Electronic Theses and Dissertations   Fogler Library

Fall 12-16-2022

Gold (I) Tetrathiomolybdate Clusters: Synthesis, Characterization, Computational Studies, and Reactivity With Thiophenol and Selenophenol

Dhirgam Humaidy
University of Maine, dhirgam.humaidy@maine.edu

Recommended Citation

GOLD (I) TETRATHIOMOLYBDATE CLUSTERS: SYNTHESIS, CHARACTERIZATION, COMPUTATIONAL
STUDIES, AND REACTIVITY WITH THIOPHENOL AND SELENOPHENOL

By

Dhirgam Humaidy

B.Sc. University of Kufa, 2005

M.Sc. Al-Nahrain University, 2011

A DISSERTATION

Submitted in Partial Fulfillment of the

Requirements for the Degree of

Doctor of Philosophy

(in Chemistry)

The Graduate School

The University of Maine

December 2022

Advisory Committee:

      Alice E. Bruce, Professor of Chemistry, Co-Advisor

      Mitchell R. M. Bruce, Professor of Chemistry, Co-Advisor

      Touradj Solouki, Professor of Chemistry and Biochemistry, Baylor University

      Matthew Brichacek, Associate Professor of Chemistry

      Michael Kienzler, Assistant Professor of Chemistry, University of Connecticut

GOLD (I) TETRATHIOMOLYBDATE CLUSTERS: SYNTHESIS, CHARACTERIZATION, COMPUTATIONAL STUDIES, AND REACTIVITY WITH THIOPHENOL AND SELENOPHENOL

By Dhirgam Humaidy

Dissertation advisors: Dr. Alice E. Bruce, and Dr. Mitchell R. M. Bruce

An Abstract of the Dissertation Presented

in Partial Fulfillment of the Requirements for the

Degree of Doctor of Philosophy

(In Chemistry)

December 2022

This thesis describes the synthesis and reactivity of heterometallic complexes containing medicinally active Au(I) and tetrathiomolybdate, $[MoS_4]^{2-}$. The research is motivated by the idea of multifunctional drugs, which are designed to treat diseases through two or more mechanisms of action. Five clusters of the general form, $[MoS_4(AuL)_2]$ were prepared: **C-1** (L=IPr), **C-2** (L=IBzMe), **C-3** (L=IMes), **C-4** (L=PPh$_3$), and **C-5** (L=PEt$_3$). The clusters with NHC ligands, **C-1**, **C-2**, and **C-3** were prepared for the first time and thoroughly characterized by ^{1}H NMR, ^{13}C{^{1}H} NMR, UV-vis, cyclic voltammetry, SCXRD, elemental analysis and mass spectrometry. **C-4** and **C-5**, which were reported previously, were prepared to compare the effect of phosphine and NHC ligands on the cluster reactivity.

Percent buried volume (% V$_{bur}$) calculations show that the steric bulkiness of the ligands increases in the order, **C-5** > **C-2** > **C-4** > **C-3** > **C-1**. A DFT calculation carried out on **C-1** suggests the presence of Au-Mo interactions, which could contribute to stabilization of the clusters in addition to the bridging sulfides. The TDDFT study showed that the lowest energy transitions are primarily υ(Au, S → Mo) and υ(S → Mo) charge transfer. This is consistent with the experimental UV-vis spectra of all five clusters which have λ_{max} = 487-491 nm.

Clusters **C-1 – C-5** were screened for antimicrobial activity by CO-ADD lab at the University of Queensland, Australia. **C-2** showed notable activity against one fungal strain, *Candida albicans*, and **C-5** showed notable activity against the gram-positive bacteria, *methicillin-resistant Staphylococcus aureus* and one fungal strain, *Cryptococcus neoformans*.

The reactivity of [MoS$_4$(AuL)$_2$] clusters with PhSH and PhSeH in DMSO-d_6 was investigated as a model for thiol- and selenol nucleophiles present in cysteine and selenocysteine proteins. In general, the clusters react with PhSH to a greater extent than with PhSeH. Cluster **C-3** was the most reactive with PhSH and PhSeH but this complex was inactive in antimicrobial cytotoxicity testing. Cluster **C-4** was not reactive with PhSH or PhSeH and it was completely inactive in cytotoxicity testing. Additional experiments are proposed as future work to better understand the complex interplay of steric and electronic effects in the [MoS$_4$(AuL)$_2$] clusters.

DEDICATION

I dedicate my dissertation work to the source of goodness and tenderness in my life, my mother. To my first teacher who inspired me with patience, wisdom and self-confidence, and his words have been like lamps that keep illuminating my path towards the success even after his death, my father. My brother and sisters never left my side and are very special. To everyone who has supported me throughout my educational journey.

TABLE OF CONTENTS

LIST OF FIGURES

LIST OF TABLES

LIST OF SCHEMES

SYNTHESIS AND REACTIVITY OF GOLD (I) TETRATHIOMOLYBDATE CLUSTERS

1.1. Overview of thesis

The objective of this thesis research is to synthesize and investigate the reactivity of a series of cluster complexes that combine two medicinally active metals, gold (I) and Mo(VI). The hypothesis is that combining gold (I) and molybdenum (VI) into one molecule will yield a compound that may show two modes of activity that are better than the sum of the parts. This hypothesis is based on the idea of multifunctional drugs, which are designed to treat diseases through two or more mechanisms of action (Scheme 1.1). The Au(I)/ Mo(VI) clusters described in this thesis are of the general form, $[MoS_4(AuL)_2]$ where L = phosphine or N-heterocyclic carbene (NHC) as shown in Figure 1.1. The central unit in these clusters is tetrathiomolybdate, $[MoS_4]^{2-}$ which coordinates to two AuL^+ cations via bridging sulfur interactions.
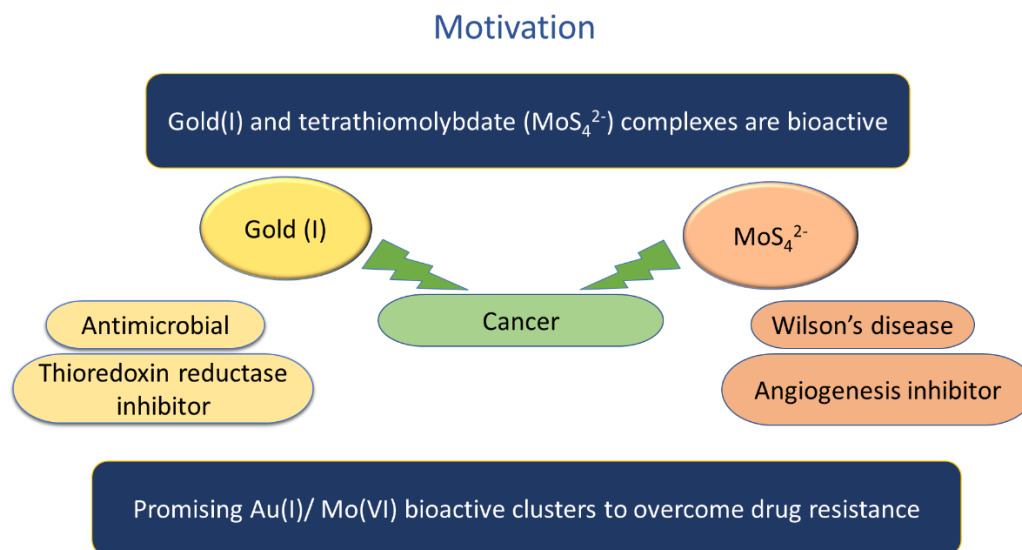
Scheme 1.1. The combination of bioactive gold (I) and tetrathiomolybdate complexes into one molecule may overcome drug resistance.

L= PR$_3$, or NHC
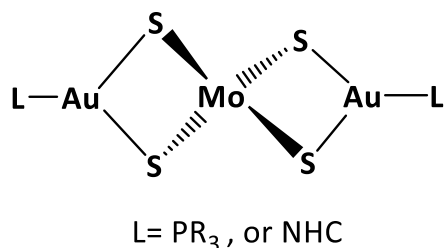
Figure 1.1. General (MoS$_4$)(AuL)$_2$ cluster structure. Mo(VI) has a tetrahedral geometry and Au(I) is trigonal planar.

1.2. Metal-based drugs

Metal-based compounds have been a cornerstone of medicine since the beginning of the 20th century. An important application of metal complexes is in the field of anticancer medicines, where platinum-based medications, such as cisplatin, are among the most widely used chemotherapeutics despite being developed more than 40 years ago.[1] Since then, clinical trials have been conducted on metal complexes that contain titanium, iron, copper, gallium, molybdenum, ruthenium, palladium, silver, gold, and bismuth.[2] Transition metal complexes have two potentially beneficial characteristics. First, they offer multiple oxidation states and multivalency, which enable the transition metals to bind with a wide range of different organic and inorganic ligands and build highly varied three-dimensional structures. Second, is their ability to access distinctive types of reactions, e.g., redox, catalytic production of active species (e.g., the production of reactive oxygen species), ligand exchange, or ligand release. These characteristics could make a significant difference in the field of medicine and complement the arsenal of organic drugs currently available.[3–5]

Cisplatin-derivatives have shown great success in treating a number of cancers including, testicular, ovarian, and head and neck cancers.[6,7] However, platinum-based complexes show non-selective interactions with DNA. Furthermore, these complexes demonstrate common problems facing drug developers, which are the resistance of some cancer cell lines and severe side effects such as kidney and gastrointestinal disorders, hearing loss, allergic reactions, and decreased immunity to infections.[8–10] This

2

has motivated researchers to develop alternatives to platinum-based drugs, employing metals that are expected to have different mechanisms of action. For example, Au(I) complexes have shown promising results in inhibiting cancer cell lines with DNA-independent mechanisms.[11] Moreover, several gold(I) compounds have shown significant activity against cisplatin-resistant cancer cell lines.[12–14] This suggests that gold(I) compounds have different modes of action than cisplatin.
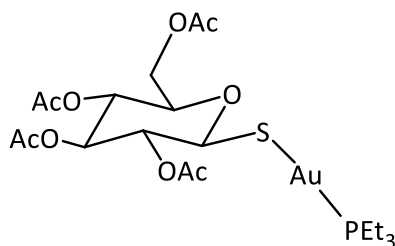
Figure 1.2. Auranofin structure, Ac= acetyl.

Auranofin, a phosphine gold (I) thiolate compound (Figure 1.2), was given clinical approval for treatment of rheumatoid arthritis in 1985.[15–17] Auranofin is in a class of drugs referred to as disease-modifying antirheumatic drugs (DMARDs). Auranofin has been shown to slow the progression of rheumatoid arthritis and in some patients, it can lead to remission of the disease. However, in recent years the clinical use of auranofin for treatment of rheumatoid arthritis has declined for a variety of reasons, including some severe side effects, the requirement for patient monitoring and the expiration of the original patent.[18] There has been great interest in repurposing auranofin to treat a variety of other conditions, including parasite infections, neurological diseases, AIDS, and bacterial infections.[19] Recently, the US Food and Drug Administration cleared auranofin for phase II clinical studies as a cancer treatment.[20] Although the mechanism of therapeutic action of auranofin is not completely understood, many studies have focused on the inhibition of sulfur- and selenium- containing enzymes, especially thioredoxin reductases (TrxR), which are a crucial part of the cellular antioxidant system.[21–23] The increasing interest in developing new metal-based drugs as well as renewed interest in repurposing

auranofin have prompted investigations of a wide variety of gold (I) compounds for medicinal applications.[24]

The types of ligands in metal complexes have a big effect on the activity and toxicity of a metal-based drug. For example, phosphine and N-heterocyclic carbene (NHC) ligands have attracted researchers for future drug design of Au(I)-based complexes. These ligands have tunable lipophilicity/hydrophilicity through changing the substituents binding to phosphine or on the imidazolium salt precursor of NHC ligands. Lipophilicity/hydrophilicity balance is an important factor in determining drug delivery to the target tissue and drug permeability through cell membranes.[25] The possibility of changing the substituents on phosphine or NHC ligands can be used to fine-tune the lipophilicity and reactivity of gold (I) complexes.[26]

1.3. Chemistry of gold

Gold has an atomic number 79 and the chemical symbol Au, derived from the Latin word *aurum*. Gold is one of the higher atomic number elements that are naturally occurring. It is a bright, slightly reddish-yellow, dense, soft, malleable, and ductile metal in its purest form. Gold is a group 11 element and is a transition metal in terms of chemistry. Gold is not affected by oxygen or sulfur although it reacts quickly with aqua regia due to the combined acting of oxidation by nitric acid and coordination of Au(III) by chloride ions (Scheme 1.2).[27]

Gold has the highest initial electron affinity (222.8 kJ mol^{-1}) of any metal (i.g. for comparison Cu, 118.5 kJ mol^{-1} and Ag, 125.7 KJ mol^{-1}) and is quite close to the halogens' values (Br, 324.7 KJ mol^{-1} and I, 295.2 KJ mol^{-1}) making Au$^-$ as accessible oxidation state.[28]

Furthermore gold in cationic form may accept electrons from practically any source (reducing agents) to generate neutral gold atoms. Gold often exists in the oxidation states Au(I) (aurous compounds) and Au(III) (auric compounds). Many Au(III) complexes are toxic to cells because they are

potent oxidizing agents and are reduced to Au(I). This reduction can be driven by thiol or thioether

reductants such as tetrahydrothiophene (THT, SC_4H_8) as shown in Scheme 1.3.[29]

$$Au_{(s)} + 3NO_3^-{}_{(aq)} + 6H^+ \rightleftharpoons Au^{3+}{}_{(aq)} + 3NO_{2(g)} + 3H_2O_{(l)}$$

$$Au^{3+}{}_{(aq)} + 4Cl^-{}_{(aq)} \rightleftharpoons AuCl_4^-{}_{(aq)}$$
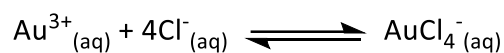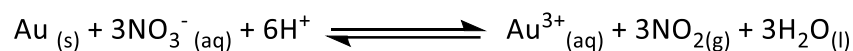
Scheme 1.2. Reaction of gold with aqua regia (the images show dissolving a gold coin in aqua regia

over time).

The complex, Au(tht)Cl is a common starting material for preparing gold (I) complexes because the

tht ligand can easily be displaced by other ligands like phosphines or N-heterocyclic carbenes (NHC).

Au(I) has a d^{10} closed-shell configuration and prefers two-coordinate, linear compounds, which are the

most prevalent coordination geometry. Three-coordinate, trigonal and four-coordinate, tetrahedral, are

rarely observed.[30]

$$HAuCl_{4(aq)} + 2\ SC_4H_{8(aq)} + H_2O_{(l)} \longrightarrow AuCl(SC_4H_8)_{(s)} + OSC_4H_{8(aq)} + 3\ HCl_{(aq)}$$
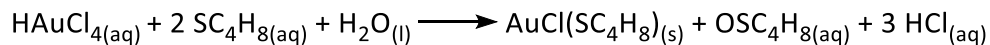
Scheme 1.3. $HAuCl_4$ reduction to Au(tht)Cl by THT.

1.4. Gold(I) complexes in medicine

Gold compounds have been used for therapeutic purposes since ancient times. In the modern era, gold compounds have been used in medicine since Robert Koch discovered that gold(I) dicyanide has anti-tubercular properties.[31] The use of gold formulations in medicine, particularly for the treatment of inflammatory conditions including rheumatoid arthritis and joint pain, is known as "chrysotherapy".[32] The physician Jacque, Forestier introduced Au(I) thiolate complexes which are considered less toxic than gold cyanide to treat rheumatoid arthritis.[33] As time went on, it was seen that patients who had chrysotherapy for arthritis had reduced rates of malignancy evidence, leading to the hypothesis that gold compounds might have anti-cancer actions.[34–38] Auranofin (Figure 1.2) showed a potential to inhibit the proliferation of tumor cells in vitro, and then was discovered to have anticancer efficacy in a mouse tumor model in vivo.[39,40] Since then, a wide range of other linear two-coordinate Au (I) phosphine complexes have been demonstrated to suppress the development of tumor cell cultures in vitro. Thiolate-ligands are frequently included in these complexes like thiosugars, thionucleobases and dithiocarbamates derivatives. [34,41–46]

McKeage, et al. stated that auranofin and Et_3PAuCl both alter mitochondrial function.[47] Later, these findings were interpreted as the induction of mitochondrial apoptotic pathways. In recent years, antitumor activity has been reported for linear Au(I) complexes with N-heterocyclic carbene (NHC), cyclodiphosphazene, phosphole, and N,N′-disubstituted cyclic thiourea ligands.[48–50] Some studies revealed that the limited anticancer effect of auranofin in vivo was constrained by its strong reactivity to protein thiols.[51] With the intention of lowering the high thiol reactivity of auranofin and other gold (I) complexes, chelating diphosphines such as 1,2-bis-diphenylphosphino-ethane (dppe) were used to create the cationic $[Au(dppe)_2]Cl$ complexes (Figure 1. 3).[51] Despite $[Au(dppe)_2]Cl$'s significant antitumor activity against a variety of tumor models in mice, clinical development of the drug was stopped after toxicological studies in dogs and rabbits revealed severe toxicities to the heart, liver, and lung due to

6

mitochondrial dysfunction.[52,53] A family of imidazolium salt precursors were used to create a series of

linear, cationic Au(I)NHC complexes [(R$_2$Im)$_2$Au]$^+$ (Figure 1. 3), where the lipophilicity was adjusted by

adding various functional groups (from log P = - 1.09 (R = Me) to 1.73 (R = cyclohexyl)).[54] Certain

compounds from this series were demonstrated to be selectively toxic to two highly tumorigenic breast

cancer cell lines while not being hazardous to normal breast cells, and the degree of selectivity and

potency were adjusted by changing the substituents.[54]
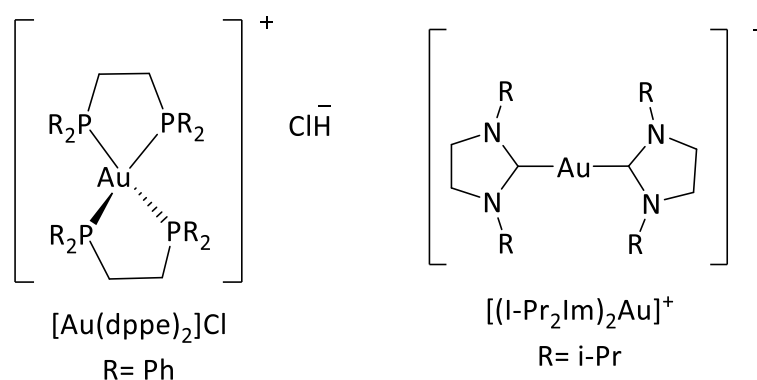
Figure 1. 3. Examples of cationic gold(I) anticancer compounds.
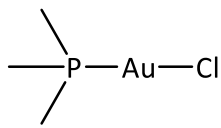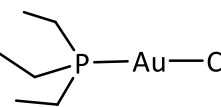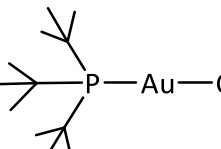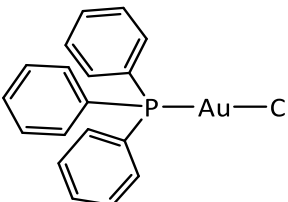
1.4.1. Gold(I) phosphines

Auranofin's rising popularity sparked the creation of gold (phosphine) complexes as possible metal-

based drugs. Phosphines are effective donors and easily bond to the gold ions. Complexes R$_3$PAuCl with

ethyl substituents (R) were more successful than methyl, isopropyl, or n-butyl complexes at producing a

therapeutic response and raising serum Au (I) levels.[17] However, Et$_3$PO has been found in the urine of

patients who have been treated with auranofin and studies with [195]Au, ^{35}S, and ^{32}P-radiolabelled

auranofin in dogs showed that the ^{35}S and ^{32}P are excreted more rapidly than [195]Au.[55,56] It has been

found that the acetylthioglucose ligand in auranofin is replaced upon binding to serum albumin, and the

phosphine ligand is released slowly (with formation of Et$_3$PO).[57] The seleno-auranofin (Se-AF) analogue

was inactive in the orally administered carragenan-induced assay in rats because of the rapid metabolism of Se-AF, presumably due to a greater extent of ligand exchange reactions and more rapid formation of Et_3PO during the reaction with serum albumin.[58] From the standpoint of ligand design, phosphine confers membrane solubility and changes the pharmacological profile of the Au (I) complex, including cell absorption. Initial research on arylphosphines was lacking, but later studies shown that triphenylphosphine Au (I) complexes are more active in the rat model of arthritis.[59] As a significant class of anticancer medicines, gold(I) phosphine complexes have shown promising results in numerous biochemical and pharmacological studies. A comparison investigation on the cytotoxic potential, cellular uptake, and nuclear uptake of several R_3PAuCl (R= Me, Et, t-But, Ph) complexes was conducted by Ott and colleagues (Table 1.1).[60] Electrothermal atomic absorption spectrometry was used to evaluate the amounts of cellular and nuclear gold in HT-29 colon cancer and MCF-7 breast cancer cells.

Table 1.1 lists the antiproliferative effects of the investigated gold phosphine complexes in two human tumor cell lines. In both tested cell lines, all examined complexes demonstrated considerable antiproliferative activities. Gold levels in the cellular and nuclear compartments were elevated, particularly for complexes R_3PAuCl with phenyl substituents (R), indicating a beneficial effect of bigger and more lipophilic substituents.[60] Phosphine gold (I) thiolate complexes have been combined with the chemotherapy drug, 5-flourouracil. Cerrada, et al. reported that the combination of the two compounds acted through a synergistic mechanism to kill colon cancer cells. Furthermore, the dose required was significantly less than the dose required for the individual compounds to achieve the same effect.[61]

Table 1.1. Anticancer activity of complexes R_3PAuCl vs colon cancer (HT-29) and breast cancer (MCF-7) cells (IC_{50} is the half maximal inhibitory concentration).[60]

Compound	IC$_{50}$ of cancer cell line	
	HT-29 (μM)	MCF-7 (μM)
P—Au—Cl	5.2 ± 0.6	3.9 ± 0.9
P—Au—Cl	5.3 ± 1.9	3.2 ± 1.3
P—Au—Cl	5.2 ± 2.1	3.1 ± 0.4
P—Au—Cl	4.2 ± 0.9	2.6 ± 0.1

1.4.2. Gold(I) N-heterocyclic carbenes

In modern organometallic chemistry, NHCs are among the most significant and extensively researched ligand classes.[62] This intense level of attention is mostly attributable to NHC-metal complexes' exceptional activity in homogeneous chemical catalysis.[63–65] NHCs have been substituted for phosphines in the construction of catalysts because numerous studies have demonstrated that they interact with metals in a manner that is like that of phosphines, perhaps most notably for the second-generation Grubbs catalyst.[64,66] As far as ligand design is concerned, NHCs are appealing since they offer considerable synthetic flexibility and the synthesis of imidazolium salts (NHC.HX) is frequently simple (Scheme 1.4).[64]
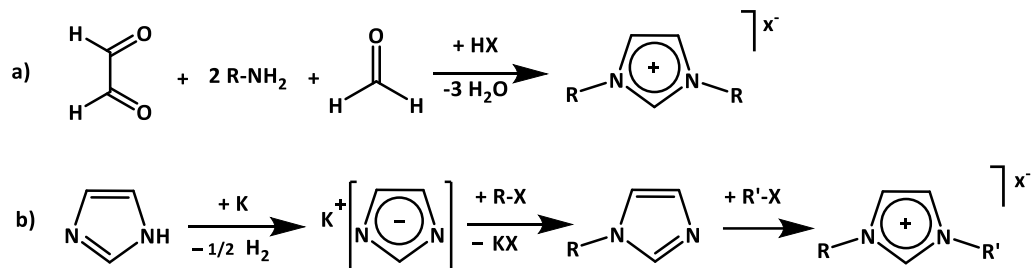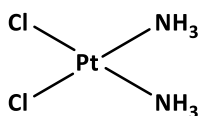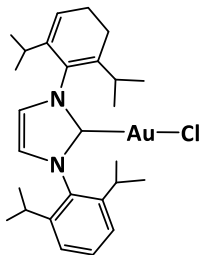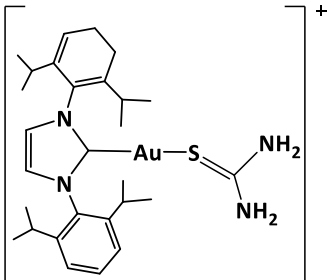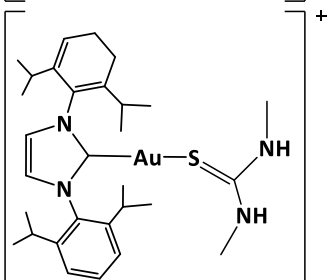
Scheme 1.4. Convenient synthetic routes to imidazolium salts, a) the same R substituents, b) different R substituents where R = any aromatic or aliphatic group.[64]
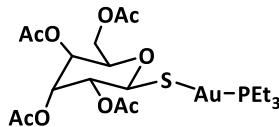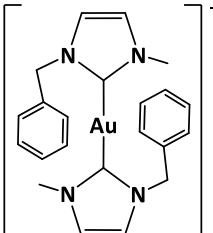
Gold (I)-NHC complexes frequently exhibit improved stability to air and moisture compared to phosphines. This stability is due to the stable metal-carbene bond and the electron-donating characteristics of NHCs. Several review articles discuss recent advancements in the medicinal inorganic chemistry of NHC-metal complexes, which has seen a significant increase in interest in recent years.[67–71] Isab, et al. tested the in vitro cytotoxicity of some (NHC)AuX complexes (Table 1.2) against human colon cancer (HCT15), human osteosarcoma (MG-63), and human cervical cancer (HeLa) cell lines and compared their cytotoxicity with cisplatin.[72] The table shows that (NHC)Au-thiolate complexes were more active than (NHC)AuCl against all cancer cell lines. Arambula, et al. tested the in vitro cytotoxicity of a bis-NHC Au(I) complex against lung cancer cells (A549). The potency of the cationic complex, $[Au(NHC)_2]^+$ was found to be about 2-fold greater than auranofin (Table 1.3).[73]
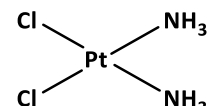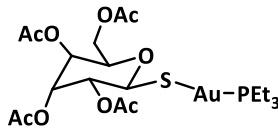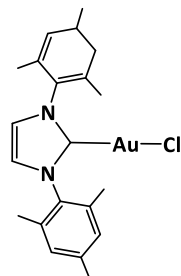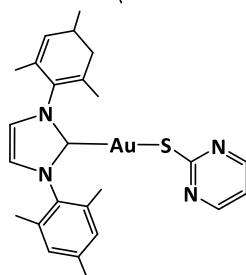
Table 1.2. Anticancer activity of complexes (NHC)AuX and cisplatin vs HCT15 (colon), MG-63 (osteosarcoma) and HeLa (cervical) cancer cells. [72]

Compound	IC$_{50}$ of cancer cell line		
	HCT15 (µM)	MG-63 (µM)	HeLa (µM)
Cisplatin	31.9 ± 0.6	33.4 ± 1.2	21.6 ± 0.7
	119.8 ± 10.6	61.6 ± 3.7	171.6 ± 12.0
	6.6 ± 0.2	1.8 ± 0.2	9.2 ± 0.2
	23.9 ± 1.2	14.7 ± 1.0	42.7 ± 6.0

Table 1.3. Anticancer activity of complexes [Au(NHC)$_2$]$^+$ and auranofin vs A549 (lung) cancer cells. [73]

Compound	IC$_{50}$ of cancer cell line
	A549 (μM)
	1.67 ± 0.05
	0.71 ± 0.03

Table 1.4. Anticancer activity of complexes (NHC)AuX, cisplatin and auranofin vs A2780S (sensitive to cisplatin) and A2780R (cisplatin resistant) ovarian cancer cells. [74]

Compound	IC$_{50}$ of cancer cell line	
	A2780S (μM)	A2780R (μM)
	3.3 ± 0.5	18.2 ± 1.0
	1.25 ± 0.5	1.5 ± 0.5
	4.5 ± 1.5	4.9 ± 2.0
	2.6 ± 0.7	2.8 ± 1.4

12

Another investigation involved (NHC)AuX complexes which were tested against human ovarian cancer cell lines that are sensitive to cisplatin (A2780S) and cisplatin resistant (A2780R), respectively (Table 1.4). The fact that the gold complexes were more cytotoxic to the cisplatin-resistant cell line suggests that they were able to overcome the resistance. Notably, the 2-pyrimidinethiolato derivative of the NHC Au(I) complex was generally more effective than the chloride derivative. Since Au-thiolate moieties and metal-NHC linkages are typically stable, Casini and colleagues suggested that the chloride ligand may be the more labile ligand at the gold center, making the chloride derivatives more reactive and susceptible to being deactivated by various cellular components.[74]

1.4.3. NHC ligand modification effect on anticancer activity of gold complexes

Gust, et al. prepared several NHC gold(I) and NHC gold (III) complexes and tested their cytotoxicity against some cancer cell lines. The NHC ligand was derived from 4,5-diarylimidazoles in which the aromatic rings on positions 4 and 5 of the imidazol-2-ylidene ring were substituted with OMe or F on different positions on the aromatic ring (Figure 1.4).[75] They found that the growth inhibitory effects of the compound toward breast cancers (MCF-7 and MDA-MB 231) as well as colon cancer (HT-29) cell lines were affected by the type of substituent on the aryl rings (OMe or F). They reported that adding aryl rings to the imidazol-2-ylidene ring at positions 4 and 5 improved the growth-inhibitory properties. Moreover, the substituents at positions 1 and 3 of the imidazol-2-ylidene ring were examined too, it was discovered that these substituents and the metal's oxidation state Au (I) and Au (III) had a less significant impact on the biological features of the complexes. However, methoxy groups at these rings did not alter the growth-inhibitory characteristics, whereas F-substituents in the ortho-position significantly boosted activity.
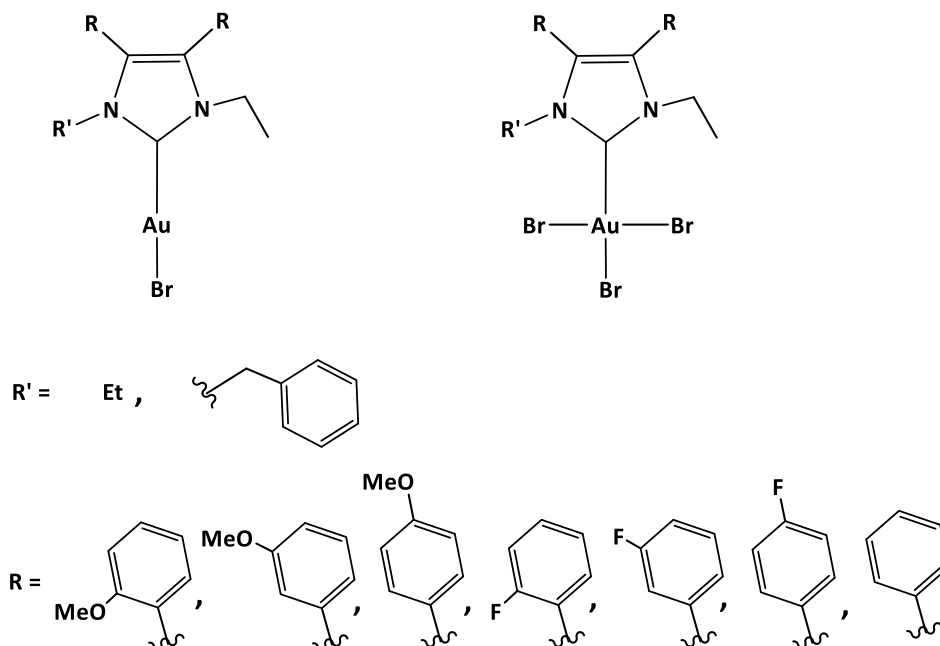
Figure 1.4. Au(I)NHC and Au(III)NHC halide complexes derived from 4,5-diarylimidazoles.[75]
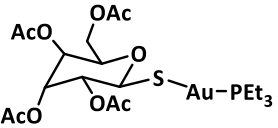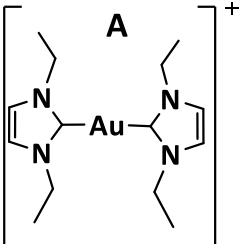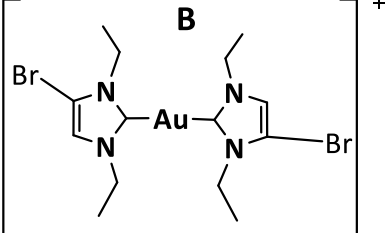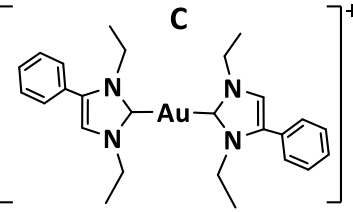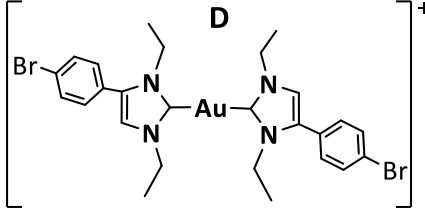
Contel, et al. reported the effect of NHC ligands on the heterometallic compounds (**AuTi**) along with those of monometallic (**Au**) precursors against renal (Caki-1), prostate (PC3, DU145), and colon (DLD1) cancer cell lines (Figure 1.5).[76] They found that the heterometallic compounds (**AuTi**) were more toxic than monometallic (**Au**) precursors. In general, all compounds showed cytotoxicity againt Caki-1, PC3, DU145 and DLD1 cancer cell lines but there was not a strong correlation between the type of NHC ligand employed and the cytotoxicity of monometallic (**Au**). However, the SIPr ligand (Figure 1.5) showed higher activity than IPr and IMes ligands in the heterometallic compounds (**AuTi**). The IMes ligand of **AuTi** compounds showed slightly higher activity than the IPr ligand on DU145, Caki-1 and DLL1 but lower activity on the PC3 cancer cell line. Another example that illustrates design of a heterometallic compound containing gold (I) was reported by Arambula, et al. who prepared ferrocene complexes derivatized with Au (I) NHC.[73] The heterometallic complexes had a higher antiproliferation activity on lung cancer cells than did the homometallic complexes individually. They found that the higher activity came from the formation of reactive oxygen species (ROS) via multiple mechanisms.[61]
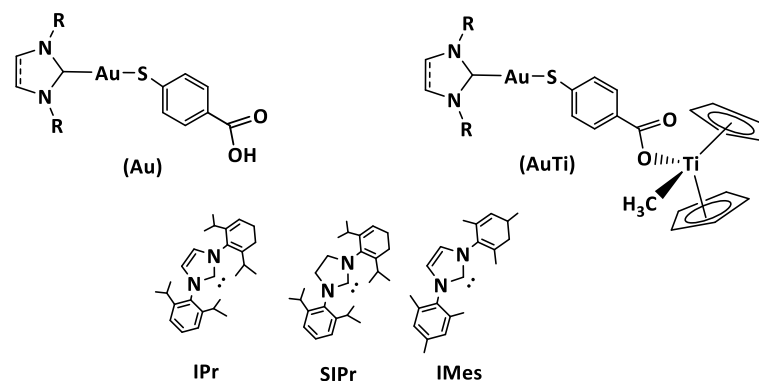
Figure 1.5. [Au(NHC)(Hmba)] (Au) and [(η^5-C$_5$H$_5$)$_2$ Ti(CH$_3$){OC(O)-*p*-C$_6$H$_4$SAu(NHC)}] (AuTi) complexes, NHC= IPr, SIPr and IMes.[76]

Ott and colleagues tested a series of gold (I) complexes with two N-heterocyclic carbene ligands [Au(NHC)$_2$]$^+$ and auranofin against cancer cell lines, pathogenic bacteria and in thioredoxin reductase (TrxR) inhibition studies.[77] The cancer cell lines were colon (HT-29) and breast (MCF-7, MDA-MB-231). The pathogenic bacteria were Gram-negative strains (*A. baumannii, E. coli, K. pneumoniae, P. aeruginosa*) and Gram-positive strains (*E. faecium*, MRSA RKI, MRSA DSM). Cancer cells and Gram-positive bacteria showed evidence of suppressed proliferation, whereas Gram negative bacteria were not significantly affected by the complexes. They found that adding aryl rings to the imidazol-2-ylidene ring at positions 4 and 5 substituent on the aryl ring as well as a bromine significantly improved the anti-cancer activity (Table 1.5, **C** and **D**). The compounds containing bromine had more anticancer activity than the compounds without bromine ((Table 1.5, **B** and **D**). The most anticancer-active compound was complex **D**. The strongest TrxR inhibitor was auranofin and complex **D**. Interestingly, complex **C** showed lower anti-cancer activity than **D** but showed higher growth inhibition of Gram-negative bacteria than complex **D**. The TrxR inhibition study showed that complex **D** had higher inhibition of rat TrxR than complex **C** but had lower inhibition of bacterial TrxR (*E. coli*) than complex **C** (Table 1.5).

Table 1.5. Anticancer and antibacterial activities, and TrxR inhibition of complexes [Au(NHC)$_2$]$^+$ and auranofin vs selected cancer cells, one strain of Gram-positive (MRSA DMS) and one strain of Gram-negative bacteria, and TrxR of rat and bacteria (*E. coli*).[77]

Compound	IC$_{50}$ for anticancer			MIC* for antibacterial		IC$_{50}$ for TrxR inhibition	
	HT-29 (µM)	MCF-7 (µM)	MDA-MB-231 (µM)	MRSA DSM (µM)	*E. coli* (µM)	Rat (µM)	*E. coli* (µM)
Auranofin structure	3.79 ± 0.18	2.00 ± 0.05	1.54 ± 0.12	0.4 ± 0.3	45.7 ± 5.1	0.09 ± 0.01	0.30 ± 0.07
A	5.54 ± 0.79	4.20 ± 0.72	5.08 ± 0.60	79.0 ± 29.2	>100 ± 0.0	127.8 ± 6.1	410.9 ± 42.1
B	1.51 ± 0.10	0.72 ± 0.07	1.08 ± 0.06	12.2 ± 8.0	>100 ± 0.0	71.9 ± 5.4	57.2 ± 6.2
C	0.15 ± 0.01	0.16± 0.03	0.18 ± 0.02	1.7 ± 0.4	47.7 ± 10.7	30.3 ± 4.6	30.0 ± 7.1
D	0.14 ± 0.02	0.06 ± 0.00	0.18 ± 0.01	9.6 ± 3.4	>100 ± 0.0	16.3 ± 3.2	96.6 ± 13.4

MIC = Minimal inhibitory concentrations which was defined in the experimental part as the lowest concentration that completely suppressed growth of bacteria.

1.5. Chemistry of molybdenum

Molybdenum has an atomic number 42 and the chemical symbol Mo, derived from the Latin word

molybdos. It is a silvery metal, with an extremely high melting point (2623 °C). Molybdenum is a group 6

element and a transition metal in terms of chemistry. Molybdenum is found naturally in oxidation states

between -2 to +6. Taube reported that Mo(VI) and Mo(V) are labile metals but Mo(III) is inert.[78] The

metal is readily accessible to humans, animals, and plants since it is soluble in water as molybdate,

$[MoO_4]^{2-}$. Molybdate is transferred into prokaryotes and eukaryotes using the typical active transport

mechanisms for phosphate and sulfate.[79] Sulfidation of molybdate occurs in four steps (Scheme 1.5).[80]

The formation of tetrathiomolybdate (TTM, $[MoS_4]^{2-}$) depends on the pH of the solution.

$$[MoO_4]^{2-} \xrightarrow[HS^-]{H^+} [MoO_3S]^{2-} \xrightarrow[HS^-]{H^+} [MoO_2S_2]^{2-} \xrightarrow[HS^-]{H^+} [MoOS_3]^{2-} \xrightarrow[HS^-]{H^+} [MoS_4]^{2-}$$
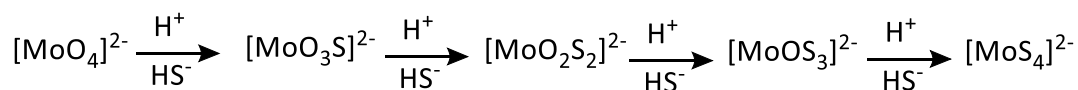
Scheme 1.5. Reaction profile of the interconversion of the $[MoO_xS_{4-x}]$ (x= 0-4) dianions.[80]

The sulfides in the TTM dianion function as ligands to coordinate metal ions in diverse bonding

modes, such as monodentate, bidentate, tridentate, and ambient bidentate, either terminal or

bridging. The ability of TTM to form heterobimetallic trinuclear clusters such as $([MoS_4]MX_n,$

M=Fe,Cu,Au,Ag, X=Cl⁻, CN⁻, PR₃) was investigated by several groups in the 1980 's (Scheme 1.6).[80–82]

R= Et, or Ph
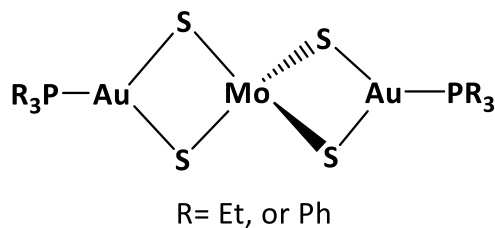
Scheme 1.6. Heterobimetallic trinuclear cluster complexes coordination of TTM.

1.5. 1. Tetrathiomolybdate complex in medicine

Ammonium tetrathiomolybdate (Figure 1.6) has an interesting use in treating chronic copper toxicity in sheep.[83] It has also been studied for the treatment of Wilson's disease, a genetic disorder associated with excessive copper accumulation.[83,84] TTM can combine with proteins (such as ceruloplasmin and albumin) and copper to form a stable tripartite complex (Figure 1.7).[84]

$$\left[\; NH_4 \; \right]_2 \left[\begin{array}{c} S \quad\quad S \\ Mo \\ S \quad\quad S \end{array} \right]$$
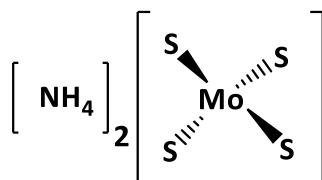
Figure 1.6. Ammonium tetrathiomolybdate structure.

In vivo, tetrathiomolybdate weakly complexes or binds free Cu^{2+} with serum albumin while being absorbed into the blood. This complex slowly excretes through the bile and urine, has no biological activity, and is no longer accessible for cellular absorption.[85] Due to the copper role to stimulate blood vessel formation and maturation (angiogenesis), and to the fact that tumor growth needs to build up new blood vessels, ammonium tetrathiomolybdate has been investigated against cancer cell lines and has shown a promising result to inhibit tumor growth and treat metastatic tumors.[86,87]

Chisholm, et al. found that the copper ATPase transporter protein (ATP7A) contributed to cisplatin-resistance in a breast cancer cell line and acted to reduce drug uptake and contribute to treatment failure. Moreover, they reported that ammonium tetrathiomolybdate reduced the ATP7A level and enhanced cisplatin treatment in a cisplatin-resistant breast cancer.[88] TTM can be regarded as a crucial agent that participates in angiogenesis.[85] Pre-clinical research revealed that TTM could be used to reduce tumor development and angiogenesis via copper depletion (CD).[89,90] In a phase I study, TTM was well tolerated and led to stabilization but not reduction of metastatic tumors.[91] In a phase II study of women with high-risk breast cancer, the use of TTM following the end of adjuvant/standard therapy led

to encouraging overall survival, particularly for triple-negative breast cancer.[92] Hence, TTM can be considered as a complementary drug in the treatment of metastatic tumor.
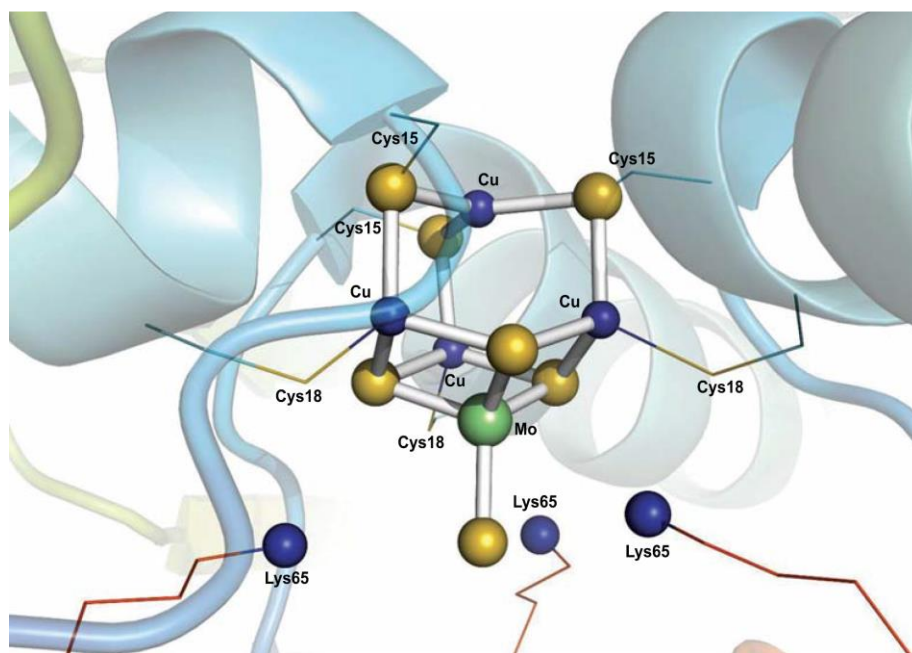
Figure 1.7. Ball-and-stick model of the $S_6Cu_4MoS_4$ cluster structure (yellow balls, sulfur atoms; blue balls, copper atoms; lime ball, molybdenum atoms).[84]

1.6. Thesis objectives & organization

This thesis describes the synthesis and characterization of [$MoS_4(AuL)_2$] clusters (L= PR_3; NHC), computational studies of the steric properties of the ligands, DFT calculations on [$MoS_4(AuIPr)_2$] (IPr= 1,3-Bis(2,6-diisopropylphenyl-imidazol-2-ylidene), and investigation of the reactivity with thiol and selenol compounds. Antimicrobial activity data, obtained in collaboration with a lab at University of Queensland, is also reported.

The thesis is organized as follows, Chapter 2 presents the synthesis and characterization of five [$MoS_4(AuL)_2$] clusters. Two of the clusters with L= PEt_3 and PPh_3 have been reported previously.[81,82] The three clusters with N-heterocyclic carbene ligands are new (L= 1,3-bis(2,6-diisopropylphenyl-imidazol-2-

19

ylidene)**,** 1-benzyl-3-methyl-imidazol-2-ylidene**,** and 1,3-bis(2,4,6-trimethylphenyl)imidazol-2-ylidene).

All clusters are characterized by ^{1}H NMR, either ^{13}C{^{1}H} NMR or ^{31}P{^{1}H} NMR, UV-Vis, elemental analyses, ESI-MS, and cyclic voltammetry. The three NHC containing clusters are further characterized by SC-XRD.

Chapter 3 describes the percent buried volume calculations on the [MoS$_4$(AuL)$_2$] clusters, which is a measure of steric bulk of the phosphine and NHC ligands. DFT calculations for [MoS$_4$(AuIPr)$_2$] are reported and the calculated values are compared to the experimental UV-Vis, ^{1}H NMR and ^{13}C{^{1}H} NMR spectra. The calculation is used to gain insight into the electronic structure of [MoS$_4$(Au(NHC))$_2$] clusters.

Chapter 4 describes the antimicrobial data obtained for several [MoS$_4$(AuL)$_2$] clusters. The antimicrobial data were collected and published in collaboration with the Community for Open Antimicrobial Drug Discovery initiative (CO-ADD, co-add.org) funded by The Wellcome Trust and the University of Queensland. The primary focus of the chapter is on the investigation of the reactivity of [MoS$_4$(AuL)$_2$] clusters with thiophenol and selenophenol. Reactions were monitored by ^{1}H NMR for clusters with NHC ligands, and by ^{1}H NMR and ^{31}P{^{1}H} NMR for clusters with phosphine ligands. The relative rates of the reaction of [MoS$_4$(AuL)$_2$] clusters with thiophenol and selenophenol are discussed. All the clusters showed low to moderate reactivity in general with thiophenol or selenophenol and the reactivity with selenophenol was lower than thiophenol.

Characterization data are collected in the appendices. Appendix A has all the NMR spectra. Appendix B has the UV- vis spectra and cyclic voltammograms. Appendix C has the single-crystal X-ray diffraction data. Appendix D collects the elemental analysis and mass spectrometry data. Appendix E contains the published article and supporting information: "Metal Complexes as Antifungals? From a Crowd-Sourced Compound Library to the First In Vivo Experiments", *JACS Au* 2022, 2, 10, 2277–2294.

1.7. Chapter References

(1)   Rosenberg, B.; VanCamp, L.; Trosko, J. E.; Mansour, V. H. Platinum Compounds: A New Class of
        Potent Antitumour Agents. *Nature* **1969**, *222* (5191), 385–386.
        https://doi.org/10.1038/222385a0.

(2)   Medina-Franco, J. L.; López-López, E.; Andrade, E.; Ruiz-Azuara, L.; Frei, A.; Guan, D.; Zuegg, J.;
        Blaskovich, M. A. T. Bridging Informatics and Medicinal Inorganic Chemistry: Toward a Database
        of Metallodrugs and Metallodrug Candidates. *Drug Discov Today* **2022**, *27* (5), 1420–1430.
        https://doi.org/https://doi.org/10.1016/j.drudis.2022.02.021.

(3)   Boros, E.; Dyson, P. J.; Gasser, G. Classification of Metal-Based Drugs According to Their
        Mechanisms of Action. *Chem* **2020**, *6* (1), 41–60. https://doi.org/10.1016/j.chempr.2019.10.013.

(4)   Lovering, F.; Bikker, J.; Humblet, C. Escape from Flatland: Increasing Saturation as an Approach
        to Improving Clinical Success. *J Med Chem* **2009**, *52* (21), 6752–6756.
        https://doi.org/10.1021/jm901241e.

(5)   Lovering, F. Escape from Flatland 2: Complexity and Promiscuity. *Medchemcomm* **2013**, *4* (3),
        515–519. https://doi.org/10.1039/C2MD20347B.

(6)   Raveendran, R.; Braude, J. P.; Wexselblatt, E.; Novohradsky, V.; Stuchlikova, O.; Brabec, V.;
        Gandin, V.; Gibson, D. Pt(Iv) Derivatives of Cisplatin and Oxaliplatin with Phenylbutyrate Axial
        Ligands Are Potent Cytotoxic Agents That Act by Several Mechanisms of Action. *Chem Sci* **2016**,
        7 (3), 2381–2391. https://doi.org/10.1039/C5SC04205D.

(7)   Dasari, S.; Bernard Tchounwou, P. Cisplatin in Cancer Therapy: Molecular Mechanisms of Action.
        Eur J Pharmacol **2014**, *740*, 364–378. https://doi.org/10.1016/j.ejphar.2014.07.025.

(8)   Dasari, S.; Bernard Tchounwou, P. Cisplatin in Cancer Therapy: Molecular Mechanisms of Action.
        Eur J Pharmacol **2014**, *740*, 364–378.
        https://doi.org/https://doi.org/10.1016/j.ejphar.2014.07.025.

(9)   Rocha, C. R. R.; Silva, M. M.; Quinet, A.; Cabral-Neto, J. B.; Menck, C. F. M. DNA Repair Pathways

        and Cisplatin Resistance: An Intimate Relationship. *Clinics* **2018**, *73*, e478s.

        https://doi.org/10.6061/clinics/2018/e478s.

(10)   Zhu, X.; Zhu, H.; Luo, H.; Zhang, W.; Shen, Z.; Hu, X. Molecular Mechanisms of Cisplatin

        Resistance in Cervical Cancer. *Drug Des Devel Ther* **2016**, 1885.

        https://doi.org/10.2147/DDDT.S106412.

(11)   Yeo, C.; Ooi, K.; Tiekink, E. Gold-Based Medicine: A Paradigm Shift in Anti-Cancer Therapy?

        Molecules **2018**, *23* (6), 1410. https://doi.org/10.3390/molecules23061410.

(12)   Marzano, C.; Gandin, V.; Folda, A.; Scutari, G.; Bindoli, A.; Rigobello, M. P. Inhibition of

        Thioredoxin Reductase by Auranofin Induces Apoptosis in Cisplatin-Resistant Human Ovarian

        Cancer Cells. *Free Radic Biol Med* **2007**, *42* (6), 872–881.

        https://doi.org/10.1016/j.freeradbiomed.2006.12.021.

(13)   Estrada-Ortiz, N.; Guarra, F.; de Graaf, I. A. M.; Marchetti, L.; de Jager, M. H.; Groothuis, G. M.

        M.; Gabbiani, C.; Casini, A. Anticancer Gold *N* -Heterocyclic Carbene Complexes: A Comparative

        in Vitro and Ex Vivo Study. *ChemMedChem* **2017**, *12* (17), 1429–1435.

        https://doi.org/10.1002/cmdc.201700316.

(14)   Li, H.; Hu, J.; Wu, S.; Wang, L.; Cao, X.; Zhang, X.; Dai, B.; Cao, M.; Shao, R.; Zhang, R.; Majidi, M.;

        Ji, L.; Heymach, J. v.; Wang, M.; Pan, S.; Minna, J.; Mehran, R. J.; Swisher, S. G.; Roth, J. A.; Fang,

        B. Auranofin-Mediated Inhibition of PI3K/AKT/MTOR Axis and Anticancer Activity in Non-Small

        Cell Lung Cancer Cells. *Oncotarget* **2016**, *7* (3), 3548–3558.

        https://doi.org/10.18632/oncotarget.6516.

(15)   Sutton, B. M. Gold Compounds for Rheumatoid Arthritis. *Gold Bull* **1986**, *19* (1), 15–16.

        https://doi.org/10.1007/BF03214639.

(16)   Kean, W. F.; Hart, L.; Buchanan, W. W. Auranofin. *Rheumatology* **1997**, *36* (5), 560–572.

https://doi.org/10.1093/rheumatology/36.5.560.

(17)   Sutton, B. M.; McGusty, E.; Walz, D. T.; DiMartino, M. J. Oral Gold. Antiarthritic Properties of

Alkylphosphinegold Coordination Complexes. *J Med Chem* **1972**, *15* (11), 1095–1098.

https://doi.org/10.1021/jm00281a001.

(18)   Casini, A.; Wai-Yin Sun, R.; Ott, I. Medicinal Chemistry of Gold Anticancer Metallodrugs. In

Metallo-Drugs: Development and Action of Anticancer Agents; Sigel, A., Sigel, H., Freisinger, E.,

Sigel, R., Eds.; Walter de Gruyter GmbH: Berlin, 2018; Vol. 18, pp 199–217.

https://doi.org/10.1515/9783110470734-007.

(19)   Roder, C.; Thomson, M. J. Auranofin: Repurposing an Old Drug for a Golden New Age. *Drugs R D*

2015, *15* (1), 13–20. https://doi.org/10.1007/s40268-015-0083-y.

(20)   Roder, C.; Thomson, M. J. Auranofin: Repurposing an Old Drug for a Golden New Age. *Drugs R D*

2015, *15* (1), 13–20. https://doi.org/10.1007/s40268-015-0083-y.

(21)   Liu, N.; Li, X.; Huang, H.; Zhao, C.; Liao, S.; Yang, C.; Liu, S.; Song, W.; Lu, X.; Lan, X.; Chen, X.; Yi,

S.; Xu, L.; Jiang, L.; Zhao, C.; Dong, X.; Zhou, P.; Li, S.; Wang, S.; Shi, X.; Dou, P. Q.; Wang, X.; Liu, J.

Clinically Used Antirheumatic Agent Auranofin Is a Proteasomal Deubiquitinase Inhibitor and

Inhibits Tumor Growth. *Oncotarget* **2014**, *5* (14), 5453–5471.

https://doi.org/10.18632/oncotarget.2113.

(22)   Fan, C.; Zheng, W.; Fu, X.; Li, X.; Wong, Y.-S.; Chen, T. Enhancement of Auranofin-Induced Lung

Cancer Cell Apoptosis by Selenocystine, a Natural Inhibitor of TrxR1 in Vitro and in Vivo. *Cell

Death Dis* **2014**, *5* (4), e1191–e1191. https://doi.org/10.1038/cddis.2014.132.

(23)   Fiskus, W.; Saba, N.; Shen, M.; Ghias, M.; Liu, J.; Gupta, S. das; Chauhan, L.; Rao, R.;

Gunewardena, S.; Schorno, K.; Austin, C. P.; Maddocks, K.; Byrd, J.; Melnick, A.; Huang, P.;

Wiestner, A.; Bhalla, K. N. Auranofin Induces Lethal Oxidative and Endoplasmic Reticulum Stress

and Exerts Potent Preclinical Activity against Chronic Lymphocytic Leukemia. *Cancer Res* **2014**, *74* (9), 2520–2532. https://doi.org/10.1158/0008-5472.CAN-13-2033.

(24)   Lu, Y.; Ma, X.; Chang, X.; Liang, Z.; Lv, L.; Shan, M.; Lu, Q.; Wen, Z.; Gust, R.; Liu, W. Recent Development of Gold(<scp>i</Scp>) and Gold(<scp>iii</Scp>) Complexes as Therapeutic Agents for Cancer Diseases. *Chem Soc Rev* **2022**, *51* (13), 5518–5556. https://doi.org/10.1039/D1CS00933H.

(25)   Atrián-Blasco, E.; Gascón, S.; Rodríguez-Yoldi, M. J.; Laguna, M.; Cerrada, E. Novel Gold(I) Thiolate Derivatives Synergistic with 5-Fluorouracil as Potential Selective Anticancer Agents in Colon Cancer. *Inorg Chem* **2017**, *56* (14), 8562–8579. https://doi.org/10.1021/acs.inorgchem.7b01370.

(26)   Storr, T. Therapeutic Gold Compounds. In *Ligand Design in Medicinal Inorganic Chemistry*; John Wiley & Sons: Chennai, India, **2014**; pp 227–248.

(27)   Wiberg Egon; Wiberg Nils; Holleman A. F. *Inorganic Chemistry*, first.; Academic Press: San Diego, Berlin, 2001.

(28)   Jansen, M. The Chemistry of Gold as an Anion. *Chem Soc Rev* **2008**, *37* (9), 1826–1835. https://doi.org/10.1039/B708844M.

(29)   Usón, R.; Laguna, A. POLYARYL DERIVATIVES OF GOLD(I), SILVER(I) AND GOLD(III). In *Organometallic Syntheses*; King, R. B., Eisch, J. J., Eds.; Elsevier: Amsterdam, **1986**; pp 322–342. https://doi.org/https://doi.org/10.1016/B978-0-444-42607-9.50090-5.

(30)   Gimeno MC. The Chemistry of Gold. In *Modern Supramolecular Gold Chemistry: Gold-Metal Interactions and Applications*; Laguna Antonio, Ed.; Wiley: Weinheim, **2008**.

(31)   Kean, W. F.; Forestier, F.; Kassam, Y.; Buchanan, W. W.; Rooney, P. J. The History of Gold Therapy in Rheumatoid Disease. *Semin Arthritis Rheum* **1985**, *14* (3), 180–186. https://doi.org/10.1016/0049-0172(85)90037-X.

(32)   Berners-Price, S. J.; Filipovska, A. Gold Compounds as Therapeutic Agents for Human Diseases. *Metallomics* **2011**, *3* (9), 863–873. https://doi.org/10.1039/c1mt00062d.

(33)   Stillman, M. Biological Inorganic Chemistry. Structure and Reactivity. Edited by Ivano Bertini, Harry B. Gray, Edward I. Stiefel and Joan S. Valentine. *Angewandte Chemie International Edition* **2007**, *46* (46), 8741–8742. https://doi.org/https://doi.org/10.1002/anie.200785504.

(34)   Maiore, L.; Cinellu, M. A.; Michelucci, E.; Moneti, G.; Nobili, S.; Landini, I.; Mini, E.; Guerri, A.; Gabbiani, C.; Messori, L. Structural and Solution Chemistry, Protein Binding and Antiproliferative Profiles of Gold(I)/(III) Complexes Bearing the Saccharinato Ligand. *J Inorg Biochem* **2011**, *105* (3), 348–355. https://doi.org/10.1016/j.jinorgbio.2010.11.016.

(35)   Ward, J. R. Role of Disease-Modifying Antirheumatic Drugs versus Cytotoxic Agents in the Therapy of Rheumatoid Arthritis. *Am J Med* **1988**, *85* (4), 39–44. https://doi.org/10.1016/0002-9343(88)90361-0.

(36)   Fries, J. F.; Bloch, D.; Spitz, P.; Mitchell, D. M. Cancer in Rheumatoid Arthritis: A Prospective Long-Term Study of Mortality. *Am J Med* **1985**, *78* (1), 56–59. https://doi.org/10.1016/0002-9343(85)90247-5.

(37)   Lorenzen, I. Treatment of Rheumatoid Arthritis with Cytostatic Drugs. *Ann Clin Res* **1975**, *7* (3), 195–201.

(38)   Tiekink, E. R. T. Gold Derivatives for the Treatment of Cancer. *Crit Rev Oncol Hematol* **2002**, *42* (3), 225–248. https://doi.org/10.1016/S1040-8428(01)00216-5.

(39)   Mirabelli, C. K.; Johnson, R. K.; Sung, C. M.; Faucette, L.; Muirhead, K.; Crooke, S. T. Evaluation of the in Vivo Antitumor Activity and in Vitro Cytotoxic Properties of Auranofin, a Coordinated Gold Compound, in Murine Tumor Models. *Cancer Res* **1985**, *45* (1), 32–39.

(40)   Simon, T. M.; Kunishima, D. H.; Vibert, G. J.; Lorber, A. Inhibitory Effects of a New Oral Gold

Compound on Hela Cells. *Cancer* **1979**, *44* (6), 1965–1975. https://doi.org/10.1002/1097-

0142(197912)44:6<1965::AID-CNCR2820440602>3.0.CO;2-6.

(41)   Gandin, V.; Fernandes, A. P.; Rigobello, M. P.; Dani, B.; Sorrentino, F.; Tisato, F.; Björnstedt, M.;

Bindoli, A.; Sturaro, A.; Rella, R.; Marzano, C. Cancer Cell Death Induced by Phosphine Gold(I)

Compounds Targeting Thioredoxin Reductase. *Biochem Pharmacol* **2010**, *79* (2), 90–101.

https://doi.org/10.1016/j.bcp.2009.07.023.

(42)   Fernández-Moreira, V.; Herrera, R. P.; Gimeno, M. C. Anticancer Properties of Gold Complexes

with Biologically Relevant Ligands. *Pure and Applied Chemistry* **2019**, *91* (2), 247–269.

https://doi.org/10.1515/pac-2018-0901.

(43)   Vesna, M.; Dolores, F.; Q. Ping, D. Gold Complexes as Prospective Metal-Based Anticancer Drugs.

Histol Histopathol **2008**, *23* (1), 101–108. https://doi.org/10.14670/HH-23.101.

(44)   Bagowski, C. P.; You, Y.; Scheffler, H.; Vlecken, D. H.; Schmitz, D. J.; Ott, I. Naphthalimide Gold(i)

Phosphine Complexes as Anticancer Metallodrugs. *Dalton Transactions* **2009**, No. 48, 10799–

10805. https://doi.org/10.1039/B912378D.

(45)   Srinivasa Reddy, T.; Privér, S. H.; Rao, V. v; Mirzadeh, N.; Bhargava, S. K. Gold(i) and Gold(Iii)

Phosphine Complexes: Synthesis, Anticancer Activities towards 2D and 3D Cancer Models, and

Apoptosis Inducing Properties. *Dalton Transactions* **2018**, *47* (43), 15312–15323.

https://doi.org/10.1039/C8DT01724G.

(46)   Kim, J. H.; Reeder, E.; Parkin, S.; Awuah, S. G. Gold(I/III)-Phosphine Complexes as Potent

Antiproliferative Agents. *Sci Rep* **2019**, *9* (1), 12335. https://doi.org/10.1038/s41598-019-48584-

5.

(47)   McKeage, M. J.; Maharaj, L.; Berners-Price, S. J. Mechanisms of Cytotoxicity and Antitumor
         Activity of Gold(I) Phosphine Complexes: The Possible Role of Mitochondria. *Coord Chem Rev*
         2002, *232* (1), 127–135. https://doi.org/https://doi.org/10.1016/S0010-8545(02)00048-6.

(48)   Suresh, D.; Balakrishna, M. S.; Rathinasamy, K.; Panda, D.; Mobin, S. M. Water-Soluble
         Cyclodiphosphazanes: Synthesis, Gold(i) Metal Complexes and Their in Vitro Antitumor Studies.
         Dalton Transactions **2008**, No. 21, 2812–2814. https://doi.org/10.1039/B804026P.

(49)   Viry, E.; Battaglia, E.; Deborde, V.; Müller, T.; Réau, R.; Davioud-Charvet, E.; Bagrel, D. A Sugar-
         Modified Phosphole Gold Complex with Antiproliferative Properties Acting as a Thioredoxin
         Reductase Inhibitor in MCF-7 Cells. *ChemMedChem* **2008**, *3* (11), 1667–1670.
         https://doi.org/10.1002/cmdc.200800210.

(50)   Yan, K.; Lok, C.-N.; Bierla, K.; Che, C.-M. Gold(i) Complex of N,N'-Disubstituted Cyclic Thiourea
         with in Vitro and in Vivo Anticancer Properties—Potent Tight-Binding Inhibition of Thioredoxin
         Reductase. *Chemical Communications* **2010**, *46* (41), 7691–7693.
         https://doi.org/10.1039/C0CC01058H.

(51)   Berners-Price, S. J.; Mirabelli, C. K.; Johnson, R. K.; Mattern, M. R.; McCabe, F. L.; Faucette, L. F.;
         Sung, C. M.; Mong, S. M.; Sadler, P. J.; Crooke, S. T. In Vivo Antitumor Activity and in Vitro
         Cytotoxic Properties of Bis[1,2-Bis(Diphenylphosphino)Ethane]Gold(I) Chloride. *Cancer Res* **1986**,
         46 (11), 5486–5493.

(52)   Hoke, G. D.; Macia, R. A.; Meunier, P. C.; Bugelski, P. J.; Mirabelli, C. K.; Rush, G. F.; Matthews,
         W. D. In Vivo and in Vitro Cardiotoxicity of a Gold-Containing Antineoplastic Drug Candidate in
         the Rabbit. *Toxicol Appl Pharmacol* **1989**, *100* (2), 293–306. https://doi.org/10.1016/0041-
         008X(89)90315-3.

(53)   Smith, P. F.; Hoke, G. D.; Alberts, D. W.; Bugelski, P. J.; Lupo, S.; Mirabelli, C. K.; Rush, G. F.

Mechanism of Toxicity of an Experimental Bidentate Phosphine Gold Complexed Antineoplastic

Agent in Isolated Rat Hepatocytes. *J Pharmacol Exp Ther* **1989**, *249* (3), 944–950.

(54)   Baker, M. v; Barnard, P. J.; Berners-Price, S. J.; Brayshaw, S. K.; Hickey, J. L.; Skelton, B. W.;

White, A. H. Cationic, Linear Au(i) N-Heterocyclic Carbene Complexes: Synthesis, Structure and

Anti-Mitochondrial Activity. *Dalton Transactions* **2006**, No. 30, 3708–3715.

https://doi.org/10.1039/B602560A.

(55)   Blodgett, R. C.; Heuer, M. A.; Pietrusko, R. G. Auranofin: A Unique Oral Chrysotherapeutic Agent.

Semin Arthritis Rheum **1984**, *13* (3), 255–273. https://doi.org/10.1016/0049-0172(84)90029-5.

(56)   Intoccia, A. P.; Flanagan, T. L.; Walz, D. T.; Gutzait, L.; Swagzdis, J. E.; Flagiello, J.; Hwang, B. Y.;

Dewey, R. H.; Noguchi, H. Pharmacokinetics of Auranofin in Animals. *J Rheumatol Suppl 8*, 90–

98.

(57)   Coffer, M. T.; Shaw, C. F.; Hormann, A. L.; Mirabelli, C. K.; Crooke, S. T. Thiol Competition for

Et3PAuS-Albumin: A Nonenzymatic Mechanism for Et3PO Formation. *J Inorg Biochem* **1987**, *30*

(3), 177–187. https://doi.org/10.1016/0162-0134(87)80062-4.

(58)   Hill, D. T.; Isab, A. A.; Griswold, D. E.; DiMartino, M. J.; Matz, E. D.; Figueroa, A. L.; Wawro, J. E.;

DeBrosse, C.; Reiff, W. M.; Elder, R. C.; Jones, B.; Webb, J. W.; Shaw, C. F. Seleno-Auranofin (Et $_3$

PAuSe-Tagl): Synthesis, Spectroscopic (EXAFS, [197] Au Mössbauer, [31] P, [1] H, [13] C, and [77] Se NMR,

ESI-MS) Characterization, Biological Activity, and Rapid Serum Albumin-Induced

Triethylphosphine Oxide Generation. *Inorg Chem* **2010**, *49* (17), 7663–7675.

https://doi.org/10.1021/ic902335z.

(59)   Whitehouse, M. W.; Cookson, P. D.; Siasios, G.; Tiekink, E. R. T. Anti-Arthritic Activity in Rats of

Some Phosphinegold(I) Thionucleobases and Related Thiolates. *Met Based Drugs* **1998**, *5* (4),

245–249. https://doi.org/10.1155/MBD.1998.245.

(60)   Scheffler, H.; You, Y.; Ott, I. Comparative Studies on the Cytotoxicity, Cellular and Nuclear

Uptake of a Series of Chloro Gold(I) Phosphine Complexes. *Polyhedron* **2010**, *29* (1), 66–69.

https://doi.org/10.1016/j.poly.2009.06.007.

(61)   Atrián-Blasco, E.; Gascón, S.; Rodríguez-Yoldi, M. J.; Laguna, M.; Cerrada, E. Novel Gold(I)

Thiolate Derivatives Synergistic with 5-Fluorouracil as Potential Selective Anticancer Agents in

Colon Cancer. *Inorg Chem* **2017**, *56* (14), 8562–8579.

https://doi.org/10.1021/acs.inorgchem.7b01370.

(62)   Bourissou, D.; Guerret, O.; Gabbaï, F. P.; Bertrand, G. Stable Carbenes. *Chem Rev* **2000**, *100* (1),

39–92. https://doi.org/10.1021/cr940472u.

(63)   Herrmann, W. A.; Köcher, C. N-Heterocyclic Carbenes. *Angewandte Chemie International Edition

in English* **1997**, *36* (20), 2162–2187. https://doi.org/10.1002/anie.199721621.

(64)   Herrmann, W. A. N-Heterocyclic Carbenes: A New Concept in Organometallic Catalysis.

Angewandte Chemie International Edition **2002**, *41* (8), 1290–1309.

https://doi.org/10.1002/1521-3773(20020415)41:8<1290::AID-ANIE1290>3.0.CO;2-Y.

(65)   Díez-González, S.; Marion, N.; Nolan, S. P. N-Heterocyclic Carbenes in Late Transition Metal

Catalysis. *Chem Rev* **2009**, *109* (8), 3612–3676. https://doi.org/10.1021/cr900074m.

(66)   Scholl, M.; Ding, S.; Lee, C. W.; Grubbs, R. H. Synthesis and Activity of a New Generation of

Ruthenium-Based Olefin Metathesis Catalysts Coordinated with 1,3-Dimesityl-4,5-

Dihydroimidazol-2-Ylidene Ligands. *Org Lett* **1999**, *1* (6), 953–956.

https://doi.org/10.1021/ol990909q.

(67)   Barnard, P. J.; Berners-Price, S. J. Targeting the Mitochondrial Cell Death Pathway with Gold

Compounds. *Coord Chem Rev* **2007**, *251* (13), 1889–1902.

https://doi.org/https://doi.org/10.1016/j.ccr.2007.04.006.

(68)   Hindi, K. M.; Panzner, M. J.; Tessier, C. A.; Cannon, C. L.; Youngs, W. J. The Medicinal

Applications of Imidazolium Carbene–Metal Complexes. *Chem Rev* **2009**, *109* (8), 3859–3884.

https://doi.org/10.1021/cr800500u.

(69)   Gasser, G.; Ott, I.; Metzler-Nolte, N. Organometallic Anticancer Compounds. *J Med Chem* **2011**,

54 (1), 3–25. https://doi.org/10.1021/jm100020w.

(70)   Oehninger, L.; Rubbiani, R.; Ott, I. N-Heterocyclic Carbene Metal Complexes in Medicinal

Chemistry. *Dalton Transactions* **2013**, *42* (10), 3269–3284.

https://doi.org/10.1039/C2DT32617E.

(71)   Liu, W.; Gust, R. Metal N-Heterocyclic Carbene Complexes as Potential Antitumor Metallodrugs.

Chem Soc Rev **2013**, *42* (2), 755–773. https://doi.org/10.1039/C2CS35314H.

(72)   Sulaiman, A. A. A.; Kalia, N.; Bhatia, G.; Kaur, M.; Fettouhi, M.; Altaf, M.; Baig, N.; Kawde, A.-N.;

Isab, A. A. Cytotoxic Effects of Gold(i) Complexes against Colon, Cervical and Osteo Carcinoma

Cell Lines: A Mechanistic Approach. *New Journal of Chemistry* **2019**, *43* (36), 14565–14574.

https://doi.org/10.1039/C9NJ02063B.

(73)   Arambula, J. F.; McCall, R.; Sidoran, K. J.; Magda, D.; Mitchell, N. A.; Bielawski, C. W.; Lynch, V.

M.; Sessler, J. L.; Arumugam, K. Targeting Antioxidant Pathways with Ferrocenylated N-

Heterocyclic Carbene Supported Gold(i) Complexes in A549 Lung Cancer Cells. *Chem Sci* **2016**, *7*

(2), 1245–1256. https://doi.org/10.1039/C5SC03519H.

(74)   Schuh, E.; Pflüger, C.; Citta, A.; Folda, A.; Rigobello, M. P.; Bindoli, A.; Casini, A.; Mohr, F. Gold(I)

Carbene Complexes Causing Thioredoxin 1 and Thioredoxin 2 Oxidation as Potential Anticancer

Agents. *J Med Chem* **2012**, *55* (11), 5518–5528. https://doi.org/10.1021/jm300428v.

(75)   Liu, W.; Bensdorf, K.; Proetto, M.; Abram, U.; Hagenbach, A.; Gust, R. NHC Gold Halide

Complexes Derived from 4,5-Diarylimidazoles: Synthesis, Structural Analysis, and

Pharmacological Investigations as Potential Antitumor Agents. *J Med Chem* **2011**, *54* (24), 8605–8615. https://doi.org/10.1021/jm201156x.

(76)   Mui, Y. F.; Fernández-Gallardo, J.; Elie, B. T.; Gubran, A.; Maluenda, I.; Sanaú, M.; Navarro, O.; Contel, M. Titanocene–Gold Complexes Containing N-Heterocyclic Carbene Ligands Inhibit Growth of Prostate, Renal, and Colon Cancers in Vitro. *Organometallics* **2016**, *35* (9), 1218–1227. https://doi.org/10.1021/acs.organomet.6b00051.

(77)   Schmidt, C.; Karge, B.; Misgeld, R.; Prokop, A.; Brönstrup, M.; Ott, I. Biscarbene Gold(i) Complexes: Structure–Activity-Relationships Regarding Antibacterial Effects, Cytotoxicity, TrxR Inhibition and Cellular Bioavailability. *Medchemcomm* **2017**, *8* (8), 1681–1689. https://doi.org/10.1039/C7MD00269F.

(78)   Taube, Henry. Rates and Mechanisms of Substitution in Inorganic Complexes in Solution. *Chem Rev* **1952**, *50* (1), 69–126. https://doi.org/10.1021/cr60155a003.

(79)   Jennette, K. W. The Role of Metals in Carcinogenesis: Biochemistry and Metabolism. *Environ Health Perspect* **1981**, *40*, 233–252. https://doi.org/10.1289/ehp.8140233.

(80)   Gili, P.; Tsipis, A. C. Electronic Structure Calculations on Multiply Charged Anions Containing M⬜S Bonds (M = Cr, Mo, W) and Their Heterobimetallic Cluster Complexes. *Int J Quantum Chem* **2007**, *107* (2), 418–439. https://doi.org/https://doi.org/10.1002/qua.21087.

(81)   Charnock, J. M.; Bristow, S.; Nicholson, J. R.; Garner, C. D.; Clegg, W. Preparations, Crystal Structures, and Molybdenum-95 Nuclear Magnetic Resonance Spectroscopic Studies of Triphenylphosphine–Gold–Tetrathiomolybdate(VI) Clusters. *Journal of the Chemical Society, Dalton Transactions* **1987**, No. 2, 303–306. https://doi.org/10.1039/DT9870000303.

(82)   Kinsch, E. M.; Stephan, D. W. Synthesis and Crystal and Molecular Structure of MoS4(AuPEt3)2: A Linear Trinuclear Heterobimetallic Species. *Inorganica Chim Acta* **1985**, *96* (2), L87–L90. https://doi.org/https://doi.org/10.1016/S0020-1693(00)87570-2.

(83) de Fabregues, O.; Viñas, J.; Palasí, A.; Quintana, M.; Cardona, I.; Auger, C.; Vargas, V. Ammonium Tetrathiomolybdate in the Decoppering Phase Treatment of Wilson's Disease with Neurological Symptoms: A Case Series. *Brain Behav* **2020**, *10* (5). https://doi.org/10.1002/brb3.1596.

(84) Jurowska, A.; Jurowski, K.; Szklarzewicz, J.; Buszewski, B.; Kalenik, T.; Piekoszewski, W. Molybdenum Metallopharmaceuticals Candidate Compounds - The "Renaissance" of Molybdenum Metallodrugs? *Curr Med Chem* **2016**, *23* (29), 3322–3342. https://doi.org/10.2174/0929867323666160504103743.

(85) Redman, B. G.; Esper, P.; Pan, Q.; Dunn, R. L.; Hussain, H. K.; Chenevert, T.; Brewer, G. J.; Merajver, S. D. Phase II Trial of Tetrathiomolybdate in Patients with Advanced Kidney Cancer1. *Clinical Cancer Research* **2003**, *9* (5), 1666–1672.

(86) Brewer, G. Copper Lowering Therapy With Tetrathiomolybdate as an Antiangiogenic Strategy in Cancer. *Curr Cancer Drug Targets* **2005**, *5* (3), 195–202. https://doi.org/10.2174/1568009053765807.

(87) Jurowska, A.; Jurowski, K.; Szklarzewicz, J.; Buszewski, B.; Kalenik, T.; Piekoszewski, W. Molybdenum Metallopharmaceuticals Candidate Compounds - The "Renaissance" of Molybdenum Metallodrugs? *Curr Med Chem* **2016**, *23* (29), 3322–3342. https://doi.org/10.2174/0929867323666160504103743.

(88) Chisholm, C. L.; Wang, H.; Wong, A. H.-H.; Vazquez-Ortiz, G.; Chen, W.; Xu, X.; Deng, C.-X. Ammonium Tetrathiomolybdate Treatment Targets the Copper Transporter ATP7A and Enhances Sensitivity of Breast Cancer to Cisplatin. *Oncotarget* **2016**, *7* (51), 84439–84452. https://doi.org/10.18632/oncotarget.12992.

(89) Pan, Q.; Kleer, C. G.; van Golen, K. L.; Irani, J.; Bottema, K. M.; Bias, C.; de Carvalho, M.; Mesri, E. A.; Robins, D. M.; Dick, R. D.; Brewer, G. J.; Merajver, S. D. Copper Deficiency Induced by

Tetrathiomolybdate Suppresses Tumor Growth and Angiogenesis. *Cancer Res* **2002**, *62* (17), 4854–4859.

(90)   Pan, Q.; Rosenthal, D. T.; Bao, L.; Kleer, C. G.; Merajver, S. D. Antiangiogenic Tetrathiomolybdate Protects against Her2/Neu-Induced Breast Carcinoma by Hypoplastic Remodeling of the Mammary Gland. *Clinical Cancer Research* **2009**, *15* (23), 7441–7446. https://doi.org/10.1158/1078-0432.CCR-09-1361.

(91)   Brewer, G. J.; Dick, R. D.; Grover, D. K.; LeClaire, V.; Tseng, M.; Wicha, M.; Pienta, K.; Redman, B. G.; Jahan, T.; Sondak, V. K.; Strawderman, M.; LeCarpentier, G.; Merajver, S. D. Treatment of Metastatic Cancer with Tetrathiomolybdate, an Anticopper, Antiangiogenic Agent: Phase I Study. *Clin Cancer Res* **2000**, *6* (1), 1–10.

(92)   Chan, N.; Willis, A.; Kornhauser, N.; Ward, M. M.; Lee, S. B.; Nackos, E.; Seo, B. R.; Chuang, E.; Cigler, T.; Moore, A.; Donovan, D.; Vallee Cobham, M.; Fitzpatrick, V.; Schneider, S.; Wiener, A.; Guillaume-Abraham, J.; Aljom, E.; Zelkowitz, R.; Warren, J. D.; Lane, M. E.; Fischbach, C.; Mittal, V.; Vahdat, L. Influencing the Tumor Microenvironment: A Phase II Study of Copper Depletion Using Tetrathiomolybdate in Patients with Breast Cancer at High Risk for Recurrence and in Preclinical Models of Lung Metastases. *Clinical Cancer Research* **2017**, *23* (3), 666–676. https://doi.org/10.1158/1078-0432.CCR-16-1326.

SYNTHESIS AND CHARACTERIZATION OF GOLD-MOLYBDENUM CLUSTERS [MoS₄(AuL)₂] (L=NHC, PR₃)

2.1 Introduction

This chapter is about the synthesis and characterization of the five Au-Mo-S clusters shown in Scheme 2.1. The clusters with N-heterocyclic carbene ligands (**C-1**, **C-2**, **C-3**) are new and the two clusters with phosphine ligands (**C-4**, **C-5**) have been reported previously.[1,2] All clusters are characterized by ^{1}H NMR, either ^{13}C{^{1}H} NMR or ^{31}P{^{1}H} NMR, UV-Vis, elemental analyses, electrospray ionization mass spectrometry and cyclic voltammetry. Clusters **C-1**, **C-2** and **C-3** are further characterized by SC-XRD.
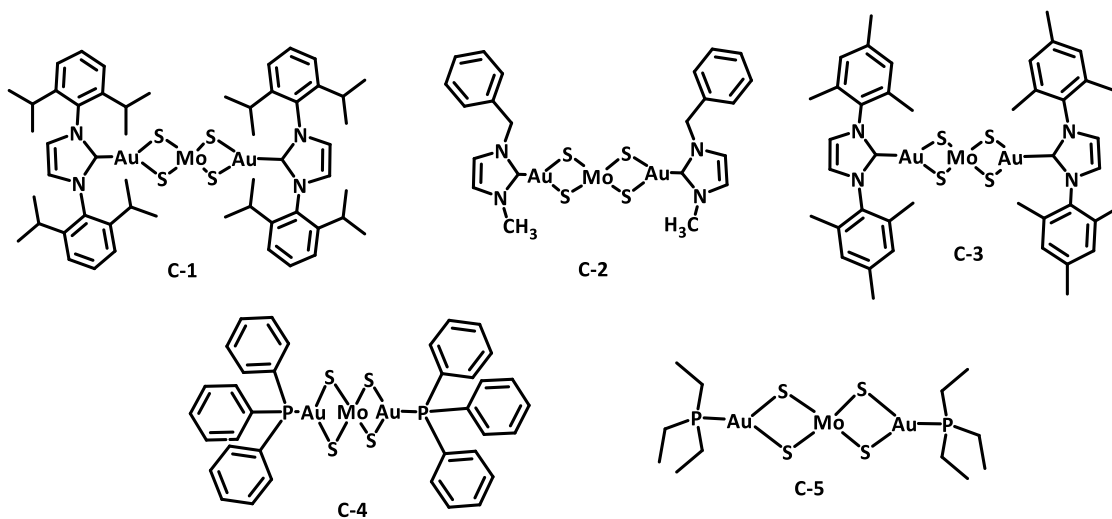
Scheme 2.1. Au-Mo-S complexes synthesized and studied in this thesis.

2.2. Experimental Section

2.2.1. General Consideration

A Canadian Gold Maple Leaf coin (gold content of 99.99%) purchased from ModernCoinMart was used to prepare Au(tht)Cl. Ammonium tetrathiomolybdate ([NH₄]₂[MoS₄], 99%), tetrahydrothiophene (THT; C₄H₈S, 99%), tetraethylammonium hydroxide ((C₂H₅)₄N(OH), 35wt. % in H₂O), triphenylphosphine

(Ph$_3$P, 99%), triethylphosphine (PEt$_3$, 99%), 1-(2,6-diisopropylphenyl)-3-(2,4,6-trimethylphenyl)-4,5-dihydroimidazolium chloride (IPr.HCl; C$_{24}$H$_{33}$ClN$_2$, 97%), 1-benzyl-3-methylimidazolium chloride (IBzMe.HCl; C$_{11}$H$_{13}$ClN$_2$, 97%), 1,3-bis(2,4,6-trimethylphenyl)imidazolium chloride (IMes.HCl; C$_{21}$H$_{25}$ClN$_2$, 95%), acetylacetone (CH$_3$COCH$_2$COCH$_3$, 99%), tetrabutylammonium hydroxide solution (n-Bu$_4$N(OH), 0.1 M in water), potassium carbonate (K$_2$CO$_3$, 99%), sodium sulfate (Na$_2$SO$_4$, 99%) and tetrabutylammonium hexafluorophosphate (TBAH) (electrochemical analysis, ≥99.0%) were obtained from Sigma-Aldrich and used as received. Concentrated hydrochloric acid (HCl), concentrated nitric acid (HNO$_3$), diethyl ether (Et$_2$O), acetone (CH$_3$COCH$_3$), acetonitrile (CH$_3$CN), pentane (CH$_3$(CH$_2$)$_3$CH$_3$), heptane (C$_7$H$_{16}$), methanol (CH$_3$OH) and methylene chloride (CH$_2$Cl$_2$) were purchased from Fisher Scientific. Dimethyl sulfoxide (DMSO; CH$_3$SOCH$_3$), was purchased from Acros Organics. Ethanol (CH$_3$CH$_2$OH) was purchased from Pharmco by Greenfield Global. Deuterated solvents: dichloromethane-d_2 (CH$_2$Cl$_2$-d$_2$), dimethyl sulfoxide-d_6 (DMSO-d_6), chloroform-d (CDCl$_3$) and acetonitrile-d_3 (CD$_3$CN) were purchased from Cambridge Isotope Laboratories, Inc. Monocrystalline Diamond Suspension (1 μm) was received from Buehler.

All reactions were carried out in the air unless otherwise stated. Reactions carried out under a nitrogen atmosphere were conducted using standard Schlenk techniques. All glassware was oven-dried prior to use.

^{1}H NMR,^{13}C{^{1}H} NMR and ^{31}P{^{1}H} NMR spectra were obtained using Varian Inova 400 MHz or Bruker Avance NEO 500 MHz NMR spectrometers at room temperature. The chemical shifts of ^{1}H NMR spectra were referenced to residual proton signals of the deuterated solvents and ^{13}C{^{1}H} NMR were referenced to ^{13}C signals of the solvents. ^{31}P{^{1}H} NMR spectra were referenced to 85% H$_3$PO$_4$ (external standard). All ^{1}H, ^{13}C{^{1}H} and ^{31}P {^{1}H} NMR spectra are collected in Appendix A. Ultraviolet–visible light (UV-vis) spectra were collected using a Perkin Elmer Lambda 25 spectrophotometer. A Potentiostat/Galvanostat Model 273 was used to conduct cyclic voltammetry (CV) and experiments were carried out in air in a one compartment cell. The working electrode was a platinum disk (1 mm). A platinum coil and saturated

calomel (SCE, Hg_2Cl_2) were used as counter and reference electrodes, respectively. The electrolyte solution was tetrabutylammonium hexafluorophosphate (TBAH; 0.1 M) in the dichloromethane or acetonitrile. The analyzed compounds (1.5mM) were prepared in electrolyte solution. UV-Vis and CVs of **C-1**, **C-2**, **C-3**, **C-4, C-5** and ammonium tetrathiomolybdate data are collected in Appendix B.

Single-crystal X-ray diffraction measurements (SC-XRD) for **C-1**, **C-2** and **C-3** were collected using a Bruker D8 QUEST ECO diffractometer with a sealed tube source (Mo-Kα λ = 0.71073 Å) running at 50 mV/20 mA with a Photon 50 detector. The crystals were mounted on dual thickness MiTeGen micro loop with an immersion oil (type NVH, Cargille laboratories). The structures were solved through direct methods using the APEX 3 (Bruker, 2017) suite of programs. Further refinement on the solved structure was done by the Olex2 (V1.2.10) program[3] using the SHELXL refinement package.[4] All hydrogen atoms were geometrically calculated by the software and finally refined. SCXRD data of **C-1**, **C-2** and **C-3** data are collected in Appendix C.

Elemental analyses (CHN) were performed by Galbraith Laboratories, Inc., Knoxville, Tennessee, USA. Electrospray ionization mass spectrometry (ESI-MS) was performed by Kyle Wilhelm in Professor Touradj Solouki's lab at Baylor University, Texas. Elemental analysis reports for **C-1**, **C-2** and **C-3** as well as mass spectra of **C-1**, **C-2**, **C-3** and **C-4** are collected in Appendix D.

The synthesis of all metal complexes, including those that have been previously reported, are described here for completeness.

2.2.2. Synthesis of Au(tht)Cl

Gold (3.4 g, 17.2 mmol) was dissolved in 300 mL of aqua regia (3:1 conc. HC1: conc. HNO_3). The solution was heated slowly to 70 °C in a water bath (liquid nitrogen was on hand to quickly quench the reaction if it became too vigorous.) The round-bottom flask was connected to a vacuum aspirator via a Tygon tube and the reaction mixture was stirred for 7 h to remove NOxs. Concentrated hydrochloric acid (1 mL) was added into the solution after 30 min, 2 h, and after all the gold had dissolved. The reaction

mixture was cooled to room temperature and then kept in an ice bath. A 10 % excess of tetrahydrothiophene (3.34 mL, 37.84 mmol) and 200 mL of absolute ethanol were added into the reaction mixture at 0 °C. First a yellow precipitate of $AuCl_3$(tht) formed, and then after 15 min with stirring at 0 °C, a white solid of Au(tht)Cl formed. The white precipitate was filtered, washed with two 10 mL portions of cold ethanol, and vacuum dried. Yield 4.9 g (90%).

2.2.3. Synthesis of [Et$_4$N]$_2$[MoS$_4$]

[Et$_4$N]$_2$[MoS$_4$] was prepared by slight modification of published procedures.[1,5] A 35 % aqueous solution of Et$_4$NOH (5.04 mL, 12.31 mmol), 40 mL water and [Et$_4$N]$_2$[MoS$_4$] (1.6 gm, 6.15 mmol) were placed under vacuum with stirring for 2h to remove NH_3. The solution was filtered after adding 100 mL of isopropanol and 25 mL diethyl ether and washed with isopropanol and then diethyl ether. The orange solid was dissolved in 200 mL acetonitrile and reprecipitated by adding 100 mL diethyl either. Yield 2.2 g (74%). UV-vis. λ_{max} (nm) in acetonitrile (245 , 322, 474) (see Fig B.1).

2.2.4. Synthesis of Au(IPr)Cl

Au(IPr)Cl was prepared by slight modification of published procedures.[6–8] Au(tht)Cl (0.5 gm, 1.56 mmol), K_2CO_3 powder (0.43 gm, 3.12 mmol) and 1-(2,6-diisopropylphenyl)-3-(2,4,6-trimethylphenyl)-4,5-dihydroimidazolium chloride (IPr.HCl; 0.66 gm, 1.56 mmol) were dissolved in 100 mL acetone in a round-bottom flask and stirred for 15 min. The mixture was refluxed at 60 °C for 2.5 h. The acetone was removed under vacuum and CH_2Cl_2 (20 mL) was added. The solution was filtered through a thin pad of silica and washed with 5 mL of CH_2Cl_2. Heptane (5 mL) was added to the filtrate and left in an evaporating dish for 5-6 h to yield white crystalline precipitate. The crystals were collected by filtration, washed with pentane (5 mL) and dried under vacuum. Yield 0.9 gm (92%).
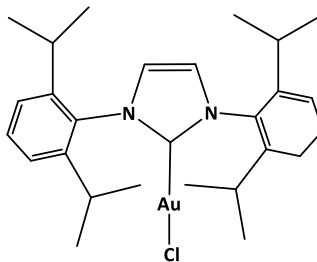
δ ^{1}H NMR (400 MHz, CH$_2$Cl$_2$-d_2) 7.57 (2 H, t, J 7.8), 7.35 (4 H, d, J 7.8), 7.24 (2 H, s), 2.56 (4 H, hept, J 6.9), 1.34 (12H, d, J 6.9), 1.23 (12 H, d, J 6.9) ppm. δ ^{13}C{^{1}H} NMR (101 MHz, CH$_2$Cl$_2$-d_2) 175.62, 146.29, 134.56,131.29, 124.89, 123.95, 29.40, 24.66, 24.22 ppm. δ ^{1}H NMR and δ ^{13}C{^{1}H} NMR (see Fig A.1 and Fig A.2)

2.2.5. Synthesis of Au(IBzMe)Cl

Au(IBzMe)Cl was prepared by slight modification of published procedures.[6–9] A 0.1 M tetrabutylammonium hydroxide aqueous solution (17.20 mL , 1.72 mmol) and acetylacetone (0.18 mL,1.72 mmol) were mixed and stirred for 10h. The solution was dried under vacuum to give a yellow solid [Bu$_4$N][acac]. Au(tht)Cl (0.5 gm, 1.56 mmol), and 1-benzyl-3-methylimidazolium chloride (IBzMe.HCl; 0.27 gm, 1.56 mmol) were added to the yellow solid and dissolved in 100 mL CH$_2$Cl$_2$ in a round-bottom flask and stirred for 2 h. The solution was filtered through a thin pad of silica and sodium sulfate. Heptane (5 mL) was added and leave the solution in the evaporating dish for 5-6 h to get white crystals in heptane. The crystals were collected by filtration, washed with pentane (5 mL) and dried under vacuum. Yield 0.51 gm (81%).
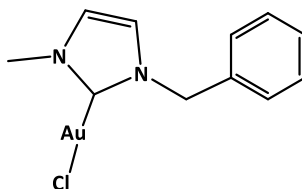
δ ^{1}H NMR (400 MHz, CH$_2$Cl$_2$-d_2) 7.43 – 7.29 (5 H, m), 6.97 (1 H, d, J 2.0), 6.92 (1 H, d, J 2.0), 5.37 (2 H, s), 3.84 (3 H, s) ppm. δ ^{13}C{^{1}H} NMR (101 MHz, CH$_2$Cl$_2$-d_2) 172.00, 136.08, 129.50, 129.09, 128.47, 122.93, 121.03, 55.43, 38.84 ppm. δ ^{1}H NMR and δ ^{13}C{^{1}H} NMR (see Fig A.3 and Fig A.4)

2.2.6. Synthesis of Au(IMes)Cl

Au(IMes)Cl was prepared by modified the previous published procedures.[6–8] Au(tht)Cl (0.5 gm, 1.56 mmol), K$_2$CO$_3$ powder (0.65 gm, 4.68 mmol) and 1,3-Bis(2,4,6-trimethylphenyl)imidazolium chloride (IMes.HCl; 0.53 gm, 1.56 mmol) were dissolved in 100 mL acetone under air in a round-bottom flask and stirred for 15 min. The mixture was refluxed at 60 ℃ for 4h. The acetone was removed under vacuum and CH$_2$Cl$_2$ (20 mL)was added. The solution was filtered through thin pad of silica and added 5 mL of CH$_2$Cl$_2$ to wash the silica pad. Heptane (5 mL) was added and leave the solution in the evaporating dish for 5-6 h to get white crystals in heptane. The crystals were collected by filtration, washed with pentane (5 mL) and dried under vacuum. Yield 0.76 gm (91%).
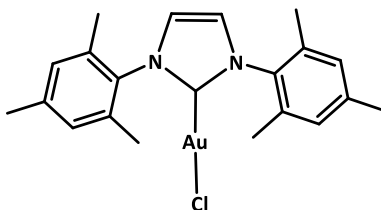
δ ^{1}H NMR (400 MHz, CH$_2$Cl$_2$-d_2) 7.16 (2 H, s), 7.07 (4 H, s), 2.38 (6 H, s), 2.12 (12 H, s) ppm. δ ^{13}C{^{1}H} NMR (101 MHz, CH$_2$Cl$_2$-d_2) 173.53, 140.54, 135.44, 135.27, 129.90 , 122.89 , 21.52, 18.08 ppm. δ ^{1}H NMR and δ ^{13}C{^{1}H} NMR (see Fig A.5 and Fig A.6)

2.2.7 Synthesis of Ph$_3$PAuCl

Ph$_3$PAuCl was prepared by slight modification of published procedures.[10,11] Au(tht)Cl (0.5 gm, 1.56 mmol) and Ph$_3$P (0.41 gm, 1.56 mmol) were weighed in air then placed under nitrogen. CH$_2$Cl$_2$ (50 mL) was purged under nitrogen gas and transferred via cannula to the mixture flask and the mixture was

stirred at room temperature for 30 min. The volume of the solution was reduced to 1 mL under vacuum and Et$_2$O was added (5 mL) resulting in the precipitation of the complex. The solid was collected by filtration, washed with Et$_2$O (5 mL) and dried under vacuum. Yield 0.69 gm (90%).
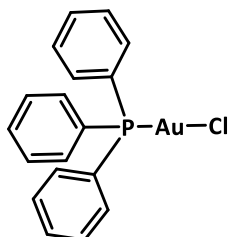
δ ^{1}H NMR (400 MHz, CH$_2$Cl$_2$-d_2) 7.47-7.59 (15 H, m) ppm. δ ^{31}P{^{1}H} NMR (162 MHz, CH$_2$Cl$_2$-d_2) 33.69 ppm. δ ^{1}H NMR and δ ^{31}P{^{1}H} NMR (see Fig A.7 and Fig A.8)

2.2.8. Synthesis of Et$_3$PAuCl

Et$_3$PAuCl was prepared by slight modification of published procedures.[12,13] Au(tht)Cl (0.5 gm, 1.56 mmol) was weighed in air then placed under nitrogen. Acetone (50 mL) was purged under nitrogen gas and transferred via cannula to the flask containing Au(tht)Cl. The solution was cooled to 0 °C and Et$_3$P (0.23 mL, 1.56 mmol) was added slowly using a glass syringe. The mixture was stirred for 60 min and allowed to come to room temperature. The solvent was removed under vacuum. CH$_2$Cl$_2$ (5 mL) was added and then the solution was filtered in air through a thin pad of silica and washed with 2 mL of CH$_2$Cl$_2$. The volume of the solution was reduced to 2 mL under vacuum, heptane (2 mL) was added, and left in an evaporating dish for 2-3 h to get white solid in heptane. The solid was collected by filtration, washed with pentane (5 mL) and dried under vacuum. Yield 0.42gm (76%).
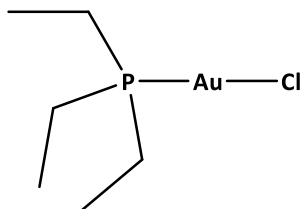
δ ^{1}H NMR (400 MHz, CH$_2$Cl$_2$-d_2) 1.85 (6 H, dq, J 10.4, 7.6), 1.19 (9 H, dt, J 18.9, 7.6) ppm. δ ^{31}P{^{1}H} NMR (162 MHz, CH$_2$Cl$_2$-d_2) 32.27 ppm. δ ^{1}H NMR and δ ^{31}P{^{1}H} NMR (see Fig A.9 and Fig A.10)

2.2.9. Synthesis of [C-1; [MoS$_4$(AuIPr)$_2$])

A solution of Au(IPr)Cl (0.31 gm, 0.50 mmol) in chloroform (10 mL) was added slowly to a solution of [Et$_4$N]$_2$[MoS$_4$] (0.12 gm, 0.25 mmol) in acetonitrile (7 mL). The mixture was heated under reflux (61℃) for 2 hours, and then all solvents were evaporated under reduced pressure. The solid was dissolved in diethyl ether and filtered through a thin layer of silica gel, the filtrate was dried under reduced pressure. The orange residue was recrystallized from diethyl ether-heptane (1:1) at room temperature in an open flask to yield red crystals (0.26 gm, 76%).
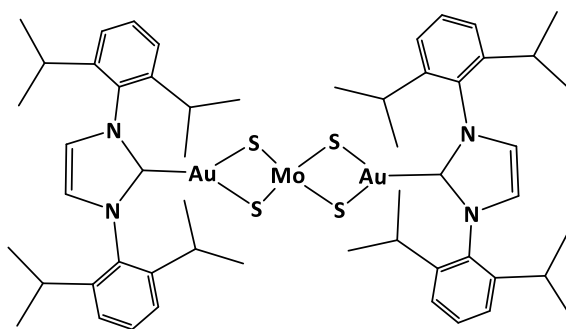
δ ^{1}H NMR (CH$_2$Cl$_2$-d_2, 400 MHz): 7.44 (4H, t, H$_{Ar}$), 7.44 (4H, s, H$_{imid}$), 7.25 (8H, d, H$_{Ar}$, J 7.8), 2.81 (8H, hept,H-CH_2), 1.21 (48 H, dd, J 6.8, 1.0, H-CH_3) ppm. δ ^{13}C{^{1}H} NMR (CH$_2$Cl$_2$-d_2, 100 MHz): 186.97 (2C, C$_{Au}$), 147.27, 135.69, 130.47, 124.30, 123.80, 29.26, 24.75, 23.77 ppm. δ ^{1}H NMR and δ ^{13}C{^{1}H} NMR (see Fig A.11 and Fig A.12). UV-vis. measurements of maximum wavelength (λ_{max}; nm) and extinction coefficient (ε; M^{-1} cm^{-1}) in acetonitrile were (270 , 290 , 357 , 491), (25k, 31k, 18k, 7k). UV-vis. measurements (see Fig B.3-6) and cyclic voltammetry (CV) measurements (see Fig B.23). SCXRD data (table C.1 and table C4). Anal. Calcd. for MoAu$_2$S$_4$N$_4$C$_{54}$H$_{72}$ (1395.31): C, 46.48; H, 5.20; N, 4.01. Found: C, 46.46; H, 5.10; N, 4.08. Elemental analysis report (Fig. D.2). ESI-MS in acetonitrile (positive ion mode): m/z1391.2966 ([M+H$^+$], calcd 1391.3072). ESI-MS measurements (Fig. D.4).

2.2.10. Synthesis of [C-2; [MoS$_4$(AuIBzMe)$_2$])

A solution of Au(IBeMe)Cl (0.24 gm, 0.60 mmol) in dichloromethane (20 mL) was added slowly to a solution of [Et$_4$N]$_2$[MoS$_4$] (0.15 gm, 0.30 mmol) in acetonitrile (10 mL). The mixture was allowed to stir at room temperature for 18 hours. The resulting dark red solid was isolated via vacuum filtration and washed with cold ethanol and Et$_2$O. The dark-orange residue was recrystallized from dichloromethane-heptane (1:1) at ambient temperature in an open flask to yield red crystals (0.13 gm, 44%).
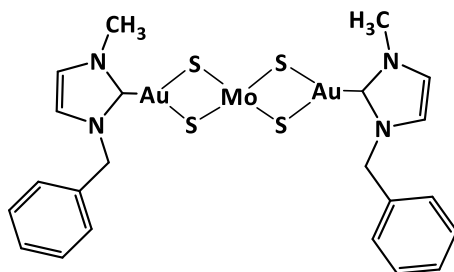
δ ^{1}H NMR (CH$_2$Cl$_2$-d_2, 400 MHz): 7.45 – 7.31 (m, 10H , H$_{Ar}$), 7.19 (4H,dd, H$_{imid}$, J 21.8, 1.9), 5.60 (4H, s, H$_{Ar}$), 4.04 (6H, s, H-CH_3) ppm. δ ^{13}C{^{1}H} NMR (CH$_2$Cl$_2$-d_2, 100 MHz): 181.05 (2C, C$_{Au}$), 136.51, 129.44, 128.94, 123.39, 121.44, 56.53, 40.04 ppm. δ ^{1}H NMR and δ ^{13}C{^{1}H} NMR (see Fig A.13 and Fig A.14). UV-vis. measurements of maximum wavelength (λ_{max} ; nm) and extinction coefficient (ε; M^{-1} cm^{-1}) in acetonitrile were (288 , 354 , 491), (25k, 14k,5k). UV-vis. measurements (see Fig B.7-10) and cyclic voltammetry (CV) measurements (see Fig B.24). SCXRD data (table C.2 and table C5). Anal. Calcd. for MoAu$_2$S$_4$N$_4$C$_{22}$H$_{24}$ (962.58): C, 27.45; H, 2.51; N, 5.82. Found: C, 27.39; H, 2.53; N, 5.77. Elemental analysis report (Fig. D.2). ESI-MS in acetonitrile (positive ion mode): *m/z* 958.9260 ([M+H$^+$], calcd 958.9295). ESI-MS measurements (Fig. D.5).

2.2.11. Synthesis of [C-3; [MoS$_4$(AuIMes)$_2$])

A solution of Au(IMes)Cl (0.27gm, 0.50 mmol) in chloroform (12 mL) was added slowly to a solution of [Et$_4$N]$_2$[MoS$_4$] (0.12 gm, 0.25 mmol) in acetonitrile (7 mL). The mixture was heated under reflux (61°C) for 4 hours, and then all solvents were evaporated under reduced pressure. The orange solid was

dissolved in dichloromethane and filtered through a thin layer of silica gel (standard grade 60 A), the filtrate was dried under reduced pressure. The orange residue was crystallized by dissolving it in a hot ethanol 65 °C and let the temperature goes down slowly to yield red crystals (0.23 gm, 75%).
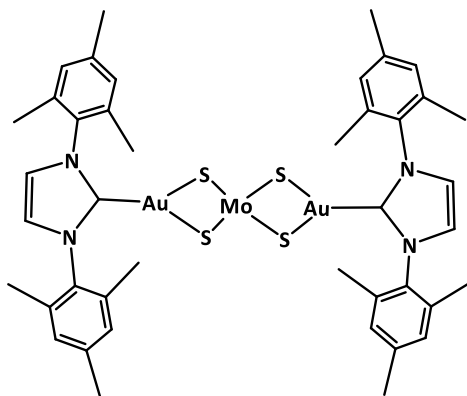
δ ^{1}H NMR (CH$_2$Cl$_2$-d_2, 400 MHz): 7.34 (4H, s, H$_{imid}$), 6.98 (8H, s, H$_{Ar}$), 2.30 (12H, s, H-CH_3), 2.21 (24H, s, H-CH_3) ppm. δ ^{13}C{^{1}H} NMR (CH$_2$Cl$_2$-d_2, 100 MHz): 183.48 (2C, C$_{Au}$), 140.06, 135.91, 135.76, 129.63, 123.04, 21.49, 18.35 ppm. δ ^{1}H NMR and δ ^{13}C{^{1}H} NMR (see Fig A.15 and Fig A.16). UV-vis. measurements of maximum wavelength (λ_{max}; nm) and extinction coefficient (ε; M^{-1} cm^{-1}) in acetonitrile were (265 , 290 , 359 , 491), (25k, 25k, 16k,5k). UV-vis. measurements (see Fig B.11-15) and cyclic voltammetry (CV) measurements (see Fig B.25). SCXRD data (table C.3 and table C6). Anal. Calcd. for MoAu$_2$S$_4$N$_4$C$_{42}$H$_{48}$ (1226.99): C, 41.11; H, 3.94; N, 4.57. Found: C, 41.34; H, 4.11; N, 4.91. Elemental analysis report (Fig. D.1). ESI-MS in acetonitrile (positive ion mode): m/z 1223.1176 ([M+H$^+$], calcd 1223.1225). ESI-MS measurements (Fig. D.6).

2.2.12. Synthesis of (C-4; [MoS$_4$(Au PPh$_3$)$_2$])

Synthesis of **C-4** was first reported by Garne et al.[2] In my work, the reported procedure was modified to improve the purity and eliminating the unnecessary steps like conducting the synthesis in air instead of under nitrogen. A solution of Ph$_3$PAuCl (0.65 gm, 1.31 mmol) in CH$_2$Cl$_2$ (30 mL) was added slowly to a solution of [Et$_4$N]$_2$[MoS$_4$] (0.32 gm, 0.66 mmol) in acetonitrile (12 mL). The mixture was

stirred at room temperature for 20 h, and then all solvents were evaporated under reduced pressure.

The solid was dissolved in CH_2Cl_2 (20 mL) and filtered through a thin layer of silica gel and added 4 mL of

CH_2Cl_2 to wash the silica pad. The volume of the filtered solution reduced to 10 mL and heptane (2 mL)

was added and leave the solution in unsealed round-bottom flask for 10-12 h to get orange crystals in

heptane. The crystals were collected by filtering the solution, washing with pentane (5 mL) and

removing the pentane contamination under vacuum. The yield of the orange crystals of **C-4** was 0.65

gm (87%).
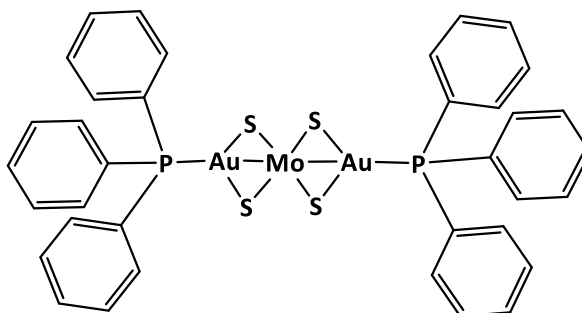
δ ^{1}H NMR (400 MHz, CH_2Cl_2-*d_2*) 7.83-7.78 (12 H, dd, J 13.3, 7.2), 7.59 – 7.50 (18 H, m) ppm. δ [31]P{[1]H}

NMR (162 MHz, CH_2Cl_2-*d_2*) 42.59 ppm. δ ^{1}H NMR and δ ^{31}P{^{1}H} NMR (see Fig A.17 and Fig A.18). UV-vis.

measurements of maximum wavelength (λ_{max} ; nm) and extinction coefficient (ε; M^{-1} cm^{-1}) in

dichloromethane were (312 , 489), (40k, 7k). UV-vis. measurements (see Fig B.16-18) and cyclic

voltammetry (CV) measurements (see Fig B.26). Anal. Calcd. for $Mo_1Au_2S_4P_2C_{36}H_{30}$ (1142.70): C, 37.84; H,

2.65. Found: C, 37.91; H, 2.86. Elemental analysis report (Fig. D.1). ESI-MS in acetonitrile (positive ion

mode): *m/z* 1138.9188 ([M+H^{+}], calcd 1138.9242). ESI-MS measurements (Fig. D.7).

2.2.13. Synthesis of (C-5; [MoS₄(AuPEt₃)₂])

Synthesis of **C-5** was first reported by Kinsch and Stephan.[1] The synthesis presented in this study

was achieved by mixing a solution of Et_3PAuCl (0.38 gm, 1.08 mmol) in EtOH (60 mL) with a solution of

[Et_4N]₂[MoS_4] (0.26 gm, 0.05 mmol) in acetonitrile (10 mL). The mixture was stirred at room

temperature for 16 h, and then all solvents were evaporated under reduced pressure. The solid was dissolved in CH_2Cl_2 (20 mL) and filtered through a thin layer of silica gel and added 4 mL of CH_2Cl_2 to wash the silica pad. The solvent was evaporated under reduced pressure. CH_3CN (5 mL) was added after dissolving all the orange solid, Et_2O (15 mL) was added. The crystal was grown by saving the solution at -10 °C for 24 h. The crystals were collected by filtering the solution, washing with Et_2O (5 mL) and removing the solvent contamination under vacuum. The yield of the orange crystals of **C-5** was 0.23 gm (50%).
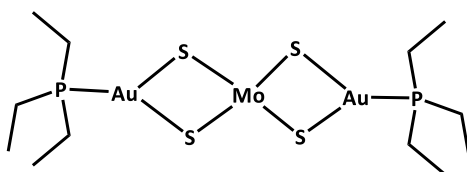
δ ^{1}H NMR (400 MHz, CH_2Cl_2-d_2) 2.09 (12 H, dq, J 10.1, 7.6), 1.36 (18 H, dt, J 19.1, 7.6) ppm. δ ^{31}P{^{1}H} NMR (162 MHz, CH_2Cl_2-d_2) 41.20 ppm. δ ^{1}H NMR and δ ^{31}P{^{1}H} NMR (see Fig A.19 and Fig A.20). UV-vis. measurements of maximum wavelength (λ_{max}; nm) and extinction coefficient (ε; M^{-1} cm^{-1}) in acetonitrile were (232 , 303 , 487), (22k, 26k, 5k). UV-vis. measurements (see Fig B.19-22) and cyclic voltammetry (CV) measurements (see Fig B.27). Anal. Calcd. for $Mo_1Au_2S_4P_2C_{12}H_{30}$ (854.45): C, 16.87; H, 3.54. Found: C, 16.96; H, 3.57. Elemental analysis report (Fig. D.3). ESI-MS has not measrured.

2.3 Results and discussion

The cluster complexes **C-1**, **C-2** and **C-3** were synthesized by mixing one equivalent of [Et_4N]$_2$[$MoS4_4$] with two equivalents of the appropriate Au(NHC)Cl complex as shown in Scheme 2.2. The clusters **C-4** and **C-5**, which were previously reported (Garne et al., Kinsch and Stephan, respectively) were prepared in a similar fashion by mixing one equivalent of [Et_4N]$_2$[$MoS4_4$] with two equivalents of the corresponding R_3PAuCl. The Au(NHC)Cl and R_3PAuCl complexes were synthesized from Au(tht)Cl as

described in Experimental section 2.2.2. All complexes which were previously reported were characterized by ^{1}H, ^{13}C, and ^{31}P NMR and the data matched literature values.

2.3.1. Elemental analyses (CHN) and mass spectrometry data

Complexes **C-1** – **C-5** were sent to Galbraith Laboratories, Inc., Knoxville, Tennessee, USA for the elemental analysis, and to Professor Touradj Solouki's lab in Baylor University for nano-electrospray ionization-mass spectrometry (ESI-MS). Elemental analysis reports of **C-1**, **C-2** and **C-3** as well as mass spectrometry of **C-1**, **C-2**, **C-3** and **C-4** are collected in Appendix D. The elemental analysis data are summarized in Table 2.1 and confirm the bulk purity of the cluster complexes **C-1** – **C-5**.

Table 2.1. Elemental analysis summary of the new clusters.

Analysis	Carbon %			Hydrogen %			Nitrogen %		
	Calc.	Expt.	|Δ|	Calc.	Expt.	|Δ|	Calc.	Expt.	|Δ|
C-1	46.48	46.46	0.02	5.20	5.10	0.10	4.01	4.08	0.07
C-2	27.45	27.39	0.06	2.51	2.53	0.02	5.82	5.77	0.05
C-3	41.11	41.34	0.23	3.94	4.11	0.17	4.57	4.91	0.34
C-4	37.84	37.91	0.07	2.65	2.86	0.21	---	---	---
C-5	16.87	16.96	0.09	3.54	3.57	0.03	---	---	---

|Δ|: absolute vale | calc. – expt|

Isotopic patterns of **C-1**, **C-2**, **C-3** and **C-4**   were confirmed by comparing their theoretically calculated isotopic patterns (red dots in Figure 2.1) with their experimentally observed isotopic patterns in broadband MS data acquisition mode. Exact masses and relative abundances were calculated using the IonSpec Exact Mass Calculator; theoretically calculated isotopic patterns (red dots) were overlaid on the experimentally acquired mass spectra (Figure 2.1). Each of the gold-molybdenum clusters exhibited unique isotopic patterns with relative abundances that are characteristic for molybdenum-containing complexes (Appendix D, Fig. D.4-7).

$^{92}Mo^{197}Au_2{}^{32}S_4{}^{14}N_4{}^{12}C_{54}{}^{1}H_{72}$

Measured: 1391.2966 *m/z*
Theoretical: 1391.3072 *m/z*
MMA: 7.6187 ppm
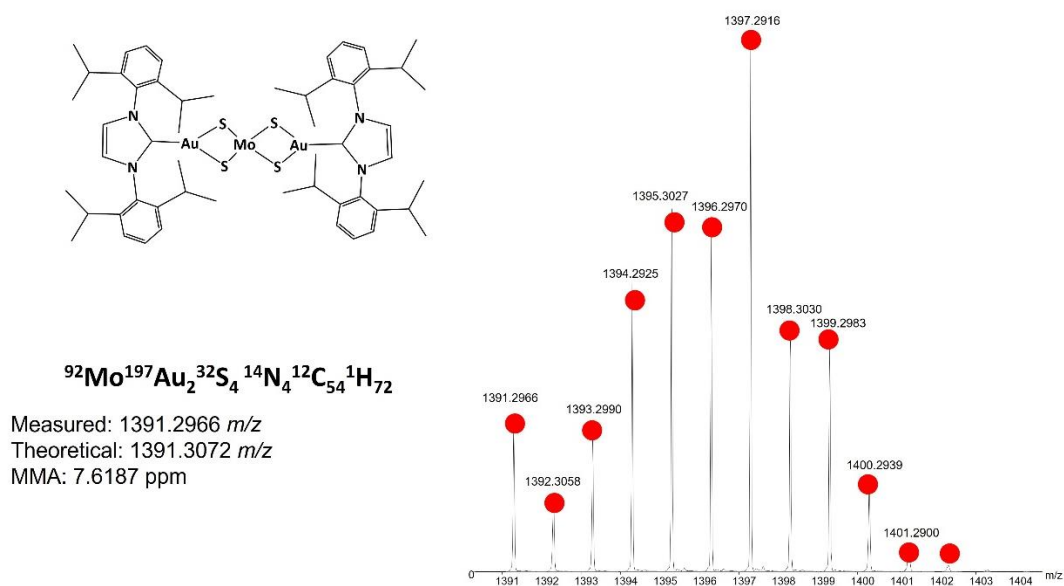
Figure 2.1. ESI-MS in acetonitrile (positive ion mode) of **C-1**; corresponding theoretically calculated isotopic patterns are indicated with red dots. MMA: mass measurement accuracy values for [M+H]$^+$.

2.3.2. NMR data

The ^{1}H and $^{13}C\{^{1}H\}$ NMR data for **C-1**, **C-2** and **C-3** are summarized in Table 2.2, where chemical shifts for each cluster are compared to the corresponding Au(NHC)Cl monomers. Scheme 2.3 illustrates the labels for ^{1}H, ^{13}C nuclei assignments in Table 2.2.

In general, the imidazole protons (H$_{imid}$) in clusters show slight downfield shifts in comparison with the precursor Au(NHC)Cl complexes. The carbon atom coordinated to Au (C$_{Au}$) in the clusters experiences an approximate 10 ppm downfield shift relative to the Au(NHC)Cl precursors.
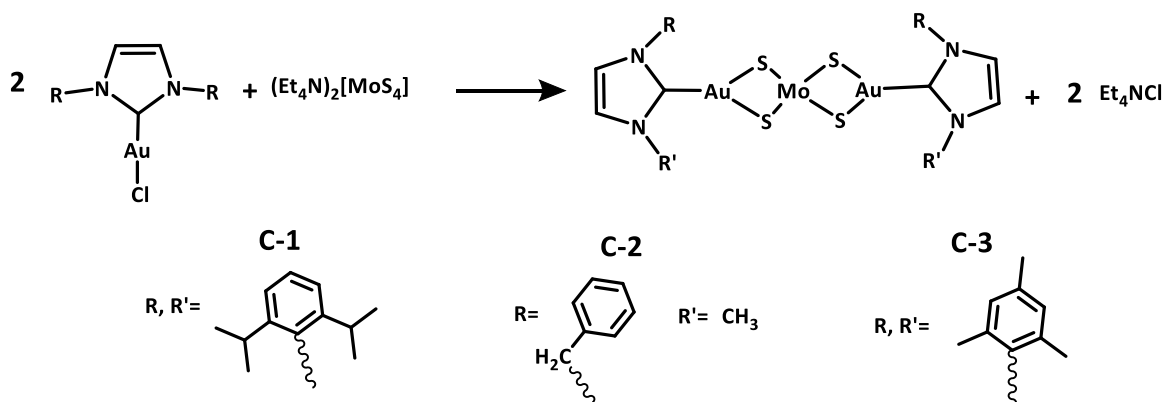
Scheme 2.2. The synthesis of **C-1**, **C-2** and **C-3**.

The solution stability of all the gold (I) compounds was assessed by ^{1}H NMR. The results show that all the compounds [except Au(tht)Cl] are stable in solution for at least 24 hours. The five cluster complexes **C-1** to **C-5** were stable in CH_2Cl_2-d_2 for at least 72 hours. It is noteworthy that solutions of **C-1** in CH_2Cl_2/Et_2O and **C-3** in $CH_2Cl_2/Et_2O/Et_2OH$ that were prepared for growing crystals, were stable at 4-6 °C for several years.

The clusters **C-1** and **C-3** have symmetrically substituted NHC ligands whereas **C-2** has asymmetrical NHC ligands. In the single crystal X-ray structure of **C-2**, the benzyl substitutes are on the same side (syn). We were interested to know whether conformers could be detected in solution. Further investigations were done on **C-2** by the variable temperature ^{1}H NMR and DOSY ^{1}H NMR.
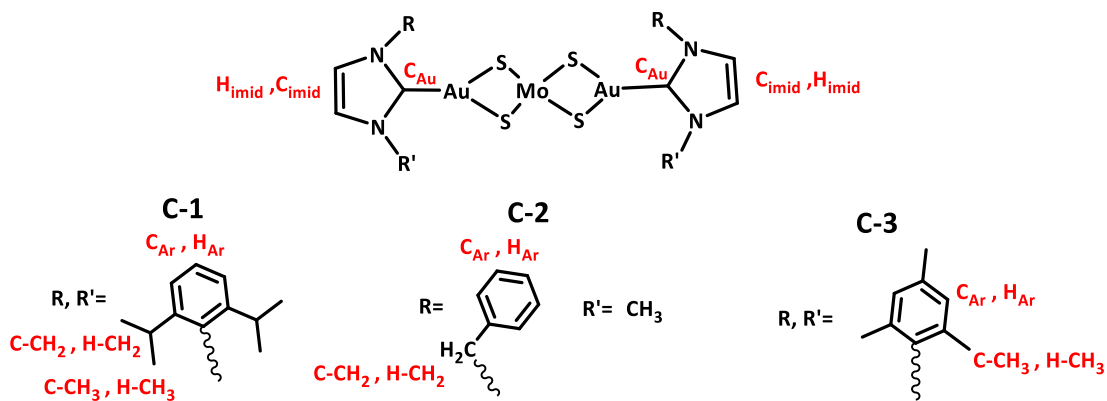
Scheme 2.3. Labels for ^{1}H, ^{13}C NMR data.

48

Table 2.2. Summary of ^1H NMR and $^{13}C\{^1H\}$ NMR chemical shifts (ppm) of **C-1**, **C-2** and **C-3** vs their Au(I) precursors in CH_2Cl_2-d_2.

Entry	NMR	C-1	Au(IPr)Cl	C-2	Au(IBzMe)Cl	C-3	Au(IMes)Cl
H$_{Ar}$	^1H NMR	(7.5-7.4), 7.3, 7.2	(7-6-7.5), (7.4-7.3)	(7.4-7.3)	(7.4-7.3)	7.0	7.1
H$_{imid}$	^1H NMR	7.4	7.2	7.2, 7.1	7.0, 6.9	7.3	7.2
H-CH_2	^1H NMR	(2.9-2.8)	(2.6-2.5)	5.6	5.4	---	---
H-CH$_3$	^1H NMR	1.2, 1.2	1.3, 1.2	4.0	3.8	2.3, 2.2	2.4, 2.1
C$_{Au}$	$^{13}C\{^1H\}$ NMR	187.0	175.6	181.1	172.0	183.5	173.5
C$_{Ar+imid}$	$^{13}C\{^1H\}$ NMR	147.3, 135.7, 130.5, 124.3, 123.8	146.3, 134.6, 131.3, 124.6, 123.9	136.5, 129.4, 128.9, 128,9, 123.4, 121.4	136.1, 129.5, 129.1, 128.5, 122.9, 121.1	140.1, 135.9, 135.8, 129.6, 123.0	140.5, 135.4, 135.3, 129.9, 122.9
C-CH_2+CH_3	$^{13}C\{^1H\}$ NMR	29.3, 24.7, 23.8	29.4, 24.7, 24.2	56.5, 40.0	55.4, 38.8	21.5, 18.4	21,5, 18.1

Bertrand, et al. studied NHC-phosphinidene bond rotation (Scheme 2.4) by variable temperature (VT) NMR. Adducts bearing unsaturated NHC backbones showed free rotation around the C-P bond at room temperature while saturated NHC's did not, revealing a greater degree of double-bond character between phosphorus and the saturated NHC.[14] VT ^1H NMR spectroscopy in CH_2Cl_2-d_2 was used to investigate the dynamic rotation of the Au-C bond in **C-2** at (20, 0, -20, -70 °C). Metal carbon bonds in NHC carbene complexes are described in the literature as single or double bonds. The greater the double bond character in the Au-C bond, the more restricted the rotation. If there is a barrier to rotation, we might expect to see separate peaks for syn and anti-conformers of **C-2** at lower temperatures. Alternatively, we would expect fast rotation for Au-C single bond. Fast rotation results in the observed signal being an average of all species present in solution i.e., signals for separate conformers would not be detected.[15] Another possibility is that there is a Au-C double bond with a significant barrier to rotation resulting in only one conformer in solution.
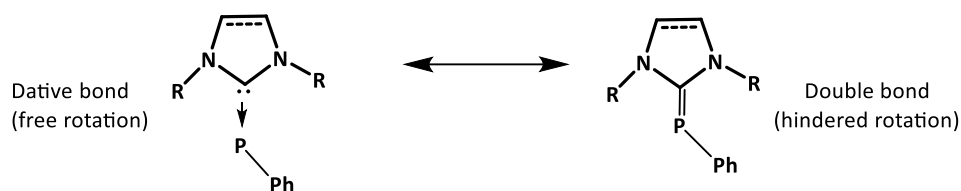
Scheme 2.4. Bonding effect on the rotation of NHC-phosphinidene adducts.

The VT ^{1}H NMR spectra for **C-2** in CH$_2$Cl$_2$-d_2 are identical from 20°C to -70°C (Figure 2.2). This suggests that the barrier for rotation of the Au-C$_{(NHC)}$ bond is low and the conformers interconvert rapidly on the NMR timescale Baker, et. al. studied [Au(NHC)$_2$]$^+$ complexes by VT ^{1}H NMR and they found that the Au-C$_{(NHC)}$ rotation was fast on the NMR timescale (at -60°C).[16] In practice, Au-C$_{(NHC)}$ bond coordination is generally drawn as a single bond rather than a double bond, with π contributions being restricted to delocalization within the NHC ring.[16,17] This representation best reflects the experimentally observed potential for rotation about the Au-C$_{(NHC)}$ bond in **C-2** and emphasizes the differences between NHCs and conventional Fischer or Schrock carbene ligands.[17]
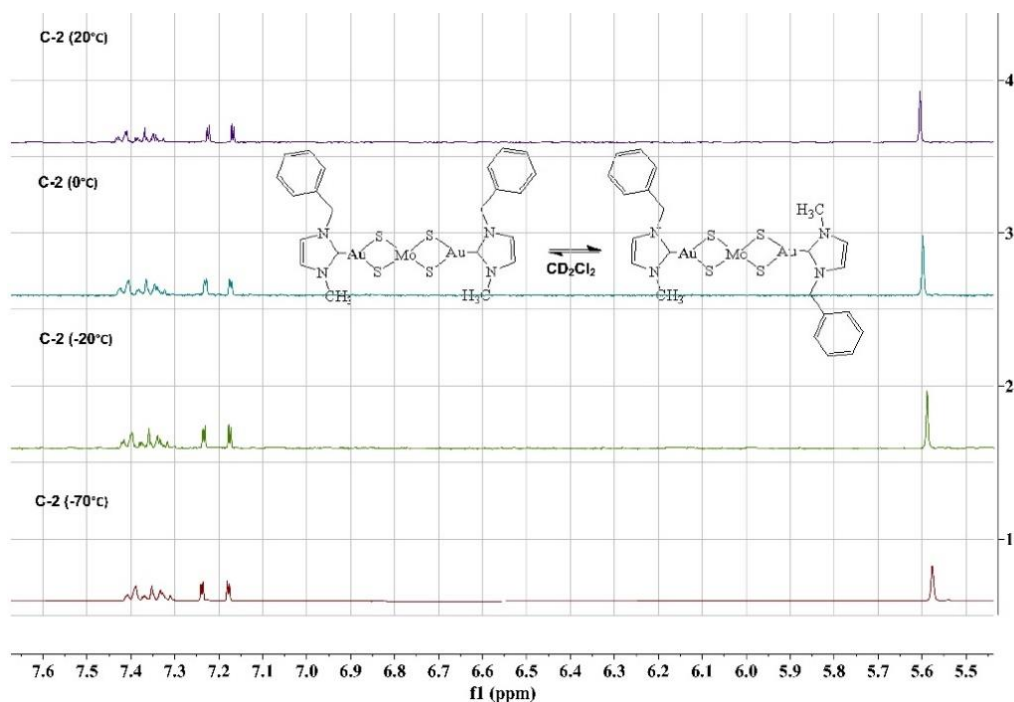
Figure 2.2. VT ^{1}H NMR of **C-2** in CH$_2$Cl$_2$-d_2**.**

Another NMR technique that can be used to assess the possibility of two conformers in solution is diffusion ordered spectroscopy (DOSY). DOSY has been used to characterize two structural isomers that have different shapes but identical mass fragmentation patterns.[18,19] It turns out that spherical molecules diffuse faster than ellipsoidal ones. This difference in diffusion coefficient is tentatively explained by microfriction effects of the solvent.[20–22] DOSY ^{1}H NMR data of **C-2** showed only one species in solution; i.e. there was no evidence for conformational isomers (Figure 2.3). The measured diffusion coefficient of **C-2** at 23°C in CH_2Cl_2-d_2 was 8.5×10^{-10} m^2/s, SD= ± 5×10^{-12}.
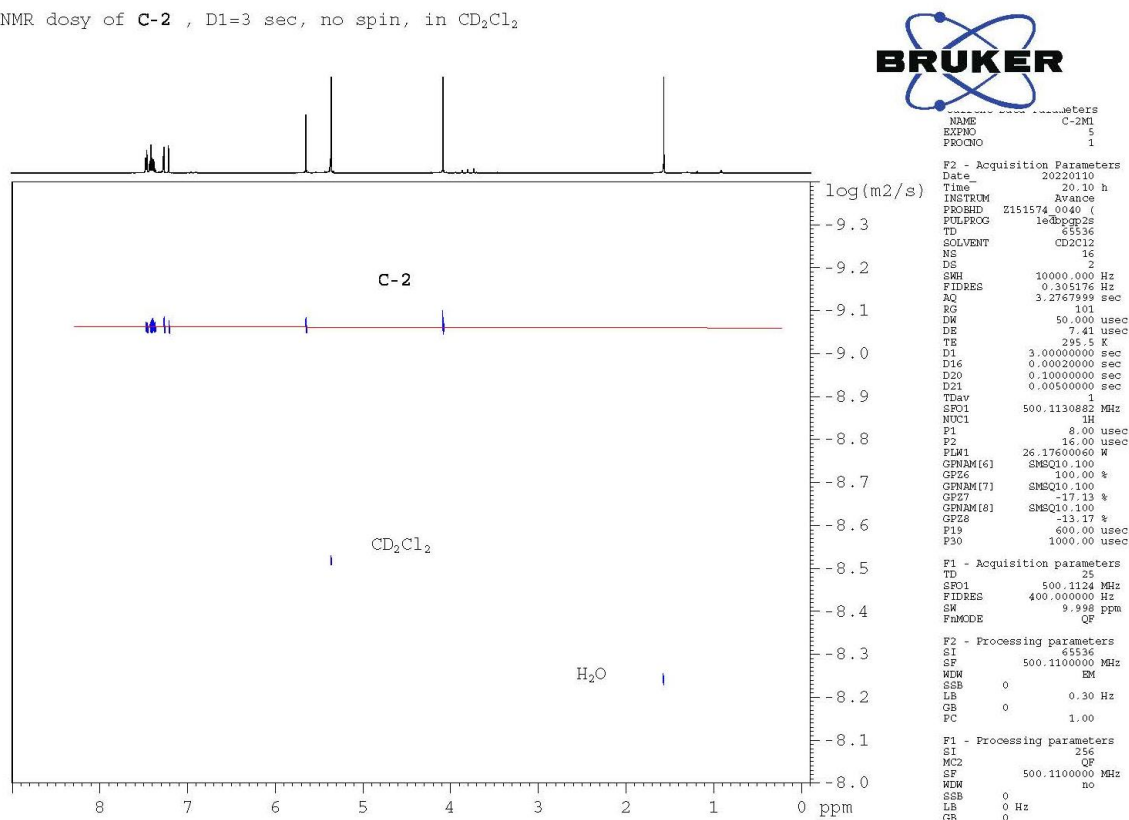
X axis represents ^{1}H NMR chemical shift in (ppm), Y axis represents the log of diffusion coefficient (m^2/s), SD calculated from the average of diffusion coefficient for each peak in **C-2** (Fig.A. 21)

Figure 2.3. DOSY ^{1}H NMR data of **C-2**.

2.3.3. UV-vis data

The UV-vis spectroscopy data for the clusters and [Et$_4$N]$_2$[MoS$_4$] are summarized in Table 2.3. All complexes are in acetonitrile solution except for **C-4** which is in dichloromethane because it is not soluble in acetonitrile. Figure 2.4 illustrates the spectrum of one cluster, **C-1** in acetonitrile to [Et$_4$N]$_2$[MoS$_4$]. All the Au(NHC)Cl and Ph$_3$PAuCl complexes have no absorption bands in the visible. Therefore, the visible absorbance of the clusters is primarily due to the MoS$_4^{2-}$ unit, which is perturbed by bonding to Au(I)-L. Müller, et al. assigned the visible bands in MoS$_4^{2-}$ complexes as primarily sulfur to metal charge transfer in character.[23,24] The assignments for the clusters will be discussed in Chapter 3 where the results of a TDDFT calculation on **C-1** will be described in detail.
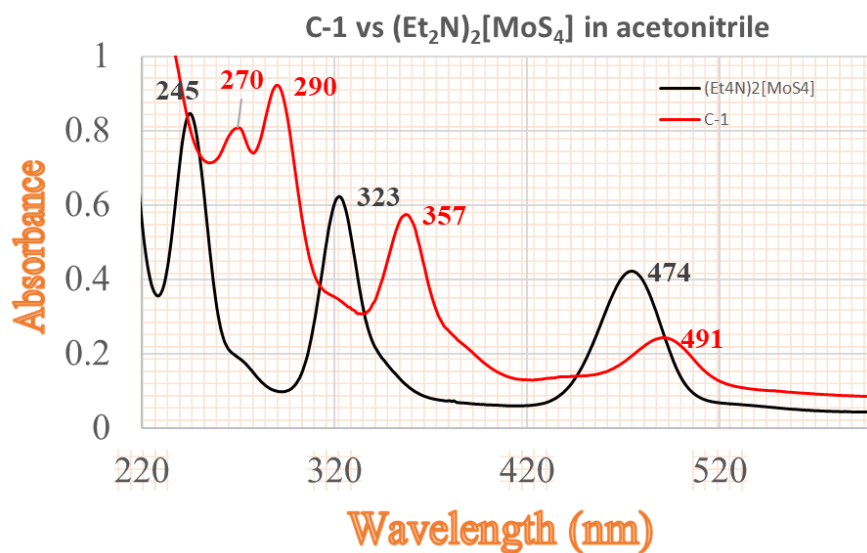
Figure 2.4. UV-vis. Scan of **C-1** vs [Et$_4$N]$_2$[MoS$_4$] in acetonitrile.

Table 2.3. UV-vis spectroscopy summary of all the clusters and **(Et$_4$N)$_2$[MoS$_4$]**.

Complex (solvent)	λ_{max} (nm)/ ε (M^{-1}Cm^{-1})*
C-1 (CH$_3$CN)	270 (25 x10^3), 290 (31 x10^3), 357 (19 x10^3), 491 (7 x10^3)
C-2 (CH$_3$CN)	288 (25 x10^3), 354 (14 x10^3), 491 (5 x10^3)
C-3 (CH$_3$CN)	265 (25 x10^3), 290 (25 x10^3), 359 (16x10^3), 491 (5 x10^3)
C-4 (CH$_2$Cl$_2$)	312 (40 x10^3), 489 (7 x10^3)
C-5 (CH$_3$CN)	232 (22 x10^3), 303 (27 x10^3), 487 (5 x10^3)
(Et$_4$N)$_2$[MoS$_4$] (CH$_3$CN)	245 (24 x10^3), 323 (17 x10^3), 474 (12-13 x10^3)

- **ε** represents extinction coefficient, **λ_{max}** represents wavelength at strongest photon absorption. Only **ε** of (Et$_4$N)$_2$[MoS$_4$] was taken from the literatures[24,25]

2.3.4. Cyclic Voltammetry (CV) data

Cyclic voltammetry experiments were conducted in acetonitrile solution, except for **C-2** and **C-4**, which were done in dichloromethane. The potential range was 0 to 2 V vs SCE   for   experiments.   The cyclic voltammetry measurements of all the L-Au(I)Cl indicate that there are no oxidations in this range. In contrast, all the clusters show irreversible oxidation peaks as summarized in Table 2.4. Moreover, [MoS$_4$]$^{2-}$ showed irreversible oxidation peaks at 0.24 and 1.38 V vs SCE. The irreversible oxidation peak at 0.24V could be considered as the oxidation of [MoS$_4$]$^{2-}$ to [MoS$_4$]$^-$. The irreversible oxidation peak at 1.38 V could be considered as the oxidation of [MoS$_4$]$^-$ to [MoS$_3$] consistent with appearance of a dark brown deposit on the electrode surface. This is similar to what G. Laperriere, et al. found for the aqueous oxidation of (NH$_4$)$_2$[MoS$_4$] to [MoS$_3$].[26] On the other hand, all the clusters showed the first oxidation peaks at higher potentials than the first oxidation peak of [MoS$_4$]$^{2-}$ consistent with removing an electron from anionic complex ([MoS$_4$]$^{2-}$) being easier than removing an electron from a neutral

cluster. The second oxidation peak of **C-1**, **C-3** and **C-5** could be assigned as Au(I)/Au(III) or some rearrangement that occurs after the first oxidation. Complete assignments of the CV 's was not conducted in this thesis.

Table 2.4. Summary of the CV oxidation potentials of **C-1** – **C-5** and $[Et_4N]_2[MoS_4]$.

Complex	E_{ox} vs (SCE)
C-1	0.98 **,** 1.57 (V) (CH$_3$CN)
C-2	0.71 (V) (CH$_2$Cl$_2$)
C-3	0.97 **,** 1.54 (V) (CH$_3$CN)
C-4	0.96 (V) (CH$_2$Cl$_2$)
C-5	0.74 **,** 1.65 (V) (CH$_3$CN)
(Et$_4$N)$_2$[MoS$_4$]	0.24 **,** 1.38 (V) (CH$_3$CN)

0.1M TBAH, 1.5mM complex,   Pt, 100 mV/s scan rate.

2.3.5. Single crystal x-ray diffraction (SCXRD) data

All the crystals of **C-1**, **C-2** and **C-3** were orange-red in color and were obtained as described in the experimental section. The crystals showed good stability in the mother liquor for over a year. However, cracks were observed when the crystals were removed from the crystallization solution. The cracking of the crystals had a negative impact on the SCXRD quality and it was not possible to solve the data for any logical structure. Immersing the crystals into a protective oil directly after taking them from the solution helped to slow down the cracking process. It was possible to collect the data within the X-ray measurement timeframe by using the oil technique. The diffraction data were collected and refined as mentioned in the experimental section. All the .cif files have been checked and analyzed by the International Union of Crystallography (https://checkcif.iucr.org/) and the detailed reports are attached at the end of Appendix D. The single crystal structure and the unit cell packing of each cluster are shown in Figures 2.3, 2.4, and 2.5. The summary of the selected bonds distance and angles are shown in Figures

2.6, 2.7, and 2.8. The Au-C(NHC) distances are 1.992(8) Å in **C-1** (IPr), 2.019(6) and 2.023(6) Å in **C-2** (IBzMe), and 2.013(18), 2.015(18) Å in **C-3** (IMes). These Au-C bond distances are similar to other reported Au-C(NHC) distances of (Au-IPr: 1.942(3), Au-IBzMe: 2.026(3), Au-IMes: 1.998(5) Å) in the compounds (NHC)AuX where X= Cl, CF$_3$.[27,28]
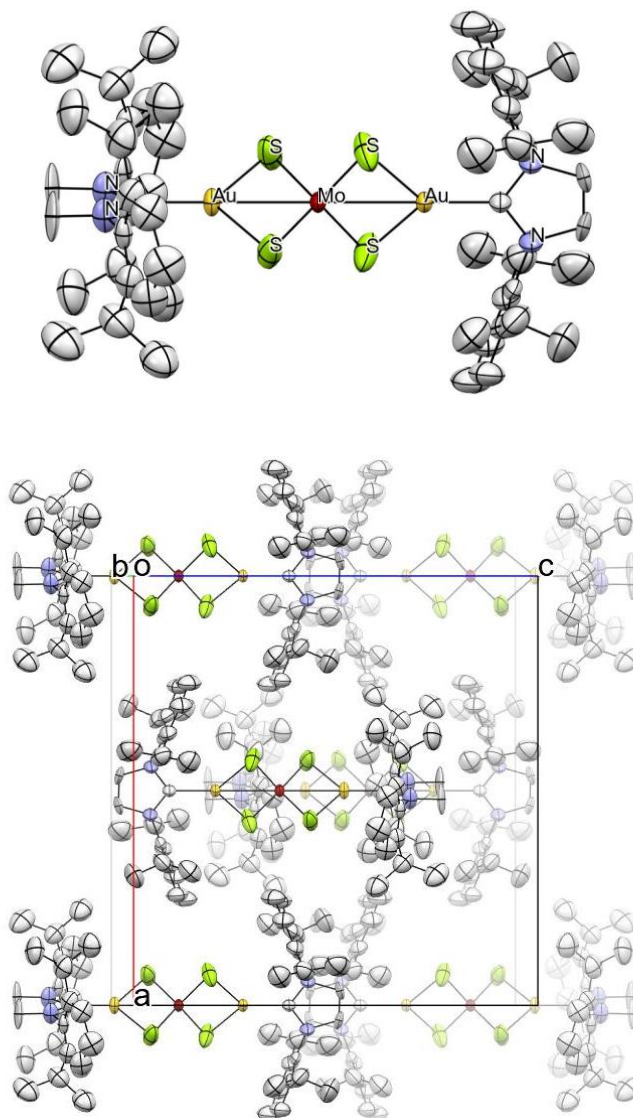
Figure 2.5. Hydrogen atoms are omitted, (top)Model molecular structure of **C-1** (ORTEP), (bottom) Packing model of **C-1** in the unit cell (ORTEP, depth cue was used to get better visualization of the packed molecules).
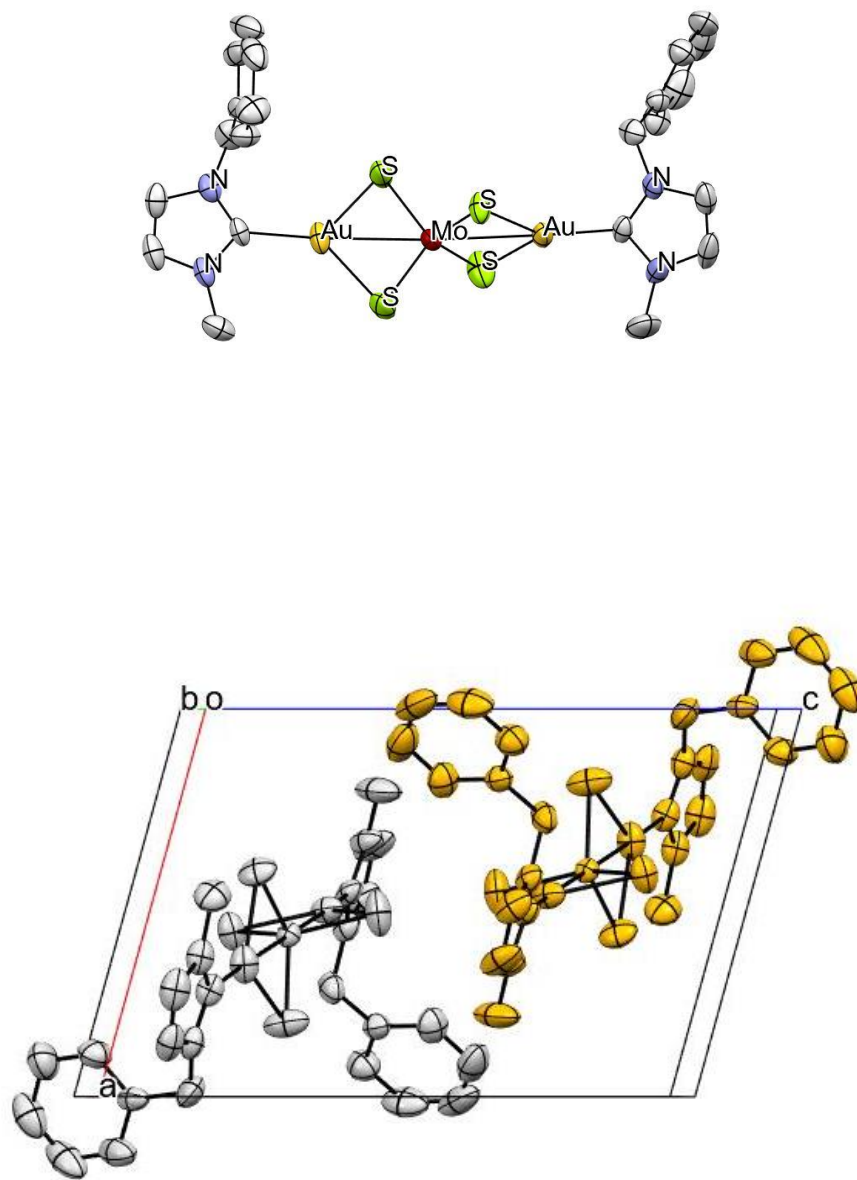
Figure 2.6. Hydrogen atoms are omitted, (top)Model molecular structure of **C-2** (ORTEP), (bottom) Packing model of **C-2** in the unit cell (ORTEP, color by symmetry operation was used to get better visualization of the packed molecules).
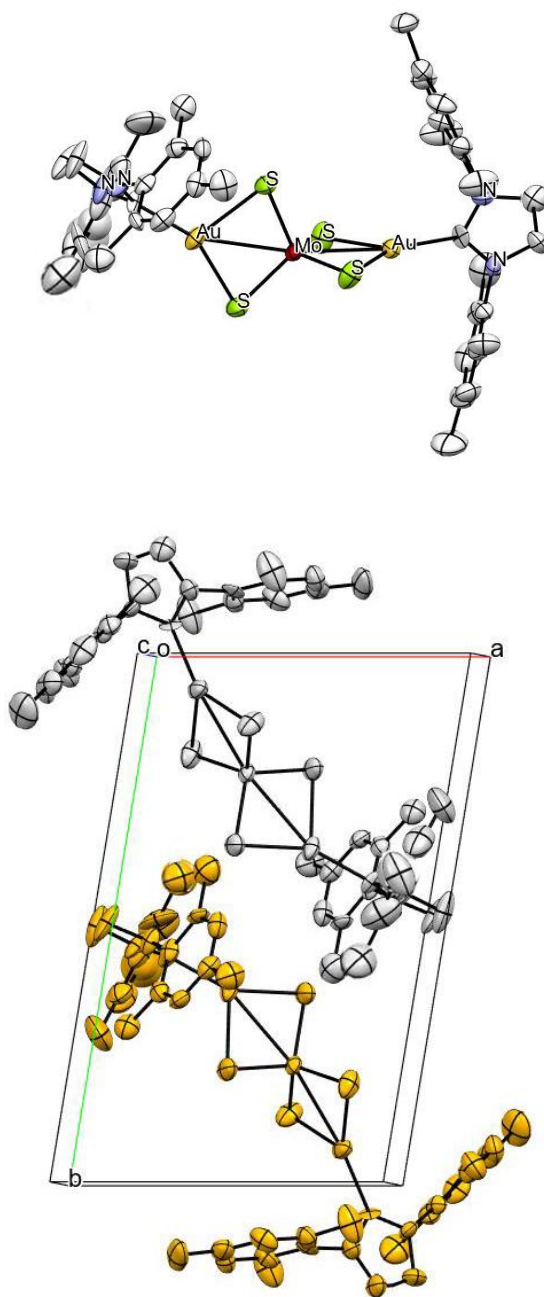
Figure 2.7. Hydrogen atoms are omitted, (top)Model molecular structure of **C-3** (ORTEP), (bottom) Packing model of **C-3** in the unit cell (ORTEP, color by symmetry operation was used to get better visualization of the packed molecules).
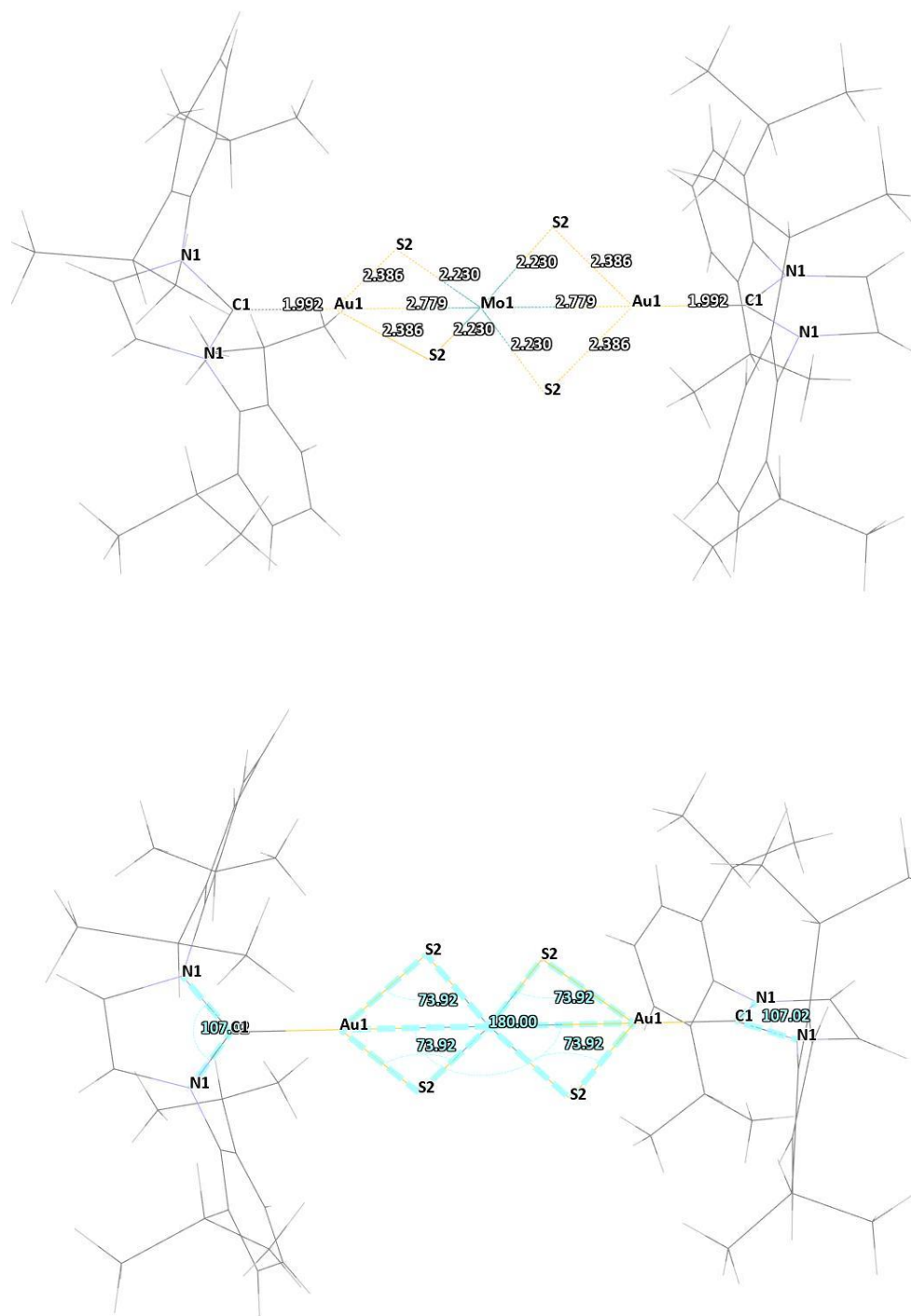
Figure 2.8. Hydrogen atoms are omitted, Wireframe model molecular structure of **C-1** (top) shows selected bond distances, (bottom) shows selected angles.
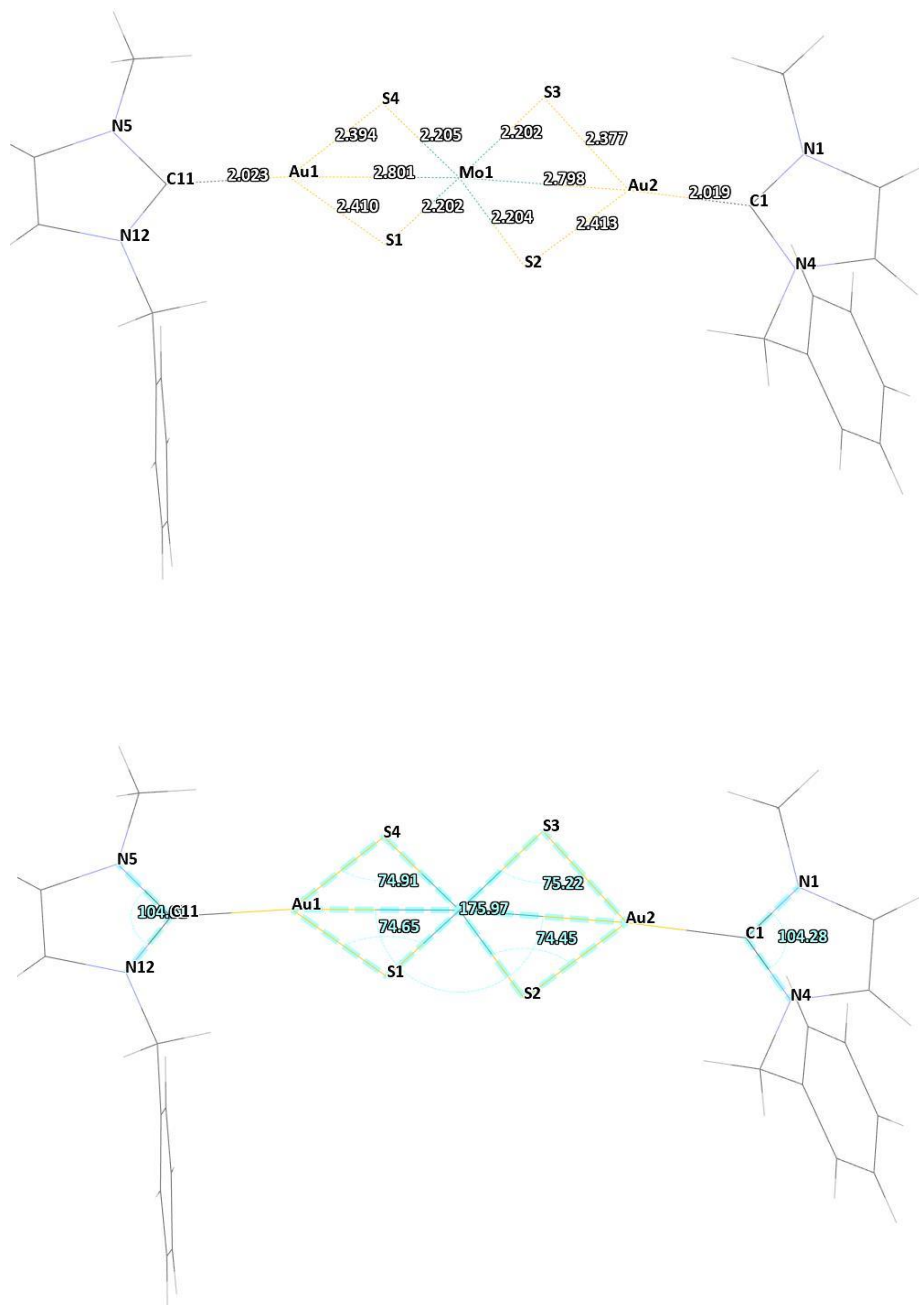
Figure 2.9. Hydrogen atoms are omitted, Wireframe model molecular structure of **C-2** (top) shows selected bond distances, (bottom) shows selected angles.
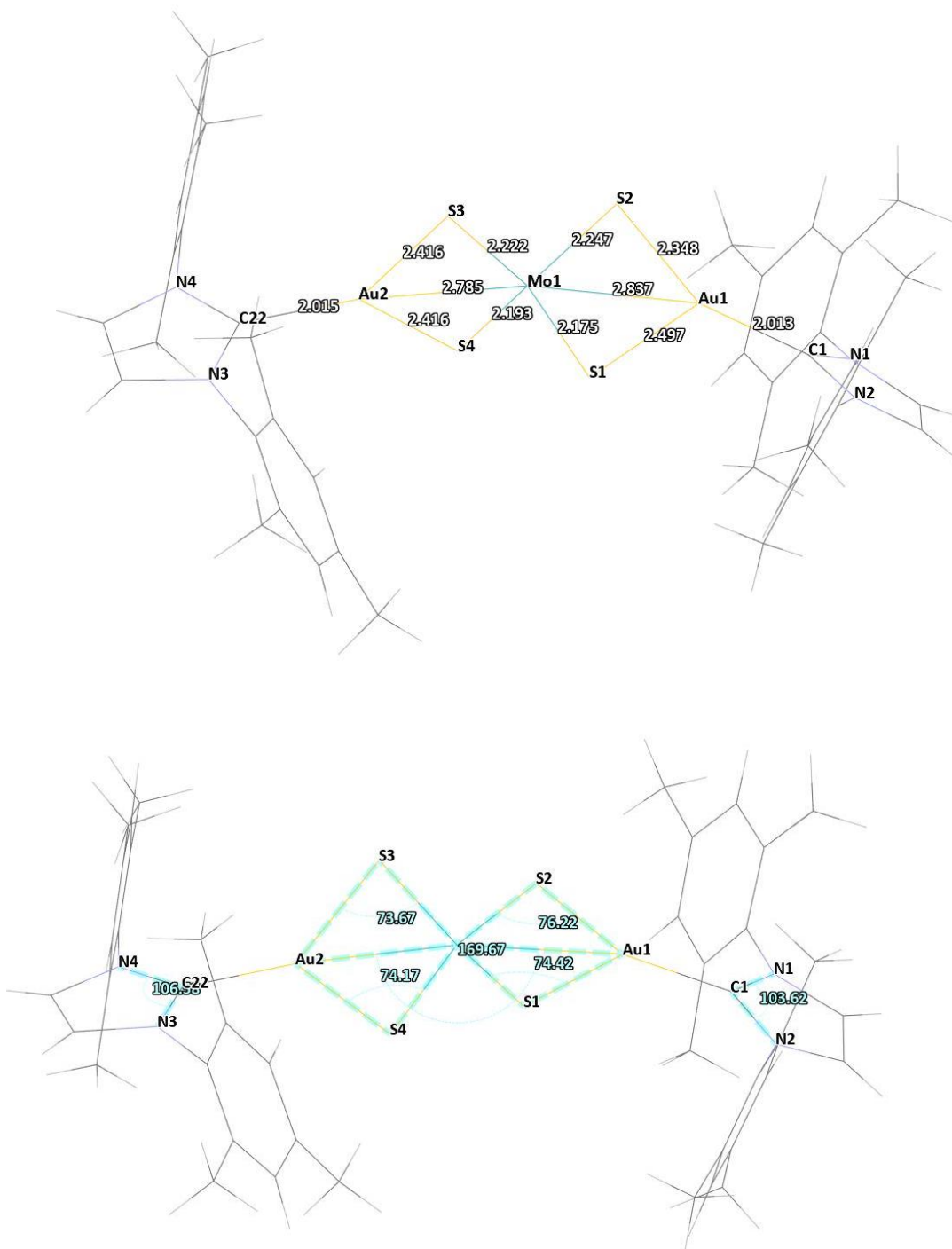
Figure 2.10. Hydrogen atoms are omitted, Wireframe model molecular structure of **C-3** (top) shows selected bond distances, (bottom) shows selected angles.

2.4. Conclusion

In conclusion, three novel clusters (**C-1**, **C-2** and **C-3**) were prepared and characterized by ^{1}H NMR, ^{13}C{^{1}H} NMR, UV-vis, cyclic voltammetry, SCXRD, elemental analysis and mass spectrometry. The clusters were pure and showed great stability in solution and in the solid state. Two clusters previously reported (**C-4** and **C-5**) were prepared using slightly modified procedures. These clusters were characterized by ^{1}H NMR, ^{31}P{^{1}H} NMR, UV-vis, cyclic voltammetry, elemental analysis, and mass spectrometry. The SCXRD of cluster **C-2** showed that both benzyl substituents on the NHC ligands are on one side and the methyl groups are on the other side (i.e. *syn* conformation). DOSY and VT ^{1}H NMR did not show evidence of conformational isomers. Either there is only one conformation present in solution or there is rapid interconversion of isomers as a result of rotation around the Au-C bond. The observation of *syn* conformation in the solid state may be preferred due to crystal packing forces.

2.5. Chapter References

(1)   Kinsch, E. M.; Stephan, D. W. Synthesis and Crystal and Molecular Structure of MoS4(AuPEt3)2: A Linear Trinuclear Heterobimetallic Species. *Inorganica Chim Acta* **1985**, *96* (2), L87–L90. https://doi.org/https://doi.org/10.1016/S0020-1693(00)87570-2.

(2)   Charnock, J. M.; Bristow, S.; Nicholson, J. R.; Garner, C. D.; Clegg, W. Preparations, Crystal Structures, and Molybdenum-95 Nuclear Magnetic Resonance Spectroscopic Studies of Triphenylphosphine–Gold–Tetrathiomolybdate(VI) Clusters. *Journal of the Chemical Society, Dalton Transactions* **1987**, No. 2, 303–306. https://doi.org/10.1039/DT9870000303.

(3)   Dolomanov, O. v; Bourhis, L. J.; Gildea, R. J.; Howard, J. A. K.; Puschmann, H. OLEX2: A Complete Structure Solution, Refinement and Analysis Program. *J Appl Crystallogr* **2009**, *42* (2), 339–341. https://doi.org/10.1107/S0021889808042726.

(4)   Sheldrick, G. M. Crystal Structure Refinement with SHELXL. *Acta Crystallographica Section C* **2015**, *71* (1), 3–8. https://doi.org/10.1107/S2053229614024218.

(5)   McDonald, J. W.; Friesen, G. D.; Rosenhein, L. D.; Newton, W. E. Syntheses and Characterization of Ammonium and Tetraalkylammonium Thiomolybdates and Thiotungstates. *Inorganica Chim Acta* **1983**, *72*, 205–210. https://doi.org/https://doi.org/10.1016/S0020-1693(00)81720-X.

(6)   Collado, A.; Gómez-Suárez, A.; Martin, A. R.; Slawin, A. M. Z.; Nolan, S. P. Straightforward Synthesis of [Au(NHC)X] (NHC = N-Heterocyclic Carbene, X = Cl, Br, I) Complexes. *Chemical Communications* **2013**, *49* (49), 5541–5543. https://doi.org/10.1039/C3CC43076F.

(7)   Johnson, A.; Gimeno, M. C. An Efficient and Sustainable Synthesis of NHC Gold Complexes. *Chemical Communications* **2016**, *52* (62), 9664–9667. https://doi.org/10.1039/C6CC05190A.

(8)   de Frémont, P.; Scott, N. M.; Stevens, E. D.; Nolan, S. P. Synthesis and Structural Characterization of N-Heterocyclic Carbene Gold(I) Complexes. *Organometallics* **2005**, *24* (10), 2411–2418. https://doi.org/10.1021/om050111c.

(9)   Maishal, T. K.; Basset, J.-M.; Boualleg, M.; Copéret, C.; Veyre, L.; Thieuleux, C. AgOC(CF3)3: An

        Alternative and Efficient Reagent for Preparing Transition Metal-NHC-Carbene Complexes.

        Dalton Transactions **2009**, No. 35, 6956–6959. https://doi.org/10.1039/B900136K.

(10)   Mézailles, N.; Ricard, L.; Gagosz, F. Phosphine Gold(I) Bis-(Trifluoromethanesulfonyl)Imidate

        Complexes as New Highly Efficient and Air-Stable Catalysts for the Cycloisomerization of Enynes.

        Org Lett **2005**, *7* (19), 4133–4136. https://doi.org/10.1021/ol0515917.

(11)   Faggiani, R.; Howard-Lock, H. E.; Lock, C. J. L.; Turner, M. A. The Reaction of

        Chloro(Triphenylphosphine)Gold(I) with 1-Methylthymine. *Can J Chem* **1987**, *65* (7), 1568–1575.

        https://doi.org/10.1139/v87-264.

(12)   Gunatilleke, S. S.; de Oliveira, C. A. F.; McCammon, J. A.; Barrios, A. M. Inhibition of Cathepsin B

        by Au(I) Complexes: A Kinetic and Computational Study. *Journal of Biological Inorganic*

        Chemistry **2008**, *13* (4), 555–561. https://doi.org/10.1007/s00775-008-0344-0.

(13)   Wang, J.; Mi, X.; Wang, J.; Yang, Y. An Efficient Approach to Chloro(Organophosphine) Gold(i)

        Complexes for the Synthesis of Auranofin. *Green Chemistry* **2017**, *19* (3), 634–637.

        https://doi.org/10.1039/C6GC02908F.

(14)   Back, O.; Henry-Ellinger, M.; Martin, C. D.; Martin, D.; Bertrand, G. 31P NMR Chemical Shifts of

        Carbene–Phosphinidene Adducts as an Indicator of the π-Accepting Properties of Carbenes.

        Angewandte Chemie International Edition **2013**, *52* (10), 2939–2943.

        https://doi.org/https://doi.org/10.1002/anie.201209109.

(15)   Huggins, M. T.; Kesharwani, T.; Buttrick, J.; Nicholson, C. Variable Temperature NMR Experiment

        Studying Restricted Bond Rotation. *J Chem Educ* **2020**, *97* (5), 1425–1429.

        https://doi.org/10.1021/acs.jchemed.0c00057.

(16)   Baker, M. v.; Barnard, P. J.; Berners-Price, S. J.; Brayshaw, S. K.; Hickey, J. L.; Skelton, B. W.;

        White, A. H. Cationic, Linear Au(I) N-Heterocyclic Carbene Complexes: Synthesis, Structure and

Anti-Mitochondrial Activity. *Dalton Transactions* **2006**, No. 30, 3708.

https://doi.org/10.1039/b602560a.

(17)   Hopkinson, M. N.; Richter, C.; Schedler, M.; Glorius, F. An Overview of N-Heterocyclic Carbenes.

Nature **2014**, *510* (7506), 485–496. https://doi.org/10.1038/nature13384.

(18)   Thureau, P.; Thévand, A.; Ancian, B.; Escavabaja, P.; Armstrong, G. S.; Mandelshtam, V. A.

Identification of Two Isomers from an Organic Mixture by Double-Stimulated-Echo NMR and

Construction of the DOSY Spectra by the Regularized Resolvent Transform Method.

ChemPhysChem **2005**, *6* (8), 1510–1513. https://doi.org/10.1002/cphc.200500192.

(19)   Yamanoi, T.; Oda, Y.; Katsuraya, K. Separation of the α- and β-Anomers of Carbohydrates by

Diffusion-Ordered NMR Spectroscopy. *Magnetochemistry* **2017**, *3* (4), 38.

https://doi.org/10.3390/magnetochemistry3040038.

(20)   Thureau, P.; Thévand, A.; Ancian, B.; Escavabaja, P.; Armstrong, G. S.; Mandelshtam, V. A.

Identification of Two Isomers from an Organic Mixture by Double-Stimulated-Echo NMR and

Construction of the DOSY Spectra by the Regularized Resolvent Transform Method.

ChemPhysChem **2005**, *6* (8), 1510–1513.

https://doi.org/https://doi.org/10.1002/cphc.200500192.

(21)   Chaudhari, S. R.; Suryaprakash, N. Diffusion Ordered Spectroscopy for Resolution of Double

Bonded Cis, Trans-Isomers. *J Mol Struct* **2012**, *1017*, 106–108.

https://doi.org/https://doi.org/10.1016/j.molstruc.2012.03.009.

(22)   Floquet, S.; Brun, S.; Lemonnier, J.-F.; Henry, M.; Delsuc, M.-A.; Prigent, Y.; Cadot, E.; Taulelle, F.

Molecular Weights of Cyclic and Hollow Clusters Measured by DOSY NMR Spectroscopy. *J Am

Chem Soc* **2009**, *131* (47), 17254–17259. https://doi.org/10.1021/ja9052619.

(23)   Kebabcioglu, R.; Müller, A. SCCC MO Calculations on the Ions WX2-4, MoX2-4 and VX3-4 (X =

         O,S,Se). *Chem Phys Lett* **1971**, *8* (1), 59–62. https://doi.org/https://doi.org/10.1016/0009-

         2614(71)80575-4.

(24)   Müller, A.; Diemann, E. Higher Energy Bands in the Electronic Absorption Spectra of CrO42−,

         RuO4, OsO4, WS42−, MoS42−, WSe42− and MoSe42−. A Note on the Assignment of the

         Electronic Spectra of Closed Shell Tetroxo-, Tetrathio- and Tetraselenoanions. *Chem Phys Lett*

         1971, *9* (5), 369–374. https://doi.org/https://doi.org/10.1016/0009-2614(71)80245-2.

(25)   McDonald, J. W.; Friesen, G. D.; Rosenhein, L. D.; Newton, W. E. Syntheses and Characterization

         of Ammonium and Tetraalkylammonium Thiomolybdates and Thiotungstates. *Inorganica Chim*

         Acta **1983**, *72*, 205–210. https://doi.org/https://doi.org/10.1016/S0020-1693(00)81720-X.

(26)   Laperriere, G.; Marsan, B.; Belanger, D. Preparation and Characterization of Electrodeposited

         Amorphous Molybdenum Sulfide. *Synth Met* **1989**, *29* (2), 201–206.

         https://doi.org/https://doi.org/10.1016/0379-6779(89)90900-4.

(27)   de Frémont, P.; Scott, N. M.; Stevens, E. D.; Nolan, S. P. Synthesis and Structural Characterization

         of N-Heterocyclic Carbene Gold(I) Complexes. *Organometallics* **2005**, *24* (10), 2411–2418.

         https://doi.org/10.1021/om050111c.

(28)   Blaya, M.; Bautista, D.; Gil-Rubio, J.; Vicente, J. Synthesis of Au(I) Trifluoromethyl Complexes.

         Oxidation to Au(III) and Reductive Elimination of Halotrifluoromethanes. *Organometallics* **2014**,

         33 (22), 6358–6368. https://doi.org/10.1021/om500669j.

CHAPTER 3

PERCENT BURIED VOLUME CALCULATIONS FOR [MoS₄(AuL)₂] (C-1 – C-5) AND DFT

CALCULATIONS FOR [MoS₄(AuIPr)₂] (C-1)

3.1. Introduction

In medicine, metal-based complexes have the potential to serve in various areas as anticancer, antimicrobial, or diagnostic agents.[1,2] This enhances the need to understand the reaction mechanisms, reactivity, and selectivity of metal-based compounds in a variety of applications. Computational chemistry plays an important role in understanding organic, inorganic, and metal-based chemistry.[3] Moreover, it can provide a quantitative representation of chemical reactivity. Density functional theory (DFT) offers high quantitative accuracy in linking theoretical studies with experimental results. Computational studies are routinely employed for spectroscopic and electrochemical analyses, as well as for interpretation of chemical reactivity and studying mechanistic details of catalytic reactions.[4–6]

The reactivity of transition metal compounds is influenced by steric and electronic effects of the ligands. Tolman developed a measure of steric bulk for phosphine ligands called cone angle (Figure 3.1, a).[7] This has been widely used for example, to rationalize the steric effect of phosphine ligands in kinetic and equilibrium data. However, cone angle measurements are less meaningful when applied to more elaborate ligands such as bidentate phosphines, biarylphosphines, or N-heterocyclic carbenes (NHC), which have different shapes than standard phosphines, PR_3. In 2003, Nolan and coworkers proposed another model to describe the total volume of a sphere occupied by a ligand coordinated to a metal, which they called "percent buried volume" ($\%V_{Bur}$) (Figure 3.1, b).[8] In 2010, Nolan and Clavier reviewed the steric properties of NHC and phosphorus-based ligands in several metal complexes using SambVca (Salerno molecular buried volume calculation) software.[9] They compared cone angle and $\%V_{Bur}$ values with different parameters such as the type of metal, the geometry of the complex, and the other ligands

connected to the metal center. Notably, there was a linear relationship between the cone angle and the %V_{Bur} values for different phosphine ligands in gold(I) compounds, which is a good indication that the two models provide similar measurements of steric properties. This model has been applied to NHC-metal complexes, including nickel, silver, gold, palladium, ruthenium, and other-NHC complexes.[10–14]
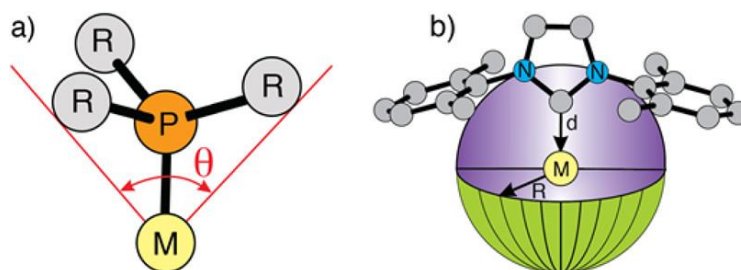
Figure 3.1. a) Tolman cone angle; b) sphere dimensions for steric parameter determination %V_{Bur} of NHC ligands.[8,15]

Rheingold, et al. described that $[MoS_4]^{2-}$ can function as a ligand for low-valent organometallic compounds.[16] Many complexes with $[MoS_4]^{2-}$ ligands have been reported to have unusual electronic properties based on chemical reactivity and spectroscopic and electrochemical measurements.[17–22] The unusual electronic properties of the $[MoS_4]^{2-}$ ligand for low-valent metals is caused by electron delocalization and metal-metal bonding interactions, where the sulfur donor atoms and Mo(VI) vacant d orbitals could interact with d orbitals of low-valent metals to result in sulfur to metal and/or metal to metal charge transfer.[22] Wu and co-workers studied the electronic structure of transition metal cluster compounds M-(μ-S)$_2$-M' where (M = V, Mo, W; M'= Fe, Co, etc.). They found that p orbitals on the bridging sulfur atoms largely contributed to the frontier molecular orbitals.[23] Shi and co-workers have assigned the three lowest energy electronic transitions of the cluster $[MS_4(M'L)_2]$ where M= Mo, W and M'= Cu, Ag, as ligand to metal charge transfer (Figure 3.2).[24] Several additional articles provide theoretical calculations of the electronic structure and nonlinear optical properties for clusters of the type $[MoS_4(M'L)_2]$ where M'= Cu, Ag, and Au. [25–27]

L= PPh$_3$, CN $^-$
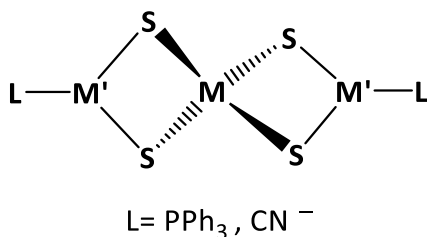
Figure 3.2. General M (Mo, W)-M'(Cu , Ag)-S cluster structure. [24]

This chapter represents the result of %V$_{Bur}$ calculations for clusters, **C-1** – **C-5**. The steric properties of the ligands are of potential importance for interpreting reactivity trends discussed in Chapter 4. Density functional theory (DFT) and time-dependent density functional theory (TDDFT) calculations were carried out on **C-1** to aid in interpreting the electronic structure and reactivity of [MoS$_4$(AuL)$_2$] clusters.

3.2. Experimental Section

3.2.1. Percent buried volume calculations

Calculations of %V$_{Bur}$ values were measured by SambVca 2.1 which requires the definition of the metal center (Au) to which the ligand is coordinated (NHC). Crystallographic CIF for **C-1**, **C-2** and **C-3** (Appendix C), **C-4** and **C-5** (Garne et al, Kinsch and Stephan respectively)[28,29] where used to provide the coordinates for %V$_{Bur}$ calculations. SambVca 2.1 is a free web application with a user-friendly interface to the SambVca 2.1 program with video tutorial for the calculation of %V$_{Bur}$ for NHC and phosphine ligands which can be found at (https://www.molnac.unisa.it/OMtools/sambvca2.1/index.html).[30] The first step was to load the CIF and then select the right side of the cluster excluding the S atoms (L-Au, H atoms were included) (Figure 3.3). Au(I) was chosen as the center of the sphere. The z axis was defined to contain gold and the carbon atom attached to gold for **C-1**, **C-2** and **C-3** or the phosphorus atom for **C-4** and **C-5**. The xz plane was defined by the nitrogen atoms in the imidazole ring for **C-1**, **C-2** and **C-3** or the two carbon atoms attached to the phosphorus atom for **C-4** and **C-5**. Only the NHC or PR$_3$ ligand atoms were selected for calculating the %V$_{Bur}$. The %V$_{Bur}$ measurements were calculated using Bondi atomic radii scaled by 1.17 and a sphere radius of 3.5Å as recommended by Cavallo, et al.[30] The distance

of the coordination point from the center of the sphere was set to zero. Mesh spacing for numerical integration was set to 0.10. Then the left side of each cluster was selected and the same steps were applied as for the right side calculations (Figure 3.3). Thus, there are two values of %V_{Bur} for each cluster and the average value for each cluster will be considered in the discussion (Table 3.1).
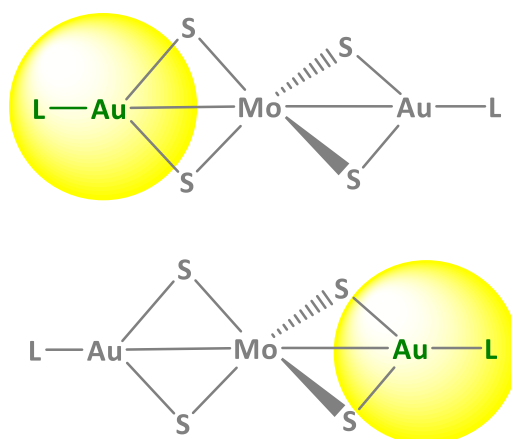
Figure 3.3. [MoS$_4$(AuL)$_2$] structure; the top structure shows the selected left side, and the bottom show the selected right side.

3.2.2. DFT calculations of the electronic structures for [MoS$_4$(AuIPr)$_2$] (C-1)

Density functional theory (DFT) and time-dependent density functional theory (TDDFT) calculations were carried out using Gaussian 16 [31] at the University of Maine High Performance Computing (HPC). A large triple-ζ valence plus two polarization functions including an effective core potential basis set (def2-TZVPP)[32–34] and the B3LYP functional which contains empirical data were applied for all the calculations.[35,36] The structure of **C-1** was fully optimized and the stationary point found. The selected computed parameters for the optimized structure are summarized in Table 3.2.
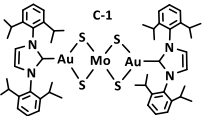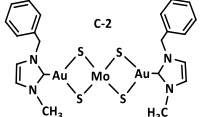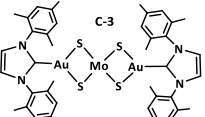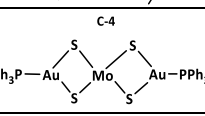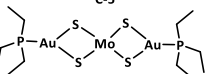
3.3. Results and discussion

3.3.1. Percent buried volume

Figures 3.4-3.7 show the results of the SambVca 2.1 calculations where the images in black background represent the selected left ligand (A) and right ligand (B) of each side of the clusters and the corresponding steric maps (A' and B') of each side. The steric maps were calculated with the SambVca package by analyzing the first coordination sphere around the metal. The %V_{Bur} of a given ligand is used in these calculations to quantify the amount of the first coordination sphere of the metal occupied by that ligand.[37] The SambVca program plots a 2D steric map from the top (i.e., looking down on the ligand along the z axis) and defines the surface of the ligand that is exposed to incoming reactants. The isocontour curves of the steric potential maps are in Å.

The steric properties are important matter to compare between the NHC and phosphine ligands because previous studies suggest that properties NHC and phosphine ligands are very similar.[38,39] The percent buried volume model (%V_{bur}) is the best tool to examine and analyze the steric characteristics of ligands. The reported %V_{bur} of L-Au(I)-Cl model complexes (L= phosphine or NHC ligands) were taken as a reference to compare with the calculated values of ligands in **C-1**, **C-2**, **C-3**, **C-4**, and **C-5** (Table 3.1). The %V_{bur} values calculated here compare well with the reported values with the exception of the IPr ligand in **C-1** which is smaller than the literature value. However, the trend is the same. In addition, there was no %V_{bur} value available for the asymmetrical NHC, which is in the cluster **C-2**.

Table 3.1. Computed %V_{bur} values for the NHC and phosphine ligands in **C-1 – C-5** vs reported %V_{bur} values for same ligand in L-Au(I)Cl complexes.

Cluster	Au-L distance (Å)	%V_{bur} / Left	%V_{bur}/ Right	Average %V_{bur}	Reported %V_{bur} in L-Au(I)Cl***
C-1	1.99	42.2	38.8	40.5	44.5
C-2	2.02	27.0	29.1	28.1	---
C-3	2.01	36.6	34.7	35.7	36.5
C-4	2.27*	31.2	30.1	30.7	29.9
C-5	2.28**	27.5	28.1	27.8	27.1

The data was taken from the references: *[28] , **[29] , ***[39]

The results show that %V_{bur} increases as a function of ligand bulk so we can arrange the clusters from the least sterically bulky to the highest as **C-5** < **C-2** < **C-4** < **C-3** < **C-1**. This arrangement could be used as a steric hindrance scale to predict the relative reactivity of the clusters with a nucleophile. Cluster **C-1** is predicted to be the most sterically hindered and least reactive and cluster **C-5** the least hindered and most reactive.

The steric maps of all the clusters show the ligand surfaces encountered by an approaching nucleophile. The predominant green area in the steric maps of the NHC complexes (Figures 3.4 – 3.6) indicate relatively flat regions of the imidazole backbone and the more positive greenish- yellow regions are where the substituents on the imidazole rings are located. The blue regions (more negative values) show more open areas, i. e. where the underlying metal is more exposed to an incoming nucleophile. The steric maps for the phosphine ligands indicate less sterically bulky regions in general, especially for the Et$_3$P ligand.
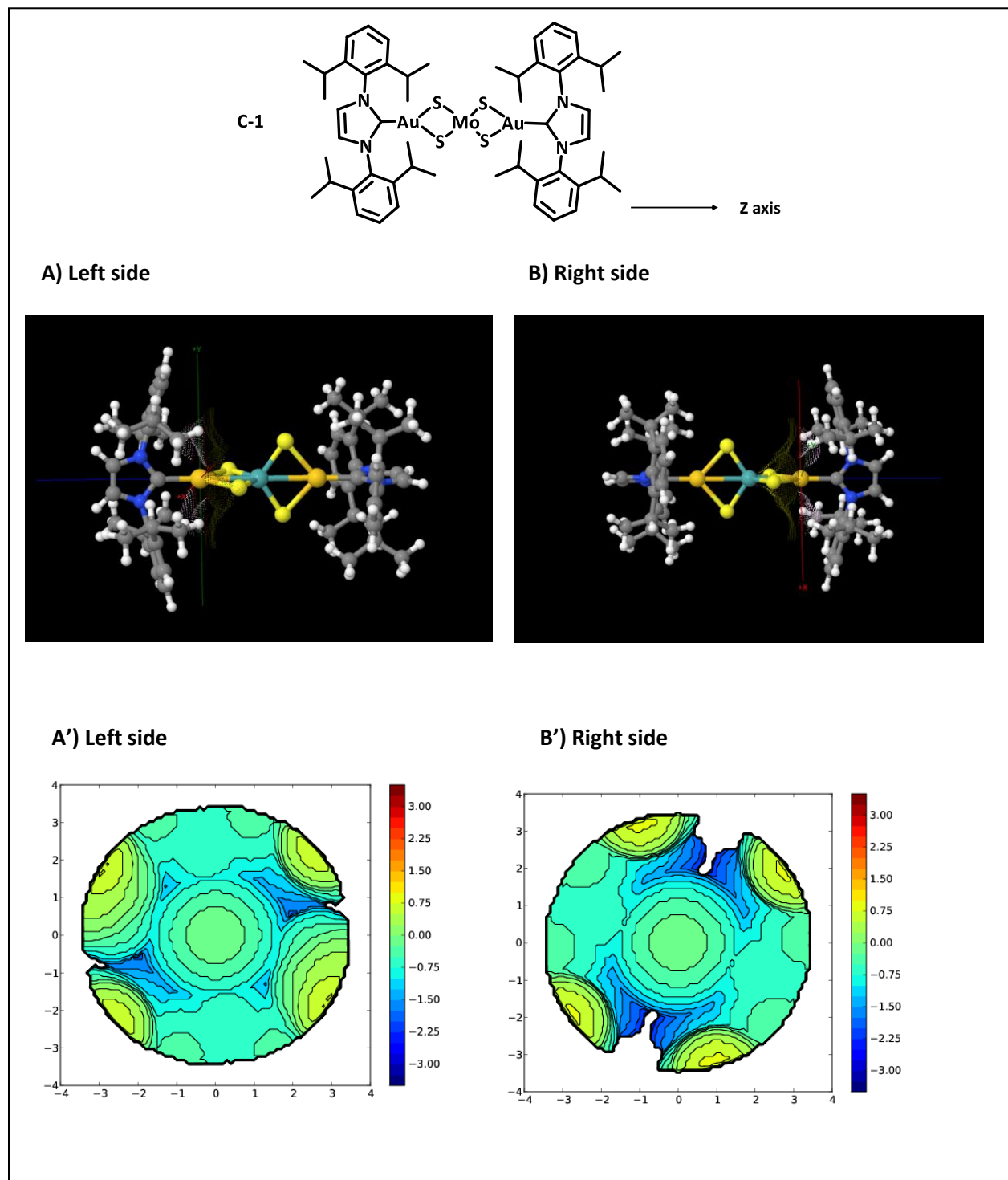
Figure 3.4. A and B show the selected ligand of left and right sides of **C-1**, A' and B' show the corresponding steric maps (viewed along the Z axis) of the left and right sides related to the upper images.
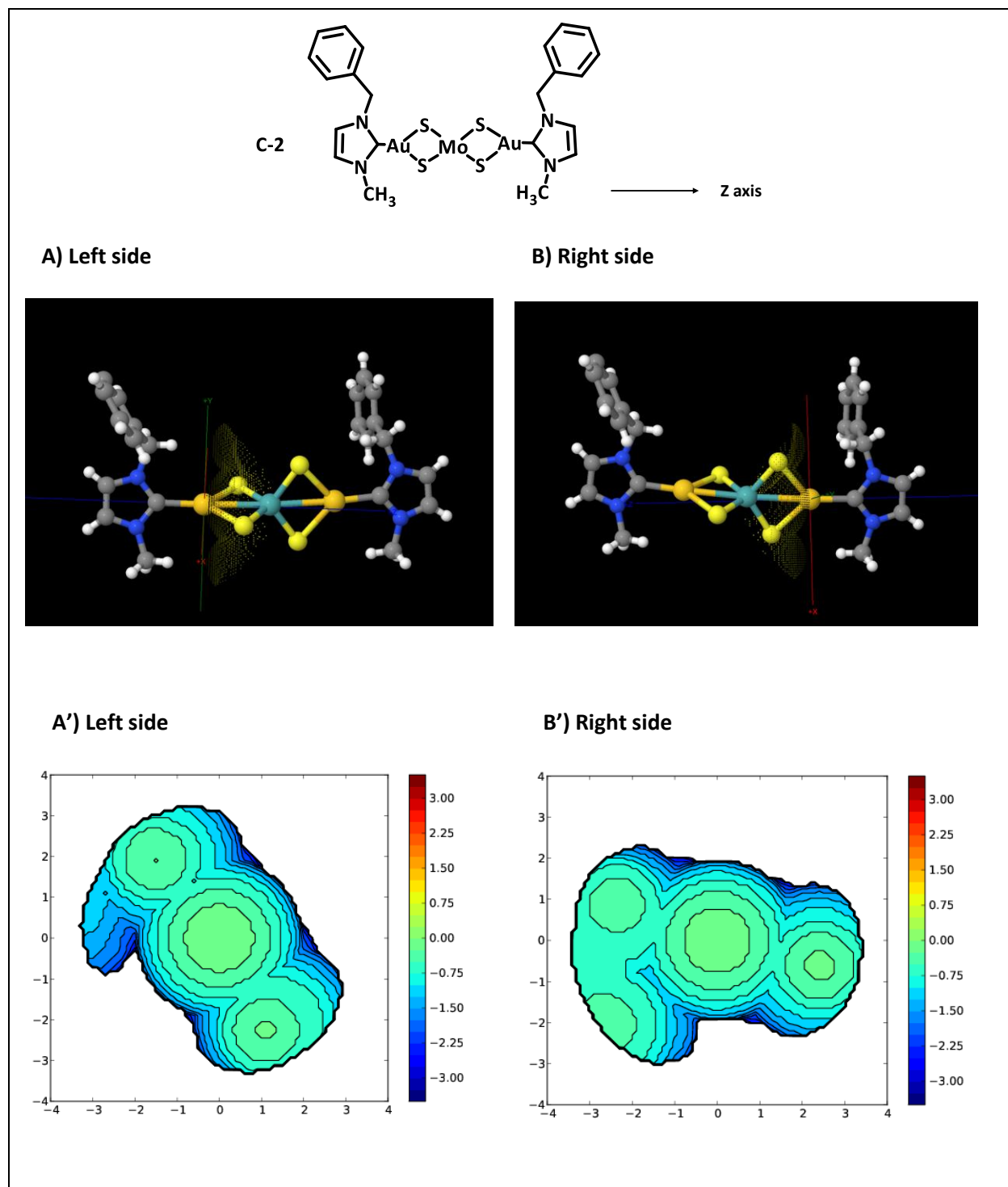
Figure 3.5. A and B show the selected ligand of left and right sides of **C-2**, A' and B' show the corresponding steric maps (viewed along the Z axis) of the left and right sides related to the upper images.
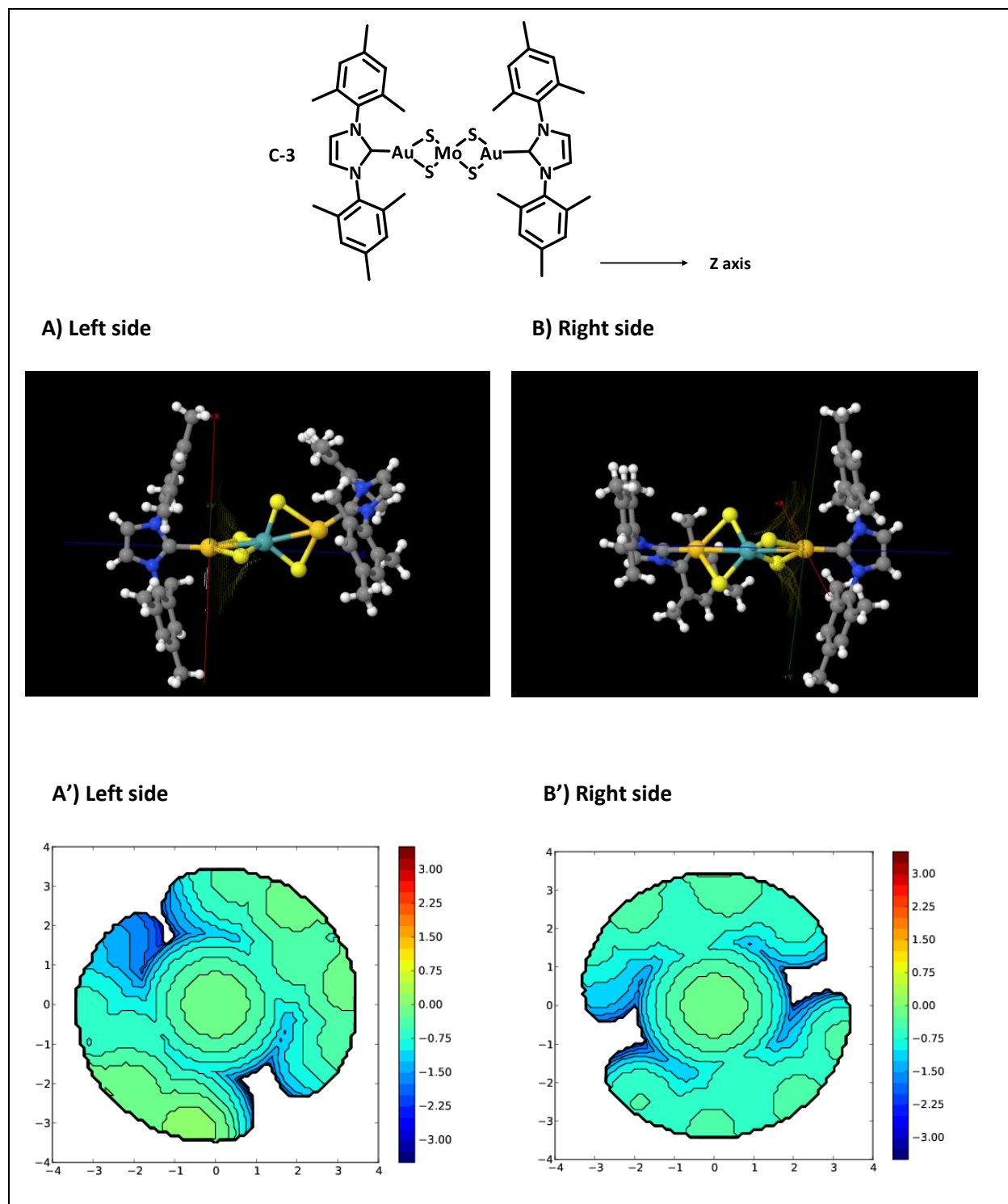
Figure 3.6. A and B show the selected ligand of left and right sides of **C-3**, A' and B' show the corresponding steric maps (viewed along the Z axis) of the left and right sides related to the upper images.
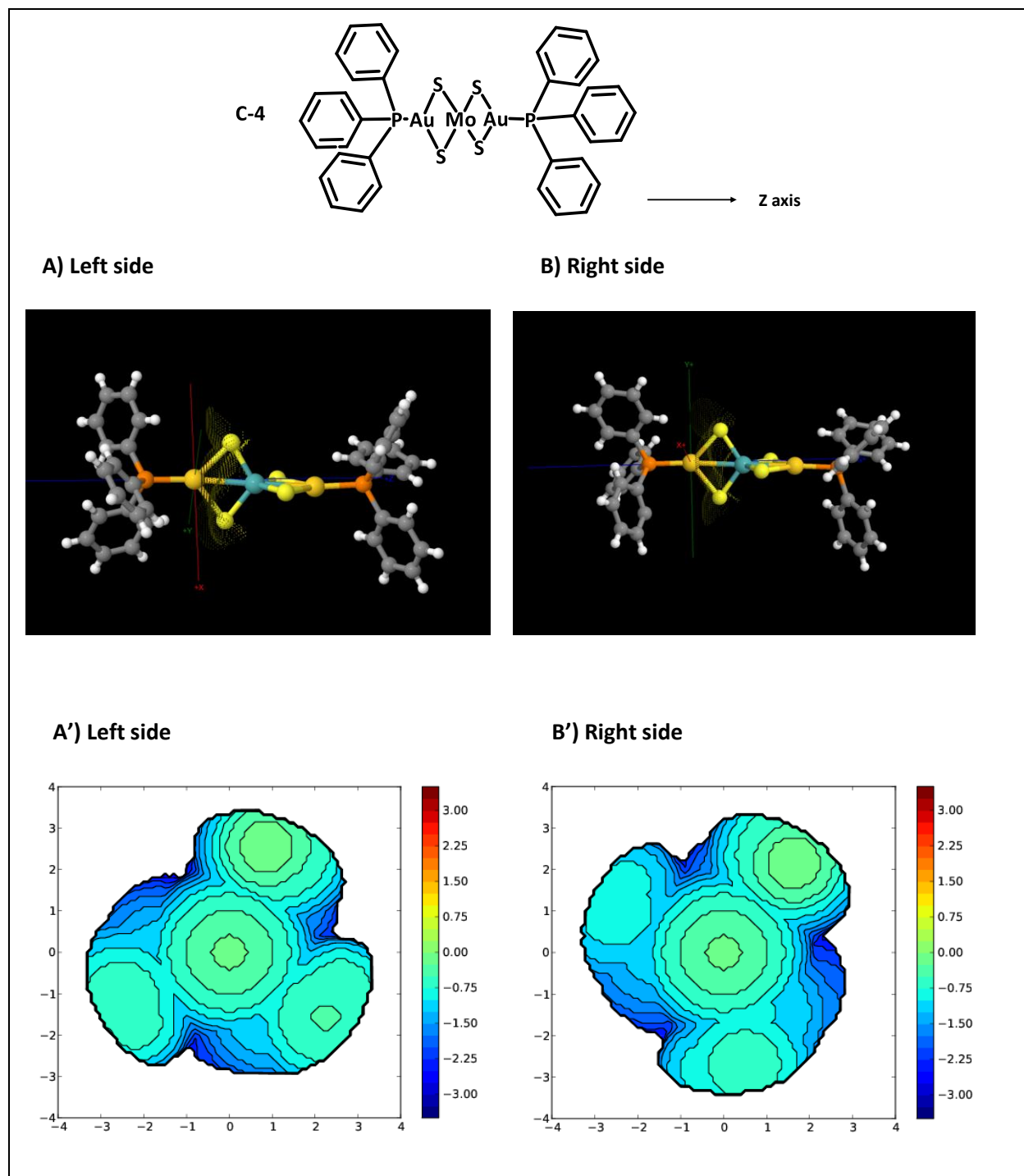
Figure 3.7. A and B show the selected ligand of left and right sides of **C-4**, A' and B' show the corresponding steric maps (viewed along the Z axis) of the left and right sides related to the upper images.
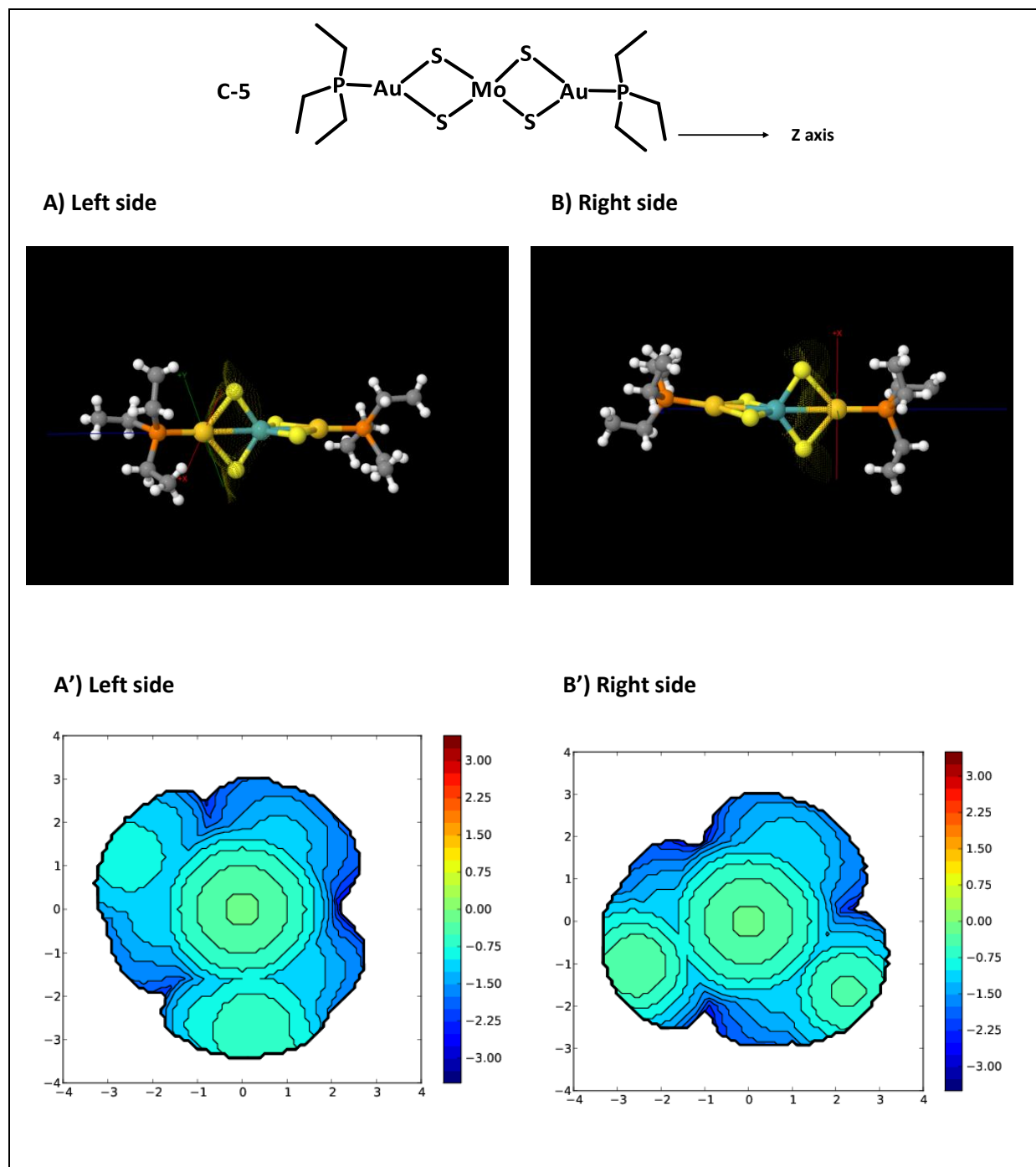
Figure 3.8. A and B show the selected ligand of left and right sides of **C-5**, A' and B' show the corresponding steric maps (viewed along the Z axis) of the left and right sides related to the upper images.

3.3.2. DFT calculations

The bond distances for the $MoS_4(Au)_2$ core in the optimized $[MoS_4(AuIPr)_2]$ structure are shown in Figure 3.9. Selected bond distances and angles of the optimized structure are compared to the SCXRD data for **C-1** in Table 3.2. There is good agreement between the optimized structure and crystallographic data. The calculated and experimental data show the coordination geometry of Au(I) can be described as trigonal planer and that of Mo(VI) as tetrahedral. The calculated Au-Mo distance is 2.89 Å and the experimental value is 2.78 Å. For comparison, Srujders, et al calculated a Au-Mo distance of 2.89 Å in **C-4** by using the LanL2Dz basis set and replacing PPh_3 with PH_3.[27] The estimated metallic radius between Au (4 coordination) and Mo (6 coordination) is 2.61 Å.[40] The van der Waals radii of Au is 1.66 Å and Mo is 2.1 Å.[41] The short Au-Mo distance in **C-1** (2.78-2.89 Å) could imply a metal-metal bonding interaction. The partial charges calculated by a Mullikan population analysis of the DFT/B3LYP orbitals are shown on each atom in the core structure in Figure 3.10 and the charges are also listed in Table 3.2. The positive charge is evenly distributed across the gold and molybdenum atoms, despite the formal Au(I) and Mo(VI) oxidation state. The negative charge is evenly distributed among the bridging sulfides. The optimized structure of **C-1** was used to calculate theoretical absolute chemical shielding tensors of ^1H NMR and $^{13}C\{^1H\}$ NMR by using def2-TZVPP. The gauge-independent atomic orbital (GIAO) plot at the B3LYP-6-311+G(2d,p) was used to show the chemical shift assignments for each atom.[42,43] All the calculated spectra are referenced to tetramethyl silane (TMS) (Figure 3.14 and Figure 3.15). The calculated chemical shift values are compared with the experimental values in Table 3.3. This good agreement between theory and experiment is an additional indication that the optimization and basis set used in the calculation were appropriately chosen.

The HOMO and LUMO molecular orbital diagrams are shown in Figure 3.11, and the calculated HOMO-LUMO energy gap is 3.46 eV. This is similar to the HOMO-LOMO gaps of 2.88-3.48 eV calculated for $[MS_4(M'PH_3)_2]$ (M=Mo, W; M'=Cu, Ag, Au).[27] The HOMO is primarily sulfur p-orbital in character with

some contribution from Au. The LUMO is primarily Mo d-orbital in character with some contribution from sulfur. Figure 3.13 shows selected molecular orbital diagrams which illustrate the delocalized nature of the bonding in the $MoS_4(Au)_2$ core, consistent with a Mo-Au bonding interaction. These findings of metal-metal bonding interaction and electron delocalization in the $MoS_4(Au)_2$ core are similar to the calculational results for tetrathiomolybdate complexes of Rh(I) reported by Koinis and co-workers who employed the def2-TZVPP basis set.[44]

Table 3.2. selected computed parameters of optimized structure (def2-TZVPP).

Distance (Å)	Optimized C-1 (SD)	SCXRD C-1 (SD)
Au-C$_{imd}$	2.04 (0.01)	1.99 (0)
Au-Mo	2.89 (0.01)	2.78 (0)
Au-S	2.47 (0.01)	2.39 (0)
Mo-S	2.22 (0.01)	2.23 (0)
Angles (°)		
Au-Mo-Au	179.9	180
Au-S-Mo	75.89 (0.18)	73.92 (0)
N-C-N	104.5 (0.01)	107.02 (0)
Other parameters		
ΔE (HOMO−LUMO)	3.46 eV	
Q(Au)	+ 0.40 (0.03)	
Q(Mo)	+ 0.38	
Q (S)	-0.47 (0.01)	

Q :Partial charges calculated by a Mulliken population analysis of the DFT/B3LYP orbitals
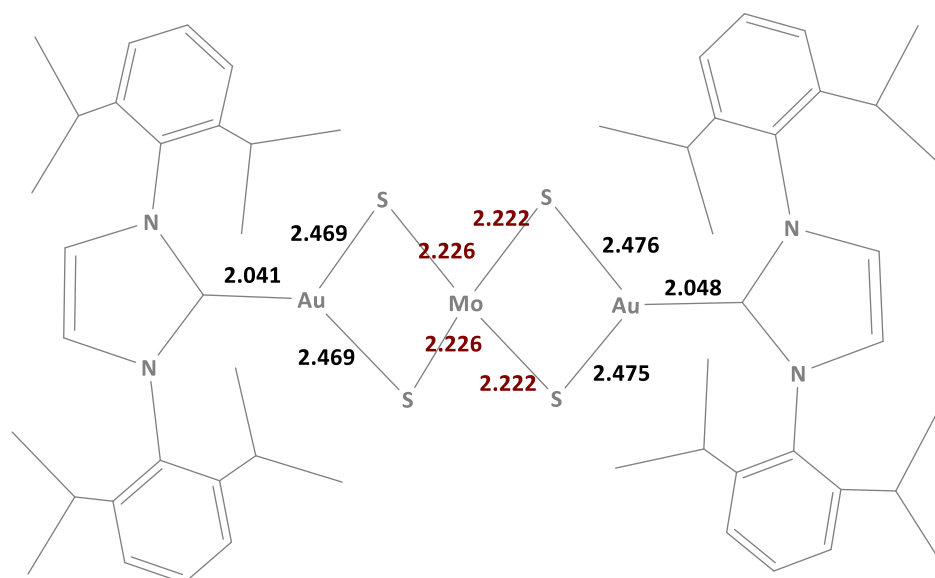
Figure 3.9. The wireframe model of the optimized molecular structure of **C-1** shows the bond distances in angstrom (Å).
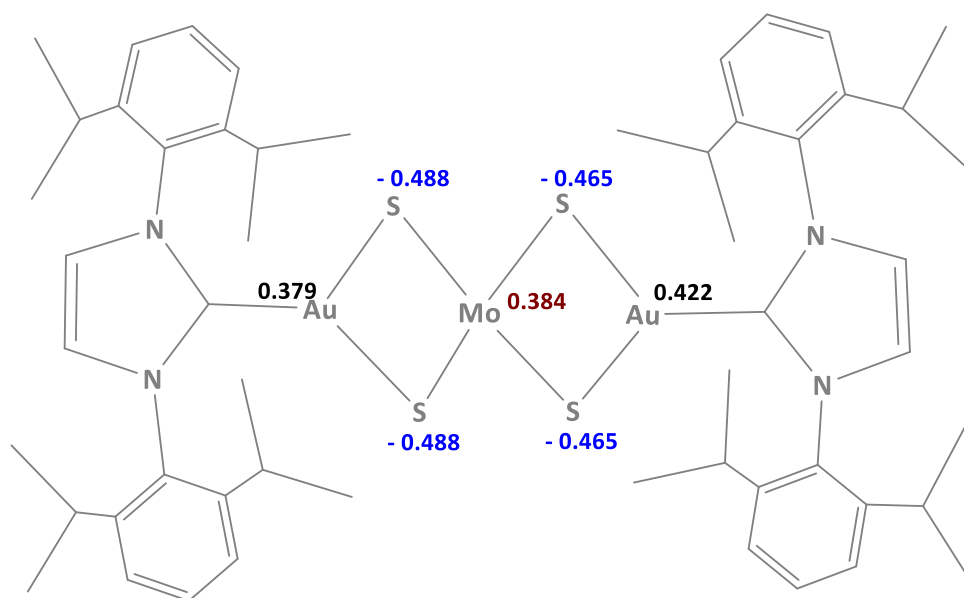
Figure 3.10. The wireframe model of the optimized molecular structure of **C-1** shows partial charges calculated by a Mulliken population analysis of the DFT/B3LYP orbitals.

LUMO

(-1.533eV)

HOMO

(-4.997eV)
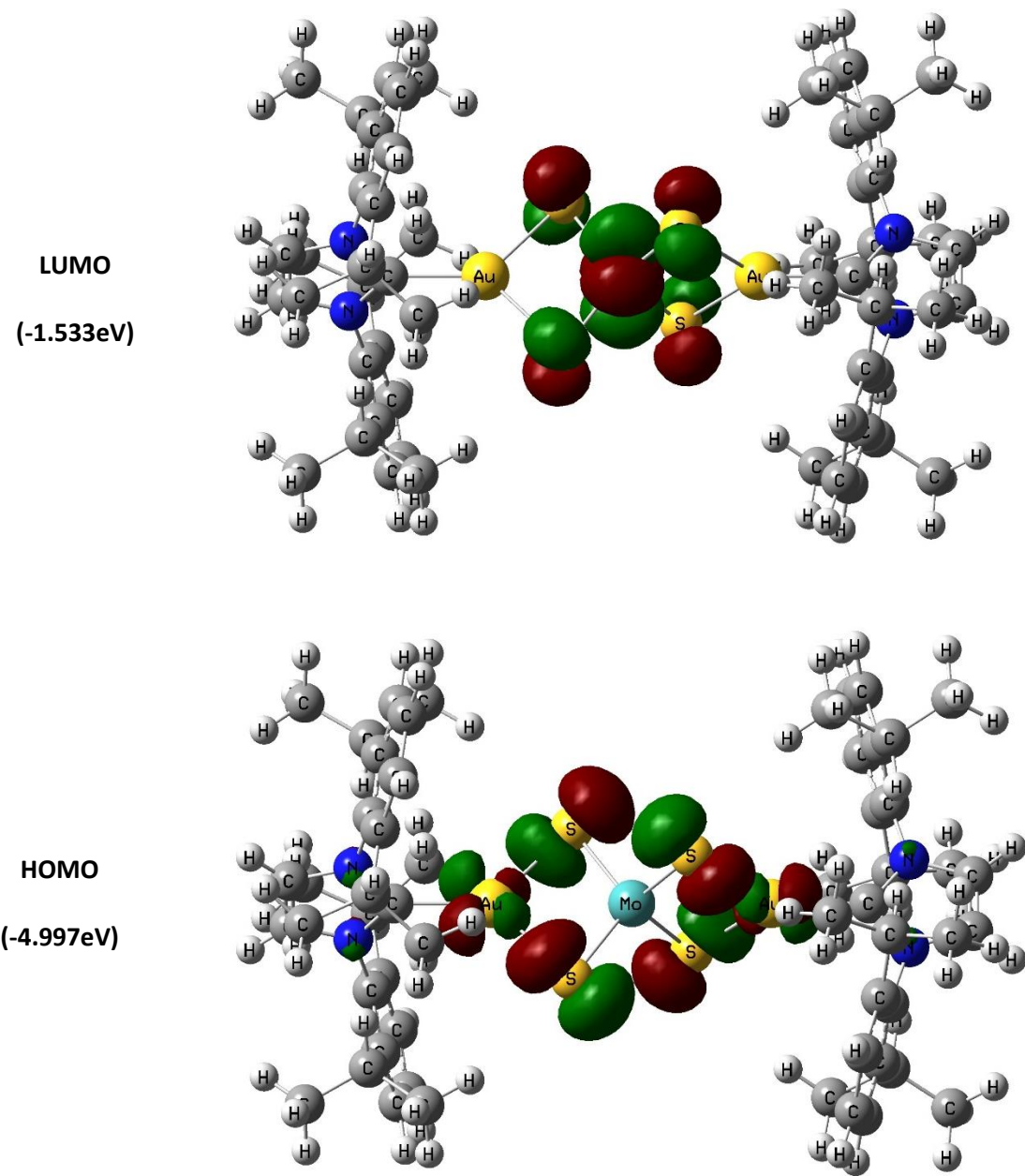
Figure 3.11. HOMO (nonbonding) and LUMO molecular orbitals for **C-1**, isovalue 0.04.

LUMO+2

(-0.782eV)

LUMO+1

(-1.275eV)

HOMO-1

(-5.004eV)

HOMO-2

(-5.019eV)
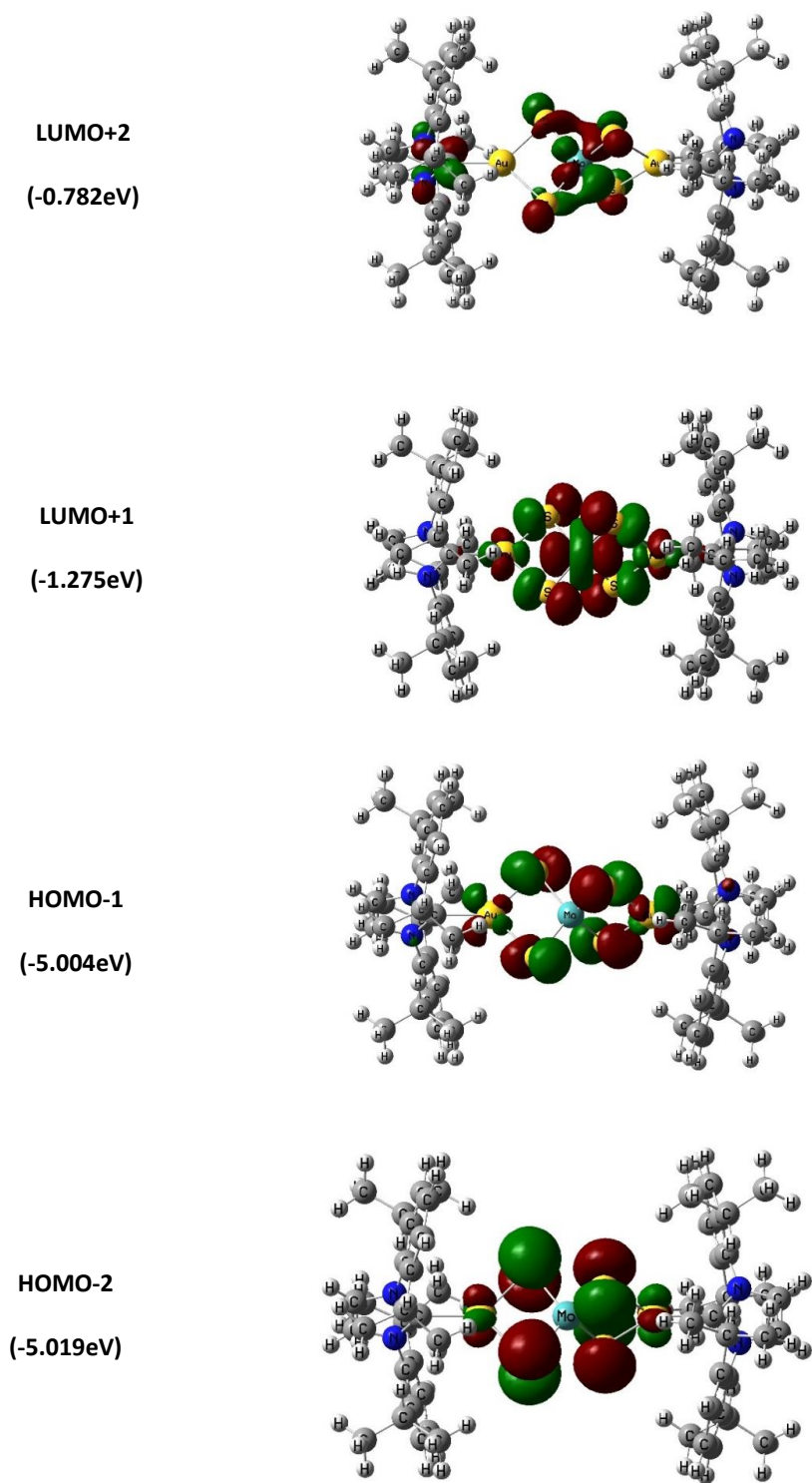
Figure 3.12. HOMO+2, HOMO+1, LUMO-1, and LUMO-2 molecular orbitals for **C-1**, isovalue 0.04.

HOMO-6

(-6.484eV)

HOMO-18

(-7.337eV)

HOMO-23

(-8.220eV)

HOMO-27

(-8.313eV)
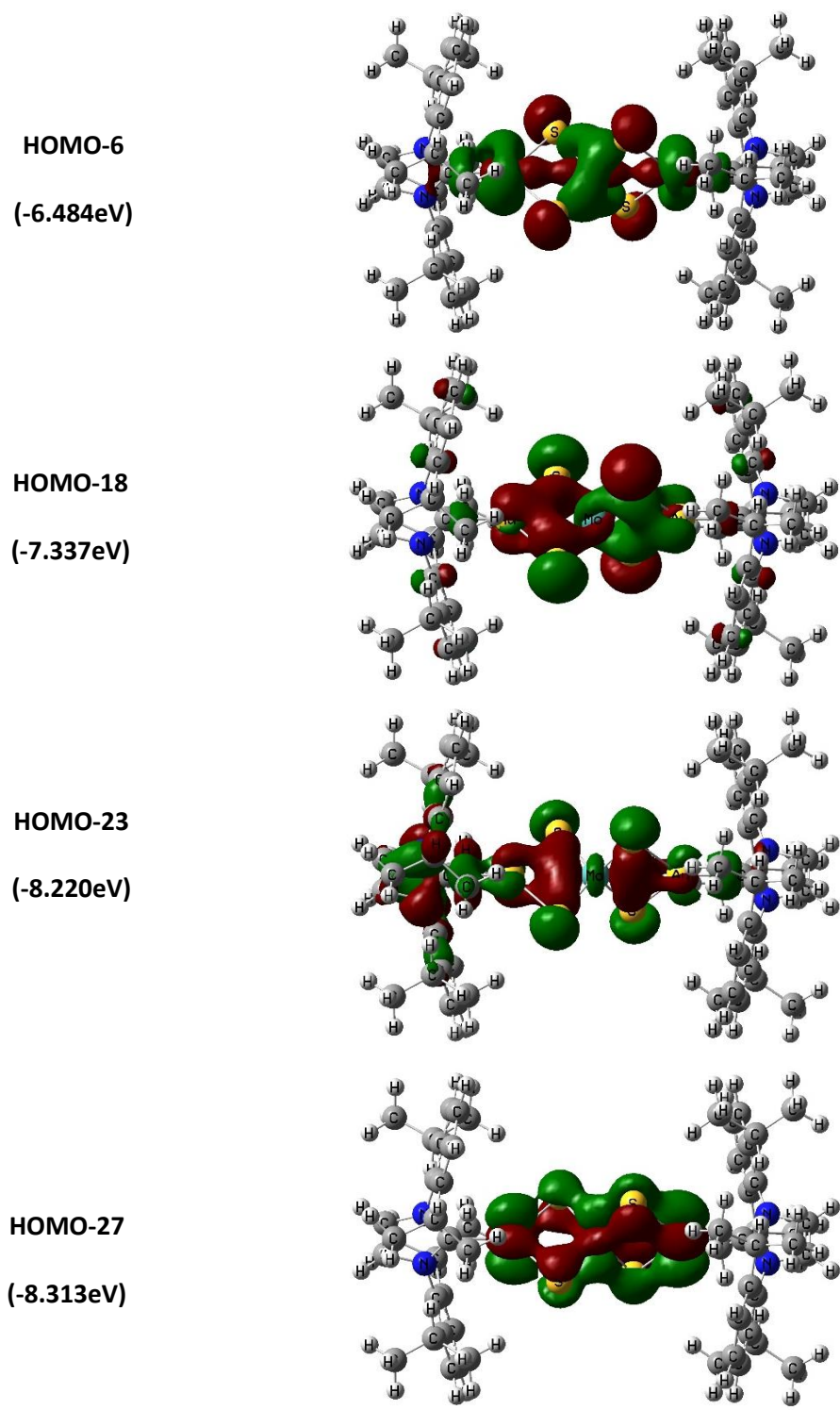
Figure 3.13. Selected molecular orbitals' bonding showing delocalized bonding in the Au(μ-S)$_2$Mo(μ-S)$_2$Au core for **C-1**, isovalue 0.04.
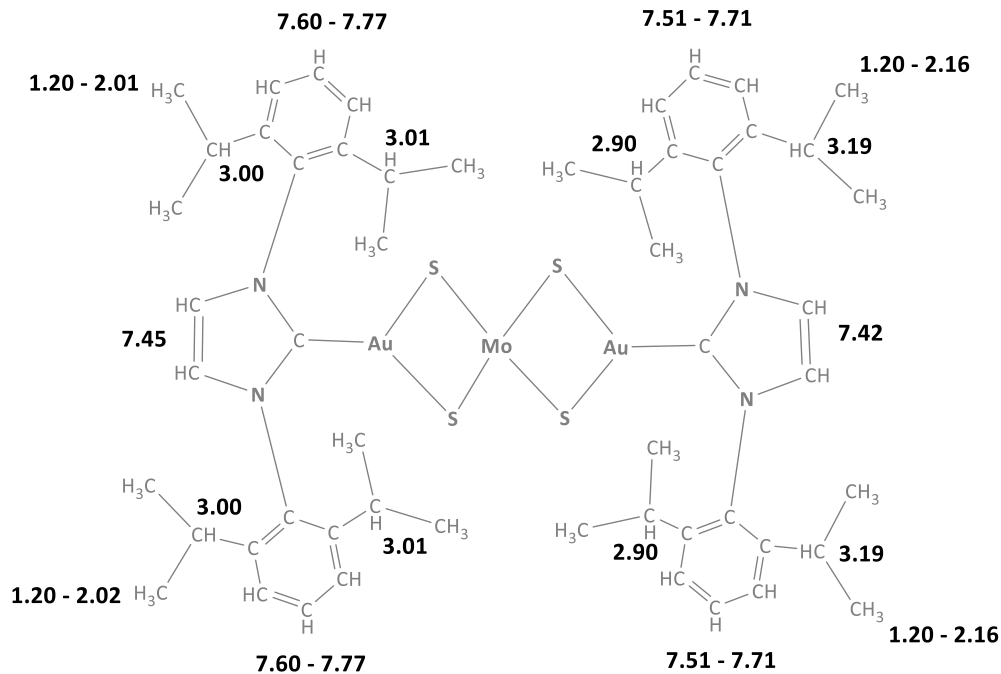
Figure 3.14. Molecular structure of **C-1** showing the computed ^{1}H NMR chemical shift (ppm).
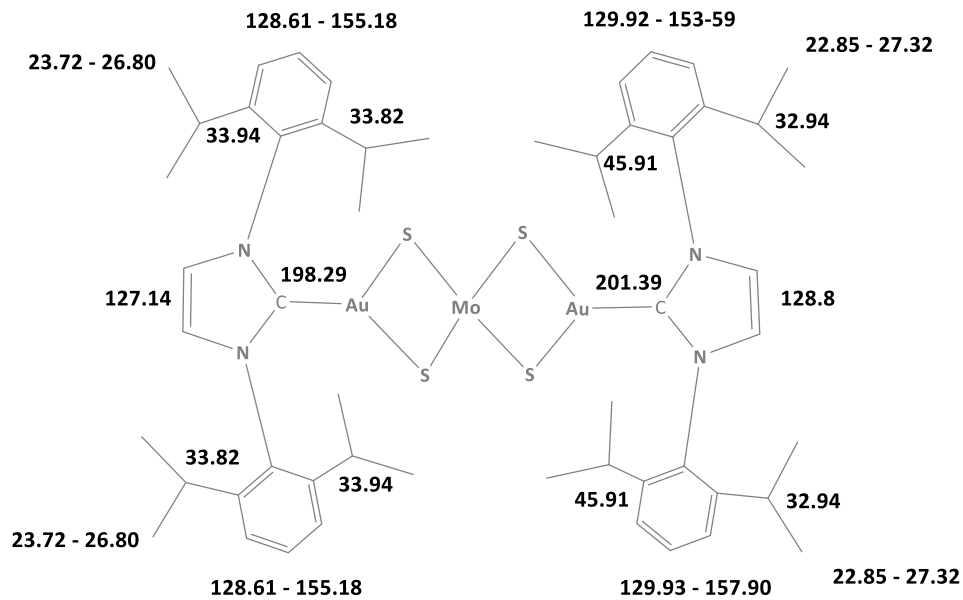
Figure 3.15. Molecular structure of **C-1** showing the computed ^{13}C{^{1}H} NMR chemical shift (ppm).

Table 3.3. Measured (CH$_2$Cl$_2$-d_2) vs computed (basis set def2-TZVPP, referenced to TMS by using B3LYP-6-311+G(2d,p) GIAO) ^{1}H NMR and ^{13}C{^{1}H} NMR for **C-1**.

Entry	NMR	C-1 Experimental	C-1 Computational
H$_{Ar}$	^{1}H NMR	(7.5-7.4), 7.3, 7.2	(7.5-7.8)
H$_{Imid}$	^{1}H NMR	7.4	7.4
H-CH_2	^{1}H NMR	(2.9-2.8)	(2.9-3.19)
H-CH$_3$	^{1}H NMR	1.2, 1.2	(1.2-2.16)
C$_{Au}$	^{13}C{^{1}H} NMR	187.0	(198.3-201.4)
C$_{Ar+Imid}$	^{13}C{^{1}H} NMR	147.3, 135.7, 130.5, 124.3, 123.8	**C**$_{Ar}$ (128.6-157.9) **C**$_{Imid}$ (127.1-128.8)
C-CH_2+CH$_3$	^{13}C{^{1}H} NMR	29.3, 24.7, 23.8	**C**H$_2$ (32.9-45.9), **C**H$_3$ (22.8-27.3)

The experimental electronic absorption spectra for **C-1** in acetonitrile solution is shown in Figure 3.16. The UV-vis spectra of all the clusters are similar in appearance (see chapter 2) with the lowest energy transition near λ_{max} = 490 nm, a higher energy transition near λ_{max} = 357 nm, and several weaker absorptions that appear as shoulders in between these two peaks. The TDDFT results are summarized and analyzed in Table 3.4. The contribution percentage values in this table were calculated by the equation: (configuration coefficient)^2 × 2 × 100%. The transitions in the visible region can be assigned as primarily υ(S →Mo) and   υ(Au, S →Mo) charge transfer, arising primarily from an essentially degenerate set of nonbonding molecular orbitals (HOMO, HOMO-1 and HOMO-2), (Figure 3.17).

C-1 UV-vis. in acetonitrile
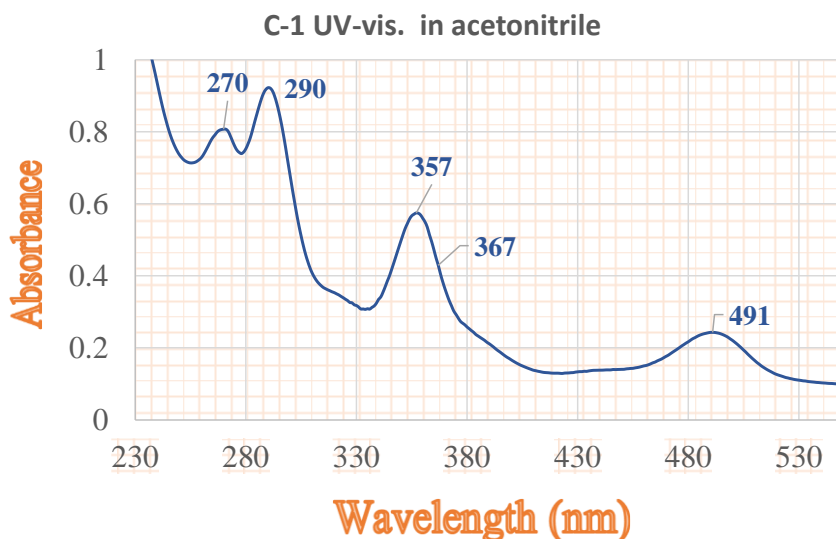
Figure 3.16. UV-vis, spectrum of **C-1** in acetonitrile.

Table 3.4. Excitation Energy (E), Oscillator Strength (f), Dominant Contributing Transitions and Associated Percent Contribution, and Assignment of **C-1**.

Excited state	Excitation Energy (eV)	Excitation Energy (nm)	Oscillator strength (f)	Dominant transitions (contribution %)	assignment
1	2.53	491	0.0010	HOMO → LUMO (82)	Au, S_{br} → Mo
2	2.53	490	0.0011	HOMO-1 → LUMO (82)	Au, S_{br} → Mo
4	2.77	448	0.0447	HOMO-2 → LUMO (90)	Au, S_{br} → Mo
5	2.87	431	0.0048	HOMO → LUMO+1 (85)	S_{br} → Mo
6	2.88	431	0.0051	HOMO-1 → LUMO+1 (85)	S_{br} → Mo
9	3.38	367	0.0023	HOMO-2 → LUMO+2 (81)	Au, S_{br} → Mo
12	3.53	351	0.4244	HOMO → LUMO+3 (37) HOMO-1 → LUMO+3 (10)	Au, S_{br} → Mo
22	3.93	316	0.0034	HOMO → LUMO+7 (37) HOMO-1 → LUMO+4 (29)	Au, S_{br} → L
27	3.98	311	0.0367	HOMO → LUMO+9 (37) HOMO-1 → LUMO+9 (37)	Au, S_{br} → Mo, L
29	4.01	309	0.0293	HOMO → LUMO+10 (44)	Au, S_{br} → Mo, L
46	4.31	288	0.4980	HOMO-4 → LUMO+1 (46) HOMO-3 → LUMO+1 (12) HOMO → LUMO+12 (15)	S_{br} → Mo Au, S_{br} → Mo
47	4.31	287	0.1337	HOMO-5 → LUMO+1 (71)	Au → S_{br}
58	4.67	266	0.0125	HOMO-1 → LUMO+14 (50) HOMO → LUMO+14 (47)	Au, S_{br} → L, Mo

S_{br} (bridging sulfide), L (NHC ligand of **C-1**)
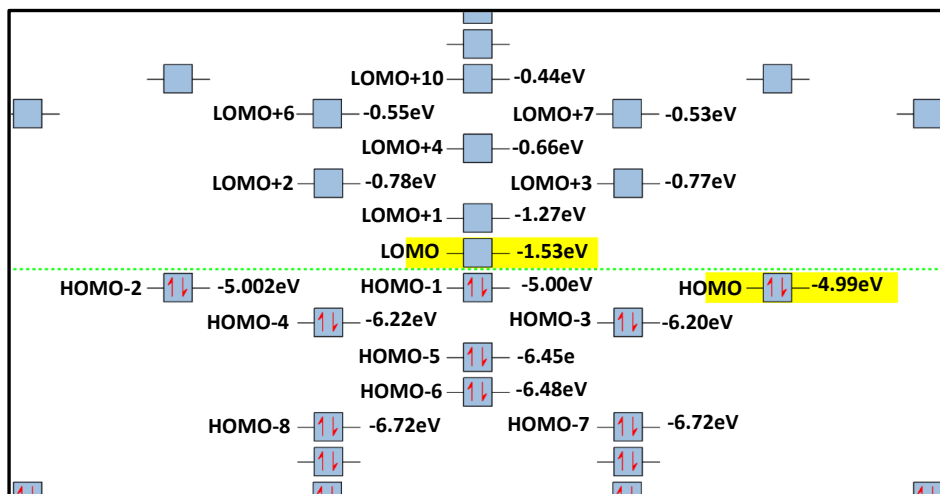
Figure 3.17. Molecular orbital diagram of **C-1**, degeneracy threshold 0.027eV (0.001Hartree).

3.4. Conclusion

In conclusion, % V_{bur} calculations show that the steric bulkiness of the ligands increases in the order, **C-5** > **C-2** > **C-4** > **C-3** > **C-1**. DFT calculations were done on **C-1** as an example of the [$MoS_4(AuNHC)_2$] cluster complex. The calculated Au-Mo distance and molecular orbitals showed there were interactions between the metal centers, which could contribute to stabilization of the clusters in addition to the bridging sulfides. The TDDFT study showed that the lowest energy transition is assigned as HOMO, HOMO-1 and HOMO-2 → LUMO, which is a mixture υ(Au, S → Mo) and υ(S → Mo) charge transfers. This is consistent with the measured UV-vis spectra of all five clusters which have a band around 487-491 nm (chapter2, Table 2.4), regardless of whether the ligands are phosphine or NHC. The ligands are involved in the transitions in the UV but they have little influence in the visible, which might indicate that the electronic properties of the ligands will have less effect on the reactivity of the clusters. However, the ligands are expected to show a noticeable steric effect and furthermore the ligands play an important role in the solubility of the clusters.

3.5. Chapter References

(1)   Tesauro, D. Metal Complexes in Diagnosis and Therapy. *Int J Mol Sci* **2022**, *23* (8), 4377–4377.

https://doi.org/10.3390/ijms23084377.

(2)   Franz, K. J.; Metzler-Nolte, N. Introduction: Metals in Medicine. *Chem Rev* **2019**, *119* (2), 727–

729. https://doi.org/10.1021/acs.chemrev.8b00685.

(3)   Lipkowitz, K. B.; Boyd, D. B.; Cundari, T. R. *Reviews in Computational Chemistry, Volume 18*; John

Wiley & Sons, Incorporated: Hoboken, UNITED STATES, 2002.

(4)   Dell'Angelo, D. 13 - Computational Chemistry and the Study and Design of Catalysts. In *Green

Chemistry and Computational Chemistry*; Mammino, L., Ed.; Elsevier, 2022; pp 299–332.

https://doi.org/https://doi.org/10.1016/B978-0-12-819879-7.00010-6.

(5)   Geerlings, P.; de Proft, F.; Langenaeker, W. Conceptual Density Functional Theory. *Chem Rev*

2003, *103* (5), 1793–1874. https://doi.org/10.1021/cr990029p.

(6)   Sperger, T.; Sanhueza, I. A.; Kalvet, I.; Schoenebeck, F. Computational Studies of Synthetically

Relevant Homogeneous Organometallic Catalysis Involving Ni, Pd, Ir, and Rh: An Overview of

Commonly Employed DFT Methods and Mechanistic Insights. *Chem Rev* **2015**, *115* (17), 9532–

9586. https://doi.org/10.1021/acs.chemrev.5b00163.

(7)   Tolman, C. A. Steric Effects of Phosphorus Ligands in Organometallic Chemistry and

Homogeneous Catalysis. *Chem Rev* **1977**, *77* (3), 313–348.

https://doi.org/10.1021/cr60307a002.

(8)   Hillier, A. C.; Sommer, W. J.; Yong, B. S.; Petersen, J. L.; Cavallo, L.; Nolan, S. P. A Combined

Experimental and Theoretical Study Examining the Binding of N-Heterocyclic Carbenes (NHC) to

the Cp*RuCl (Cp* = H5-C5Me5) Moiety: Insight into Stereoelectronic Differences between

Unsaturated and Saturated NHC Ligands. *Organometallics* **2003**, *22* (21), 4322–4326.

https://doi.org/10.1021/om034016k.

(9)   Clavier, H.; Nolan, S. P. Percent Buried Volume for Phosphine and N-Heterocyclic Carbene

        Ligands: Steric Properties in Organometallic Chemistry. *Chemical Communications* **2010**, *46* (6),

        841–861. https://doi.org/10.1039/B922984A.

(10)   Hillier, A. C.; Sommer, W. J.; Yong, B. S.; Petersen, J. L.; Cavallo, L.; Nolan, S. P. A Combined

        Experimental and Theoretical Study Examining the Binding of N-Heterocyclic Carbenes (NHC) to

        the Cp*RuCl (Cp* = H5-C5Me5) Moiety: Insight into Stereoelectronic Differences between

        Unsaturated and Saturated NHC Ligands. *Organometallics* **2003**, *22* (21), 4322–4326.

        https://doi.org/10.1021/om034016k.

(11)   Dorta, R.; Stevens, E. D.; Scott, N. M.; Costabile, C.; Cavallo, L.; Hoff, C. D.; Nolan, S. P. Steric and

        Electronic Properties of N-Heterocyclic Carbenes (NHC): A Detailed Study on Their Interaction

        with Ni(CO)4. *J Am Chem Soc* **2005**, *127* (8), 2485–2495. https://doi.org/10.1021/ja0438821.

(12)   Würtz, S.; Lohre, C.; Fröhlich, R.; Bergander, K.; Glorius, F. IBiox[(−)-Menthyl]: A Sterically

        Demanding Chiral NHC Ligand. *J Am Chem Soc* **2009**, *131* (24), 8344–8345.

        https://doi.org/10.1021/ja901018g.

(13)   Viciu, M. S.; Navarro, O.; Germaneau, R. F.; Kelly, R. A.; Sommer, W.; Marion, N.; Stevens, E. D.;

        Cavallo, L.; Nolan, S. P. Synthetic and Structural Studies of (NHC)Pd(Allyl)Cl Complexes (NHC = N-

        Heterocyclic Carbene). *Organometallics* **2004**, *23* (7), 1629–1635.

        https://doi.org/10.1021/om034319e.

(14)   Gaillard, S.; Bantreil, X.; Slawin, A. M. Z.; Nolan, S. P. Synthesis and Characterization of IPrMe-

        Containing Silver(I), Gold(I) and Gold(III) Complexes. *Dalton Transactions* **2009**, No. 35, 6967–

        6971. https://doi.org/10.1039/B907109A.

(15)   Falivene, L.; Credendino, R.; Poater, A.; Petta, A.; Serra, L.; Oliva, R.; Scarano, V.; Cavallo, L.

        SambVca 2. A Web Tool for Analyzing Catalytic Pockets with Topographic Steric Maps.

        Organometallics **2016**, *35* (13), 2286–2293. https://doi.org/10.1021/acs.organomet.6b00371.

(16)   Howard, K. E.; Rauchfuss, T. B.; Rheingold, A. L. Organometallic Derivatives of the

         Tetrathiometallates. Syntheses, Structures, and Reactions of MS4[Rh(COD)]2 and

         MS4[(C5H5)Ru(PPh3)]2 (M = Mo, W). *J Am Chem Soc* **1986**, *108* (2), 297–299.

         https://doi.org/10.1021/ja00262a020.

(17)   Siedle, A. R.; Gleason, W. B. Ternary Rhodium-Tungsten-Sulfur Clusters. *Inorg Chem* **1986**, *25*

         (22), 4054–4057. https://doi.org/10.1021/ic00242a046.

(18)   Howard, K. E.; Rauchfuss, T. B.; Wilson, S. R. Synthesis, Structure, and Reactivity of

         Organoruthenium Derivatives of Tetrathio- and Tetraselenometalates. *Inorg Chem* **1988**, *27* (10),

         1710–1716. https://doi.org/10.1021/ic00283a011.

(19)   Müller, A.; Diemann, E.; Jostes, R.; Bögge, H. Transition Metal Thiometalates: Properties and

         Significance in Complex and Bioinorganic Chemistry. *Angewandte Chemie International Edition

         in English* **1981**, *20* (11), 934–955. https://doi.org/https://doi.org/10.1002/anie.198109341.

(20)   Tieckelmann, R. H.; Silvis, H. C.; Kent, T. A.; Huynh, B. H.; Waszczak, J. v; Teo, B.-K.; Averill, B. A.

         Synthetic Molybdenum-Iron-Sulfur Clusters. Preparation, Structures, and Properties of the

         [S2MoS2Fe(SC6H5)2]2- and [S2MoS2FeCl2]2- Ions. *J Am Chem Soc* **1980**, *102* (17), 5550–5559.

         https://doi.org/10.1021/ja00537a022.

(21)   Coucouvanis, D.; Stremple, P.; Simhon, E. D.; Swenson, D.; Baenziger, N. C.; Draganjac, M.; Chan,

         L. T.; Simopoulos, A.; Papaefthymiou, V. Dinuclear Iron-Molybdenum-Sulfur Complexes

         Containing the FeS2Mo Core. Syntheses, Ground-State Electronic Structures and Crystal and

         Molecular Structures of the [(C6H5)4P]2[(C6H5S)2FeS2MoS2], [(C2H5)4N]2[(C6H5S)2FeS2WS2],

         and [(C6H5)4P]2[(S5)FeS2MS2] (M = Mo, W) Complexes. *Inorg Chem* **1983**, *22* (2), 293–308.

         https://doi.org/10.1021/ic00144a020.

(22)   Coucouvanis, D.; Simhon, E. D.; Baenziger, N. C. Successful Isolation of a Reduced

Tetrathiometallate Complex. Synthesis and Structural Characterization of the [(MoS4)2Fe]3-

Trianion. *J Am Chem Soc* **1980**, *102* (21), 6644–6646. https://doi.org/10.1021/ja00541a082.

(23)   Chen, X.; Wu, K.; Snijders, J. G.; Lin, C. Electronic Structures and Nonlinear Optical Properties of

Trinuclear Transition Metal Clusters M–(μ-S)–M' (M = Mo, W; M' = Cu, Ag, Au). *Inorg Chem*

2003, *42* (2), 532–540. https://doi.org/10.1021/ic025649e.

(24)   Hou, H.-W.; Xin, X.-Q.; Shi, S. Mo (W,V)⬜Cu (Ag)⬜S(Se) Cluster Compounds. *Coord Chem Rev*

1996, *153*, 25–56. https://doi.org/https://doi.org/10.1016/0010-8545(95)01224-9.

(25)   Che, C. M.; Xia, B. H.; Huang, J. S.; Chan, C. K.; Zhou, Z. Y.; Cheung, K. K. Photoluminescent Metal-

Sulfur Clusters Derived from Tetrathiometalates: Metal-to-Metal Charge-Transfer Excited

States of D0-D10 Heterobimetallic   Sulfido Clusters with Bulky Phosphine Ligands. *Chemistry*

(Easton) **2001**, *7* (18), 3998–4006. https://doi.org/10.1002/1521-

3765(20010917)7:18<3998::aid-chem3998>3.0.co;2-h.

(26)   Gili, P.; Tsipis, A. C. Electronic Structure Calculations on Multiply Charged Anions Containing M⬜S

Bonds (M = Cr, Mo, W) and Their Heterobimetallic Cluster Complexes. *Int J Quantum Chem*

2007, *107* (2), 418–439. https://doi.org/https://doi.org/10.1002/qua.21087.

(27)   Chen, X.; Wu, K.; Snijders, J. G.; Lin, C. Electronic Structures and Nonlinear Optical Properties of

Trinuclear Transition Metal Clusters M–(μ-S)–M' (M = Mo, W; M' = Cu, Ag, Au). *Inorg Chem*

2003, *42* (2), 532–540. https://doi.org/10.1021/ic025649e.

(28)   Charnock, J. M.; Bristow, S.; Nicholson, J. R.; Garner, C. D.; Clegg, W. Preparations, Crystal

Structures, and Molybdenum-95 Nuclear Magnetic Resonance Spectroscopic Studies of

Triphenylphosphine–Gold–Tetrathiomolybdate(VI) Clusters. *Journal of the Chemical Society,*

Dalton Transactions **1987**, No. 2, 303–306. https://doi.org/10.1039/DT9870000303.

(29)   Kinsch, E. M.; Stephan, D. W. Synthesis and Crystal and Molecular Structure of MoS4(AuPEt3)2:

A Linear Trinuclear Heterobimetallic Species. *Inorganica Chim Acta* **1985**, *96* (2), L87–L90.

https://doi.org/https://doi.org/10.1016/S0020-1693(00)87570-2.

(30)   Poater, A.; Cosenza, B.; Correa, A.; Giudice, S.; Ragone, F.; Scarano, V.; Cavallo, L. SambVca: A

Web Application for the Calculation of the Buried Volume of N-Heterocyclic Carbene Ligands.

Eur J Inorg Chem **2009**, *2009* (13), 1759–1766.

https://doi.org/https://doi.org/10.1002/ejic.200801160.

(31)   Frisch, M. J.; Trucks, G. W.; Schlegel, H. B.; Scuseria, G. E.; Robb, M. A.; Cheeseman, J. R.;

Scalmani, G.; Barone, V.; Petersson, G. A.; Nakatsuji, H.; Li, X.; Caricato, M.; Marenich, A. v;

Bloino, J.; Janesko, B. G.; Gomperts, R.; Mennucci, B.; Hratchian, H. P.; Ortiz, J. v; Izmaylov, A. F.;

Sonnenberg, J. L.; Williams; Ding, F.; Lipparini, F.; Egidi, F.; Goings, J.; Peng, B.; Petrone, A.;

Henderson, T.; Ranasinghe, D.; Zakrzewski, V. G.; Gao, J.; Rega, N.; Zheng, G.; Liang, W.; Hada,

M.; Ehara, M.; Toyota, K.; Fukuda, R.; Hasegawa, J.; Ishida, M.; Nakajima, T.; Honda, Y.; Kitao, O.;

Nakai, H.; Vreven, T.; Throssell, K.; Montgomery Jr, J. A.; Peralta, J. E.; Ogliaro, F.; Bearpark, M.

J.; Heyd, J. J.; Brothers, E. N.; Kudin, K. N.; Staroverov, V. N.; Keith, T. A.; Kobayashi, R.; Normand,

J.; Raghavachari, K.; Rendell, A. P.; Burant, J. C.; Iyengar, S. S.; Tomasi, J.; Cossi, M.; Millam, J. M.;

Klene, M.; Adamo, C.; Cammi, R.; Ochterski, J. W.; Martin, R. L.; Morokuma, K.; Farkas, O.;

Foresman, J. B.; Fox, D. J. Gaussian 16 Rev. C.01. Wallingford, CT 2016.

(32)   Weigend, F.; Ahlrichs, R. Balanced Basis Sets of Split Valence, Triple Zeta Valence and Quadruple

Zeta Valence Quality for H to Rn: Design and Assessment of Accuracy. *Physical Chemistry

Chemical Physics* **2005**, *7* (18), 3297–3305. https://doi.org/10.1039/B508541A.

(33)   Ahlrichs, R.; May, K. Contracted All-Electron Gaussian Basis Sets for Atoms Rb to Xe. *Physical

Chemistry Chemical Physics* **2000**, *2* (5), 943–945. https://doi.org/10.1039/A908859H.

(34)   Andrae, D.; Häußermann, U.; Dolg, M.; Stoll, H.; Preuß, H. Energy-Adjustedab Initio

Pseudopotentials for the Second and Third Row Transition Elements. *Theor Chim Acta* **1990**, *77*

(2), 123–141. https://doi.org/10.1007/BF01114537.

(35)   Becke, A. D. Density-Functional Exchange-Energy Approximation with Correct Asymptotic

Behavior. *Phys Rev A (Coll Park)* **1988**, *38* (6), 3098–3100.

https://doi.org/10.1103/PhysRevA.38.3098.

(36)   Lee, C.; Yang, W.; Parr, R. G. Development of the Colle-Salvetti Correlation-Energy Formula into

a Functional of the Electron Density. *Phys Rev B* **1988**, *37* (2), 785–789.

https://doi.org/10.1103/PhysRevB.37.785.

(37)   Poater, A.; Ragone, F.; Mariz, R.; Dorta, R.; Cavallo, L. Comparing the Enantioselective Power of

Steric and Electrostatic Effects in Transition-Metal-Catalyzed Asymmetric Synthesis. *Chemistry –

A European Journal* **2010**, *16* (48), 14348–14353.

https://doi.org/https://doi.org/10.1002/chem.201001938.

(38)   Kelly III, R. A.; Clavier, H.; Giudice, S.; Scott, N. M.; Stevens, E. D.; Bordner, J.; Samardjiev, I.; Hoff,

C. D.; Cavallo, L.; Nolan, S. P. Determination of N-Heterocyclic Carbene (NHC) Steric and

Electronic Parameters Using the [(NHC)Ir(CO)2Cl] System. *Organometallics* **2008**, *27* (2), 202–

210. https://doi.org/10.1021/om701001g.

(39)   Clavier, H.; Nolan, S. P. Percent Buried Volume for Phosphine and N-Heterocyclic Carbene

Ligands: Steric Properties in Organometallic Chemistry. *Chemical Communications* **2010**, *46* (6),

841–861. https://doi.org/10.1039/B922984A.

(40)   Catherine E. Housecroft; Alan G. Sharpe. Inorganic Chemistry. In *Structures and energetics of

metallic and ionic solids*; Pearson Education limited: Harlow, 2018; pp 182–183.

(41)   Alvarez, S. A Cartography of the van Der Waals Territories. *Dalton Transactions* **2013**, *42* (24),

8617–8636. https://doi.org/10.1039/C3DT50599E.

(42)   Cheeseman, J. R.; Trucks, G. W.; Keith, T. A.; Frisch, M. J. A Comparison of Models for Calculating

         Nuclear Magnetic Resonance Shielding Tensors. *J Chem Phys* **1996**, *104* (14), 5497–5509.

         https://doi.org/10.1063/1.471789.

(43)   Wolinski, K.; Hinton, J. F.; Pulay, P. Efficient Implementation of the Gauge-Independent Atomic

         Orbital Method for NMR Chemical Shift Calculations. *J Am Chem Soc* **1990**, *112* (23), 8251–8260.

         https://doi.org/10.1021/ja00179a005.

(44)   Xamonaki, N.; Asimakopoulos, A.; Balafas, A.; Dasenaki, M.; Choinopoulos, I.; Coco, S.;

         Simandiras, E.; Koinis, S. Tetrathiomolybdate Complexes of Rhodium(I) with Molybdenum–

         Rhodium Interactions. *Inorg Chem* **2016**, *55* (10), 4771–4781.

         https://doi.org/10.1021/acs.inorgchem.6b00072.

CHAPTER 4

RELATIVE REACTIVITY OF [MoS$_4$(AuL)$_2$] (C-1 – C-5) WITH THIOPHENOL AND SELENOPHENOL;

IMPLICATIONS FOR POTENTIAL ANTIMICROBIAL AND ANTICANCER ACTIVITY

4.1. Introduction

Metal-based drugs are of current interest for antimicrobial and anticancer therapy. Many scientists are motivated to develop new drugs that will overcome the increasing drug resistance shown by different type of cancers, bacteria, and fungi. Heterometallic clusters have the potential to overcome drug resistance and improve the activity of the metal-based drugs by a synergistic or cooperative effect of the combined metal, multiple mechanism of action, higher stability and/ or specific delivery of the active moieties to limited targets.[1,2] Some heterometallic clusters have been investigated for therapeutic purposes by incorporation of two different cytotoxic metals within the same molecule and have shown a promising activity.[3–5]
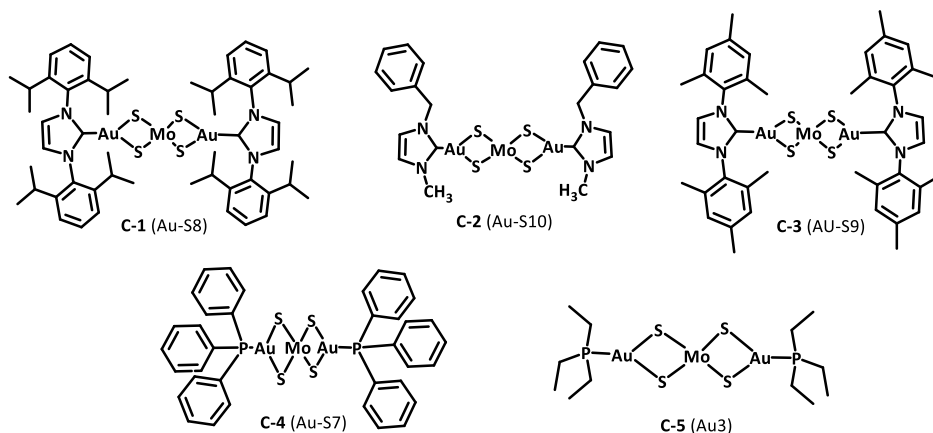
Scheme 4.1. Au-Mo-S clusters. The labels in parenthesis correspond to the abbreviation used in the published article in Appendix E.[6]

The clusters discussed in this thesis and in Scheme 4.1 were sent to the Community for Open Antimicrobial Drug Discovery initiative (CO-ADD, co-add.org) funded by The Wellcome Trust and the University of Queensland. CO-ADD offers free antimicrobial screening to chemists around the world.[7]

The initial screening for antimicrobial activity involved testing against five bacterial and two fungal pathogens commonly associated with antimicrobial resistance, as well as two types of healthy cells used to measure the cytotoxicity (Table 4.1). Antimicrobial activity was measured by minimum inhibitory concentration (MIC) which is defined as the lowest concentration of a complex (μg/mL) at which the growth of a microbe was inhibited by ≥80% (equivalent to no visible growth, i.e. cloudiness, by the eye). Toxicity against human embryonic kidney cells ((HEK-293) was measured by the concentration causing death of 50% of the viable cells (CC_{50}). Hemolysis (HC_{10}) was determined by the concentration of complex causing 10% hemolysis of human blood.[6]

Table 4.1. MIC, CC_{50} and HC_{10} values for the clusters (values given in μg/mL).

Cluster	G-ve (MIC)				G+ve (MIC)	Fungi (MIC)		HEK	RBC
	Ab	Ec	Kp	Pa	Sa	Ca	Cn	CC_{50}	HC_{10}
C-1	>32	>32	>32	>32	>32	>32	>32	n.d.	n.d.
C-2	>32	>32	>32	>32	>32	≤0.25	>32	>32	>32
C-3	>32	>32	>32	>32	>32	>32	>32	n.d.	n.d.
C-4	>32	>32	>32	>32	>32	>32	>32	n.d.	n.d.
C-5	>32	>32	>32	>32	≤0.25	16	≤0.25	>32	>32

Gram negative (G-ve) and Gram-positive (G+ve) bacteria; **Ab**, *Acinetobacter baumannii* ATCC 19606 type strain; **Ec**, *Escherichia coli* ATCC 25922 FDA control strain; **Kp**, *Klebsiella pneumoniae* ATCC 700603 ESBL; **Pa**, *Pseudomonas aeruginosa* ATCC 27853 QC control strain; **SA**, *methicillin-resistant Staphylococcus aureus* ATCC 43300; **Ca**, *Candida albicans* ATCC 90028 NCCLS11; **Cn**, *Cryptococcus neoformans* H99 ATCC 208821 type strain; **HEK**, HEK-293 human embryonic kidney cells ATCC CRL-1573; **RBC**, human red blood cells. N.d., not determined.

Clusters **C-1** – **C-5** were part of a set of 1039 metal based complexes submitted by research groups all around the world, which were subjected to the initial screening. Cluster complexes **C-1** – **C-5** were the only heteronuclear, bimetallic complexes tested and the only ones containing molybdenum.[6] Out of the original 1039 complexes, 90 showed good activity against at least one fungal strain (MIC = 16 μg/ mL), had no cytotoxicity against HEK-293 (CC50 > 32 μg/ mL) and < 10% hemolysis of red blood cells at concentrations ≥ 32 μg/ mL. From this group, 320 complexes were classified as having "high" antifungal activity, defined as MIC < 2 μg/ mL. Cluster complexes **C-2** and **C-5** were in this group of highly active and low toxicity compounds.

95

Notably, the nature of ligands in the clusters had a dramatic effect on the reactivity. Cluster **C-4** with PPh₃ ligands was completely inactive while **C-5** with PEt₃ was defined as having "high" antifungal activity. Similarly **C-1** and **C-3** with aliphatic substituents on the phenyl rings, were less active than **C-2**, which has an unsubstituted phenyl and a methyl substituent on each NHC ligand. As shown in Table 4.1 **C-2** showed "high" activity against **Ca** (*Candida albicans)* and **C-5** showed high activity against **SA** and **Cn** (*Methicillin resistant Staphylococcus aureus, Cryptococcus neoformans*), and good activity against **Ca**.

Cluster **C-5** was selected for further testing against an extended panel of fungal strains. There was good activity as shown in Table 4.2 against *Candida auris, Cryptococcus deuterogattii,* and *Cryptococcus neoformans.* However, since there was a wide variation in replicates, this complex was not advanced to the next level of testing in an *in vivo*, moth larvae model. Nevertheless, the low toxicity combined with indications of structure-activity relations in the ligands suggest that further investigation to understand the reactivity of the $[MoS_4(AuL)_2]$ clusters is warranted.

Table 4.2. Cytotoxicity of **C-5** against an extended panel of fungal strains (MIC ≥ 50 % inhibition in µM).[6]

Fungi	MIC (µM)
Candida albicans	50 – 200
Candida auris	3.13 – 6.25*
Candida glabrata	100 - 200
Cryptococcus deuterogattii	3.12 – 6.25*
Cryptococcus neoformans	3.12 – 6.25*

* MIC values that were inactive or gave a wide replicate variation when analyzed for ≥ 80 % inhibition (optically clear to slightly hazy). These were re-analyzed at 50% inhibition and gave more consistent and active values, Appendix E.

Gold(I) complexes have been found to undergo ligand exchange reactions in biological systems (Scheme 4.2).[8] Upon administering a gold(I) complex to cells, the ligand exchange process has been documented with Cys34 of serum albumin (SA) to create gold(I)-SA adducts.[9] It has been proposed that SA could work as a drug "scavenger" or as a drug carrier.[10,11] Moreover, Sadler and colleagues reported that auxiliary ligands affect the thermodynamic stability of gold(I) complexes.[8] Most likely there is not a

single mode of action given the wide variety of ligands and structures for medicinally active gold

compounds. Fortunately, some trends can be used to understand the general biological effect of gold

complexes. For example, enzymes and proteins with thiol- and selenol- containing amino acids are

particularly susceptible to attack by gold complexes. This targeting property is a result of the high

affinity of Au(I) for S and Se. Many thiol- and/ or selenol- containing enzymes, including glutathione

reductase (GR), cysteine protease, and thioredoxin reductases (TrxR), are overexpressed in cancer cells

and may therefore serve as prospective targets for gold(I)-based cancer therapies.[12,13] Auranofin and a

wide range of other gold(I) compounds containing phosphine (monodentate and bidentate) and NHC

ligands have now been shown to inhibit TrxR, which could be due to the strong covalent binding of the

gold center to a selenocysteine residue in the active site of the TrxR enzyme.[14–20]

$$R''S^{\ominus} \cdots R\text{—}Au\text{—}SR' \longrightarrow R\text{—}Au\text{—}SR'' + SR'^{\ominus} \xrightarrow{+R''S^{\ominus}} \left[R''S\text{—}Au\text{—}SR'' \right]^{\ominus} + R$$
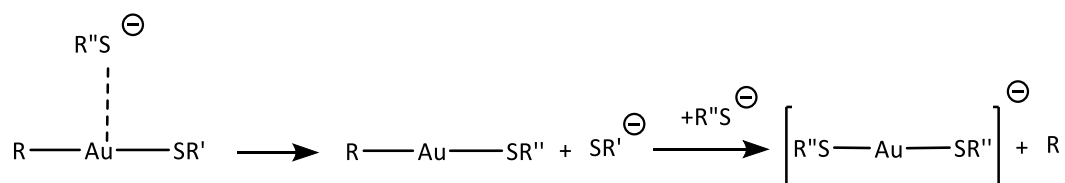
Scheme 4.2. Ligand exchange reaction of gold(I) complexes with thiolate.

The objective of the work described in this chapter is to investigate the relative reactivity of **C-1** – **C-5** with benzenethiol and benzeneselenol and to gain insight into the possible mechanism of action of

these heterometallic clusters, related to coordinating to thiol-containing and selenol-containing

proteins. Benzenethiol (PhSH) and benzeneselenol (PhSeH) were used as models for thiol or selenol

functionalities in proteins. This decision was made because alkyl selenols, such as selenocysteine, are

more rapidly oxidized in air and from diselenide. Bagno and co-workers proposed the same model of

benzenethiol (PhSH) and benzeneselenol (PhSeH) to mimic the interaction of auranofin with thiol and

selenol nucleophiles present in TrxR.[21] This is the first report of the reactivity of [MoS$_4$(AuL)$_2$] clusters

with thiol or selenol nucleophiles. The reactivity of   **C-1** – **C-5** with PhSH and PhSeH was investigated by

^{1}H NMR and ^{31}P NMR (for **C-4** and **C-5**) spectroscopy. Results are analyzed in terms of the steric effects of the ligands and the electronic structure of [MoS$_4$(AuL)$_2$] clusters as discussed in chapter 3.

4.2. Experimental Section

4.2.1. General Consideration

The synthesis of the L-Au(I)-Cl complexes, **C-1**, **C-2**, **C-3**, **C-4**, and **C-5** are described in Chapter 2. Benzenethiol (PhSH, 97%), benzeneselenol (PhSeH, 97%), and potassium carbonate (K$_2$CO$_3$, 99%) were obtained from Sigma-Aldrich and used as received. Diethyl ether (Et$_2$O), acetone (CH$_3$COCH$_3$), heptane (C$_7$H$_{16}$), and methylene chloride (CH$_2$Cl$_2$) were purchased from Fisher Scientific. Deuterated solvents: dichloromethane-d_2 (CH$_2$Cl$_2$-d_2), and dimethyl sulfoxide-d_6 (DMSO-d_6) were purchased from Cambridge Isotope Laboratories, Inc.

^{1}H NMR, and ^{31}P{^{1}H} NMR spectra were obtained on a Bruker Avance NEO 500 MHz NMR spectrometer at room temperature. The chemical shifts of ^{1}H NMR and ^{13}C NMR were referenced to residual signals of the deuterated solvents. ^{31}P{^{1}H} NMR spectra were referenced to 85% H$_3$PO$_4$ (external standard).

4.2.2. General Synthesis of L-Au-SPh and L-Au-SePh (L = PPR$_3$ or NHC)

All the complexes in Scheme 4.3 were prepared by weighing the appropriate L-Au(I)-Cl complex (0.3 mmol) into a Schlenk flask and placing it under nitrogen. Separately, K$_2$CO$_3$ (0.4 mmol) was weighed into another Schlenk flask and placed under nitrogen. Acetone (100 mL) was purged with nitrogen and then 50 mL was transferred via cannula to the flask containing the L-Au(I)-Cl complex, and 10 mL was transferred via cannula to the flask containing K$_2$CO$_3$. PhSH or PhSeH (0.3 mmol), respectively, was added slowly using a glass syringe to the K$_2$CO$_3$, solution. After 15 min., the thiolate or selenate solutions were added to the gold(I) solution and stirred for 16 hours. The solvent was removed under vacuum. CH$_2$Cl$_2$ (5 mL) was added and then the solution was filtered in air through a thin pad of silica and

washed with 2 mL of CH_2Cl_2. The volume of the solution was reduced to 2 mL under vacuum, Et_2O (2 mL) was added, and the solution was left in the freezer (-15 °C) for 24 hours. A white solid was collected by filtration, washed with Et_2O (5mL) and dried under vacuum. The **CS-1** and **CS-5** complexes in Scheme 4.3 have been previously prepared and their ^{1}H NMR matched the literature values.[22,23] **CSe-1**, **CS-2**, **CS-3**, **CSe-3**, and **CSe-5** have not been reported, and **CSe-2** was not prepared successfully. All the complexes were characterized by ^{1}H NMR, and ^{31}P{^{1}H} NMR. These complexes were prepared to aid analysis of ^{1}H NMR and ^{31}P{^{1}H} NMR spectra for the reactions between **C-1**, **C-2**, **C-3**, **C-4**, and **C-5** clusters and PhSH or PhSeH.
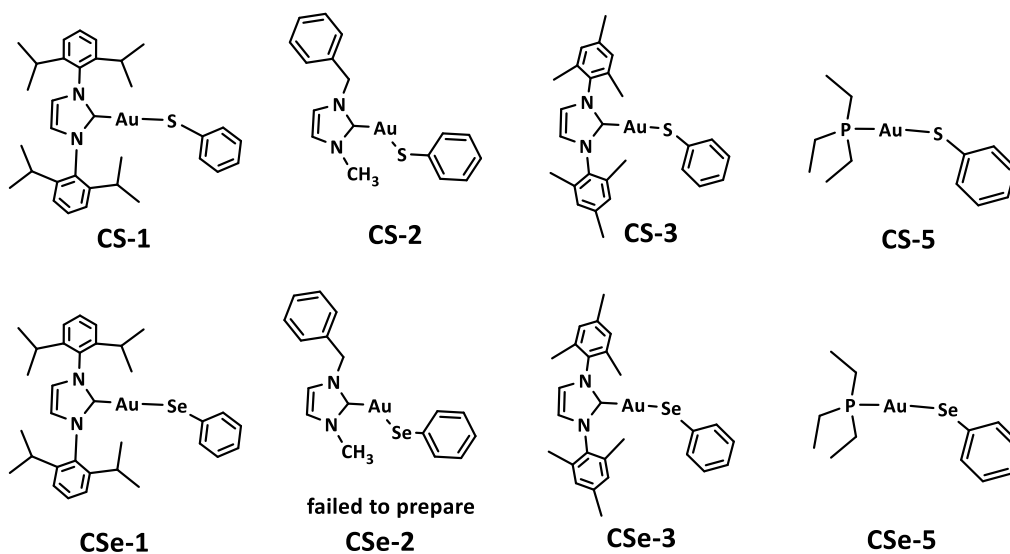
Scheme 4.3. Chemical structure of L-Au-SPh and L-Au-SePh prepared complexes.

4.2.2.1. Synthesis of CSe-1

A mixture of Au(IPr)Cl (0.19 gm, 0.3 mmol), PhSeH (32 μL, 0.3 mmol), and K_2CO_3 (0.05 gm, 0.36 mmol) in acetone (60 mL) was stirred for 16 hours. Yield 0.18 gm (80 %). δ ^{1}H NMR (500 MHz, DMSO-d_6) 7.99 (2 H, s), 7.59 (2 H, t, *J 7.8*), 7.42 (4 H, d, *J 7.8*), 6.95 – 6.58 (5 H, m), 2.56 (4 H, hept, *J 6.6*), 1.23 (24 H, dd, *J 21.4*, 6.9) (Figure 4.1).

CSe-1
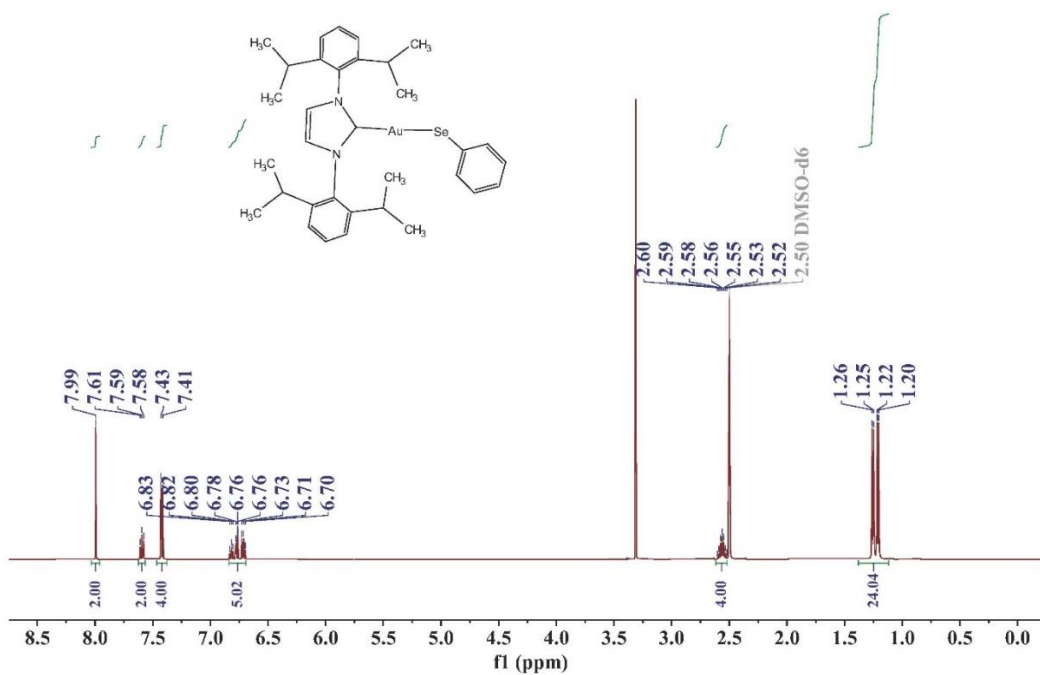
Figure 4.1. ^{1}H-NMR of **CSe-1** in DMSO-d_6 (H$_2$O 3.33 ppm).

4.2.2.2. Synthesis of CS-2

A mixture of Au(IBzMe)Cl (0.12 gm, 0.3 mmol), PhSH (31 µL, 0.3 mmol), and K$_2$CO$_3$ (0.05 gm, 0.36 mmol) in acetone (60 mL) was stirred for 16 hours. Yield 0.06 gm (41 %). δ ^{1}H NMR (500 MHz, DMSO-d_6) 7.56 (1 H, d, *J* 2.0), 7.47 (1 H, d, *J* 1.8), 7.40 – 7.28 (7 H, m), 6.98 (2 H, t, *J* 7.7), 6.86 (1 H, t, *J* 7.3), 5.38 (2 H, s), 3.80 (3 H, s)(Figure 4.2).
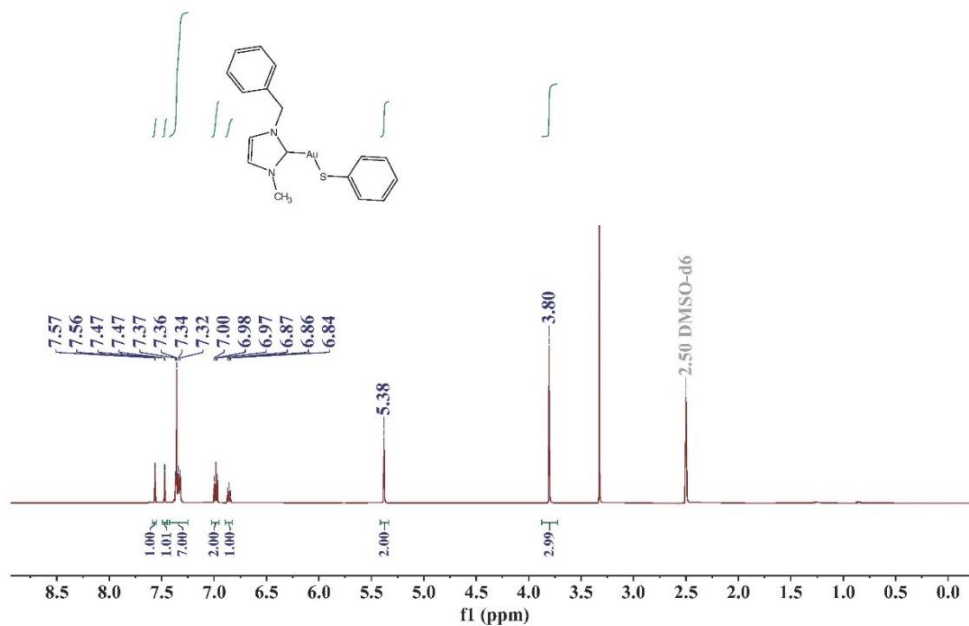
Figure 4.2. ^{1}H NMR of **CS-2** in DMSO-d_6 (H$_2$O 3.33 ppm).

4.2.2.3. Synthesis of CSe-2

A mixture of of Au(IBzMe)Cl (0.12 gm, 0.3 mmol), PhSeH (32 µL, 0.3 mmol), and K$_2$CO$_3$ (0.05 gm, 0.36 mmol) in acetone (60 mL) was stirred for 16 hours. A transparent viscous mixture of two or three products was obtained, which was not possible to separate. Yield 0.07 gm (45 %). δ ^{1}H NMR (500 MHz, DMSO-d_6) 7.65 − 7.60 (m), 7.56 (d, J 1.9), 7.52 (d, J 1.9), 7.46 (d, J 1.9), 7.40 − 7.10 (m), 6.96 (d, J 6.3), 5.37 (s), 3.81 (s) (Figure 4.3).
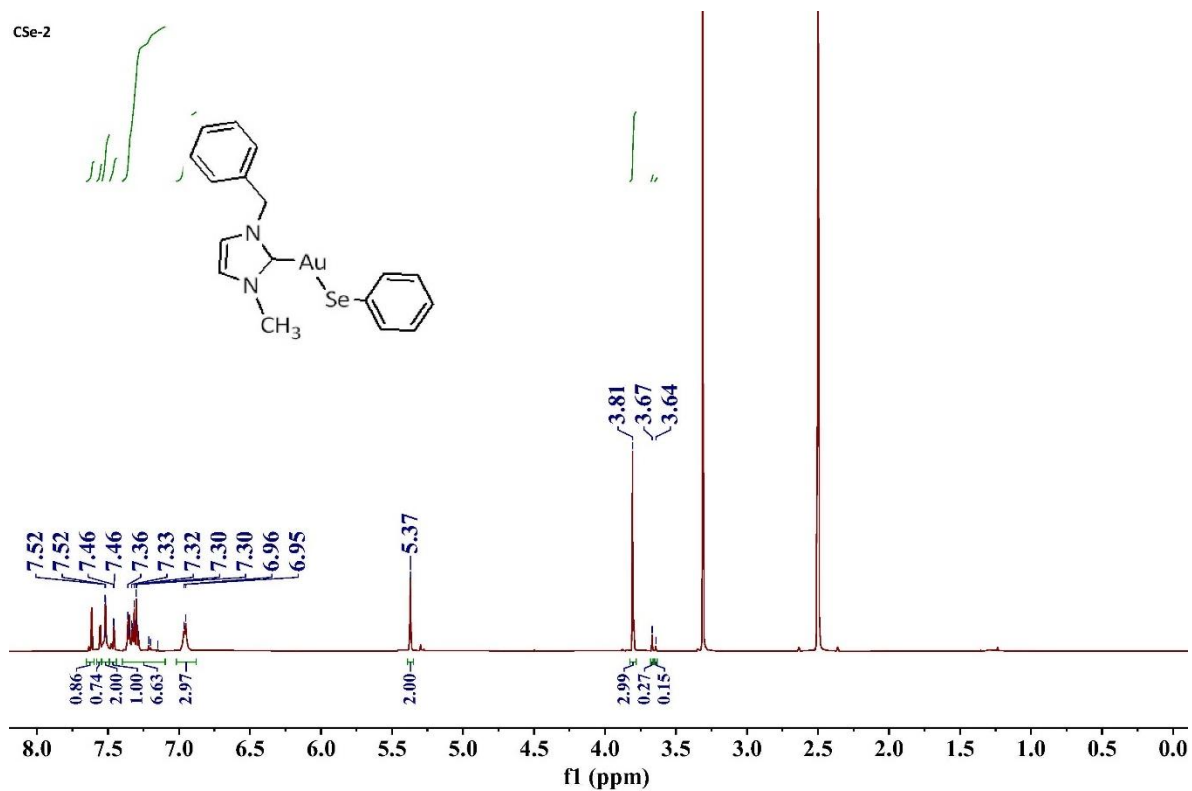
Figure 4.3. ^{1}H NMR of expected **CSe-2** in DMSO-d_6 (H$_2$O 3.33 ppm).

4.2.2.4. Synthesis of CS-3

A mixture of Au(IMes)Cl (0.16 gm, 0.3 mmol), PhSH (31 μL, 0.3 mmol), and K$_2$CO$_3$ (0.05 gm, 0.36 mmol) in acetone (60 mL) was stirred for 16 hours. Yield 0.06 gm (41 %). δ ^{1}H NMR (500 MHz, DMSO-d_6) 7.81 (2 H, s), 7.15 (4 H, s), 6.82 – 6.71 (5H, m), 2.35 (6 H, s), 2.10 (12 H, s) (Figure 4.4).
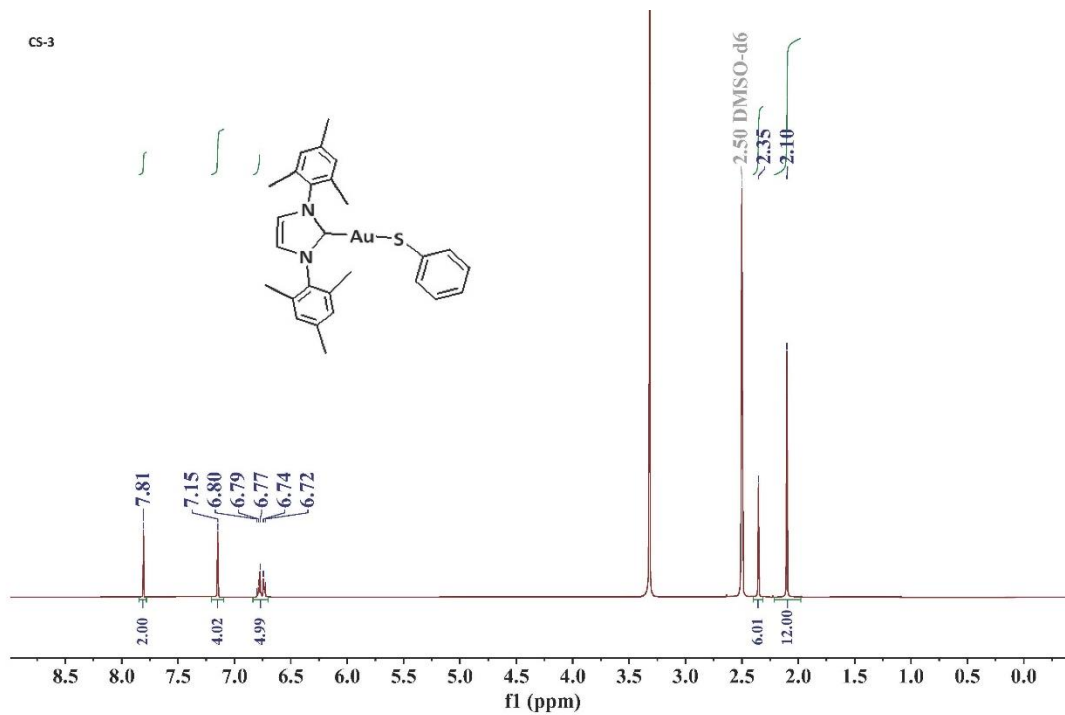
Figure 4.4. ^{1}H NMR of **CS-3** in DMSO-d_6 (H$_2$O 3.33 ppm).

4.2.2.5. Synthesis of CSe-3

A mixture of Au(IMes)Cl (0.16 gm, 0.3 mmol), PhSeH (32 μL, 0.3 mmol), and K$_2$CO$_3$ (0.05 gm, 0.36 mmol) in acetone (60 mL) was stirred for 16 hours. Yield 0.08 gm (42 %). δ ^{1}H NMR (500 MHz, DMSO-d_6) 7.80 (2 H, s), 7.14 (4 H, s), 6.93 – 6.84 (3 H, m), 6.77 (2 H, t, *J* 7.3), 2.35 (6H, s), 2.10 (12 H, s) (Figure 4.5).
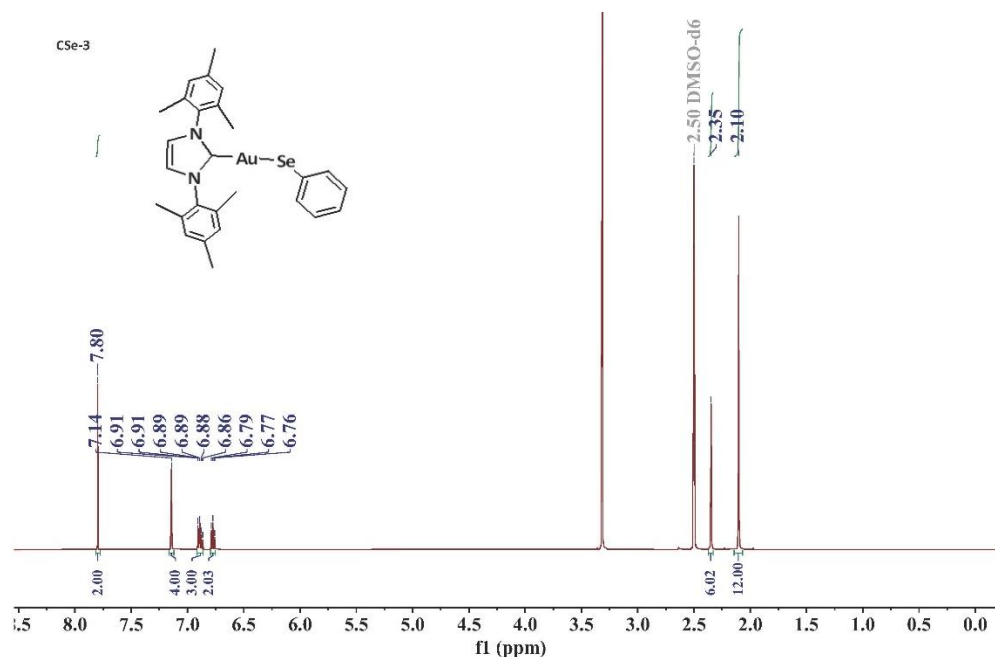
Figure 4.5. ^{1}H NMR of **CSe-3** in DMSO-d_6 (H$_2$O 3.33 ppm).

4.2.2.6. Synthesis of CSe-5

A mixture of Et$_3$PAuCl (0.10 gm, 0.3 mmol), PhSeH (32 μL, 0.3 mmol), and K$_2$CO$_3$ (0.05 gm, 0.36 mmol) in acetone (60 mL) was stirred for 16 hours. Yield 0.06 gm (43 %). δ ^{1}H NMR (500 MHz, DMSO-d_6) 7.53 – 7.48 (2 H, m), 7.08 – 6.99 (3 H, m), 1.93 (6 H, dq, J 10.2, 7.6), 1.13 (9 H, dt, J 18.8, 7.6) (Figure 4.6).δ ^{31}P{^{1}H} NMR (202 MHz, DMSO-d_6) 41.41 ppm (Figure 4.7).
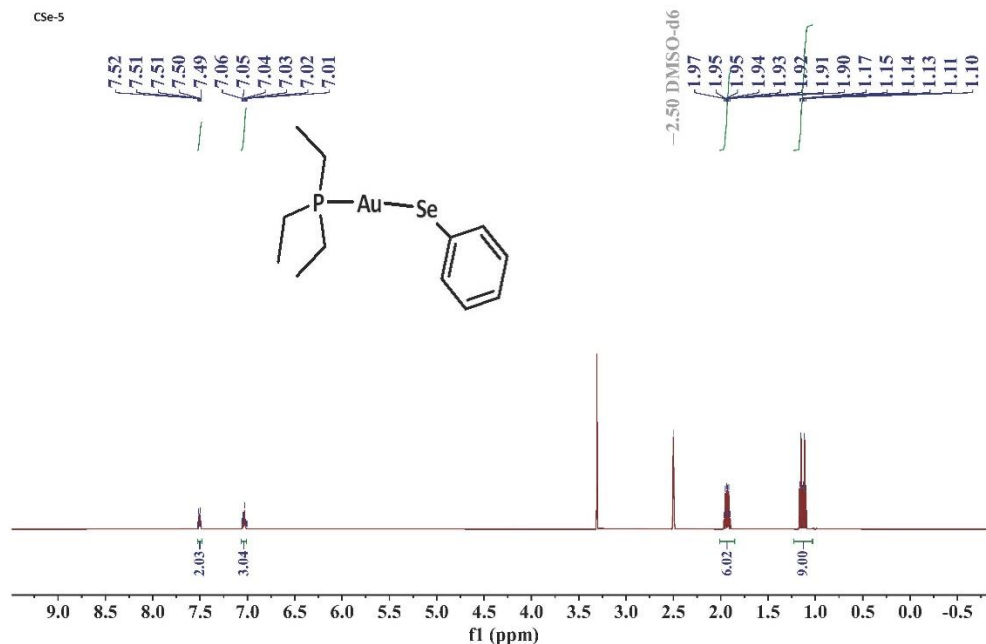
Figure 4.6. ^{1}H NMR of **CSe-5** in DMSO-d_6 (H$_2$O 3.33 ppm).
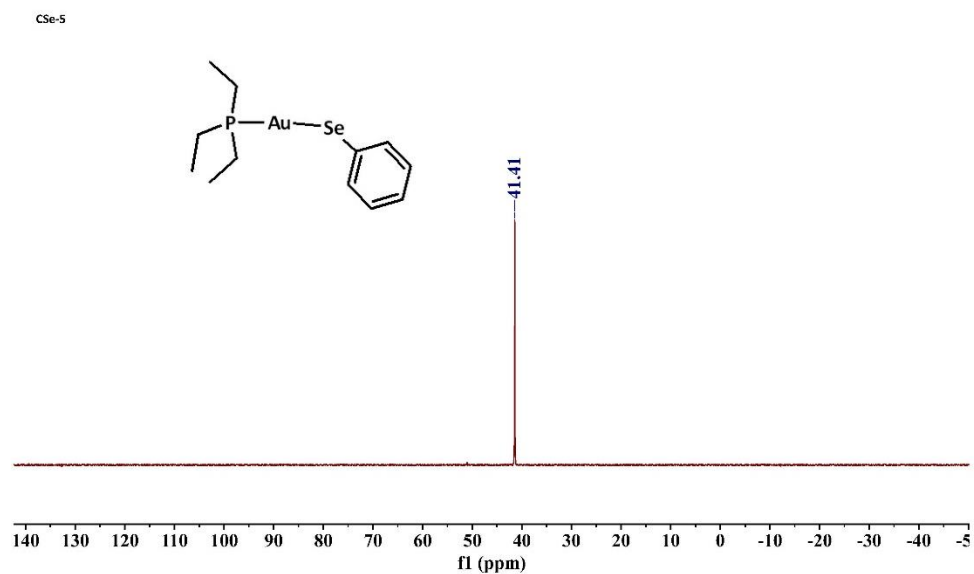
Figure 4.7. ^{31}P{^{1}H} NMR of **CSe-5** in DMSO-d_6, referenced to 85% H$_3$PO$_4$

4.2.3. Synthesis of (C-6; [MoS₄AuIPr][NEt₄])

A solution of Au(IPr)Cl (0.11 gm, 0.17 mmol) in chloroform (10 mL) was added slowly to a solution of

(Et₄N)₂[MoS₄] (0.08 gm, 0.17 mmol) in acetonitrile (7 mL). The mixture was heated under reflux (61°C)

for 2 hours, and then all solvents were evaporated under reduced pressure. The solid was dissolved in acetonitrile (10 mL) and filtered through a funnel with a fritted disc. The filtrate was concentrated to (2 mL) under reduced pressure and diethyl ether (5 mL) was added. The orange solid was filtered through Buchner funnel with fritted disc to yield orange product (0.26gm, 82 %).
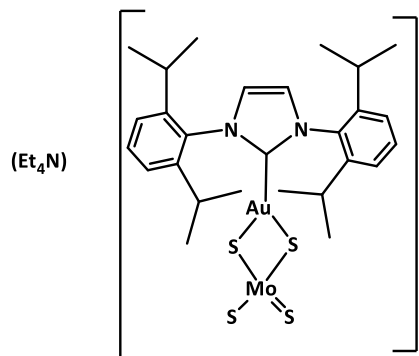
δ ^{1}H NMR (500 MHz, DMSO-d_6) 7.95 (2 H, s), 7.39 (2 H, , t, J 7.7), 7.24 (4 H, d, J 7.8), 3.20 (8 H, q, J 7.3), 2.80 (4 H, hept, J 7.0), 1.23 (12 H, d, J 6.9), 1.20 − 1.10 (24 H, m), Figure 4.8. Anal. Calcd. for MoAuS$_4$N$_3$C$_{35}$H$_{56}$ (940.01): C, 44.72; H, 6.00; N, 4.47. Found: C, 44.69; H, 6.09; N, 4.54. Elemental analysis report (Fig. D.1).

Complex **C-6** is stable as a solid but it converts into **C-1** in solution (DMSO-d_6, CH$_2$Cl$_2$-d_2, CH$_3$CN-d_3) (Figure 4.9). **C-6** was left in solution for 72 hours and the ^{1}H NMR showed about 50% of **C-6** had converted to **C-1**. The 1:1 Au:Mo complexes with the other ligands used in clusters **C-2**, **C-3**, and **C-5** were not possible to separate from the [MoS$_4$(AuL)$_2$] clusters, which also formed in the reaction mixtures. The reaction of PPh$_3$Au-Cl with (Et$_4$N)$_2$[MoS$_4$] did not show evidence of a 1: 1 Au: Mo complex and **C-4** was always formed even when a 1:2 mole ratio of PPh$_3$Au-Cl : [Et$_4$N]$_2$[MoS$_4$] was used.
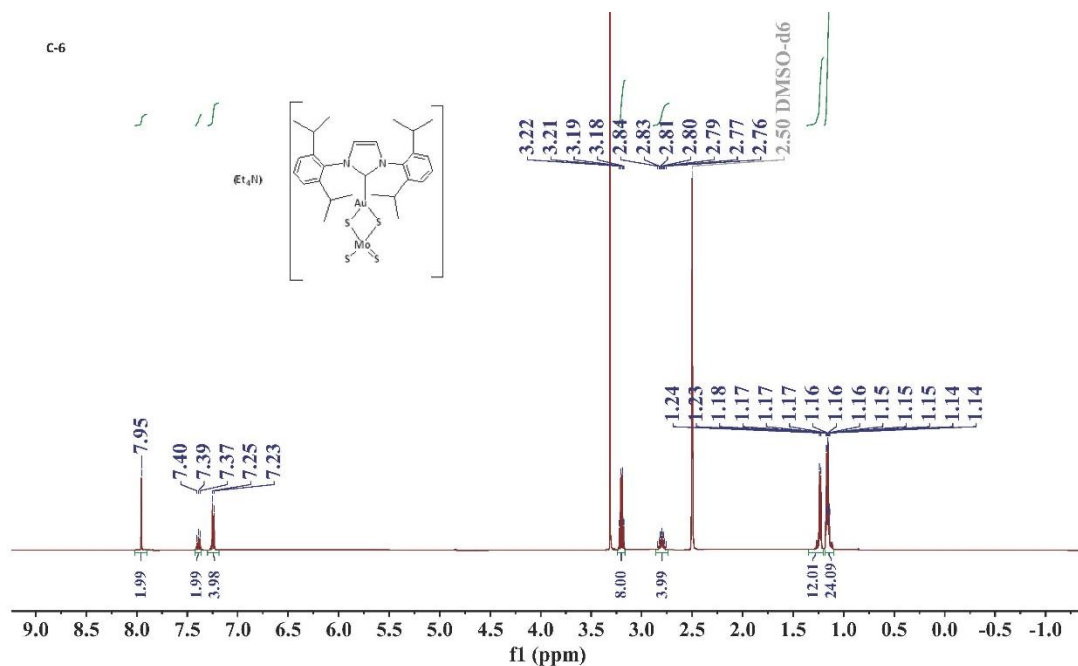
Figure 4.8. ^{1}H NMR of **C-6** in DMSO-d_6 (H$_2$O 3.33 ppm; heptane 1.24-1.14 ppm).
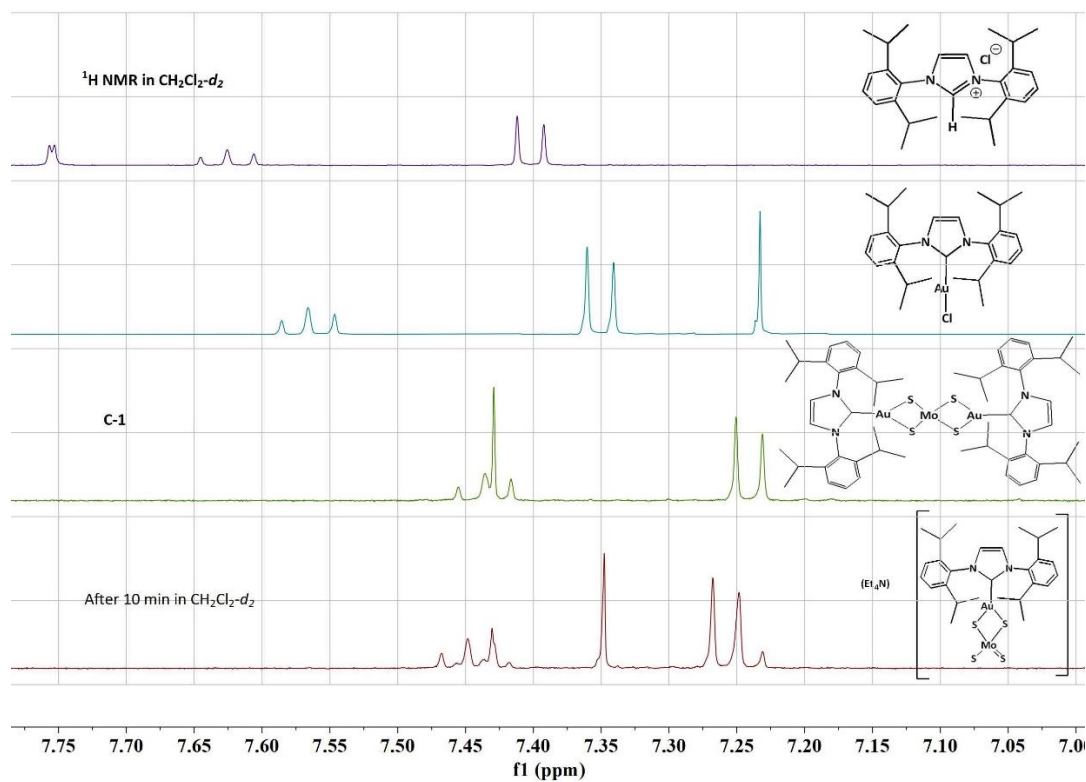
Figure 4.9. Stacked ^{1}H NMR in CH$_2$Cl$_2$-d_2 shows **C-1** formation after 10 min of dissolving **C-6**.

4.2.4. Reactivity procedure

One of the major goals of this work was to compare the relative reactivity of Au-Mo-S clusters with PhSH and PhSeH. All the reactions were done on a small scale using ≤ 2 mL of solvent (DMSO-d_6), and small quantities of each reactant. The procedure summarized in Scheme 4.4 was developed to try to limit the error in the mole ratio of the reactants (Cluster vs PhSH or PhSeH) to less than ± 5%.
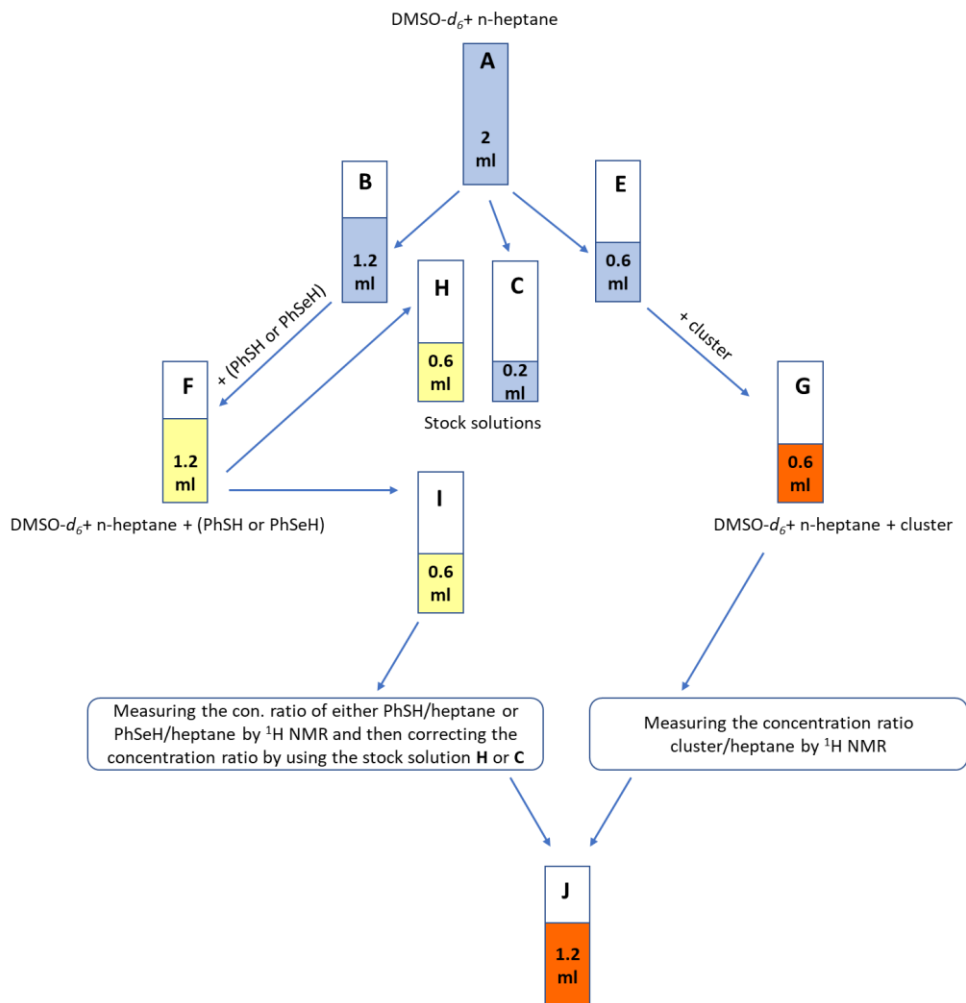
Scheme 4.4. Summary of applied procedure for the reactivity investigations.

Heptane was chosen as an internal standard because it does not react with the reactants or the expected products and moreover, the ^{1}H NMR chemical shifts do not interfere with reactant or product chemical shifts. Heptane (2 μL) was added to 2.0 mL of DMSO-d$_6$. The solution of heptane DMSO-d_6 was

divided into three vials in the amount shown in Scheme 4.4. Two vials were used to prepare a solution of the Au-Mo-S cluster at double the required final concentration and a solution of either PhSH or PhSeH at double the required final concentration. Quantitative ^{1}H NMR was used to ensure that the required concentration ratio of the cluster vs either PhSH or PhSeH was correct by using the heptane integration value. The stock solutions were used to adjust the required concentration ratio of the cluster vs either PhSH or PhSeH and then another quantitative ^{1}H NMR was done to ensure that the right ratio had been achieved. Finally, equal volumes of cluster solution, and either PhSH or PhSeH solution were mixed and the reaction was monitored by ^{1}H NMR.

4.2.5. Procedure for preparing reaction solutions

Each cluster was dissolved in 0.6 mL DMSO-d_6 solution to form a solution concentration of 16 mM (Scheme 4.4, G). A separate solution of PhSH or PhSeH was prepared to form 1.2 mL of a 32 mM solution in DMSO-d_6 (Scheme 4.4, F). The reaction mixture was prepared by adding 0.6 mL of PhSH or PhSeH solution to 0.6 mL of the cluster solution, to give final concentrations of 8 mM cluster and 16 mM PhSH or PhSeH (Scheme 4.4, J). Half (0.6 mL) of the reaction solution was transferred to an NMR tube and a series of spectra were collected over time.

4.2.6. Quantitative ^{1}H NMR

Integrals for reactants and products were normalized to the heptane integrals (Scheme 4.4, G). The ^{1}H NMR spectra acquired at the 10, 20, and 30 min time points were used for the reactivity calculations because they did not show significant disulfide formation or decomposition of the products. Quantitative ^{1}H NMR was used to determine the relative concentrations of compounds in the reaction mixtures. The 90° pulse length and T_1 relaxation time were determined. The longest T_1 relaxation was about 5-6 s for aromatic peaks and the imidazole proton T_1 relaxation was about 3-4 s. The relaxation delay was set to 15 s and the acquisition time was 3.3 s. The phase and baseline were corrected before

taking the integrations. Equation (1) was used to calculate reacted amount of each cluster and the product of each reaction within 10, 20, and 30 minutes. The initial molar concentration of a cluster was calculated by adding the integrations (I) of the unreacted cluster peaks and the gold-containing product peaks at 10 minutes and then dividing the total integrations by the number of nuclei of the cluster (N). The formula below was used to determine the molar ratio M_X / M_Y between two chemicals, X and Y:

$$\frac{M_x}{M_y} = \frac{I_x}{I_y} \times \frac{N_y}{N_x} \quad \text{................ (1)}$$

where (I) is the integral, and (N) is the number of nuclei giving rise to the signal.

The percentage was calculated by using the equation (2):

$$X\% = \frac{M_x}{M_y} \times 100 \text{ ....(2)}$$

where (M_x) represents the relative concentration of the compound under investigation and (M_y) represents the initial relative concentration of a cluster before the reaction. Malz and Jancke, found the accuracy of qNMR to be about 98.5% with parameters optimized as described above. For more accuracy, they described that further parameters should be optimized with the utmost care to attain precision with an error of less than 1.0%.[24,25]

4.3. Results and analyses

4.3.1. Reactions of clusters with PhSH and PhSeH

Benzenethiol and benzeneselenol are expected to react as nucleophiles attacking gold. If two molecules of PhSH or PhSeH react with the cluster we expect the reaction shown in Scheme 4.5, A. Alternatively, if only one PhSH or PhSeH reacts with the clusters, we expect the reaction shown in Scheme 4.5, B.
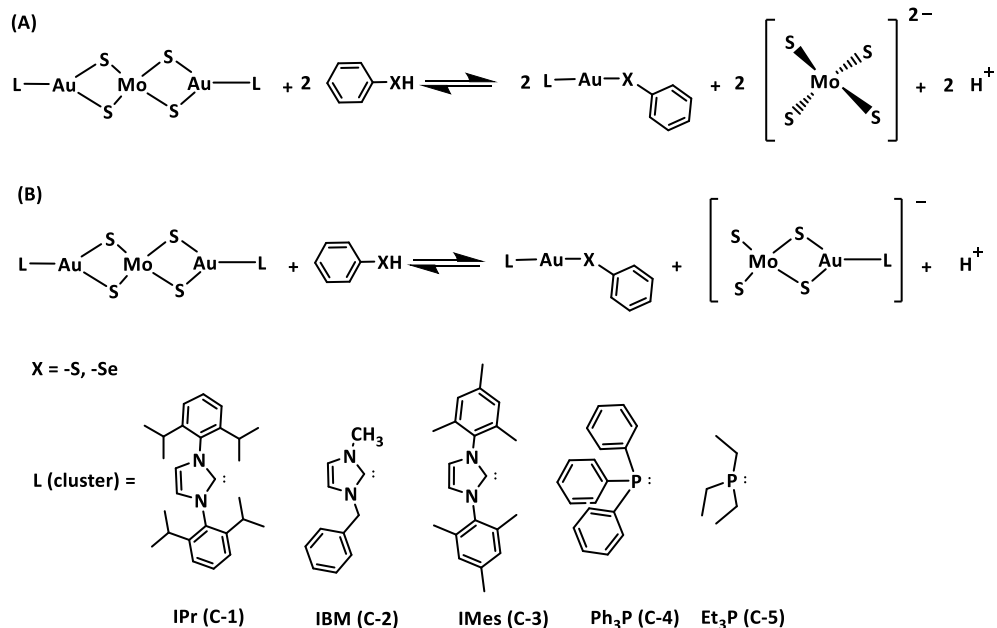
Scheme 4.5. The expected reaction of benzenethiol or benzeneselenol with **C-1 - C-5** clusters, **(A)** two molecules of PhSH or PhSeH react with the clusters, and **(B)** only one PhSH or PhSeH reacts with the clusters.

4.3.1.1. Reaction of C-1 – C-5 with PhSH

Figure 4.10 shows the ^{1}H NMR spectra in the aromatic region for the reaction of **C-1** with PhSH monitored over time. Figure 4.11 shows a stacked plot of spectra at the 40 min time point comparing the reaction mixture with the expected products. The top spectrum in the stacked plot shows a mixture of PhSH and PhSSPh. The disulfide could form via oxidation of the thiol. However, there was no evidence of disulfide formation in the reaction mixture even after 24 hours. Figure 4.12 shows the ^{1}H NMR spectrum of the reaction mixture after 4 hours with peaks assigned as shown in the equation at the top of the figure. It is evident that only one equivalent of PhSH reacts with **C-1** to form (IPr)-Au(SPh) and **C-6** as shown in Figure 4.5, B.

Separate experiments demonstrate that **C-6** is unstable in solution, converting to **C-1** (see Figure 4.9). This can also be seen in Figure 4.10 where the peak at 7.95 ppm, assigned to **C-6** increases in up to about 8 hours and then decreases.
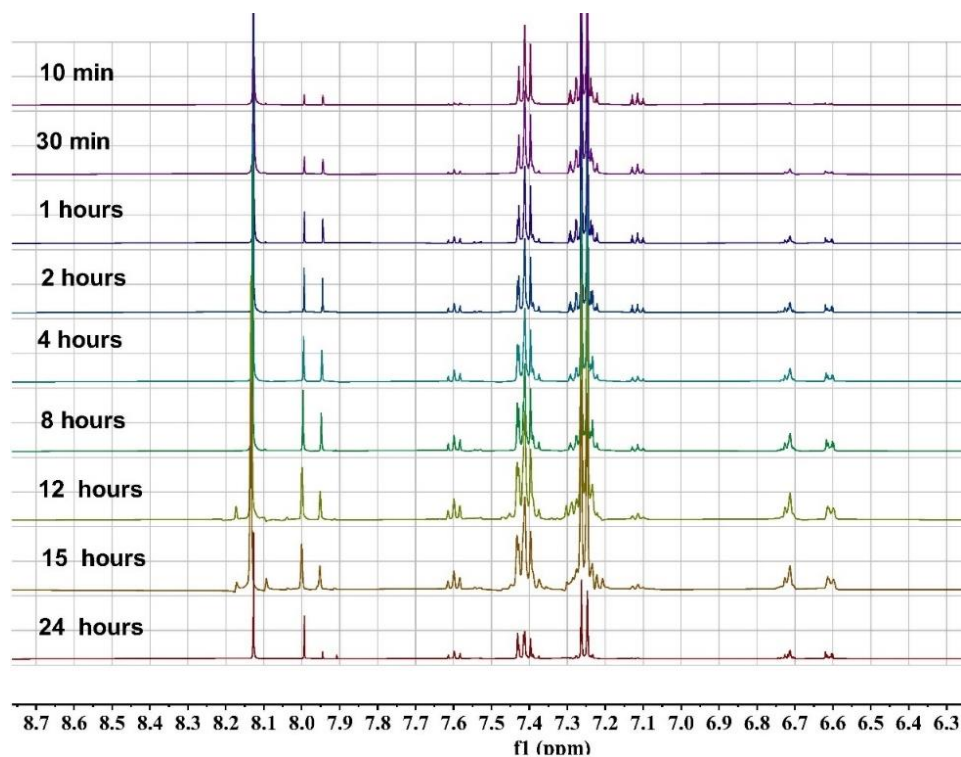
Figure 4.10. ^{1}H NMR in the aromatic region for the reaction between **C-1** (8 mM) and PhSH (16 mM) in DMSO-d_6 over time.
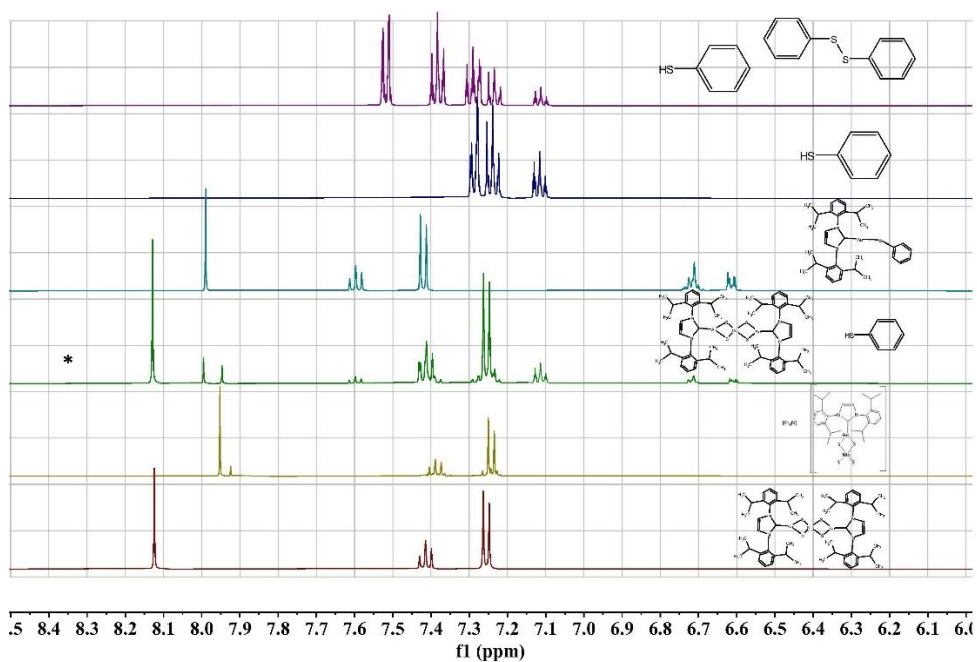
Figure 4.11. Stacked ^{1}H NMR in DMSO-d_6 of the reaction between **C-1** (8 mM) and PhSH (16 mM) after 40 min vs ^{1}H NMR of the expected compounds. * indicate the reaction mixture.
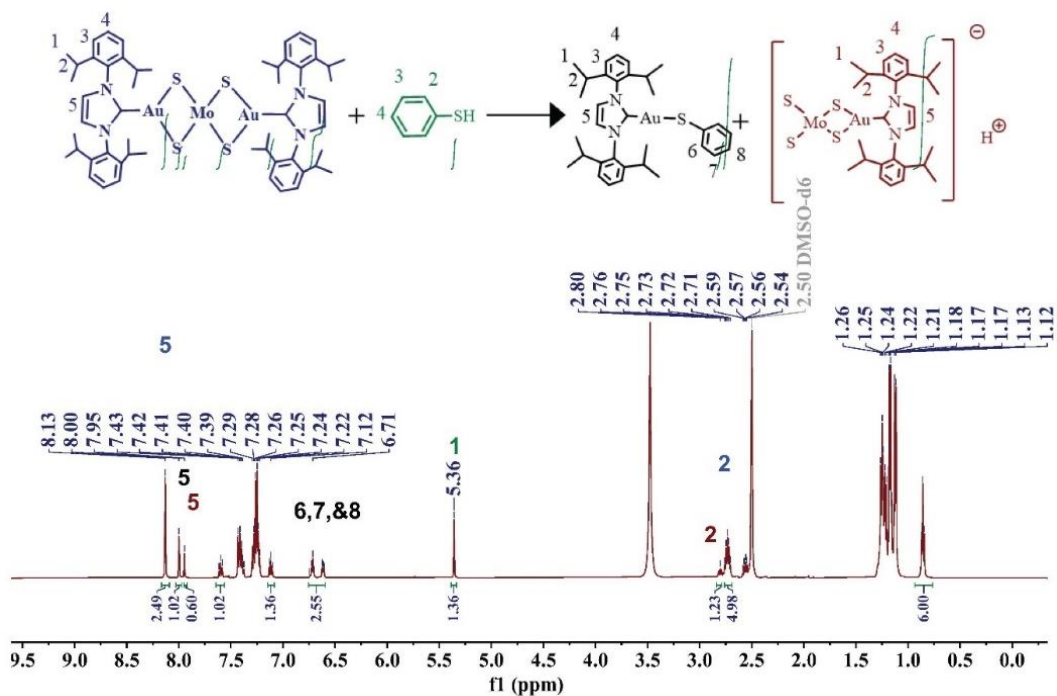
Figure 4.12. ^{1}H NMR in DMSO-d_6 of the reaction between **C-1** (8 mM) and PhSH (16 mM) after 4 hours, with peak assignments as shown.
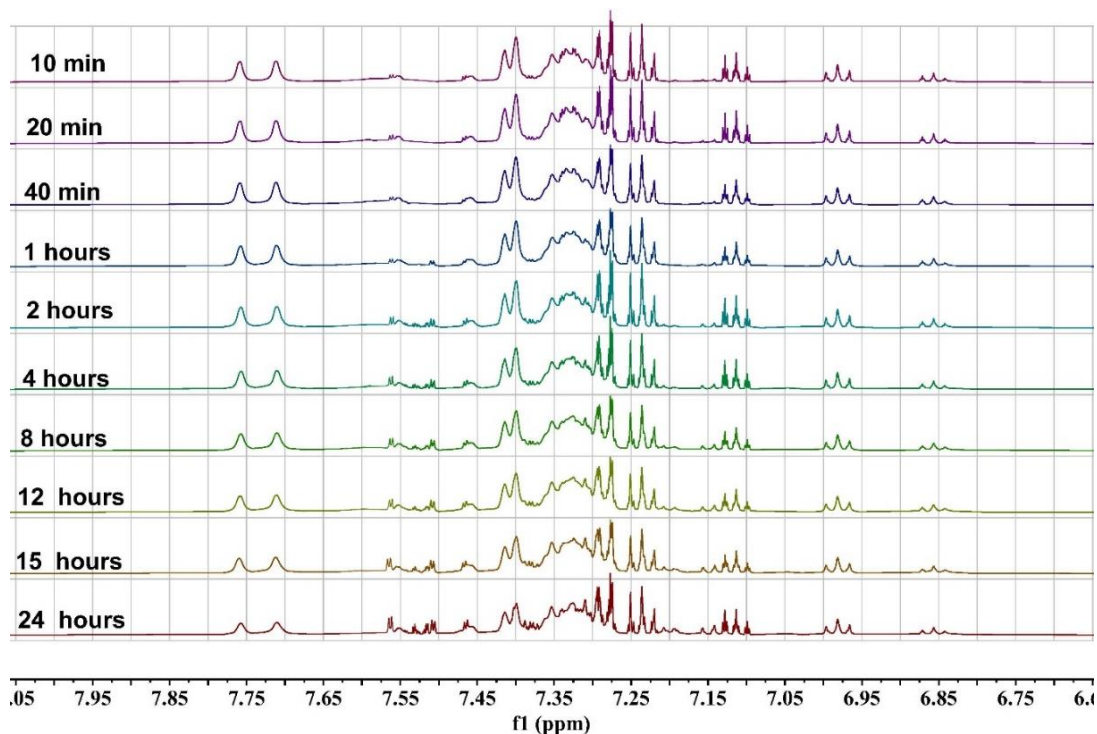
Figure 4.13. ^{1}H NMR in the aromatic region for the reaction between **C-2** (8 mM) and PhSH (16 mM) in DMSO-d_6 over time**.**

113

A similar set of ^{1}H NMR spectra in DMSO-d_6 for reaction of **C-2** and **C-3** with PhSH are collected in

Figures 4.13 – 4.18. The reaction of benzenethiol with the clusters with NHC ligands, **C-1**, **C-2**, and **C-3** all

proceed according to Scheme 4.5, B.

The reaction of **C-4** with PhSH was carried out in CH_2Cl_2-d_2 because **C-4** has very low solubility in

DMSO-d_6. Figure 4.19 shows the ^{1}H NMR stacked plots in the aromatic region for the reaction mixture

compared to expected products, while Figure 4.20 shows the ^{31}P NMR spectra. It is evident that there is

no reaction between **C-4** and PhSH even after 24 hours.

The ^{1}H NMR spectra for the reaction of **C-5** with PhSH are shown in Figures 4.21 -4.23, and the [31]P

NMR spectra are shown in Figure 4.24. Cluster **C-5**, with PEt_3 ligands, reacts similar to the clusters with

NHC ligands, according to Scheme 4.5, B.
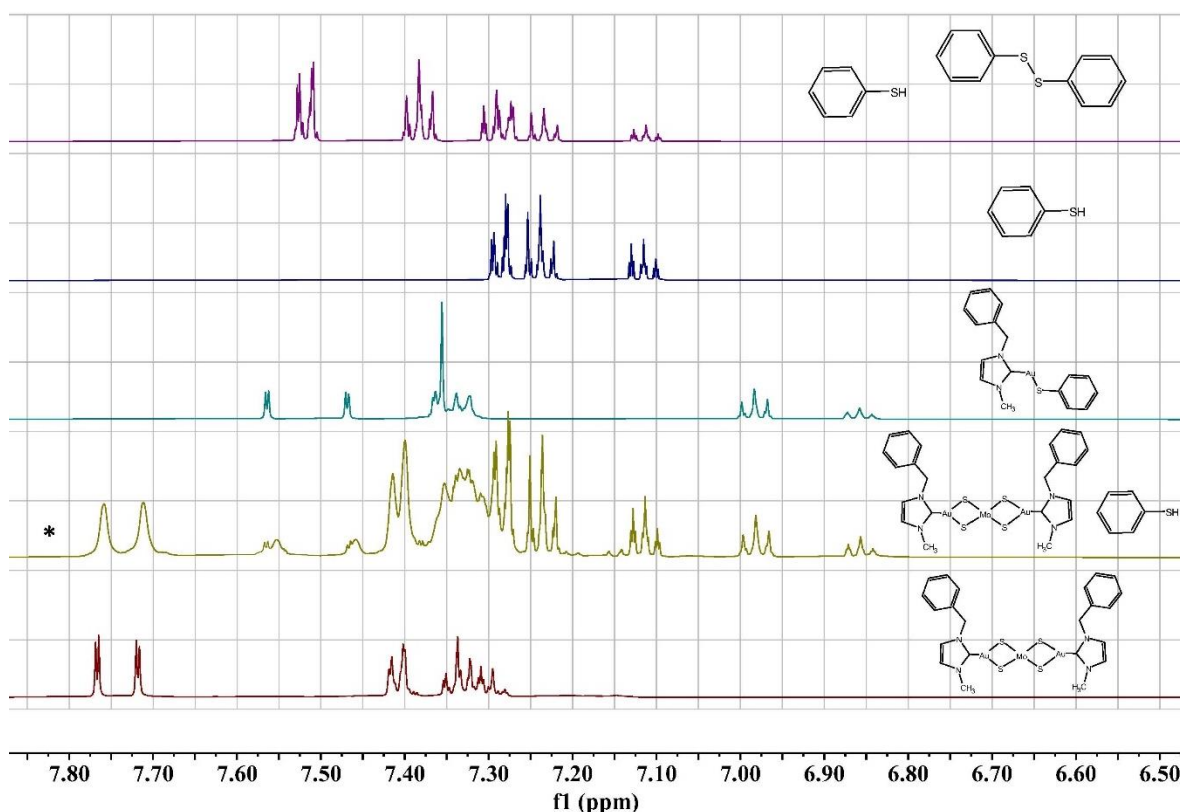
Figure 4.14. Stacked ^{1}H NMR in DMSO-d_6 of the reaction between **C-2** (8 mM) and PhSH (16 mM) after 20 min vs ^{1}H NMR of the expected compounds. * indicate the reaction mixture.
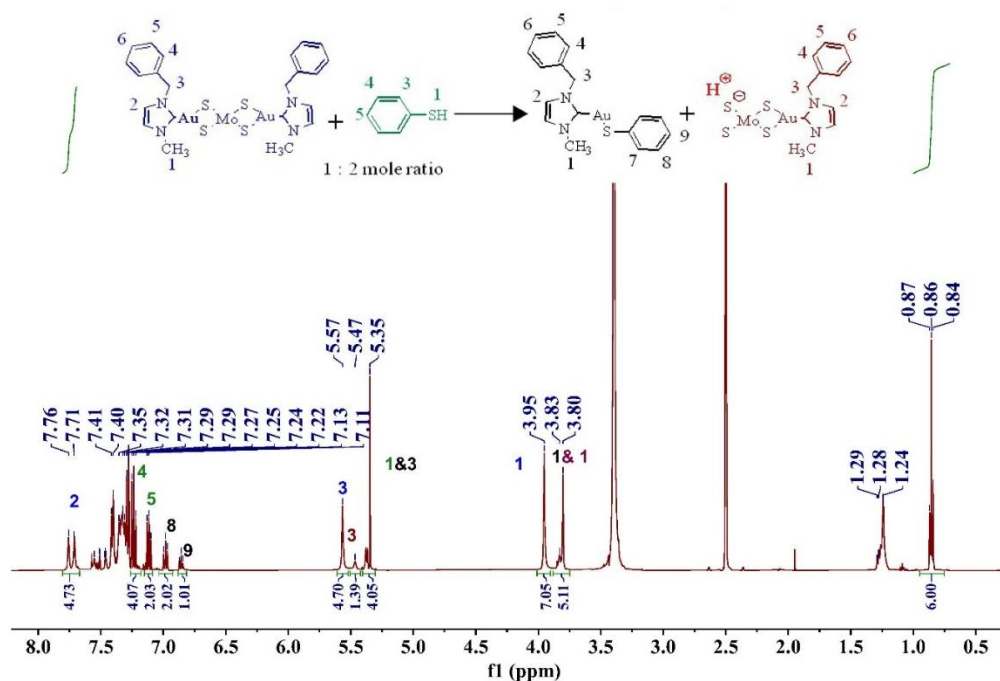
Figure 4.15. ^{1}H NMR in DMSO-d_6 of the reaction between **C-2** (8 mM) and PhSH (16 mM) after 4 hours, with peak assignments as shown.
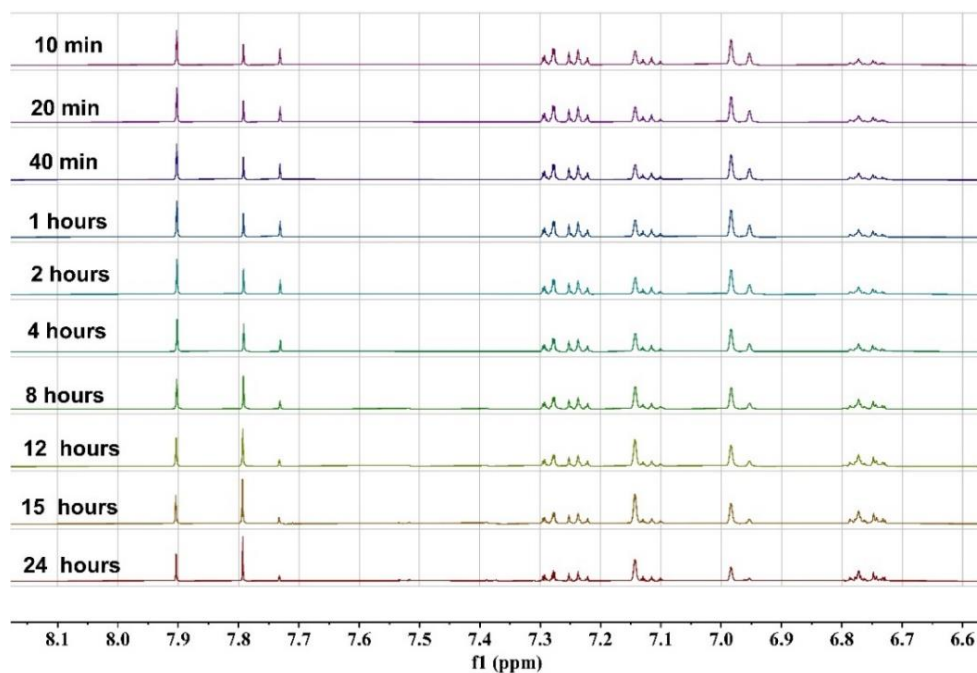
Figure 4.16. ^{1}H NMR in the aromatic region for the reaction between **C-3** (8 mM) and PhSH (16 mM) in DMSO-d_6 over time.
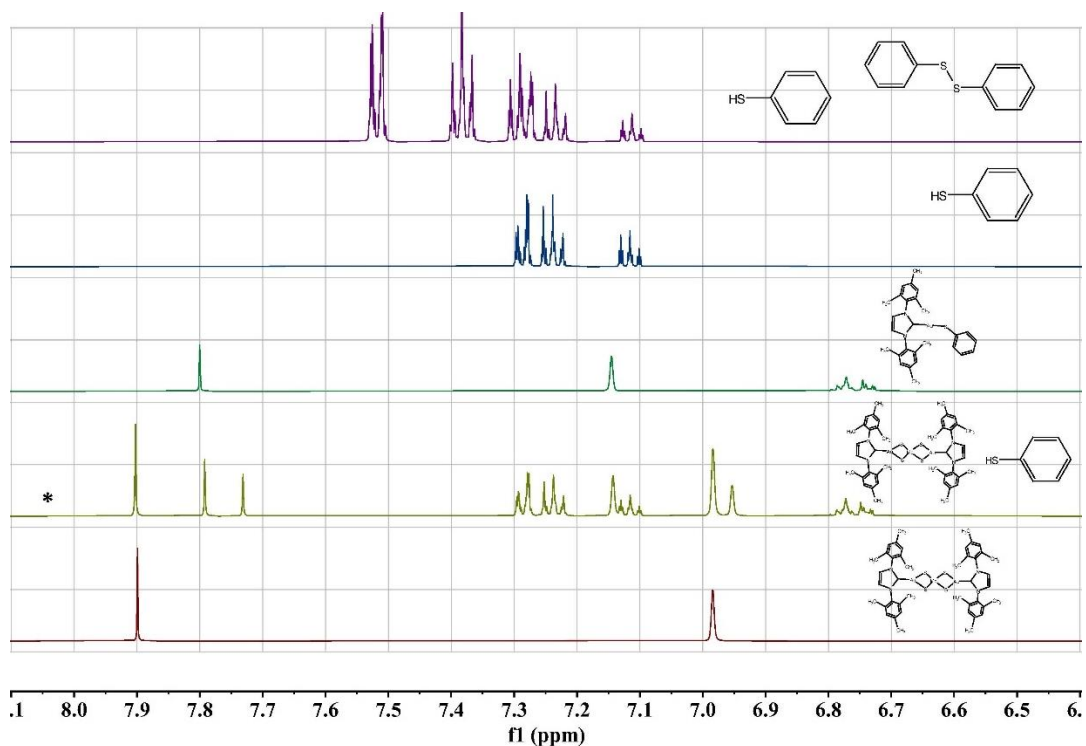
Figure 4.17. Stacked ¹H NMR in DMSO-d_6 of the reaction between **C-3** (8 mM) and PhSH (16 mM) after 30 min vs ¹H NMR of the expected compounds. * indicate the reaction mixture.
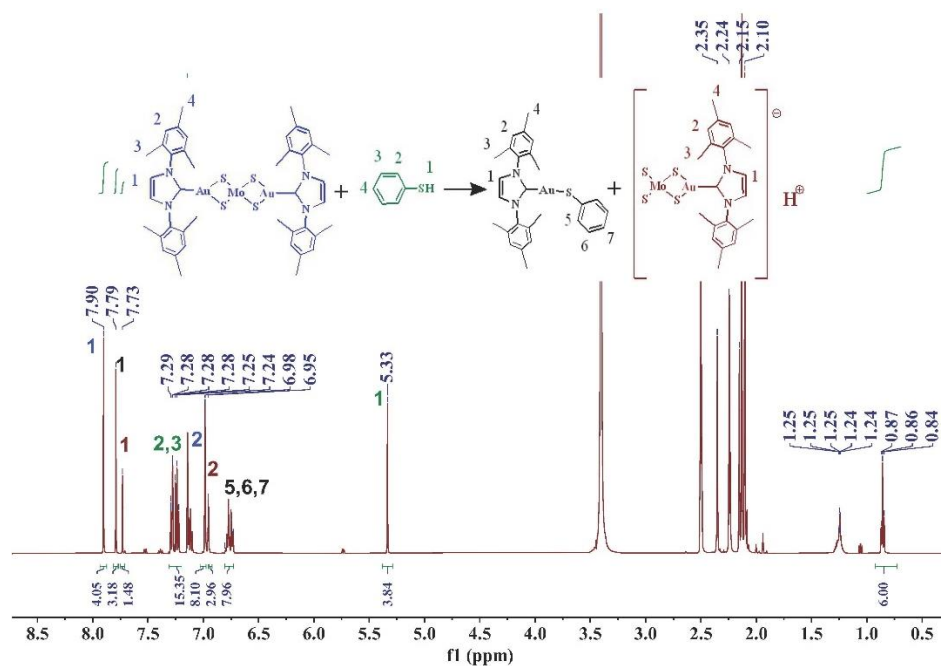
Figure 4.18. ¹H NMR in DMSO-d_6 of the reaction between **C-3** (8 mM) and PhSH (16 mM) after 4 hours, with peak assignments as shown.
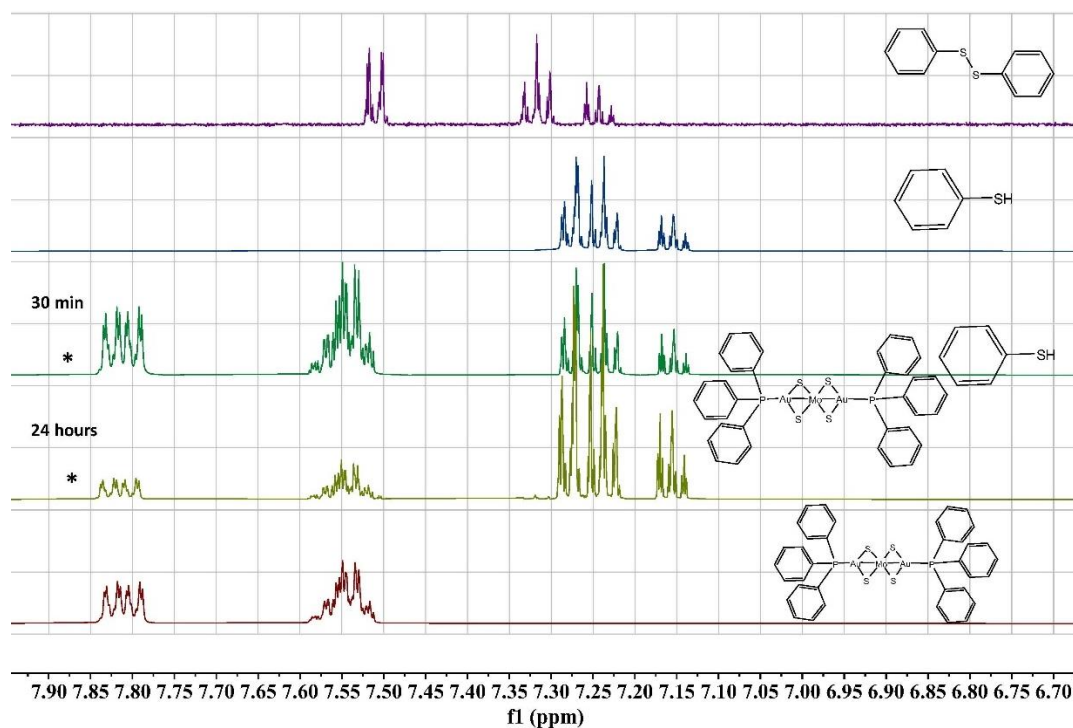
Figure 4.19. Stacked ^{1}H NMR in CH$_2$Cl$_2$-d_2 of the reaction between **C-4** (8 mM) and PhSH (16 mM) after 30 min and 24 hours vs ^{1}H NMR of the expected compounds. * indicate the reaction mixture.
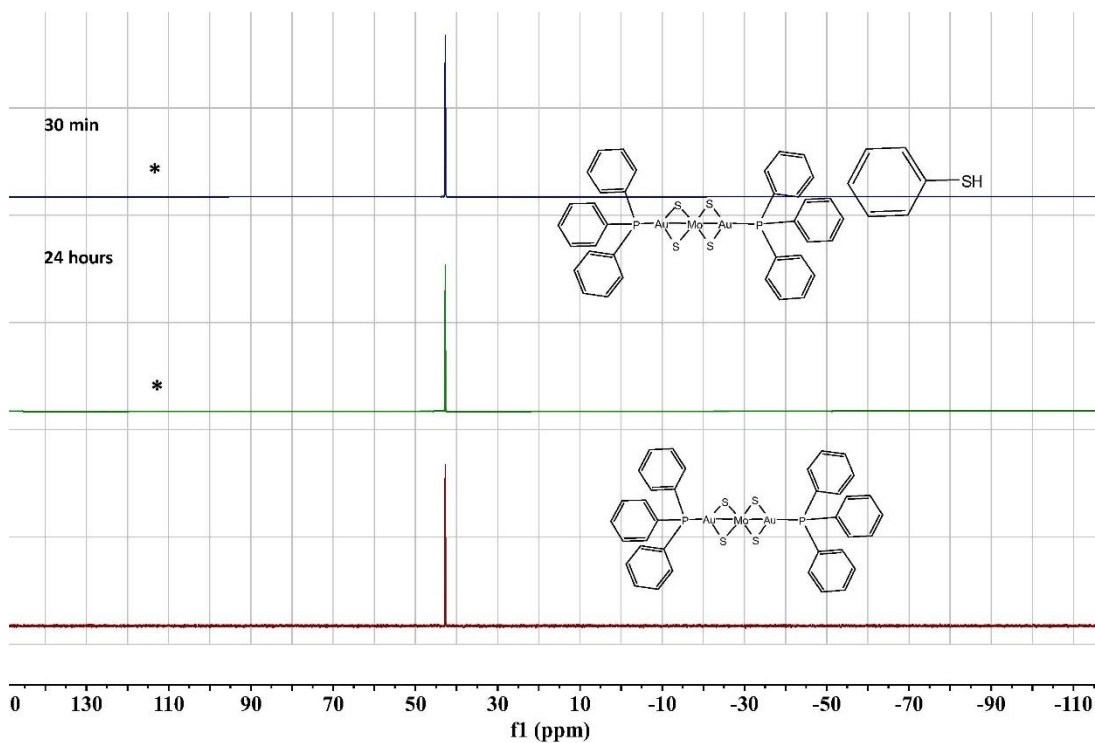
Figure 4.20. Stacked ^{31}P{^{1}H} NMR in CH$_2$Cl$_2$-d_2 of the reaction between **C-4** (8 mM) and PhSH (16 mM) after 30 min and 24 hours vs ^{31}P{^{1}H} NMR of **C-4**. * indicate the reaction mixture.
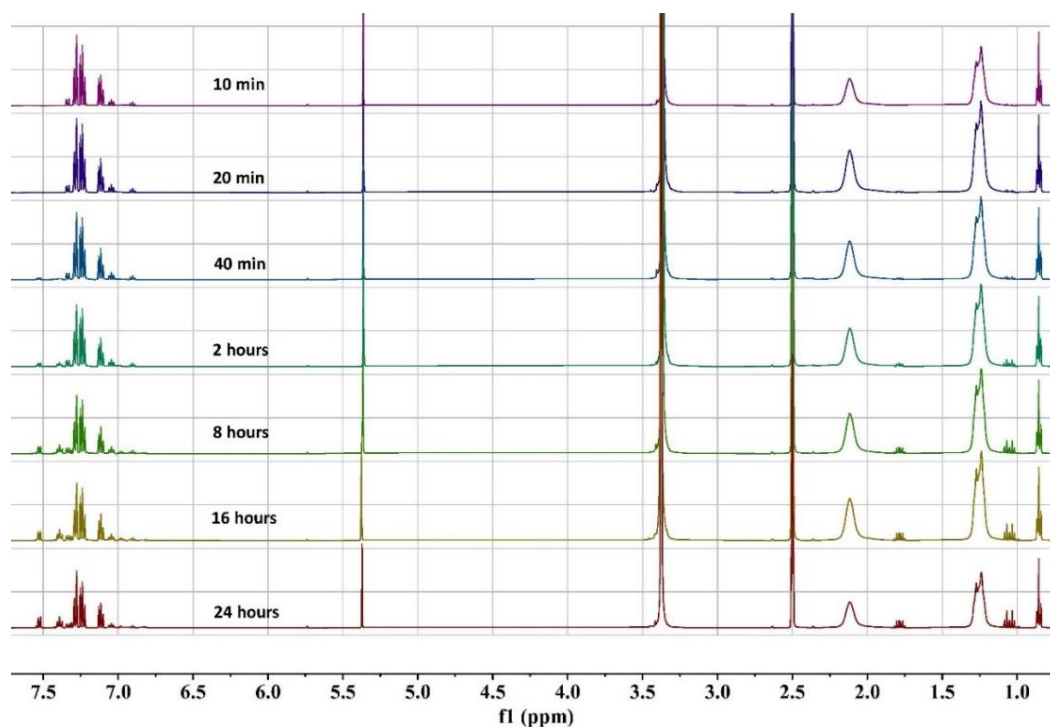
Figure 4.21. ^{1}H NMR in DMSO-d_6 of the reaction between **C-5** and PhSH over the time.
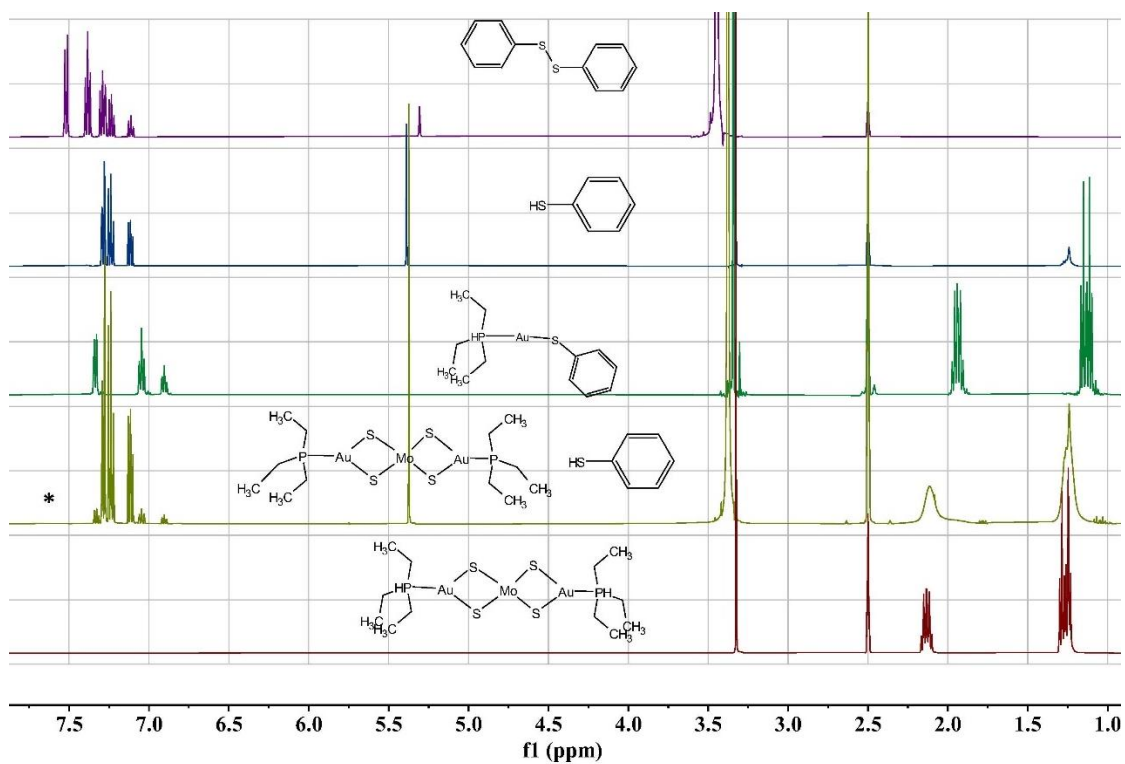
Figure 4.22. Stacked ^{1}H NMR in DMSO-d_6 of the reaction between **C-5** (8 mM) and PhSH (16 mM) after 30 min vs ^{1}H NMR of the expected compounds. * indicate the reaction mixture.
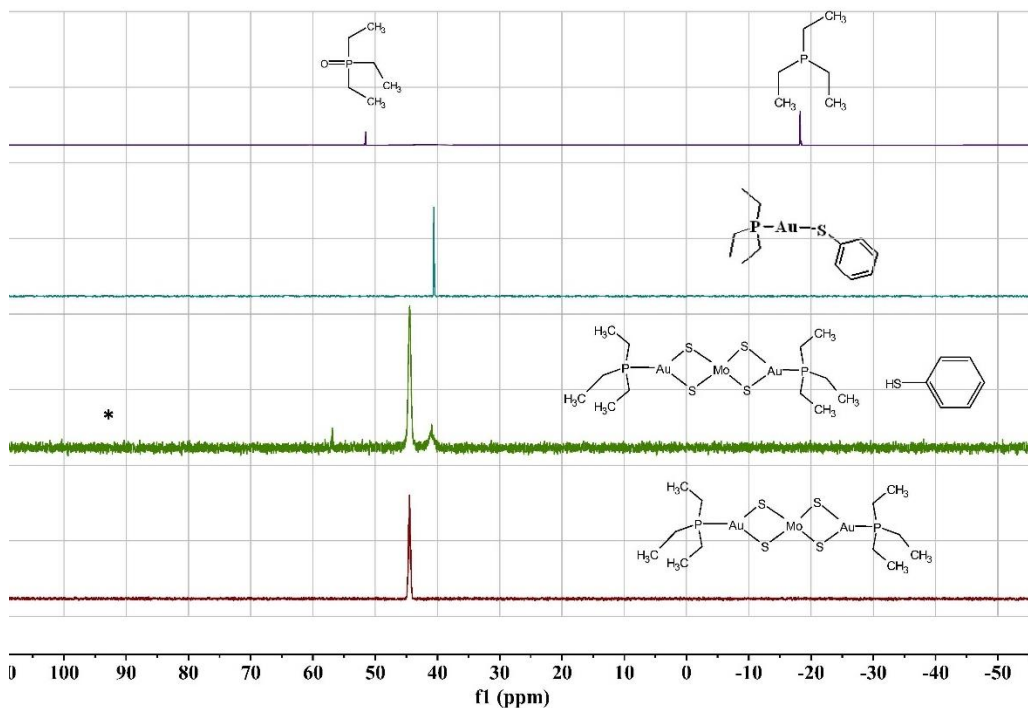
Figure 4.23. Stacked ^{31}P{^{1}H} NMR in DMSO-d_6 of the reaction between **C-5** (8 mM) and PhSH (16 mM) after 30 min vs ^{1}H NMR of **C-5**. * indicate the reaction mixture.
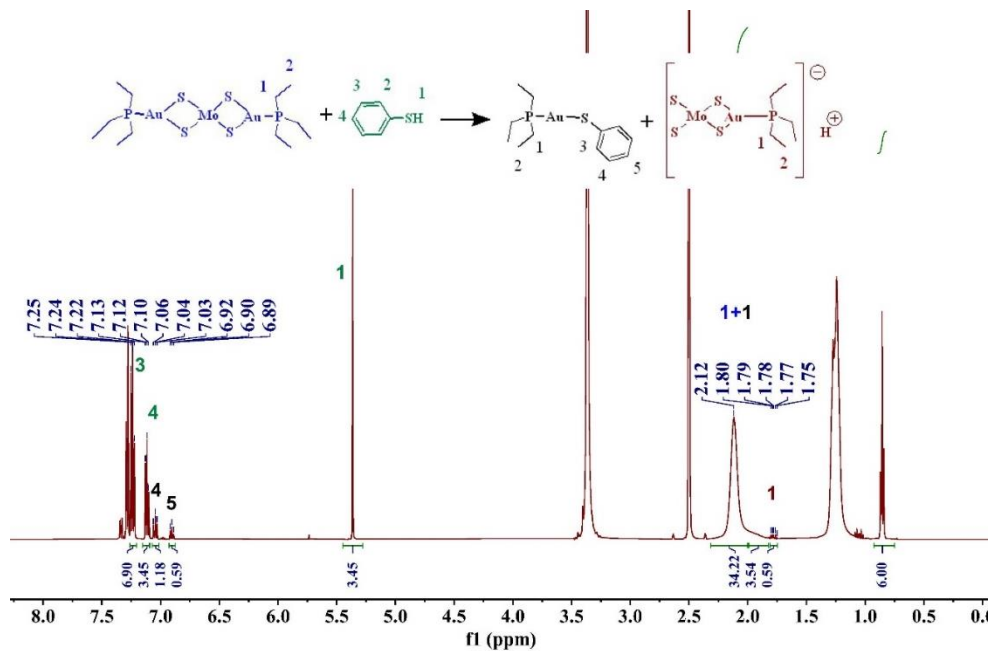
Figure 4.24. ^{1}H NMR in DMSO-d_6 of the reaction between **C-5** (8 mM) and PhSH (16 mM) after 30 minutes, with peak assignments as shown.

4.3.1.2. Reaction of C-1 – C-5 with PhSeH

The reactions of benzeneselenol with clusters **C-1 – C-5** were carried out using the same procedure as for the reaction with benzenethiol. A similar set of ^{1}H NMR spectra for reaction of NHC-containing clusters, **C-1**, **C-2**, and **C-3** are collected in Figures 4.25 – 4.33. In general, the reaction of benzeneselenol with **C-1**, **C-2**, and **C-5** is somewhat more complex than the reaction with benzenethiol. Clusters **C-1** and **C-3** react to form small amounts of (NHC)-Au(SePh) and [MoS$_4$Au(NHC)]$^-$ according to Scheme 4.5, B. In contrast, the reaction of **C-2** with PhSeH, (NHC)-Au(SePh) does not appear to form.

The ^{1}H and ^{31}P NMR spectra for the reaction of benzeneselenol with **C-4** in CH$_2$Cl$_2$-d_2 are shown in Figures 4.34 – 4.36. There is no reaction between **C-4** and PhSeH. However, there was evidence for the formation of PhSeSePh in the reaction mixture (Figure 4.35). In addition, the formation of a black precipitate suggests there was some decomposition of **C-4** after 24 hours.

The ^{1}H and ^{31}P NMR spectra for the reaction of **C-5** with PhSeH are shown in Figures 3.37 – 4.39. There is no reaction between **C-5** and PhSeH; the only product detected was a small amount of Et$_3$P=O (Figure 4.39, 24 hr). Similarly to **C-4**, there was also a black solid that formed in the reaction mixture after 24 hours.
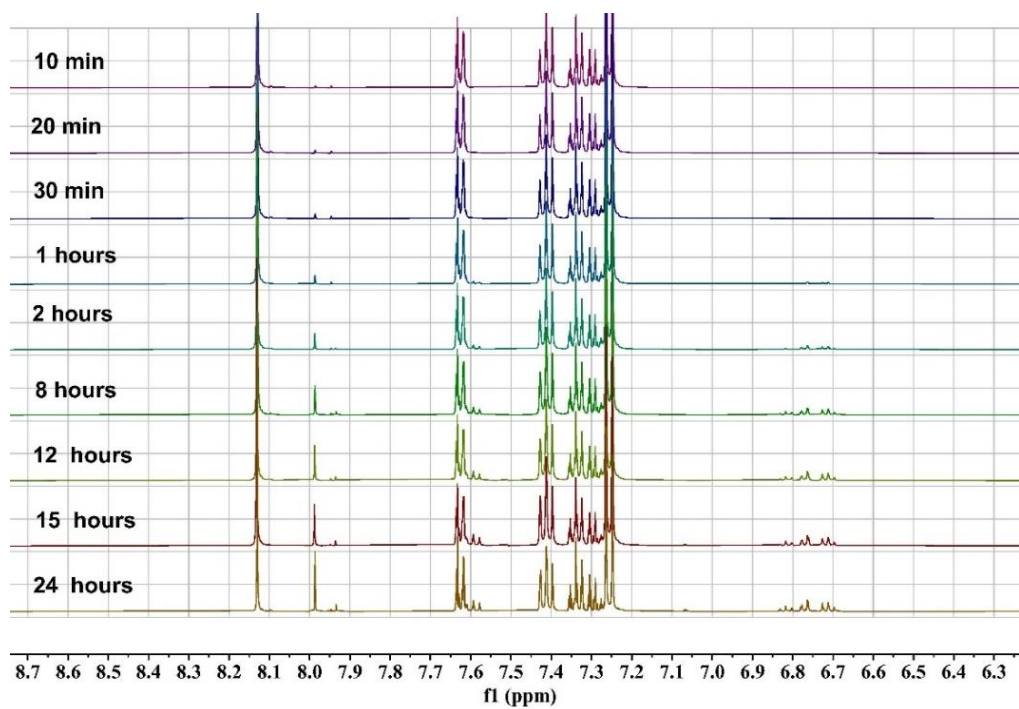
Figure 4.25. ^{1}H NMR in the aromatic region for the reaction between **C-1** (8 mM) and PhSeH (16 mM) in DMSO-d_6 over time.
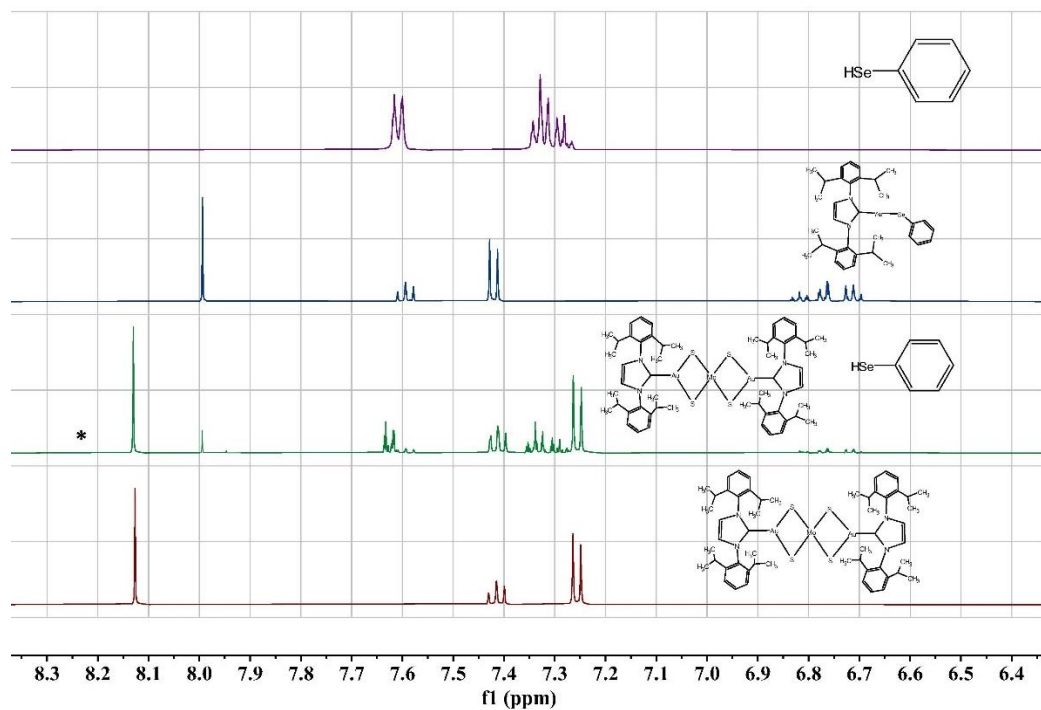
Figure 4.26. Stacked ^{1}H NMR in DMSO-d_6 of the reaction between **C-1** (8 mM) and PhSeH (16 mM) after 30min vs ^{1}H NMR of the expected compounds. * indicate the reaction mixture.
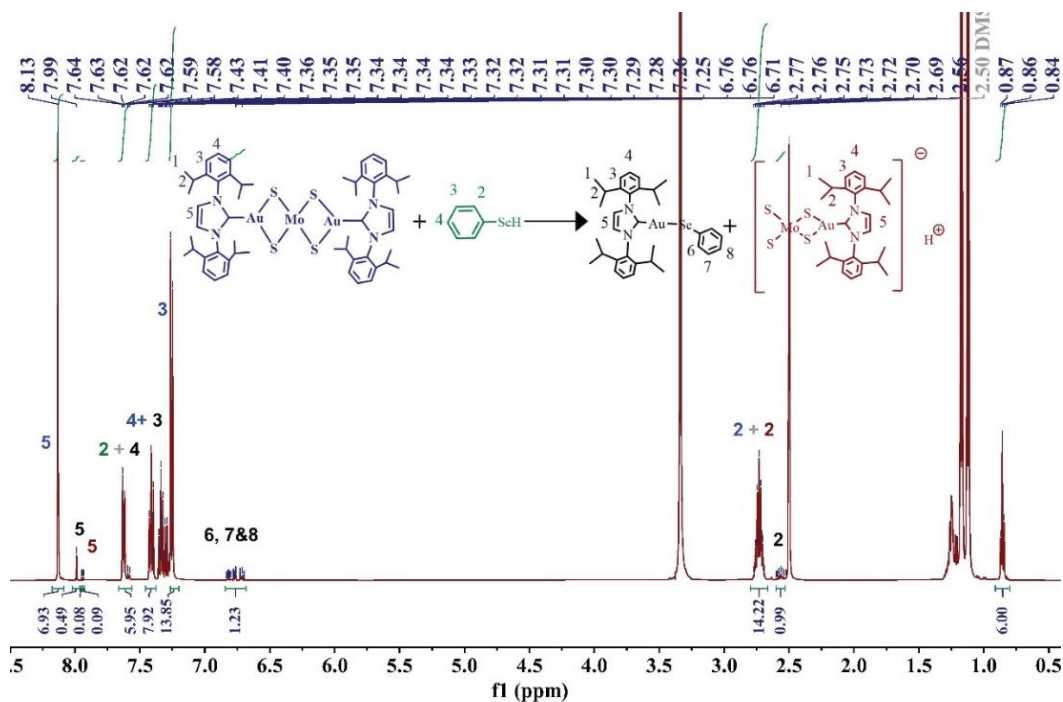
Figure 4.27. ^{1}H NMR in DMSO-d_6 of the reaction between **C-1** (8 mM) and PhSeH (16 mM) after 4 hours, with peak assignments as shown.
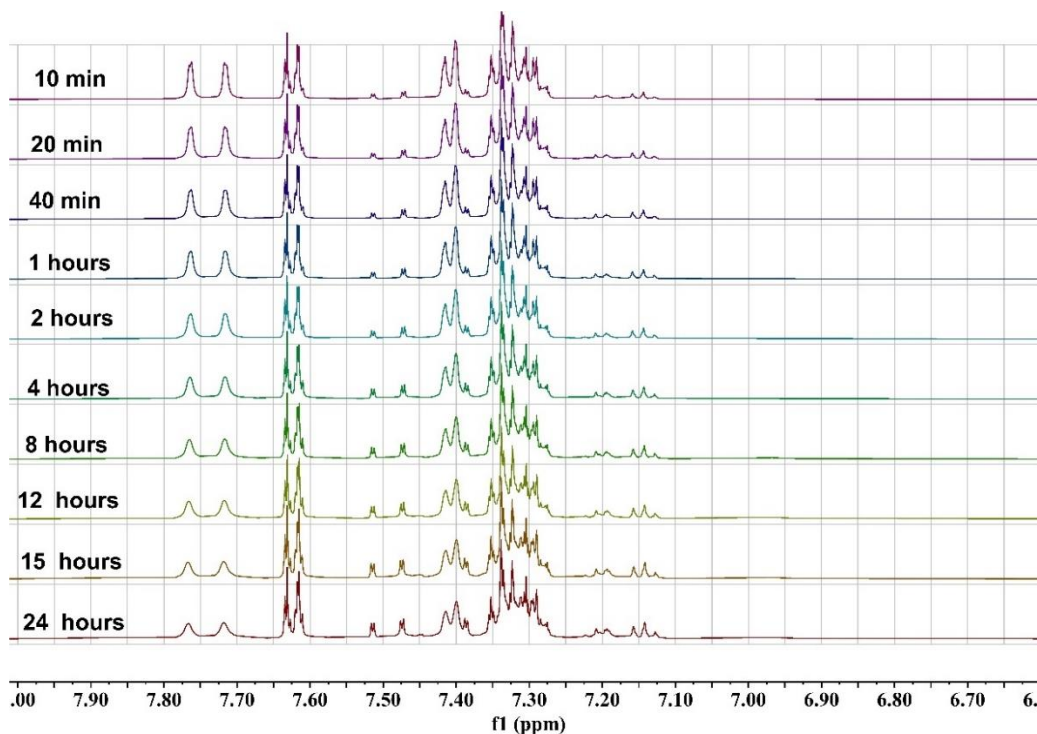
Figure 4.28. ^{1}H NMR in the aromatic region for the reaction between **C-2** (8 mM) and PhSeH (16 mM) in DMSO-d_6 over time.
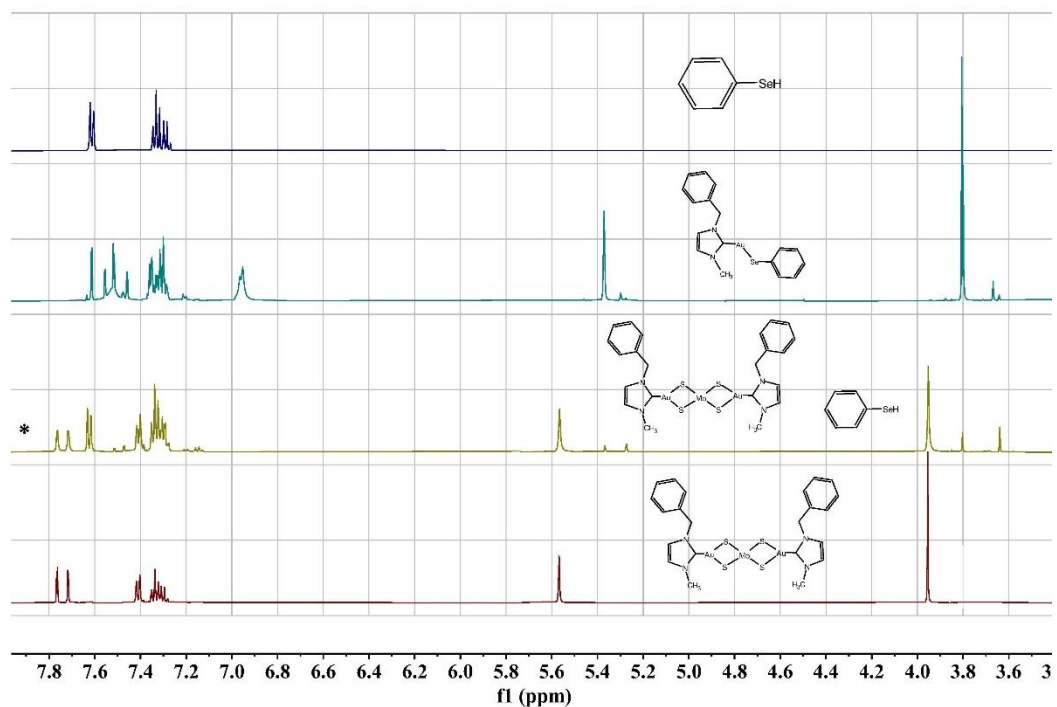
Figure 4.29. Stacked ^{1}H NMR in DMSO-d_6 of the reaction between **C-2** (8 mM) and PhSeH (16 mM) after 30min vs ^{1}H NMR of the expected compounds. * indicate the reaction mixture.
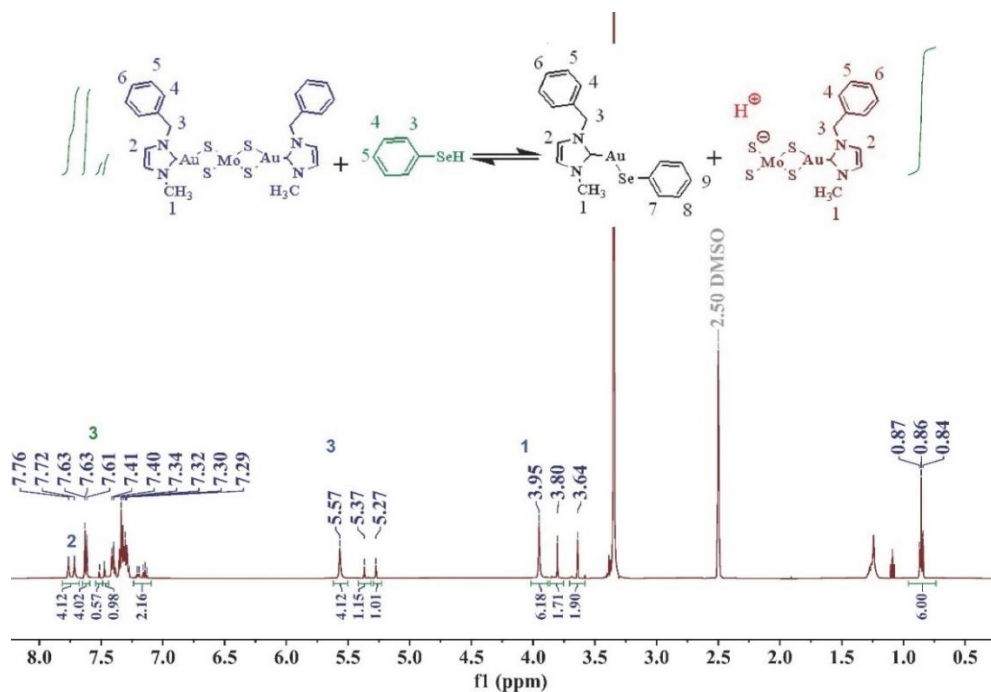
Figure 4.30. ^{1}H NMR in DMSO-d_6 of the reaction between **C-2** (8 mM) and PhSeH (16 mM) after 4 hours, with peak assignments as shown.
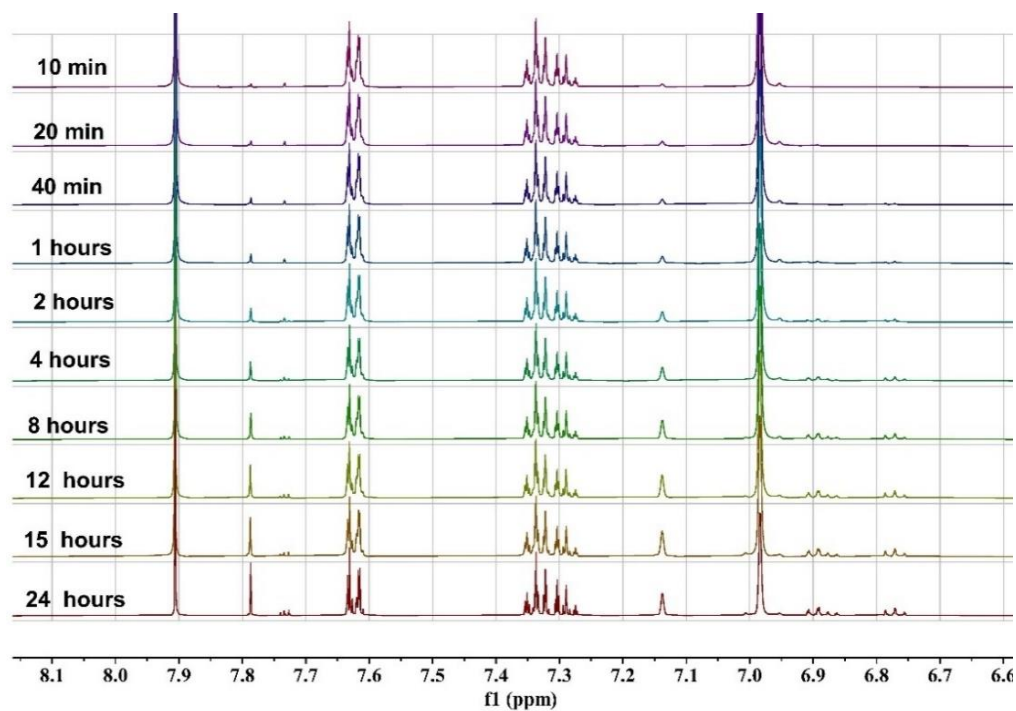
Figure 4.31. ^{1}H NMR in the aromatic region for the reaction between **C-3** (8 mM) and PhSeH (16 mM) in DMSO-d_6 over time.
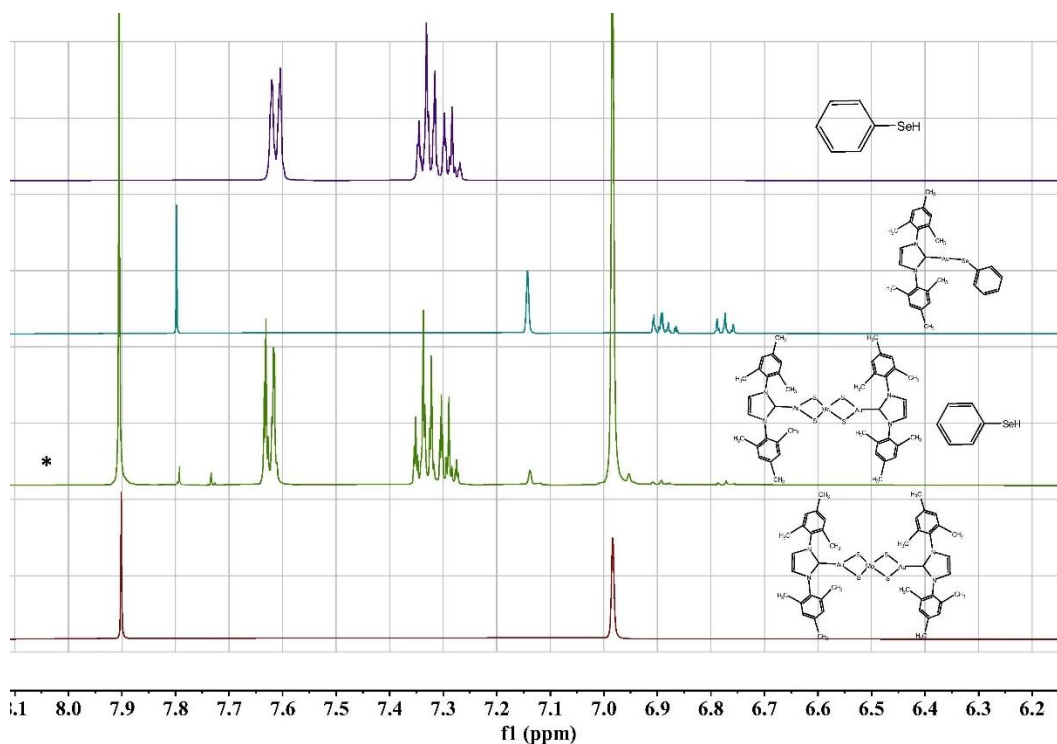
Figure 4.32. Stacked ^{1}H NMR in DMSO-d_6 of the reaction between **C-3** (8 mM) and PhSeH (16 mM) after 30min vs ^{1}H NMR of the expected compounds. * indicate the reaction mixture.
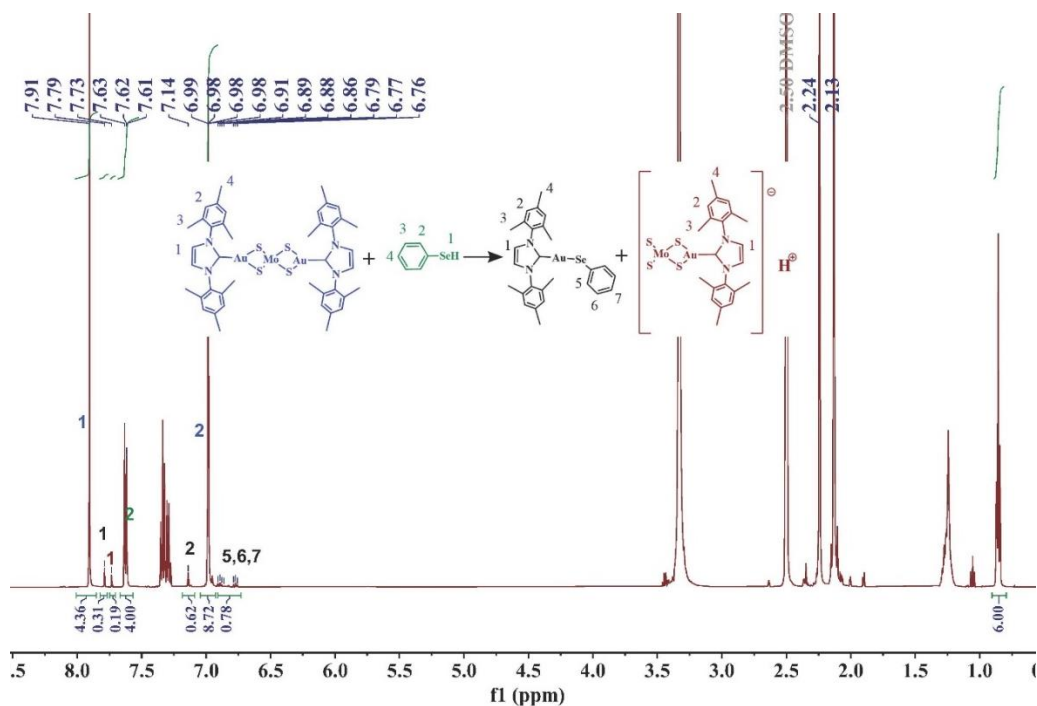
Figure 4.33. ^{1}H NMR in DMSO-d_6 of the reaction between **C-3** (8 mM) and PhSeH (16 mM) after 30 minutes, with peak assignments as shown.
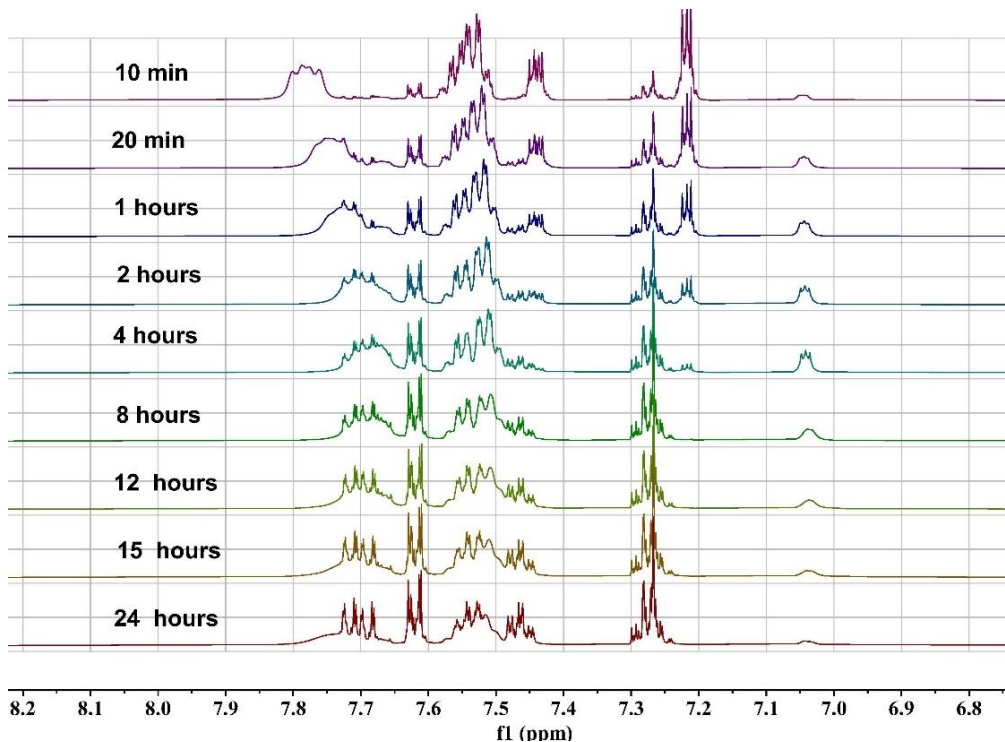
Figure 4.34. ^{1}H NMR in CH$_2$Cl$_2$-d_2 of the reaction between **C-4** (8 mM) and PhSeH (16 mM) over time.
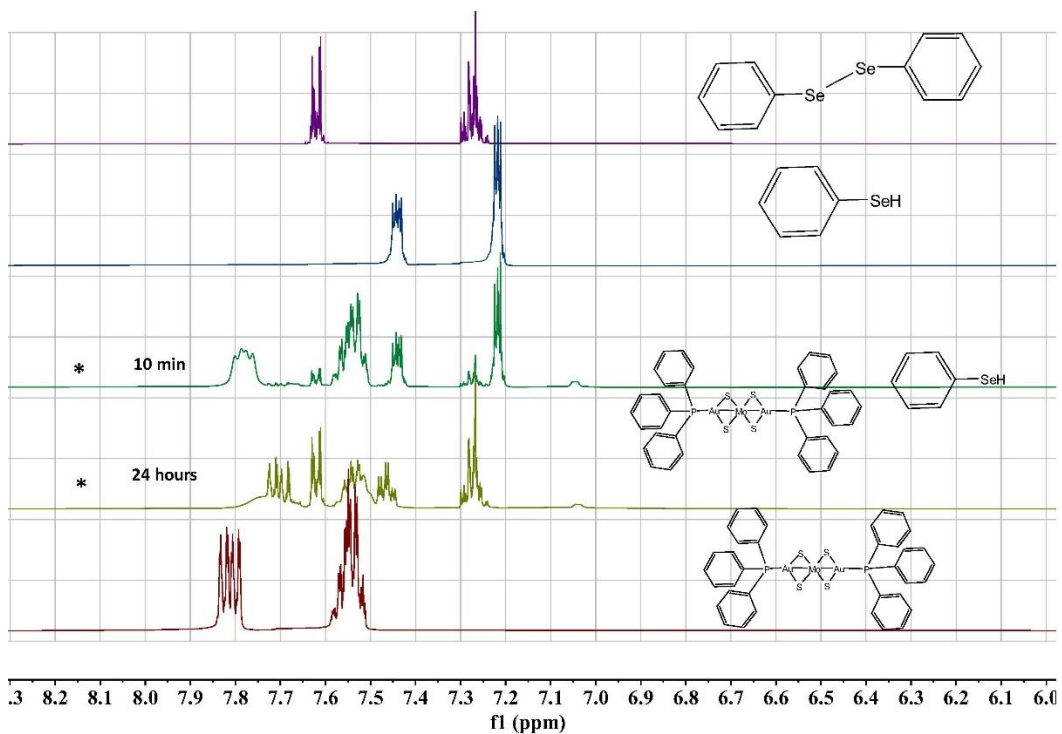
Figure 4.35. Stacked ^{1}H NMR in CH$_2$Cl$_2$-d_2 of the reaction between **C-4** (8 mM) and PhSeH (16 mM) after 10 min and 24 hours vs ^{1}H NMR of the expected compounds. * indicate the reaction mixture.
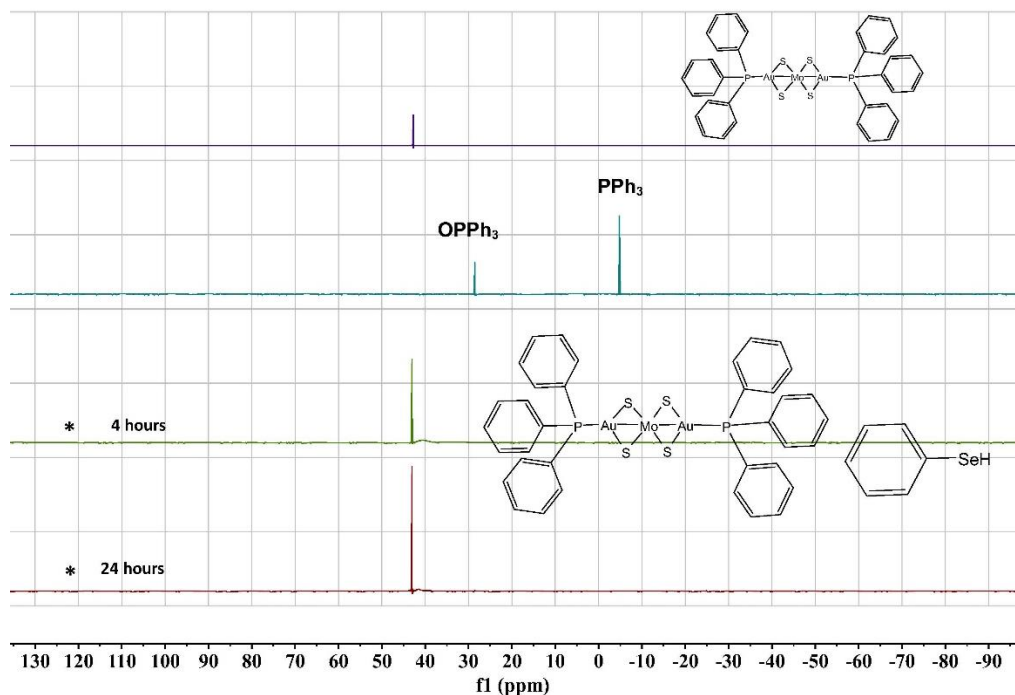
Figure 4.36. Stacked ^{31}P{^{1}H} NMR in CH$_2$Cl$_2$-d_2 of the reaction between **C-4** (8 mM) and PhSeH (16 mM) after 4 hours and 24 hours vs ^{31}P{^{1}H} NMR of the expected compounds. * indicate the reaction mixture.
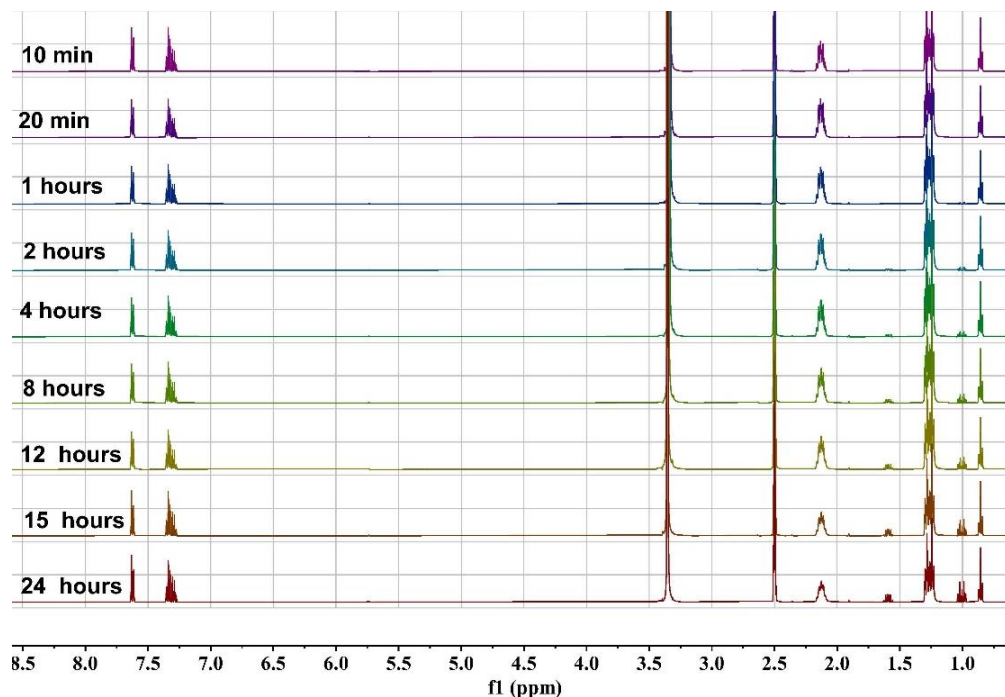
Figure 4.37. ^{1}H NMR in DMSO-d_6 of the reaction between **C-5** (8 mM) and PhSeH (16 mM) over the time.
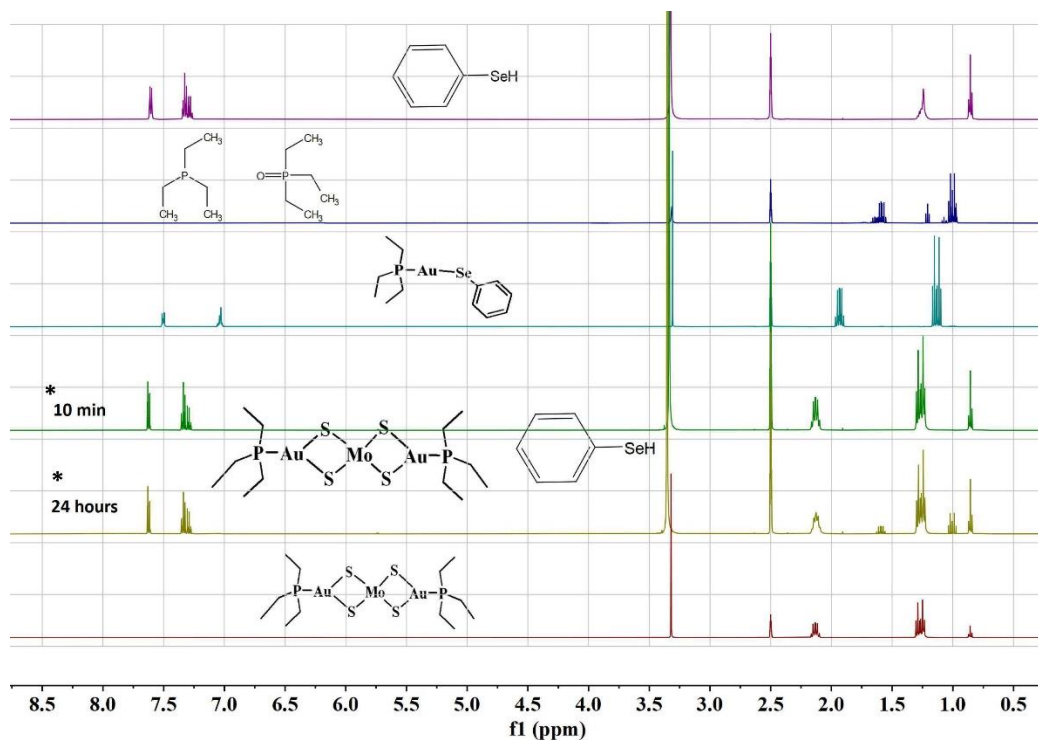
Figure 4.38. Stacked ^{1}H NMR in DMSO-d_6 of the reaction between **C-5** (8 mM) and PhSeH (16 mM) after 10 min and 24 hours vs ^{1}H NMR of the expected compounds. * indicate the reaction mixture.
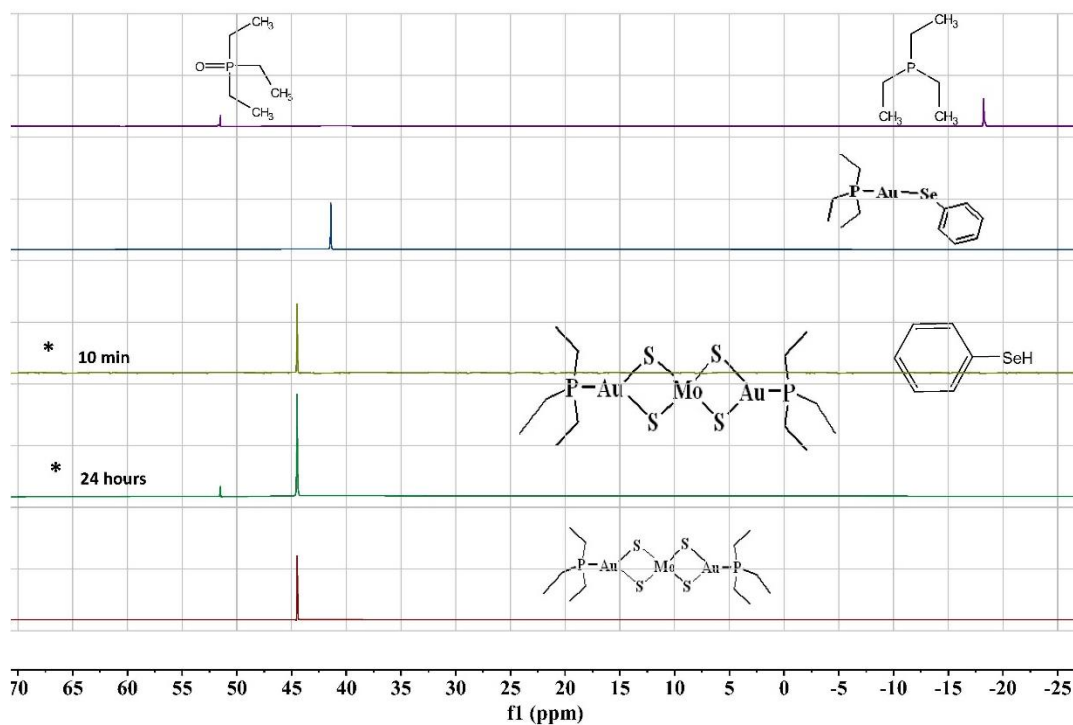
Figure 4.39. Stacked $^{31}P\{^1H\}$ NMR in DMSO-d_6 of the reaction between **C-5** (8 mM) and PhSeH (16 mM) after 10 min and 24 hours vs $^{31}P\{^1H\}$ NMR of the expected compounds. * indicate the reaction mixture.
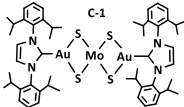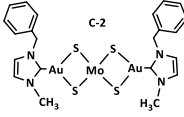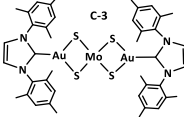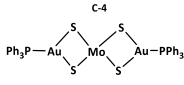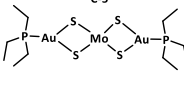
4.3.2. Relative reactivity of clusters

To compare the relative reactivity of the clusters with benzenethiol and benzeneselenol, quantitative ^1H NMR spectroscopy was used to calculate the concentration of clusters and reaction products relative to the concentration of heptane, added as an internal standard (Figures 4.40 – 4.57). The initial concentration of a cluster was calculated by summing the integrals for L (NHC or PR$_3$) in the cluster and the gold-containing products according to the reaction shown in equations 3 and 4.

$$(\text{L-Au})_2\text{MoS}_4 + \text{PhSH} \longrightarrow \text{L-Au-S-Ph} + [\text{L-Au-MoS}_4]^- \quad .... (3)$$

$$(\text{L-Au})_2\text{MoS}_4 + \text{PhSeH} \longrightarrow \text{L-Au-Se-Ph} + [\text{L-Au-MoS}_4]^- \quad .... (4)$$
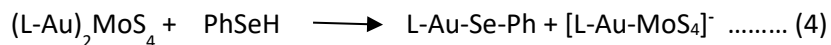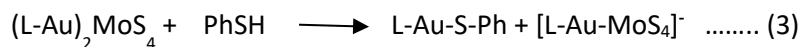
The approximate initial concentration for all clusters was 8 mM and 16 MM for PhSH or PhSeH. The percentages of clusters and reaction products, LAuSPh or LAuSePh, and [MoS$_4$(AuL)]$^-$ at the 10, 20, and 30 min. time points are shown in Table 4.3.

128

Table 4.3. The relative reactivity of **C-1** – **C-5** with PhSH or PhSeH calculated by quantitative ^{1}H NMR in DMSO-d_6.

[MoS$_4$(AuL)$_2$]	time (min)	% [MoS$_4$(AuL)$_2$] (remaining/reacted)	% L-Au-SPh	% [MoS$_4$(AuL)]$^-$	% [MoS$_4$(AuL)$_2$] (remaining/reacted)	% L-Au-SePh	% [MoS$_4$(AuL)]$^-$
C-1	10	92 / 8	8	8	98 / 2	2	2
	20	89 / 11	11	10	96 / 4	4	3
	30	85 / 15	14	12	95 / 5	4	3
C-2	10	73 / 27	27	26			
	20	71 / 29	28	24	No reaction		
	30	68 / 32	30	22			
C-3	10	58 / 42	43	41	94 / 6	6	5
	20	51 / 49	54	45	92 / 8	9	7
	30	49 / 51	57	44	89 / 11	13	8
C-4	10						
	20	No reaction			No reaction		
	30						
C-5	10	91 / 9	15	2			
	20	91 / 9	15	3	No reaction		
	30	88 / 12	15	3			

Initial concentrations: ~ 8 mM [MoS$_4$(AuL)$_2$] and ~ 16 mM PhSH or PhSeH

Cluster **C-3** was the most reactive complex in the reaction with benzenethiol and benzeneselenol. Approximately 40 % of the initial amount of **C-3** reacts with benzenethiol within the first 10 minutes. The reaction with benzeneselenol was significantly slower with only approximately 10 % of the initial amount of **C-3** reacted within 30 minutes. In general, the clusters react with benzenethiol to a greater extent than benzeneselenol. The relative reactivity of the clusters with benzenethiol is in the order **C-3** > **C-2** > **C-1** ≈ **C-5**.
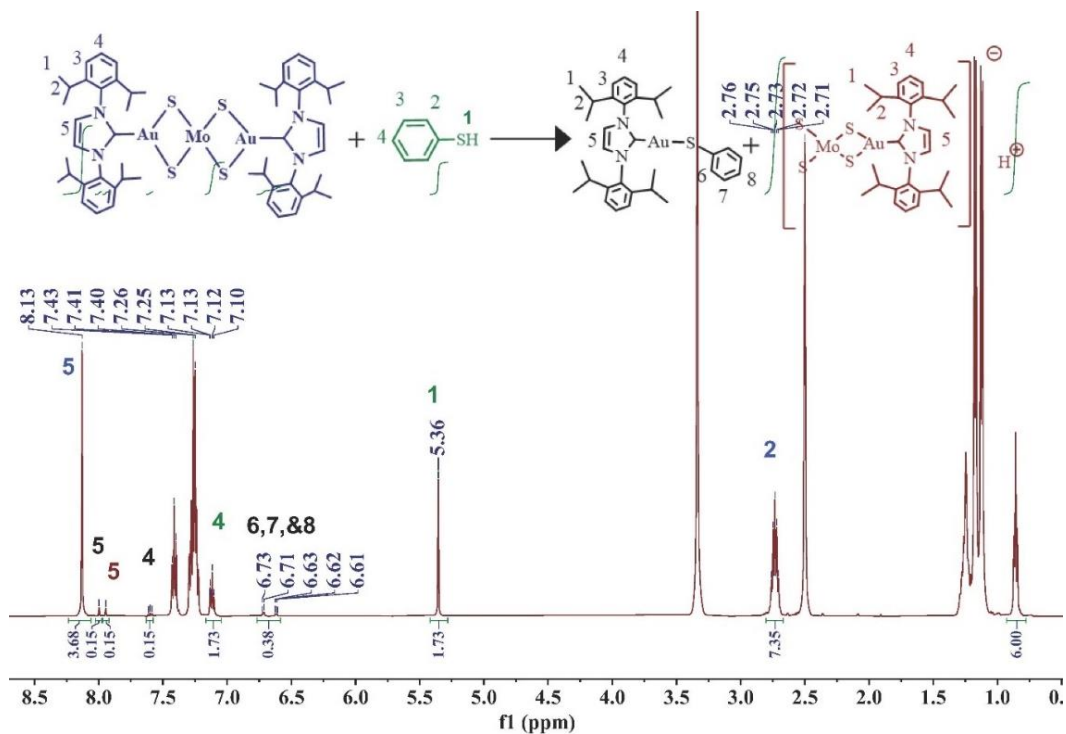
Figure 4.40. ^{1}H NMR in DMSO-*d6* of the reaction between **C-1** and PhSH after 10 min, the expected reaction equation with the relative peaks of each compound were assigned.
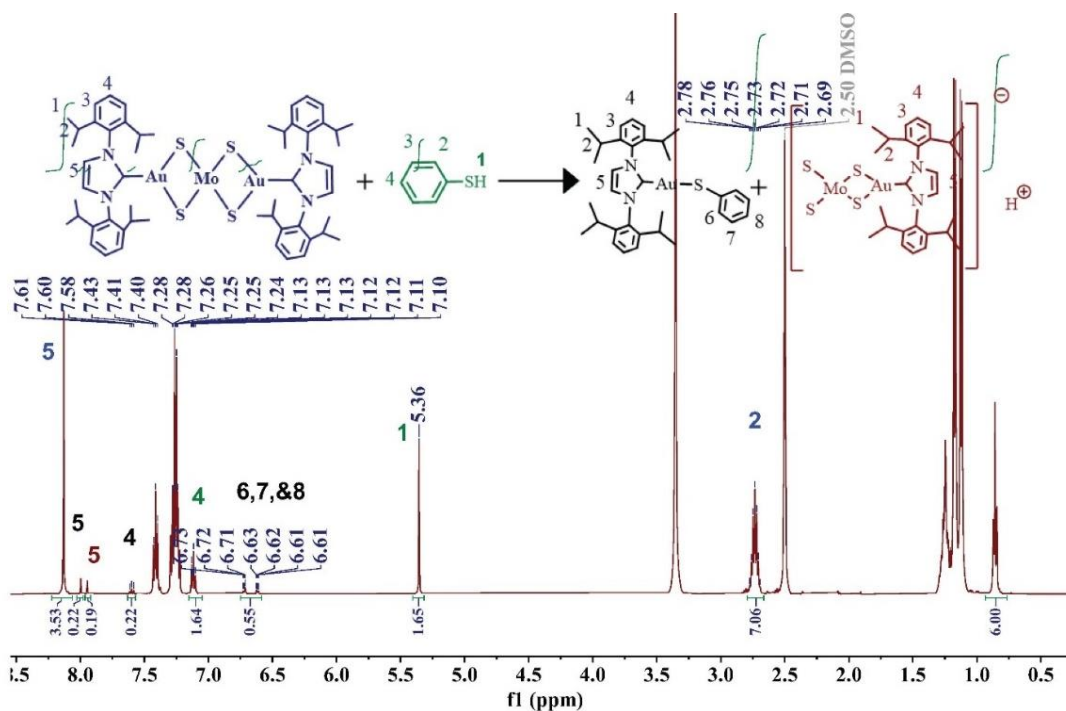
Figure 4.41. ^{1}H NMR in DMSO-*d6* of the reaction between **C-1** and PhSH after 20 min, the expected reaction equation with the relative peaks of each compound were assigned.
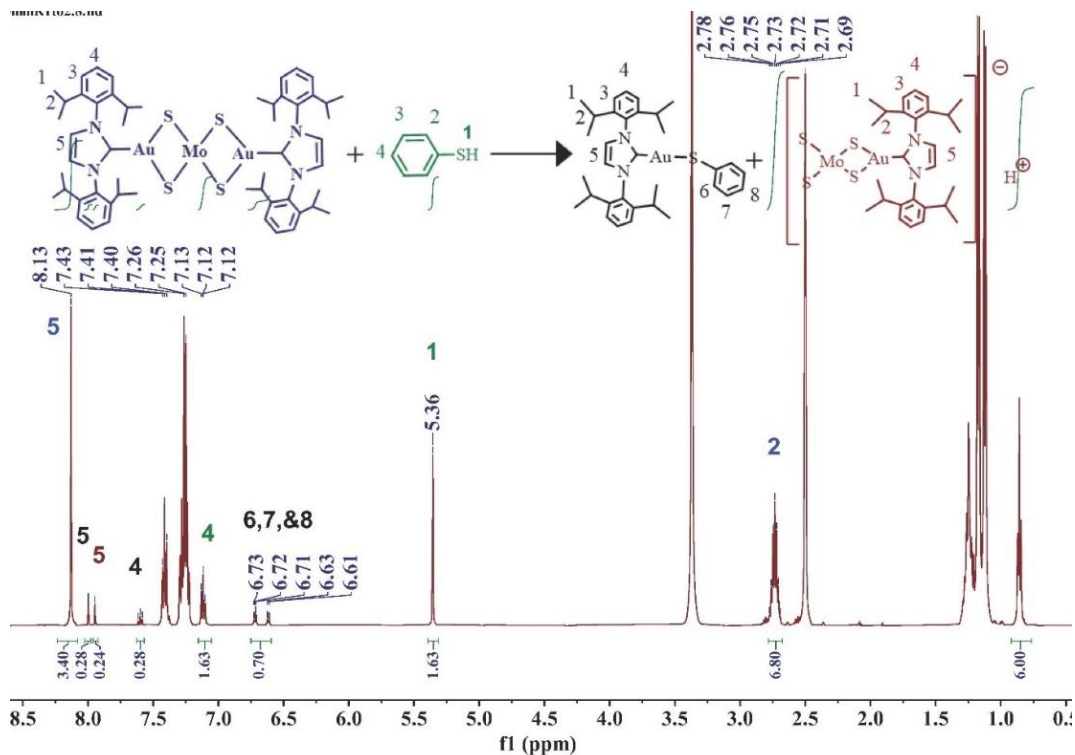
Figure 4.42. ^{1}H NMR in DMSO-d_6 of the reaction between **C-1** and PhSH after 30 min, the expected reaction equation with the relative peaks of each compound were assigned.
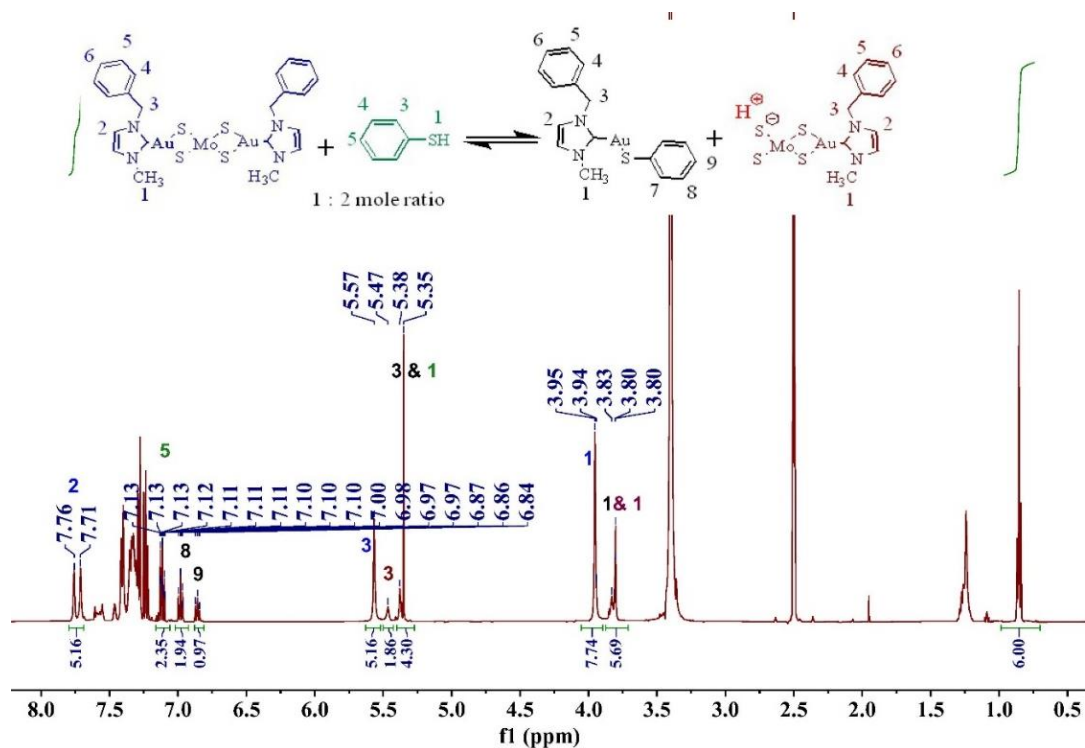
Figure 4.43. ^{1}H NMR in DMSO-d_6 of the reaction between **C-2** and PhSH after 10 min, the expected reaction equation with the relative peaks of each compound were assigned.
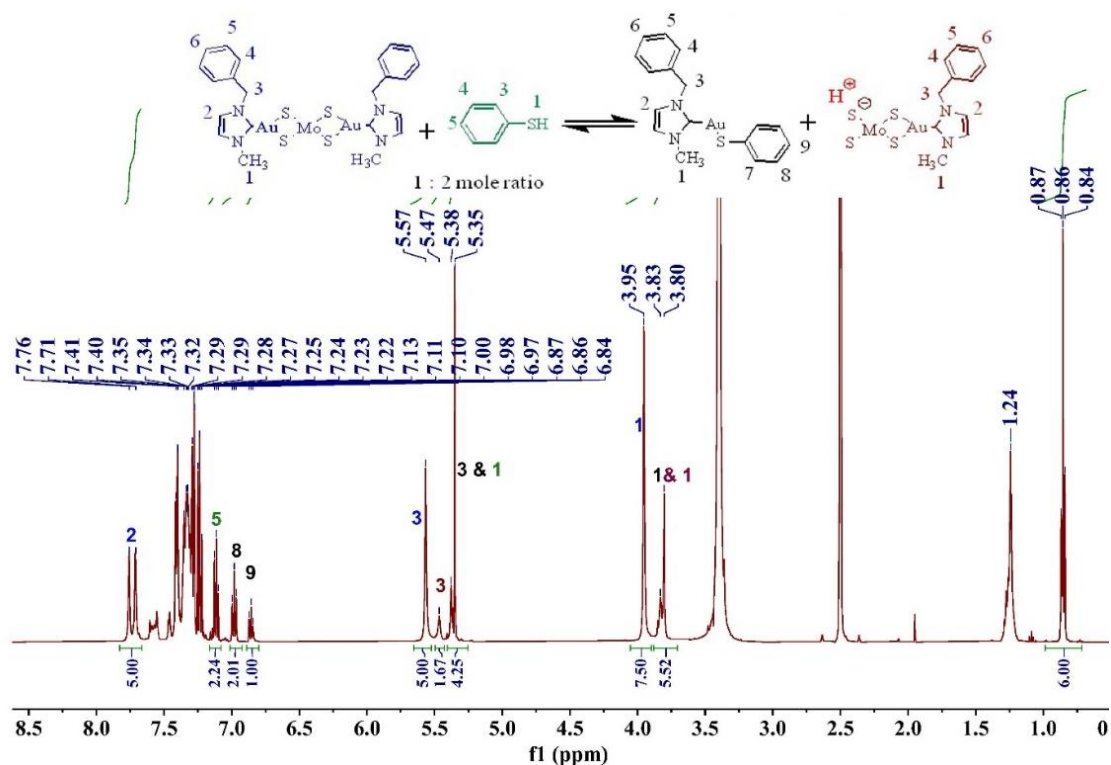
Figure 4.44. ^{1}H NMR in DMSO-d_6 of the reaction between **C-2** and PhSH after 20 min, the expected reaction equation with the relative peaks of each compound were assigned.
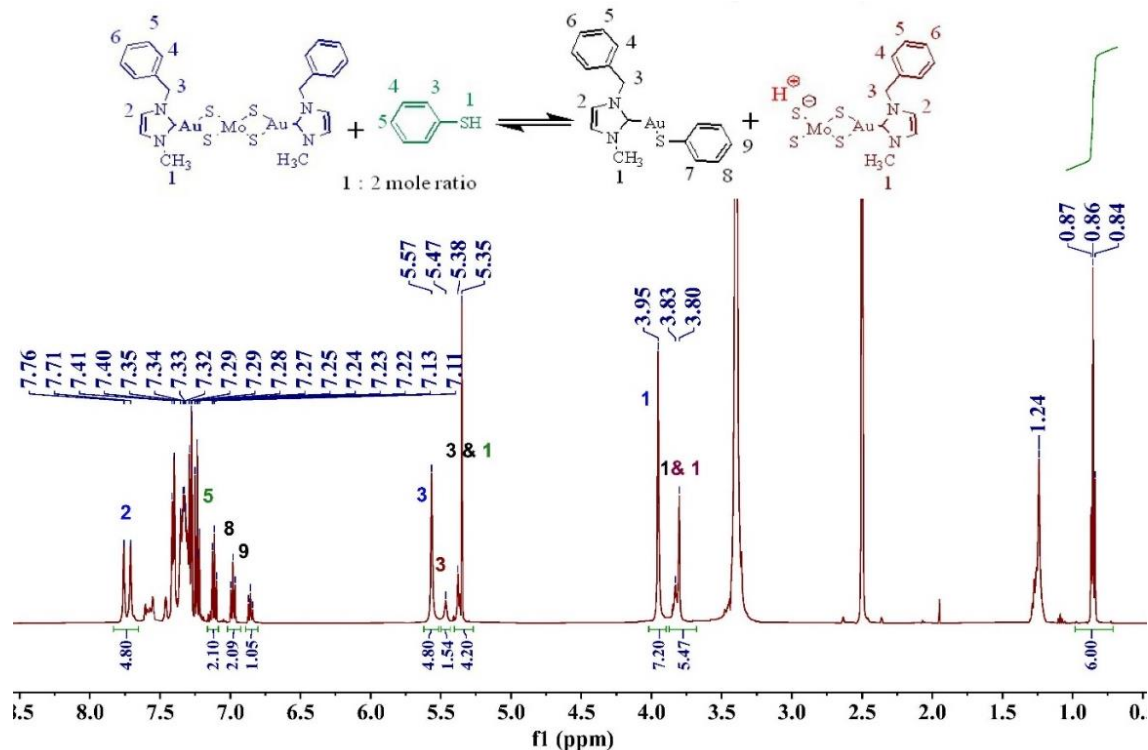
Figure 4.45. ^{1}H NMR in DMSO-d_6 of the reaction between **C-2** and PhSH after 30 min, the expected reaction equation with the relative peaks of each compound were assigned.

132
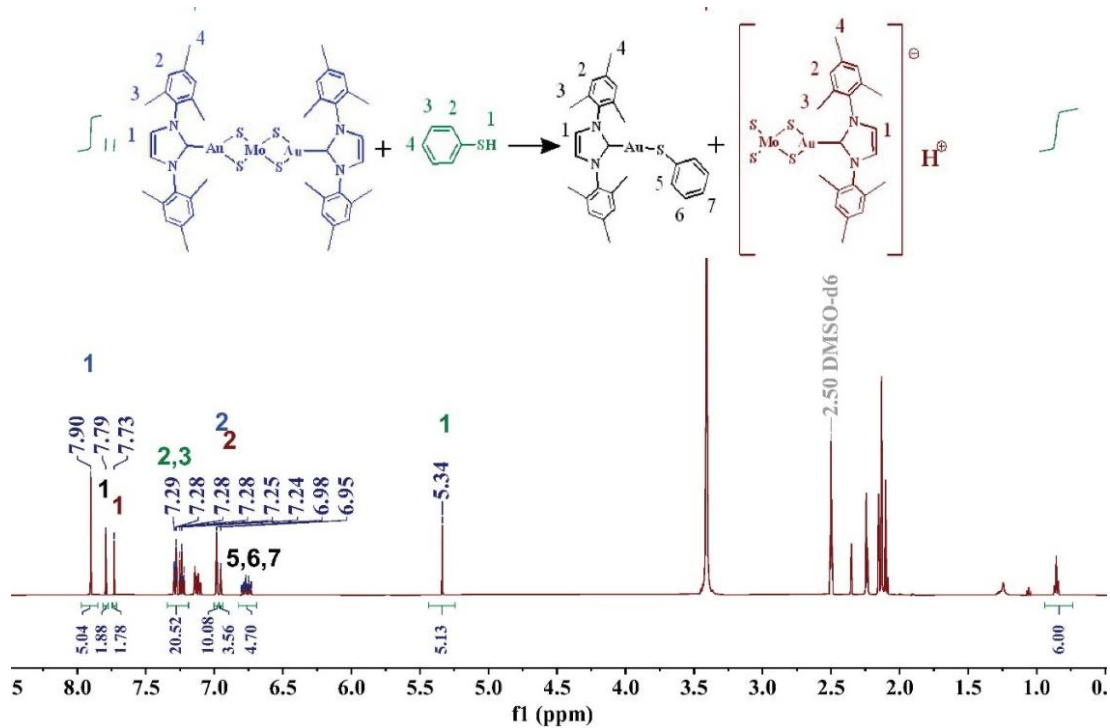
Figure 4.46. ^{1}H NMR in DMSO-d_6 of the reaction between **C-3** and PhSH after 10 min, the expected reaction equation with the relative peaks of each compound were assigned.
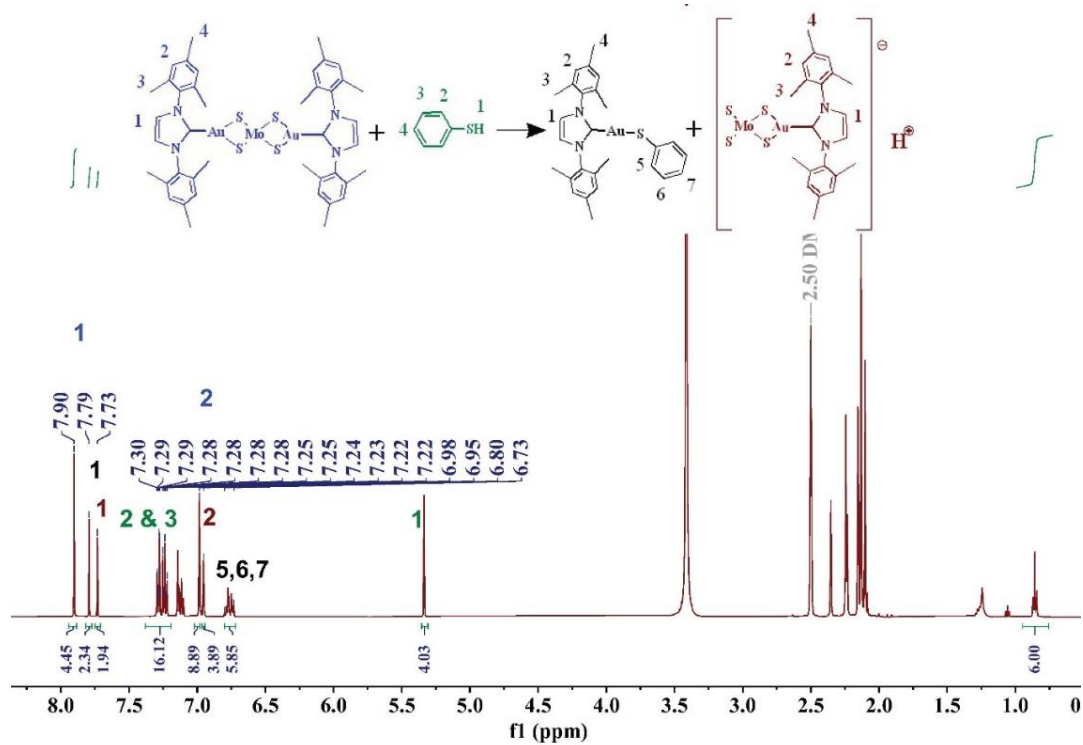
Figure 4.47. ^{1}H NMR in DMSO-d_6 of the reaction between **C-3** and PhSH after 20 min, the expected reaction equation with the relative peaks of each compound were assigned.
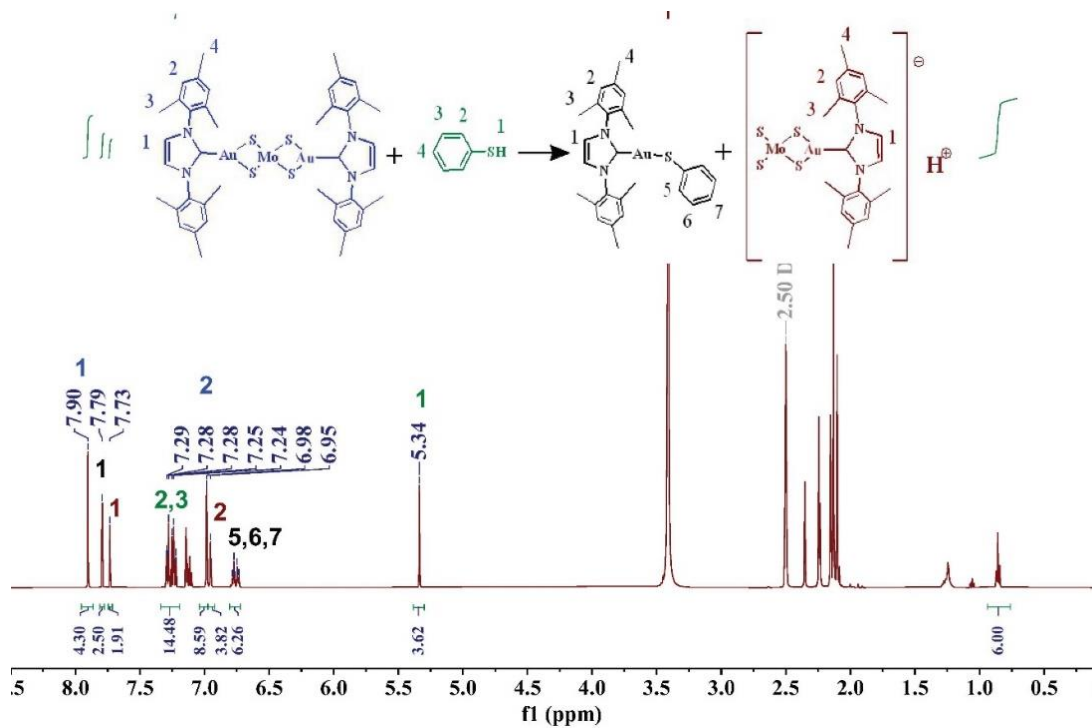
Figure 4.48. ^{1}H NMR in DMSO-d_6 of the reaction between **C-3** and PhSH after 30 min, the expected reaction equation with the relative peaks of each compound were assigned.
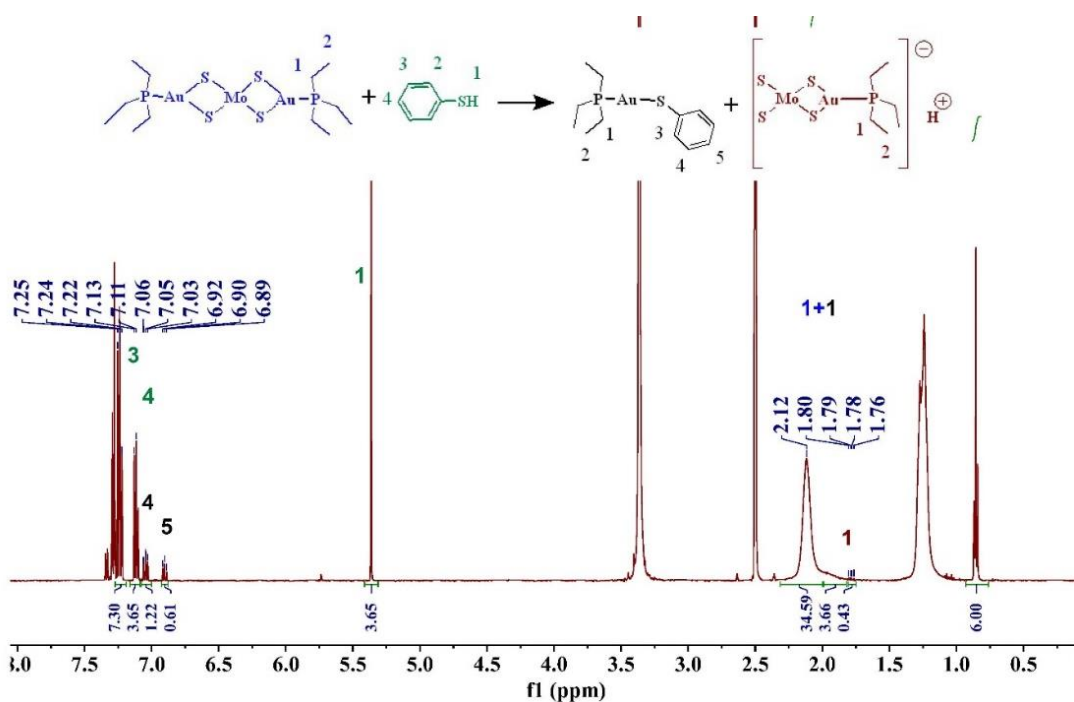
Figure 4.49. ^{1}H NMR in DMSO-d_6 of the reaction between **C-5** and PhSH after 10 min, the expected reaction equation with the relative peaks of each compound were assigned.
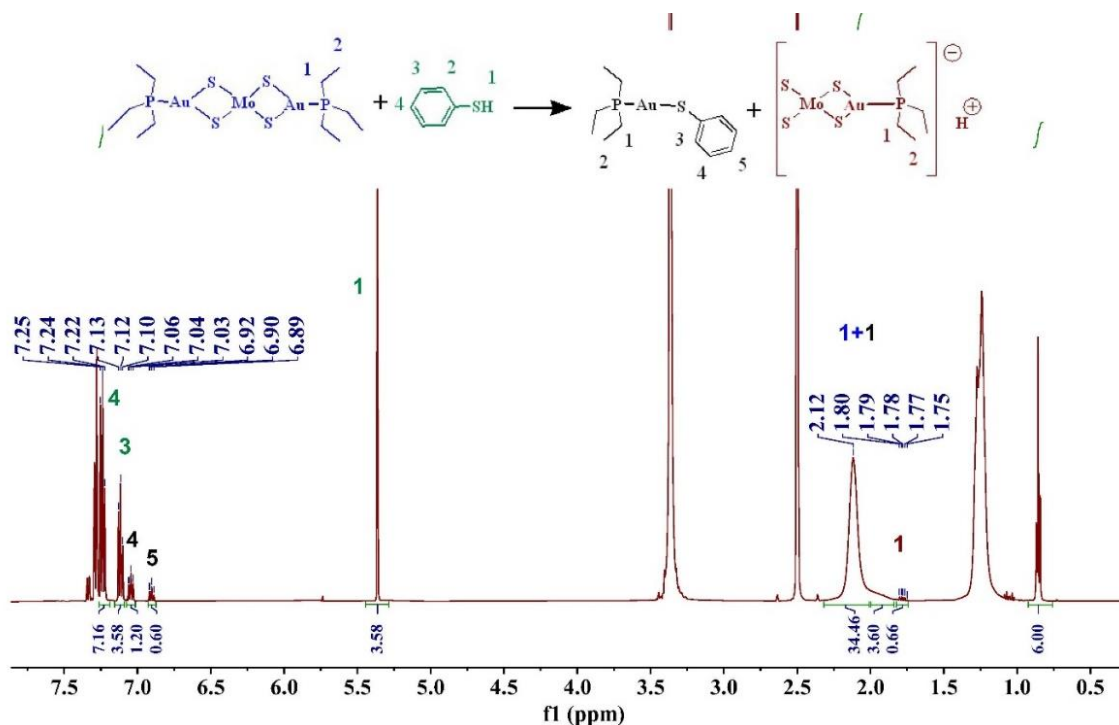
Figure 4.50. ^{1}H NMR in DMSO-d_6 of the reaction between **C-5** and PhSH after 20 min, the expected reaction equation with the relative peaks of each compound were assigned.
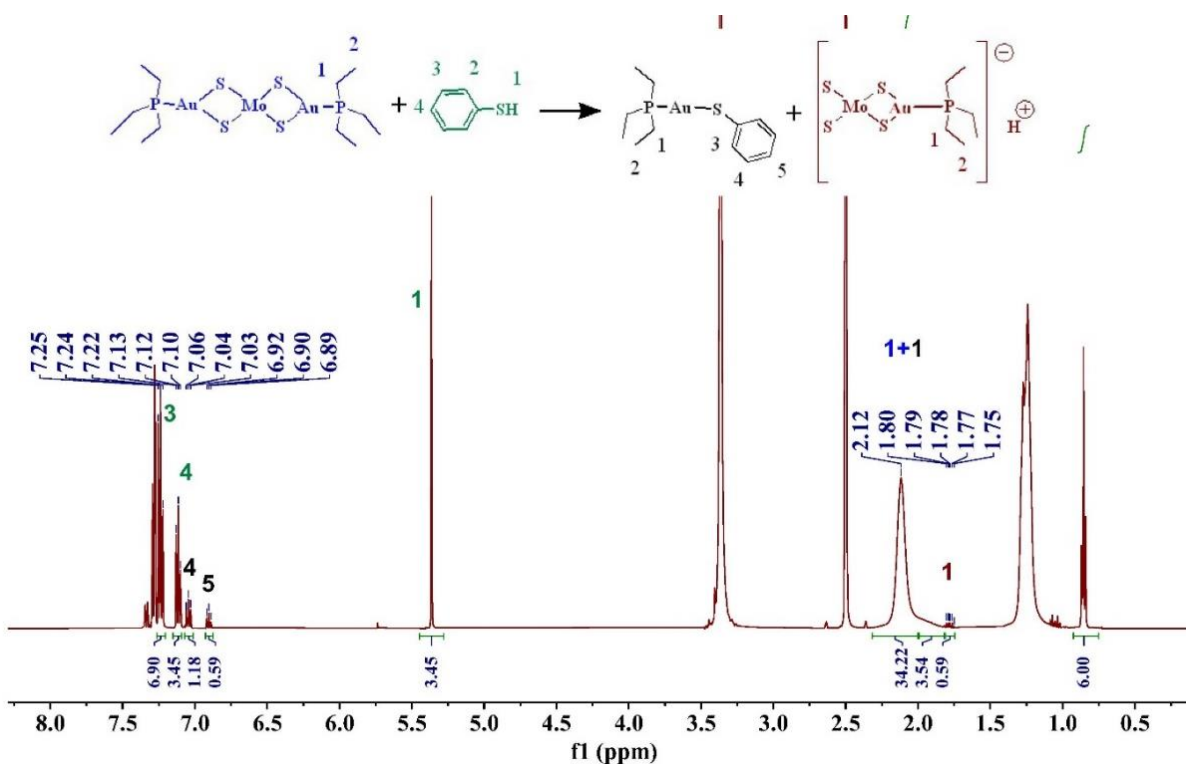
Figure 4.51. ^{1}H NMR in DMSO-d_6 of the reaction between **C-5** and PhSH after 30 min, the expected reaction equation with the relative peaks of each compound were assigned.
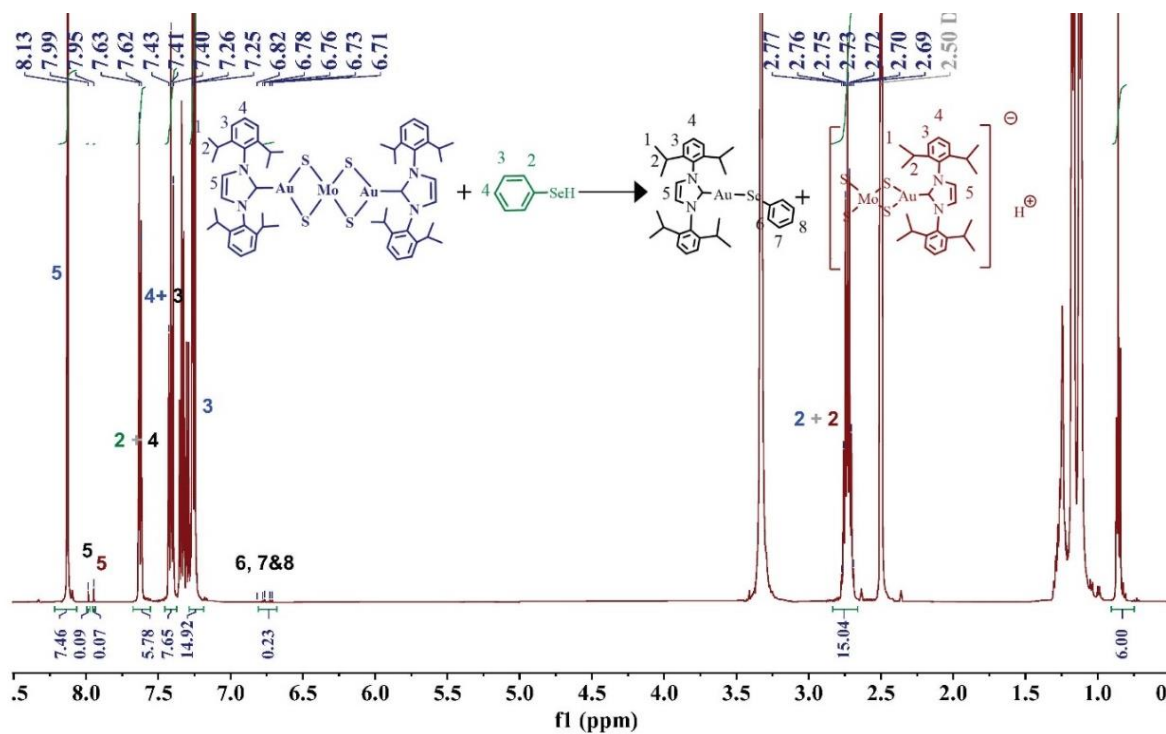
Figure 4.52. ^{1}H NMR in DMSO-d_6 of the reaction between **C-1** and PhSeH after 10 min, the expected reaction equation with the relative peaks of each compound were assigned.
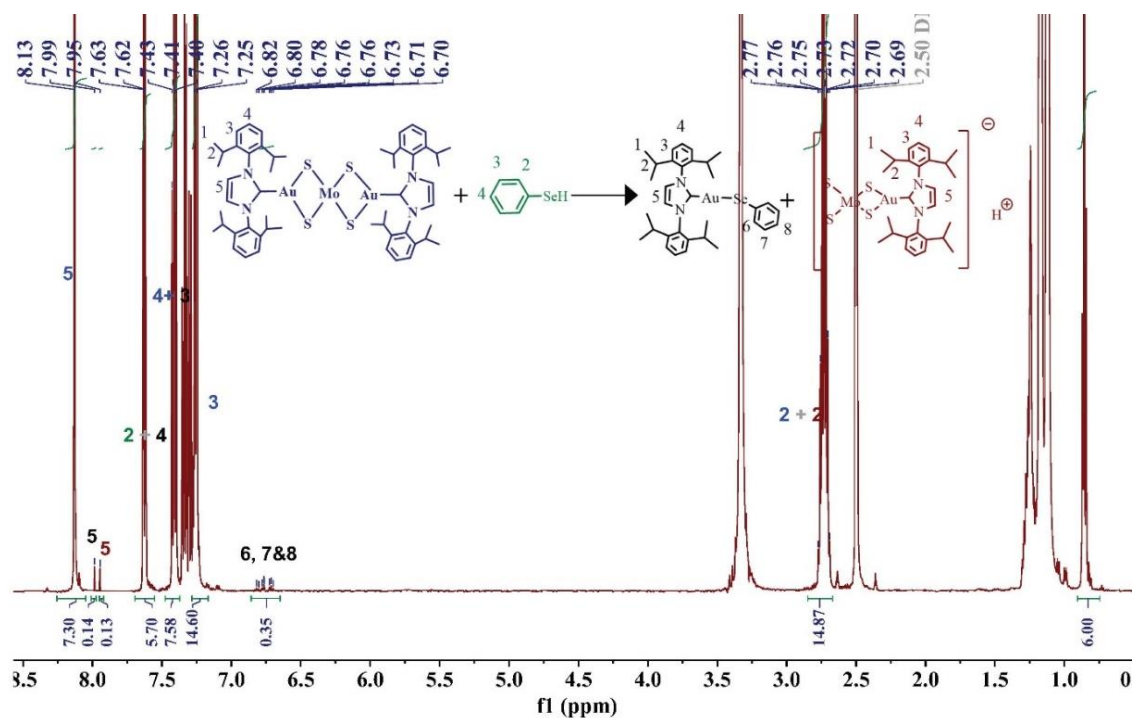
Figure 4.53. ^{1}H NMR in DMSO-d_6 of the reaction between **C-1** and PhSeH after 20 min, the expected reaction equation with the relative peaks of each compound were assigned.
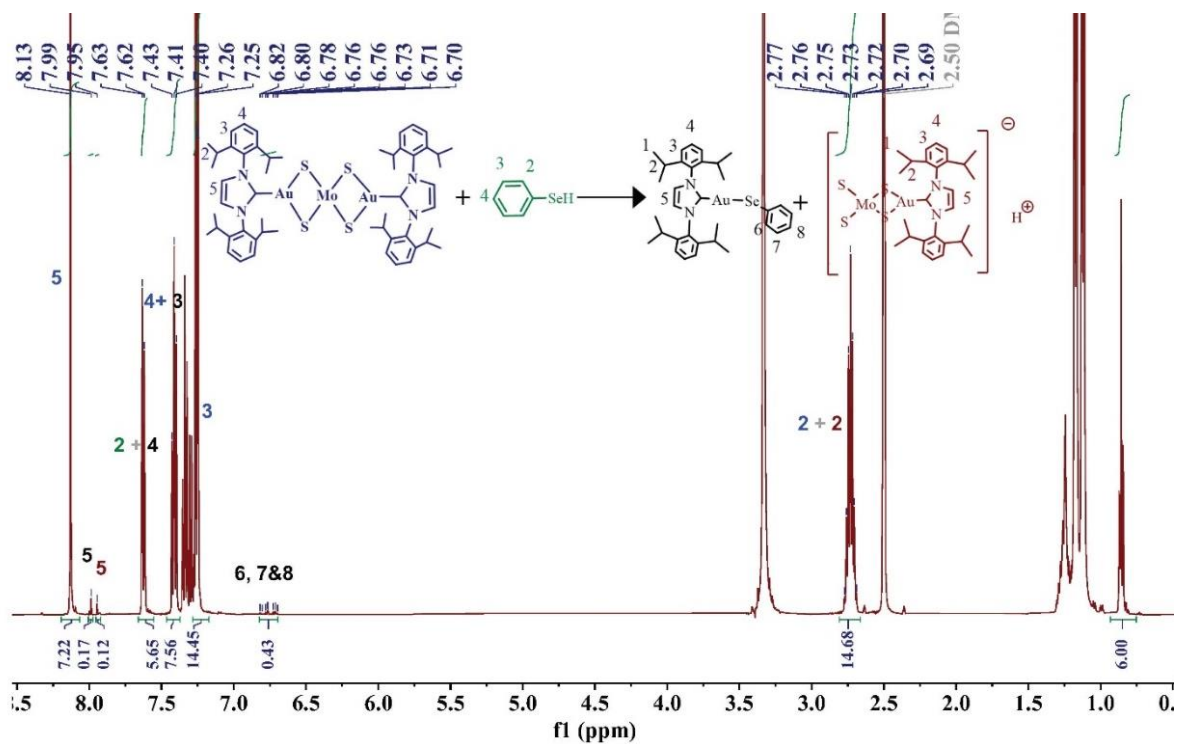
Figure 4.54. ^{1}H NMR in DMSO-d_6 of the reaction between **C-1** and PhSeH after 30 min, the expected reaction equation with the relative peaks of each compound were assigned.
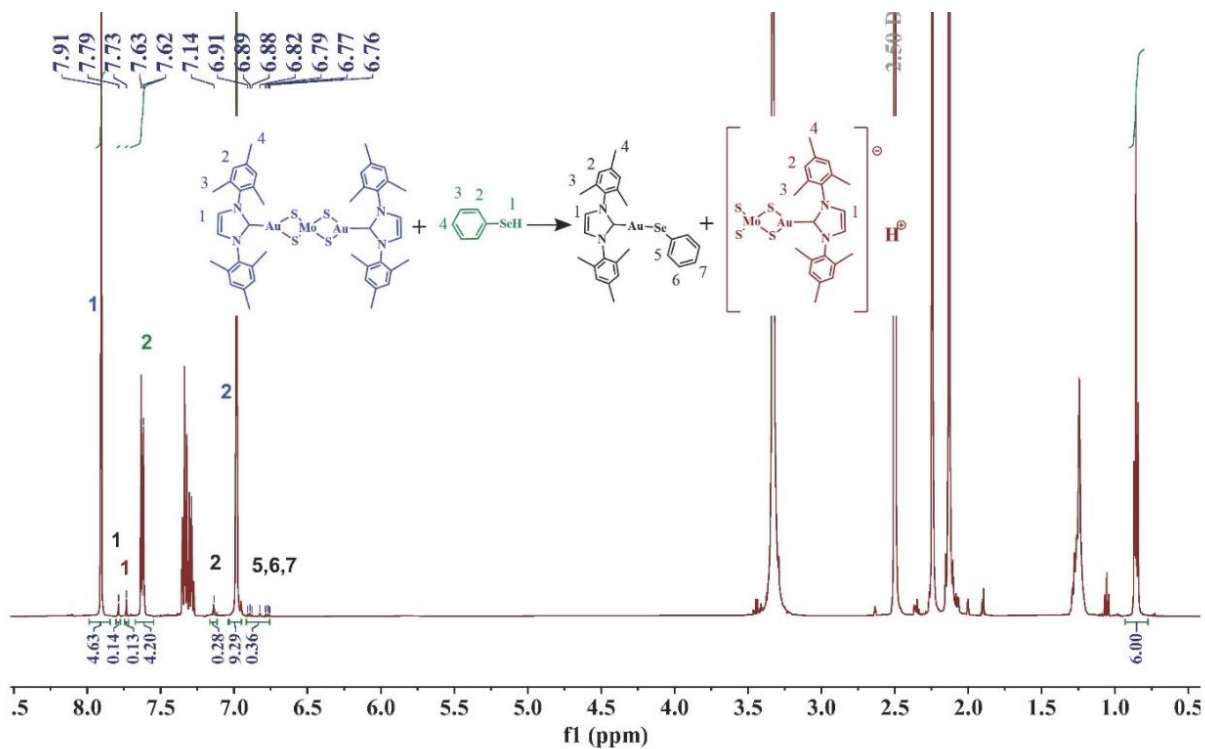
Figure 4.55. ^{1}H NMR in DMSO-d_6 of the reaction between **C-3** and PhSeH after 10 min, the expected reaction equation with the relative peaks of each compound were assigned.

137
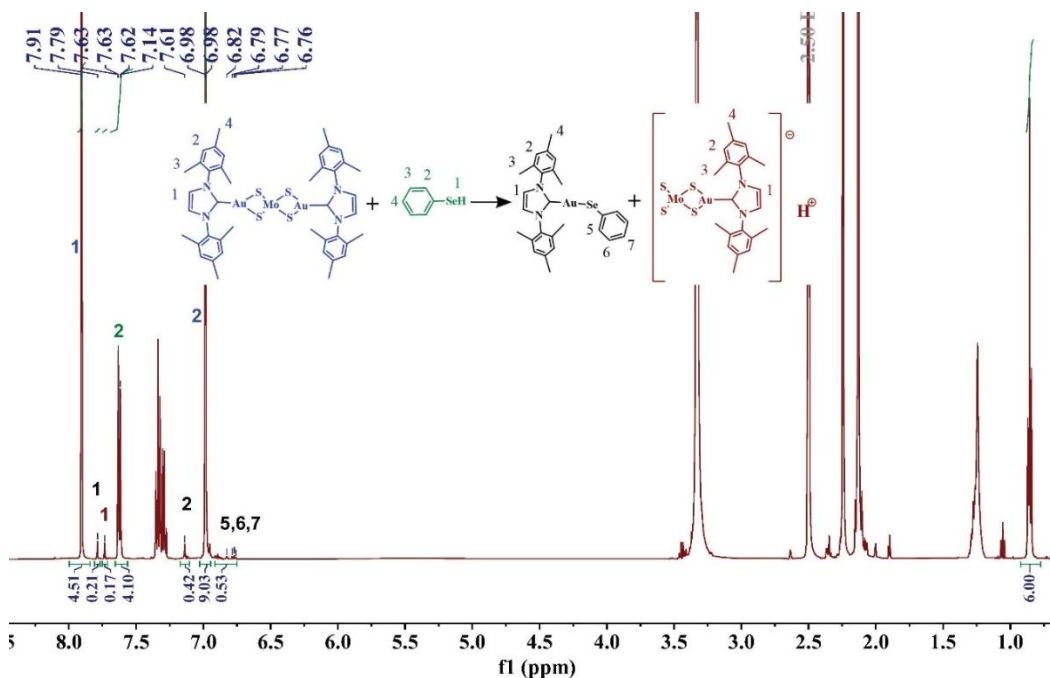
Figure 4.56. ^{1}H NMR in DMSO-d_6 of the reaction between **C-3** and PhSeH after 10 min, the expected reaction equation with the relative peaks of each compound were assigned.
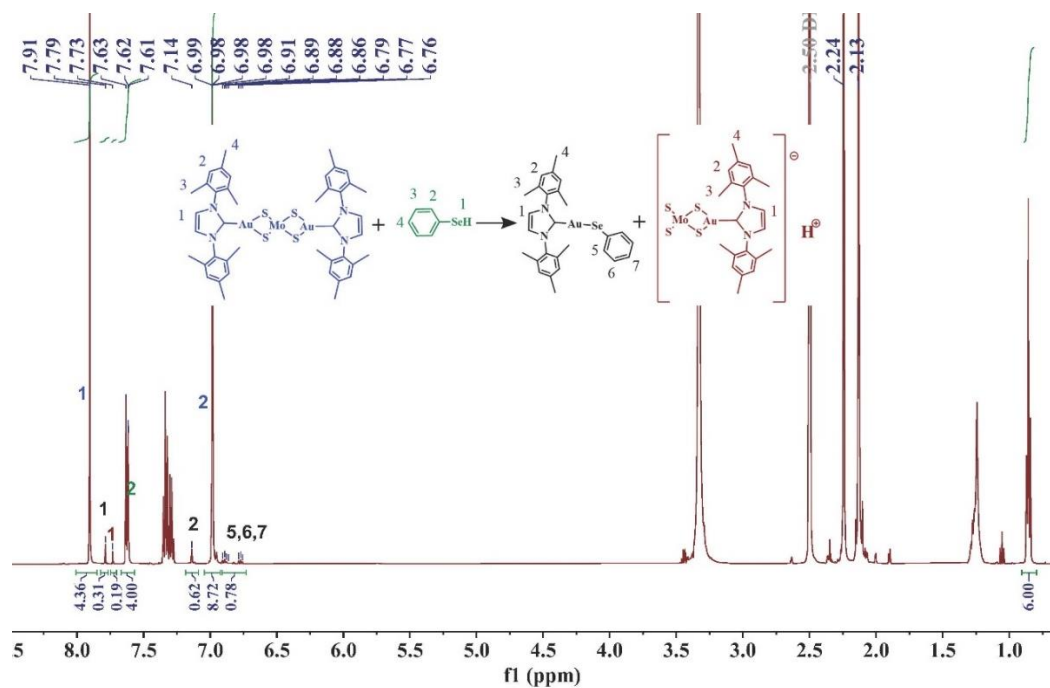
Figure 4.57. ^{1}H NMR in DMSO-d_6 of the reaction between **C-3** and PhSeH after 10 min, the expected reaction equation with the relative peaks of each compound were assigned.

4.4. Discussion and conclusions

Clusters **C-1 – C-5** were screened for antimicrobial activity by the CO-ADD lab at the University of Queensland, Australia. Four gram-negative and one gram-positive bacteria and two fungal strains were used in the initial screening (Table 4.1). Cluster **C-2** showed notable activity against one fungal strain, *Candida albicans*, and **C-5** showed notable activity against the gram-positive bacteria, *methicillin-resistant Staphylococcus aureus* and one fungal strain, *Cryptococcus neoformans*. Clusters **C-1**, **C-3**, and **C-4** did not make the cutoff of a MIC ≤ 32 μg/ mL. Clusters **C-2** and **C-5** also demonstrated low toxicity against human embryonic kidney cell lines and in the hemolysis tests on human red blood cells.

A predominant mechanism for the biological activity of gold (I) complexes is the inhibition of TrxR, an enzyme which carries out thiol-disulfide exchange and contributes to redox regulation in cells. Dysregulation of redox can result in apoptosis. TrxR plays a key role in redox homeostasis in humans, some fungi, and gram-positive bacteria. In general, gram-negative bacteria are less reliant on TrxR for maintaining redox homeostasis because the glutathione-glutaredoxin system can scavenge reactive oxygen species.[26] TrxR has been identified as a potential target for anticancer and antimicrobial drug development.[27] TrxR has a selenocysteine at the active site and the strong inhibition by gold(I) is attributed to the affinity of the soft Au(I) ion for soft selenium. Gold(I) will also bind strongly to cysteine, thereby inhibiting enzymes with sulfur at the active site, such as glutaredoxins and proteases.[28,29]

Bagno, et al. investigated the reactivity of auranofin with PhSH and PhSeH as models for thiol and selenol nucleophiles present in cysteine and selenocysteine proteins. They found that PhSH and PhSeH both substitute the thiolate ligand in auranofin and the equilibrium constant (in $CDCl_3$ solution) for substitution by PhSeH is a factor of 1000 times greater than for PhSH. The reaction in a more polar solvent (CH_3OH) is more complex, including oxidation of PhSeH to PhSeSePh, substitution of the Et_3P ligand, and formation of $Et_3P=O$.[21]

In contrast to the reactions of auranofin with sulfur and selenium nucleophiles, the reactions of the [MoS$_4$(AuL)$_2$] clusters with PhSH proceed to a greater extent than the reactions with PhSeH. The reactions were carried out in a polar solvent, DMSO-d_6, and similar to the results of Bagno and coworkers, the formation of PhSeSePh and Et$_3$P=O (for **C-5**) was observed. Cluster **C-3** was the most reactive with PhSH and PhSeH in NMR studies but this complex was inactive in antimicrobial cytotoxicity testing. Clusters **C-2** and **C-5** were the most cytotoxic in antimicrobial screening studies and both react with PhSH but not with PhSeH. Cluster **C-4** was not reactive with PhSH or PhSeH and it was completely inactive in cytotoxicity testing.

The results of DFT calculations on **C-1** discussed in chapter 3 suggest that the HOMO in the [MoS$_4$(AuL)$_2$] clusters is Au and S in character. We expect that sulfur and selenium nucleophiles would attack at the gold(I) ion, displacing the bridging sulfurs. The % V$_{bur}$ calculations indicate that the steric bulk increases in the order **C-5** ≈ **C-2** < **C-4** < **C-3** < **C-1**. Notably the least sterically hindered clusters **C-5** and **C-2** were the most cytotoxic for microorganisms. However, the cluster which reacted to the greatest extent with PhSH, **C-3**, has greater steric bulk. None of the clusters reacted to a great extent with PhSeH, perhaps in part due to the large atomic radius of selenium vs sulfur and the stability of the interaction AuL$^+$ with MoS$_4$$^{2-}$. Further investigations are needed to better understand the complex interplay of steric and electronic effects in the [MoS$_4$(AuL)$_2$] clusters.

4.5. Future work

We have presented the synthesis and reactivity of bimetallic complexes containing gold(I) and tetrathiomolybdate, [MoS$_4$(AuL)$_2$], **C-1 − C-5**. In general, the reactivity of [MoS$_4$(AuL)$_2$] with any compound has not been reported and our thesis work is the first in the field to study the reactions with benzenethiol and benzeneselenol. Further investigations are needed to better understand the complex interplay of steric and electronic effects in the [MoS$_4$(AuL)$_2$] clusters. Additional experiments should be done to determine the order of reaction and rate of reaction of these clusters with benzenethiol in

different solvents (DMSO-d_6, CH$_2$Cl$_2$-d_2). More investigations are recommended to study the reactivity of **C-1 – C-5** with aliphatic thiol and selenol compounds. Moreover, it since tetrathiomolybate tends to chelate with copper[30–32], it could be useful to broaden our scope and investigate the trans metalation reactivity between **C-1 – C-5** clusters and a copper complex (Scheme 4.6). It would also be interesting to try the reaction with other metals. This could open further applications of these clusters beside the reactivity with thiol and selenol compounds.
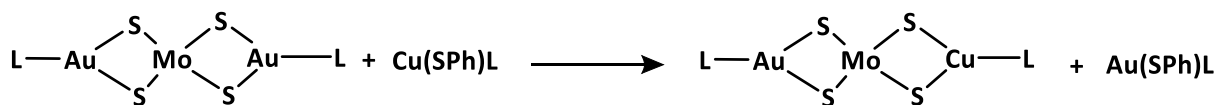
Scheme 4.6. The proposed reaction of a copper complex with **C-1 - C-5** clusters, L= NHC.

In Chapter 1 in the section "NHC ligand modification effect on anticancer activity of gold complexes", studies by Gust, et al., and Ott, et al. were discussed. These authors reported that adding aryl rings to the imidazol-2-ylidene ring at positions 4 and 5 improved the growth-inhibitory properties against cancer cell lines.[33,34] Furthermore, Gust, et al., reported that F-substituents in the ortho-position of those aryl rings significantly boosted activity.[33] Another study by Contel, et al. reported that saturated the NHC ligand, SIPr in [(η^5-C$_5$H$_5$)$_2$ Ti(CH$_3$){OC(O)-p-C$_6$H$_4$SAu(NHC)}] showed higher anticancer activity than unsaturated IPr and IMes ligands (Figure 1.6) .[35]

We suggest adding aryl rings to the imidazol-2-ylidene ring at positions 4 and 5 of the ligand used in cluster **C-2** to try to improve the reactivity, and also F-substituents in the ortho-position of the aromatic rings. Cluster **C-3**, which was the most reactive toward benzenethiol and benzeneselenol could be modified with F-substituents on the aromatic ring and the NHC ligand could also be made with a saturated backbone (SIMes) (Scheme 4.7).
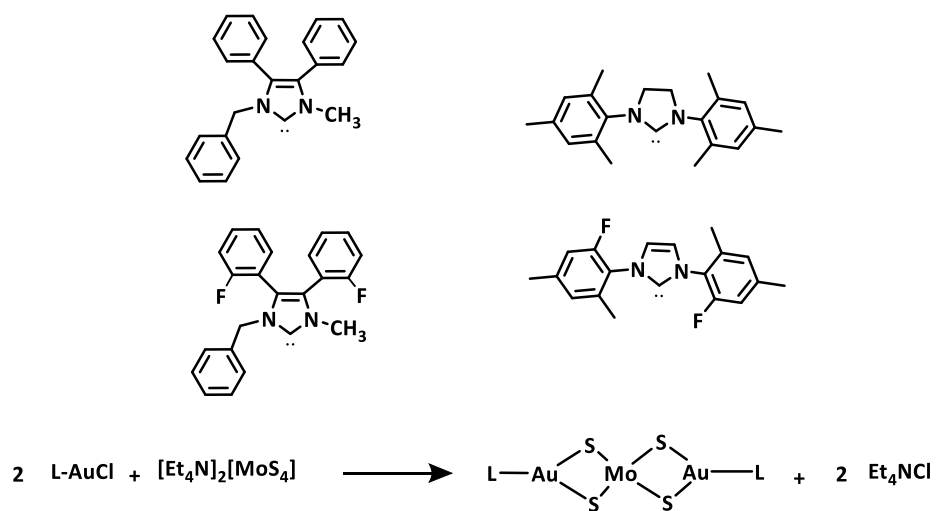
Scheme 4.7. The suggested modifications of the ligands used in cluster **C-2** and **C-3**

4.6. Chapter References

(1)   Atrián-Blasco, E.; Gascón, S.; Rodríguez-Yoldi, M. J.; Laguna, M.; Cerrada, E. Novel Gold(I)

        Thiolate Derivatives Synergistic with 5-Fluorouracil as Potential Selective Anticancer Agents in

        Colon Cancer. *Inorg Chem* **2017**, *56* (14), 8562–8579.

        https://doi.org/10.1021/acs.inorgchem.7b01370.

(2)   Arambula, J. F.; McCall, R.; Sidoran, K. J.; Magda, D.; Mitchell, N. A.; Bielawski, C. W.; Lynch, V.

        M.; Sessler, J. L.; Arumugam, K. Targeting Antioxidant Pathways with Ferrocenylated N-

        Heterocyclic Carbene Supported Gold(i) Complexes in A549 Lung Cancer Cells. *Chem Sci* **2016**, *7*

        (2), 1245–1256. https://doi.org/10.1039/C5SC03519H.

(3)   Mui, Y. F.; Fernández-Gallardo, J.; Elie, B. T.; Gubran, A.; Maluenda, I.; Sanaú, M.; Navarro, O.;

        Contel, M. Titanocene–Gold Complexes Containing N-Heterocyclic Carbene Ligands Inhibit

        Growth of Prostate, Renal, and Colon Cancers in Vitro. *Organometallics* **2016**, *35* (9), 1218–1227.

        https://doi.org/10.1021/acs.organomet.6b00051.

(4)   Arambula, J. F.; McCall, R.; Sidoran, K. J.; Magda, D.; Mitchell, N. A.; Bielawski, C. W.; Lynch, V.

        M.; Sessler, J. L.; Arumugam, K. Targeting Antioxidant Pathways with Ferrocenylated N-

        Heterocyclic Carbene Supported Gold(i) Complexes in A549 Lung Cancer Cells. *Chem Sci* **2016**, *7*

        (2), 1245–1256. https://doi.org/10.1039/C5SC03519H.

(5)   González-Pantoja, J. F.; Stern, M.; Jarzecki, A. A.; Royo, E.; Robles-Escajeda, E.; Varela-Ramírez,

        A.; Aguilera, R. J.; Contel, M. Titanocene–Phosphine Derivatives as Precursors to Cytotoxic

        Heterometallic TiAu2 and TiM (M = Pd, Pt) Compounds. Studies of Their Interactions with DNA.

        Inorg Chem **2011**, *50* (21), 11099–11110. https://doi.org/10.1021/ic201647h.

(6)   Frei, A.; Elliott, A. G.; Kan, A.; Dinh, H.; Bräse, S.; Bruce, A. E.; Bruce, M. R.; Chen, F.; Humaidy, D.;

        Jung, N.; King, A. P.; Lye, P. G.; Maliszewska, H. K.; Mansour, A. M.; Matiadis, D.; Muñoz, M. P.;

        Pai, T.-Y.; Pokhrel, S.; Sadler, P. J.; Sagnou, M.; Taylor, M.; Wilson, J. J.; Woods, D.; Zuegg, J.;

Meyer, W.; Cain, A. K.; Cooper, M. A.; Blaskovich, M. A. T. Metal Complexes as Antifungals? From a Crowd-Sourced Compound Library to the First In Vivo Experiments. *JACS Au* **2022**. https://doi.org/10.1021/jacsau.2c00308.

(7)   Blaskovich, M. A. T.; Zuegg, J.; Elliott, A. G.; Cooper, M. A. Helping Chemists Discover New Antibiotics. *ACS Infect Dis* **2015**, *1* (7), 285–287. https://doi.org/10.1021/acsinfecdis.5b00044.

(8)   Sadler, P. J.; Sue, R. E. The Chemistry of Gold Drugs. *Met Based Drugs* **1994**, *1*, 908213. https://doi.org/10.1155/MBD.1994.107.

(9)   Cottrill, S. M.; Sharma, H. L.; Dyson, D. B.; Parish, R. v; McAuliffe, C. A. The Role of the Ligand in Chrysotherapy: A Kinetic Study of 199Au- and 35S-Labelled Myocrisin and Auranofin. *Journal of the Chemical Society, Perkin Transactions 2* **1989**, No. 1, 53–58. https://doi.org/10.1039/P29890000053.

(10)   Meyer, A.; Bagowski, C. P.; Kokoschka, M.; Stefanopoulou, M.; Alborzinia, H.; Can, S.; Vlecken, D. H.; Sheldrick, W. S.; Wölfl, S.; Ott, I. On the Biological Properties of Alkynyl Phosphine Gold(I) Complexes. *Angewandte Chemie International Edition* **2012**, *51* (35), 8895–8899. https://doi.org/https://doi.org/10.1002/anie.201202939.

(11)   Berners-Price, S. J.; Filipovska, A. Gold Compounds as Therapeutic Agents for Human Diseases. *Metallomics* **2011**, *3* (9), 863–873. https://doi.org/10.1039/c1mt00062d.

(12)   Mohamed, M. M.; Sloane, B. F. Multifunctional Enzymes in Cancer. *Nat Rev Cancer* **2006**, *6* (10), 764–775. https://doi.org/10.1038/nrc1949.

(13)   Urig, S.; Fritz-Wolf, K.; Réau, R.; Herold-Mende, C.; Tóth, K.; Davioud-Charvet, E.; Becker, K. Undressing of Phosphine Gold(I) Complexes as Irreversible Inhibitors of Human Disulfide Reductases. *Angewandte Chemie International Edition* **2006**, *45* (12), 1881–1886. https://doi.org/https://doi.org/10.1002/anie.200502756.

(14)   Hickey, J. L.; Ruhayel, R. A.; Barnard, P. J.; Baker, M. v; Berners-Price, S. J.; Filipovska, A.

Mitochondria-Targeted Chemotherapeutics: The Rational Design of Gold(I) N-Heterocyclic

Carbene Complexes That Are Selectively Toxic to Cancer Cells and Target Protein Selenols in

Preference to Thiols. *J Am Chem Soc* **2008**, *130* (38), 12570–12571.

https://doi.org/10.1021/ja804027j.

(15)   Rigobello, M. P.; Scutari, G.; Boscolo, R.; Bindoli, A. Induction of Mitochondrial Permeability

Transition by Auranofin, a Gold(I)-Phosphine Derivative. *Br J Pharmacol* **2002**, *136* (8), 1162–

1168. https://doi.org/https://doi.org/10.1038/sj.bjp.0704823.

(16)   Rigobello, M. P.; Scutari, G.; Folda, A.; Bindoli, A. Mitochondrial Thioredoxin Reductase

Inhibition by Gold(I) Compounds and Concurrent Stimulation of Permeability Transition and

Release of Cytochrome c. *Biochem Pharmacol* **2004**, *67* (4), 689–696.

https://doi.org/https://doi.org/10.1016/j.bcp.2003.09.038.

(17)   Marzano, C.; Gandin, V.; Folda, A.; Scutari, G.; Bindoli, A.; Rigobello, M. P. Inhibition of

Thioredoxin Reductase by Auranofin Induces Apoptosis in Cisplatin-Resistant Human Ovarian

Cancer Cells. *Free Radic Biol Med* **2007**, *42* (6), 872–881.

https://doi.org/https://doi.org/10.1016/j.freeradbiomed.2006.12.021.

(18)   Rigobello, M. P.; Folda, A.; Dani, B.; Menabò, R.; Scutari, G.; Bindoli, A. Gold(I) Complexes

Determine Apoptosis with Limited Oxidative Stress in Jurkat T Cells. *Eur J Pharmacol* **2008**, *582*

(1), 26–34. https://doi.org/https://doi.org/10.1016/j.ejphar.2007.12.026.

(19)   Ott, I.; Qian, X.; Xu, Y.; Vlecken, D. H. W.; Marques, I. J.; Kubutat, D.; Will, J.; Sheldrick, W. S.;

Jesse, P.; Prokop, A.; Bagowski, C. P. A Gold(I) Phosphine Complex Containing a Naphthalimide

Ligand Functions as a TrxR Inhibiting Antiproliferative Agent and Angiogenesis Inhibitor. *J Med*

Chem **2009**, *52* (3), 763–770. https://doi.org/10.1021/jm8012135.

(20)   Rackham, O.; Nichols, S. J.; Leedman, P. J.; Berners-Price, S. J.; Filipovska, A. A Gold(I) Phosphine

         Complex Selectively Induces Apoptosis in Breast Cancer Cells: Implications for Anticancer

         Therapeutics Targeted to Mitochondria. *Biochem Pharmacol* **2007**, *74* (7), 992–1002.

         https://doi.org/https://doi.org/10.1016/j.bcp.2007.07.022.

(21)   di Sarra, F.; Fresch, B.; Bini, R.; Saielli, G.; Bagno, A. Reactivity of Auranofin with Selenols and

         Thiols – Implications for the Anticancer Activity of Gold(I) Compounds. *Eur J Inorg Chem* **2013**,

         2013 (15), 2718–2727. https://doi.org/https://doi.org/10.1002/ejic.201300058.

(22)   Scattolin, T.; Tzouras, N. v; Falivene, L.; Cavallo, L.; Nolan, S. P. Using Sodium Acetate for the

         Synthesis of [Au(NHC)X] Complexes. *Dalton Transactions* **2020**, *49* (28), 9694–9700.

         https://doi.org/10.1039/D0DT02240C.

(23)   Kinsch, E. M.; Stephan, D. W. A 31P Nuclear Magnetic Resonance and Fluorescence Study of the

         Interaction of an Anti-Arthritic Gold Phosphine Drug with Albumin. A Bioinorganic Approach.

         Inorganica Chim Acta **1984**, *91* (4), 263–267. https://doi.org/https://doi.org/10.1016/S0020-

         1693(00)81848-4.

(24)   Bharti, S. K.; Roy, R. Quantitative 1H NMR Spectroscopy. *TrAC Trends in Analytical Chemistry*

         2012, *35*, 5–26. https://doi.org/https://doi.org/10.1016/j.trac.2012.02.007.

(25)   Malz, F.; Jancke, H. Validation of Quantitative NMR. *J Pharm Biomed Anal* **2005**, *38* (5), 813–823.

         https://doi.org/https://doi.org/10.1016/j.jpba.2005.01.043.

(26)   Felix, L.; Mylonakis, E.; Fuchs, B. B. Thioredoxin Reductase Is a Valid Target for Antimicrobial

         Therapeutic Development Against Gram-Positive Bacteria. *Front Microbiol* **2021**, *12*.

         https://doi.org/10.3389/fmicb.2021.663481.

(27)   Godoy, J. S. R.; Kioshima, É. S.; Abadio, A. K. R.; Felipe, M. S. S.; de Freitas, S. M.; Svidzinski, T. I.

         E. Structural and Functional Characterization of the Recombinant Thioredoxin Reductase from

Candida Albicans as a Potential Target for Vaccine and Drug Design. *Appl Microbiol Biotechnol* **2016**, *100* (9), 4015–4025. https://doi.org/10.1007/s00253-015-7223-8.

(28)   Tolbatov, I.; Marrone, A.; Coletti, C.; Re, N. Computational Studies of Au(I) and Au(III) Anticancer MetalLodrugs: A Survey. *Molecules* **2021**, *26* (24), 7600. https://doi.org/10.3390/molecules26247600.

(29)   Buglak, A. A.; Kononov, A. I. Comparative Study of Gold and Silver Interactions with Amino Acids and Nucleobases. *RSC Adv* **2020**, *10* (56), 34149–34160. https://doi.org/10.1039/D0RA06486F.

(30)   de Fabregues, O.; Viñas, J.; Palasí, A.; Quintana, M.; Cardona, I.; Auger, C.; Vargas, V. Ammonium Tetrathiomolybdate in the Decoppering Phase Treatment of Wilson's Disease with Neurological Symptoms: A Case Series. *Brain Behav* **2020**, *10* (5). https://doi.org/10.1002/brb3.1596.

(31)   Jurowska, A.; Jurowski, K.; Szklarzewicz, J.; Buszewski, B.; Kalenik, T.; Piekoszewski, W. Molybdenum Metallopharmaceuticals Candidate Compounds - The "Renaissance" of Molybdenum Metallodrugs? *Curr Med Chem* **2016**, *23* (29), 3322–3342. https://doi.org/10.2174/0929867323666160504103743.

(32)   Redman, B. G.; Esper, P.; Pan, Q.; Dunn, R. L.; Hussain, H. K.; Chenevert, T.; Brewer, G. J.; Merajver, S. D. Phase II Trial of Tetrathiomolybdate in Patients with Advanced Kidney Cancer1. *Clinical Cancer Research* **2003**, *9* (5), 1666–1672.

(33)   Liu, W.; Bensdorf, K.; Proetto, M.; Abram, U.; Hagenbach, A.; Gust, R. NHC Gold Halide Complexes Derived from 4,5-Diarylimidazoles: Synthesis, Structural Analysis, and Pharmacological Investigations as Potential Antitumor Agents. *J Med Chem* **2011**, *54* (24), 8605–8615. https://doi.org/10.1021/jm201156x.

(34)   Schmidt, C.; Karge, B.; Misgeld, R.; Prokop, A.; Brönstrup, M.; Ott, I. Biscarbene Gold(i) Complexes: Structure–Activity-Relationships Regarding Antibacterial Effects, Cytotoxicity, TrxR

Inhibition and Cellular Bioavailability. *Medchemcomm* **2017**, *8* (8), 1681–1689.

https://doi.org/10.1039/C7MD00269F.

(35) Mui, Y. F.; Fernández-Gallardo, J.; Elie, B. T.; Gubran, A.; Maluenda, I.; Sanaú, M.; Navarro, O.;

Contel, M. Titanocene–Gold Complexes Containing N-Heterocyclic Carbene Ligands Inhibit

Growth of Prostate, Renal, and Colon Cancers in Vitro. *Organometallics* **2016**, *35* (9), 1218–1227.

https://doi.org/10.1021/acs.organomet.6b00051.

APPENDIX A: [1]H, ^{13}C{^{1}H} AND ^{31}P {^{1}H} NMR SPECTRA
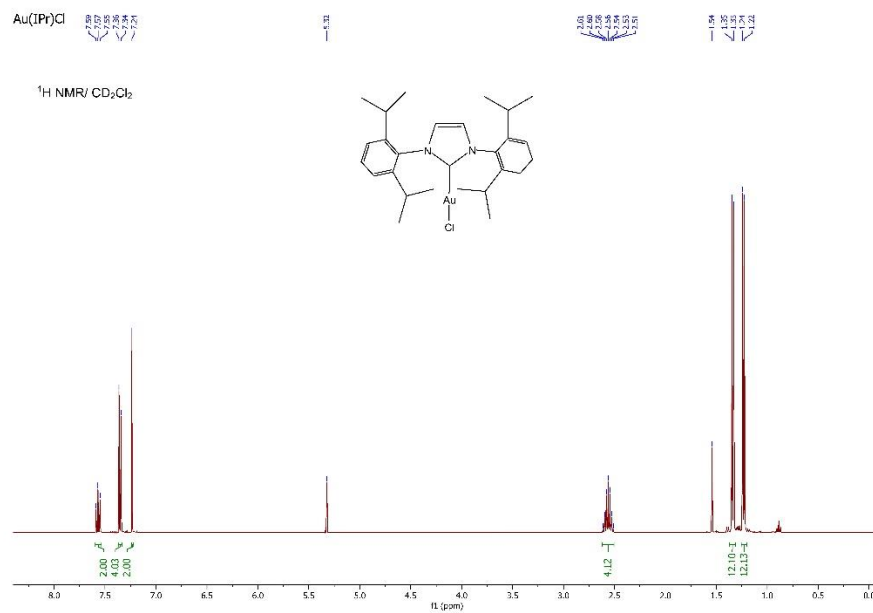
Fig. A. 1. ^{1}H NMR of Au(IPr)Cl in CH$_2$Cl$_2$-d_2.
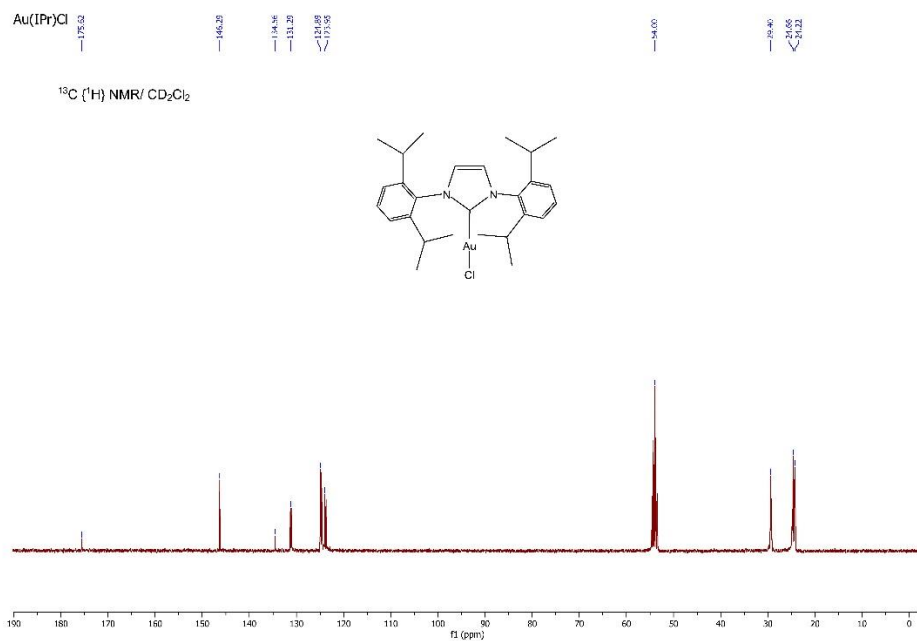
Fig. A. 2. ^{13}C{^{1}H} NMR of Au(IPr)Cl in CH$_2$Cl$_2$-d_2.
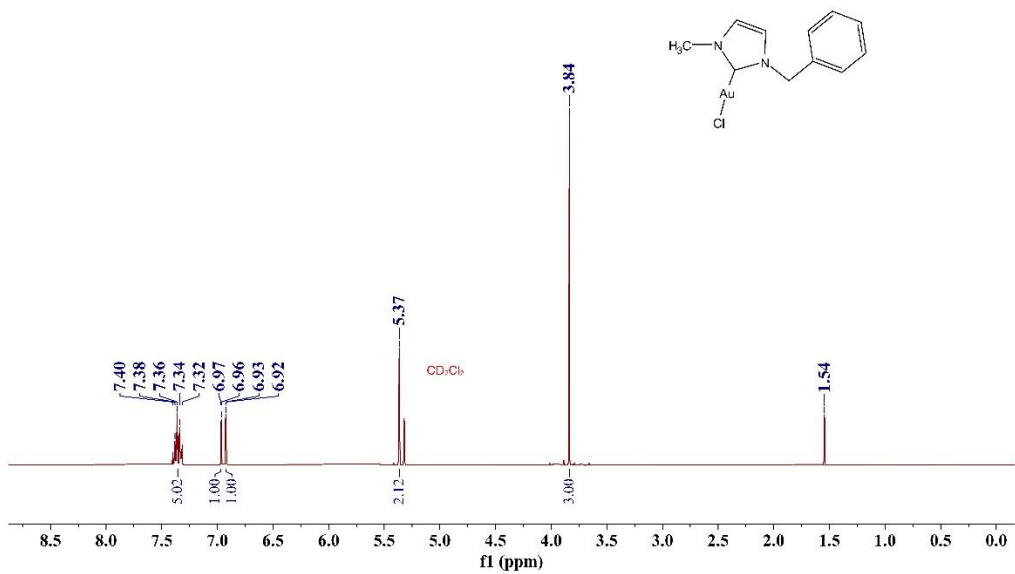
Fig. A. 3. ^{1}H NMR of Au(IBzMe)Cl in CH$_2$Cl$_2$-d_2.
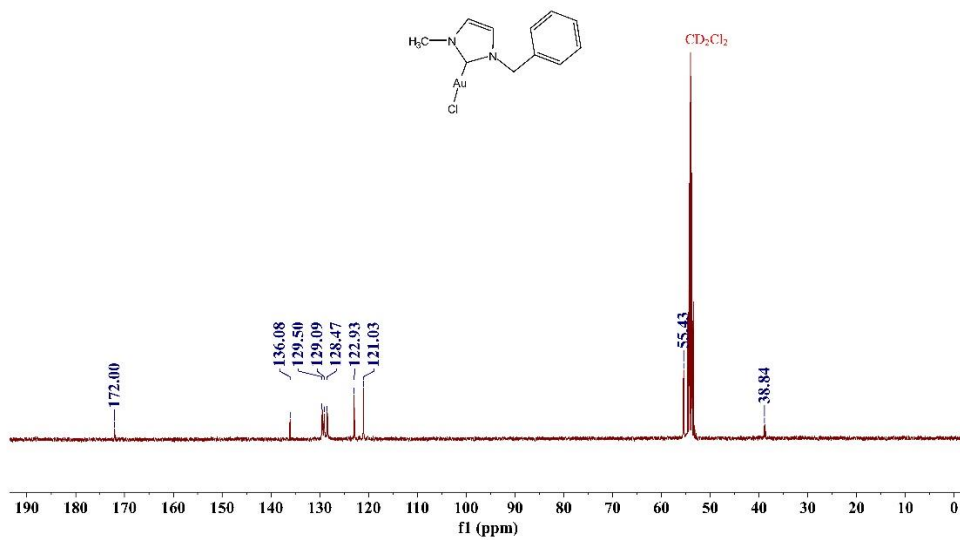
Fig. A. 4. ^{13}C{^{1}H} NMR of Au(IBzMe)Cl in CH$_2$Cl$_2$-d_2.
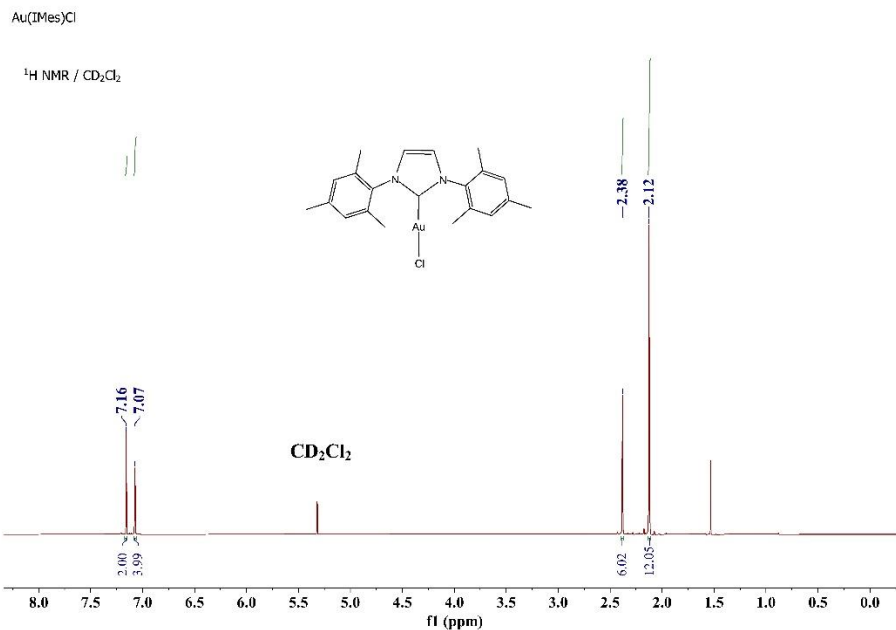
Fig. A. 5. ^{1}H NMR of Au(IMes)Cl in CH$_2$Cl$_2$-*d$_2$*.
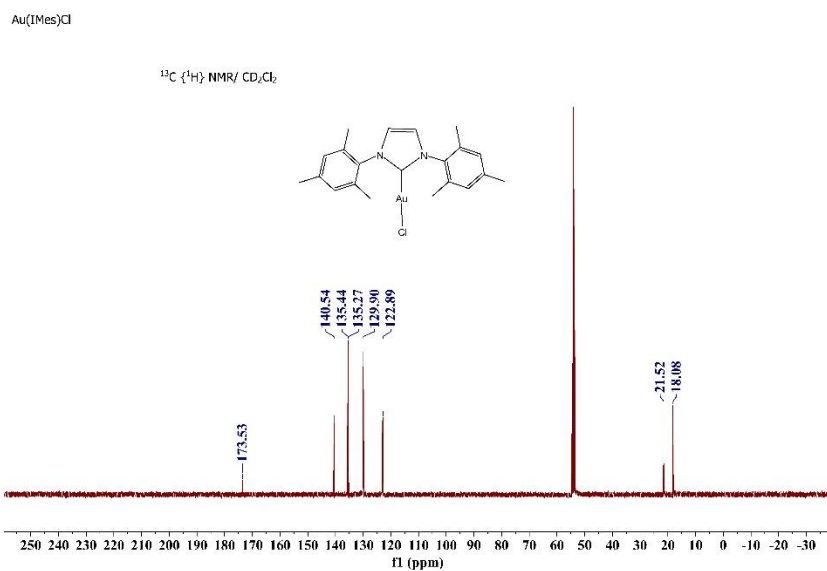
Fig. A. 6. ^{13}C{^{1}H} NMR of Au(IMes)Cl in CH$_2$Cl$_2$-*d$_2$*.
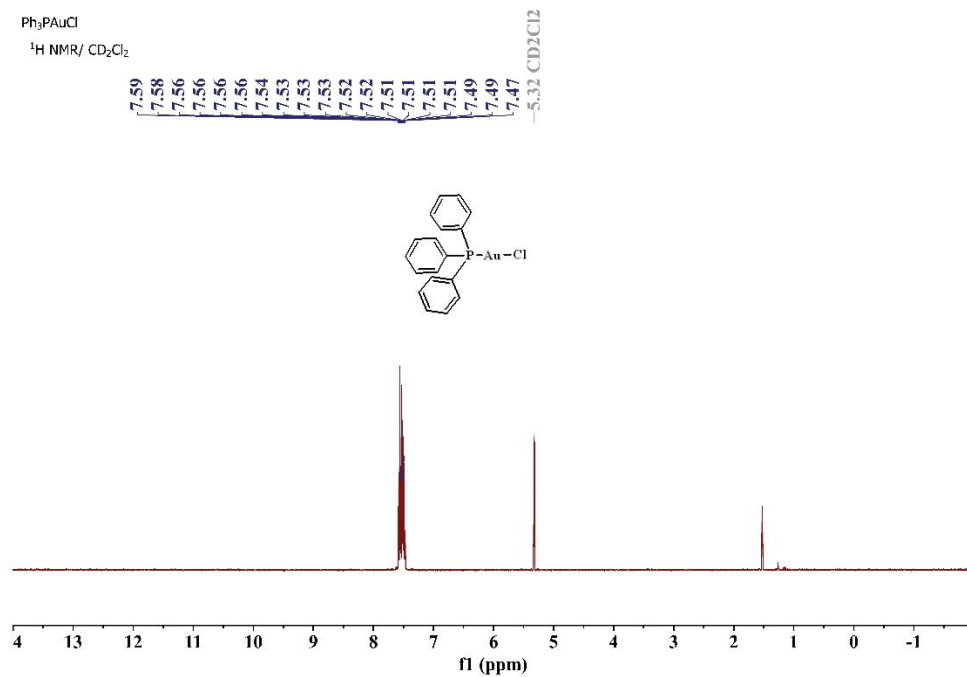
Fig. A. 7. ^{1}H NMR of Ph$_3$PAuCl in CH$_2$Cl$_2$-d_2.
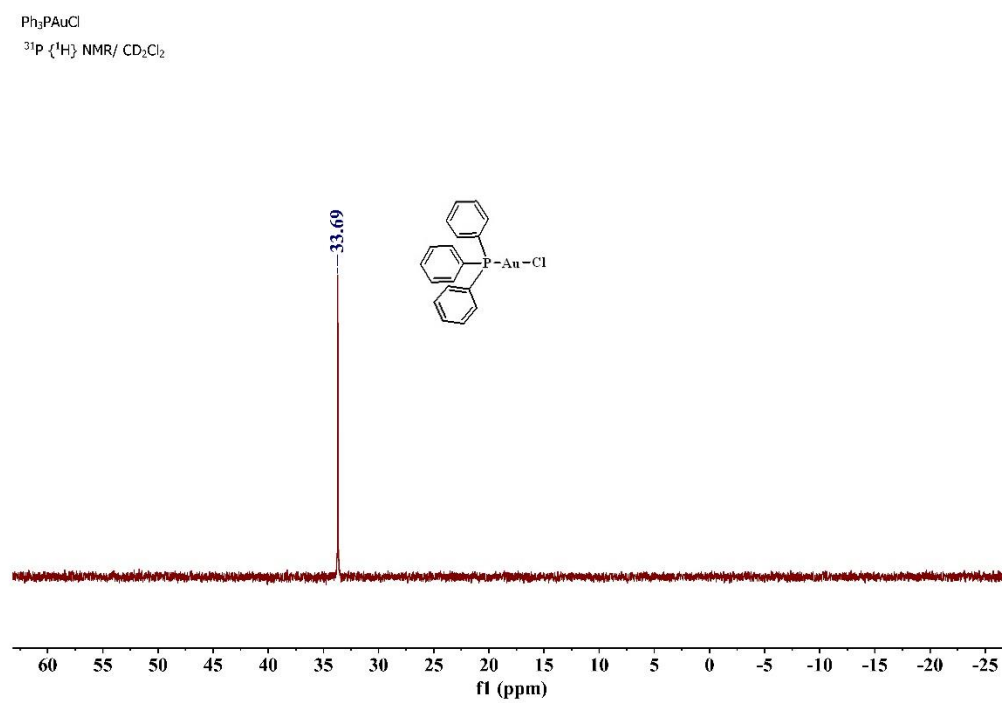
Fig. A. 8. ^{31}P{^{1}H} NMR of Ph$_3$PAuCl in CH$_2$Cl$_2$-d_2.

152
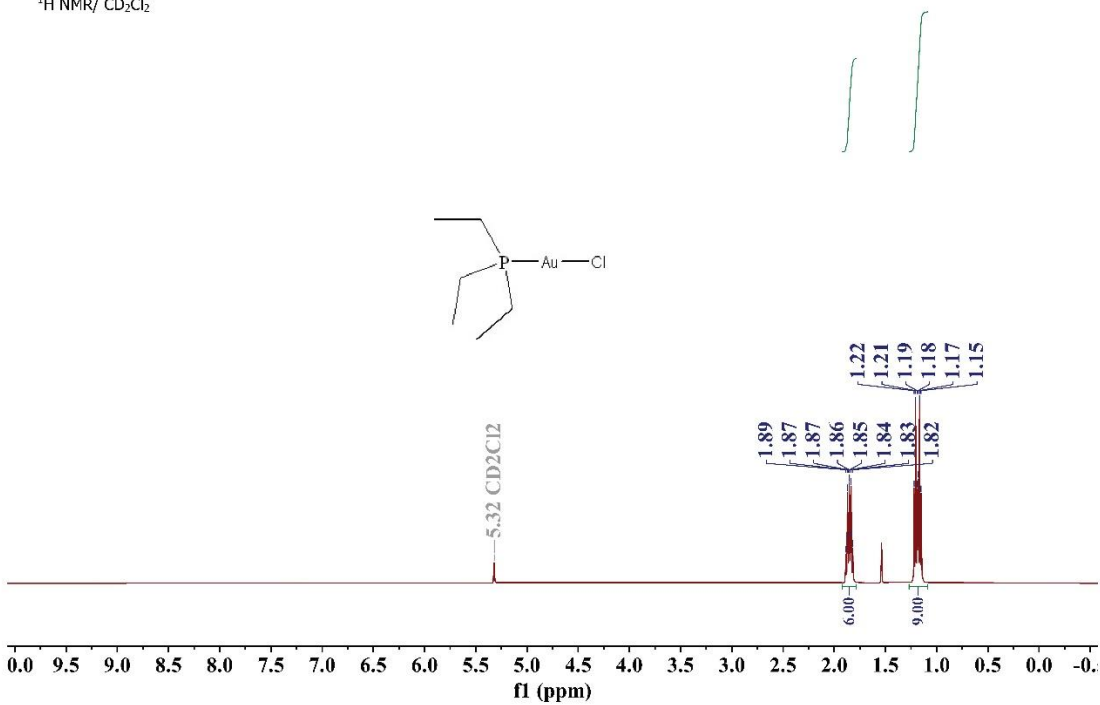
Et₃PAuCl

Fig. A. 9. ^{1}H NMR of Et$_3$PAuCl in CHCl$_3$-*d*.
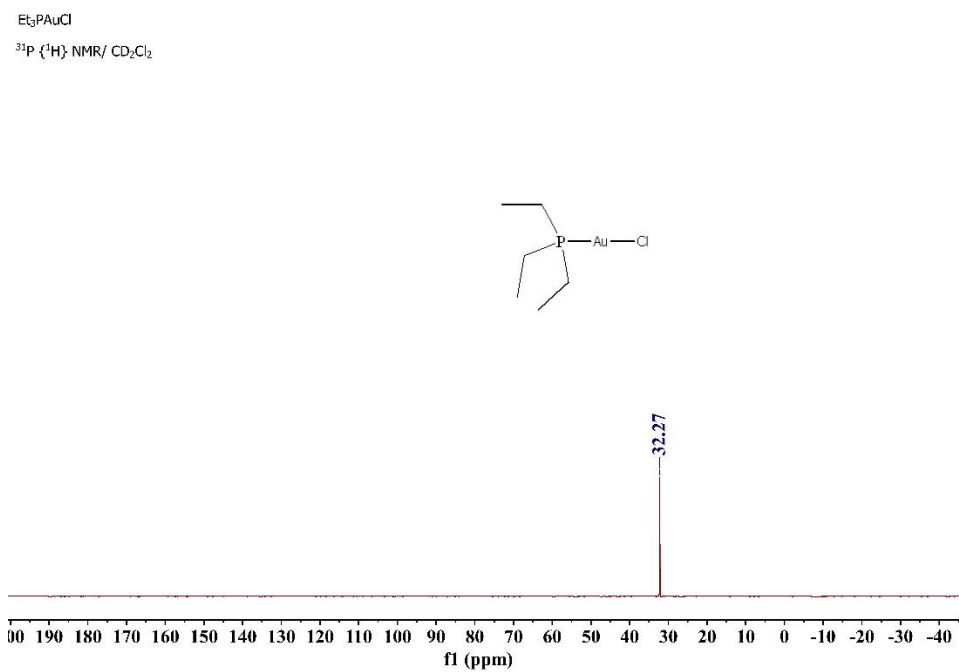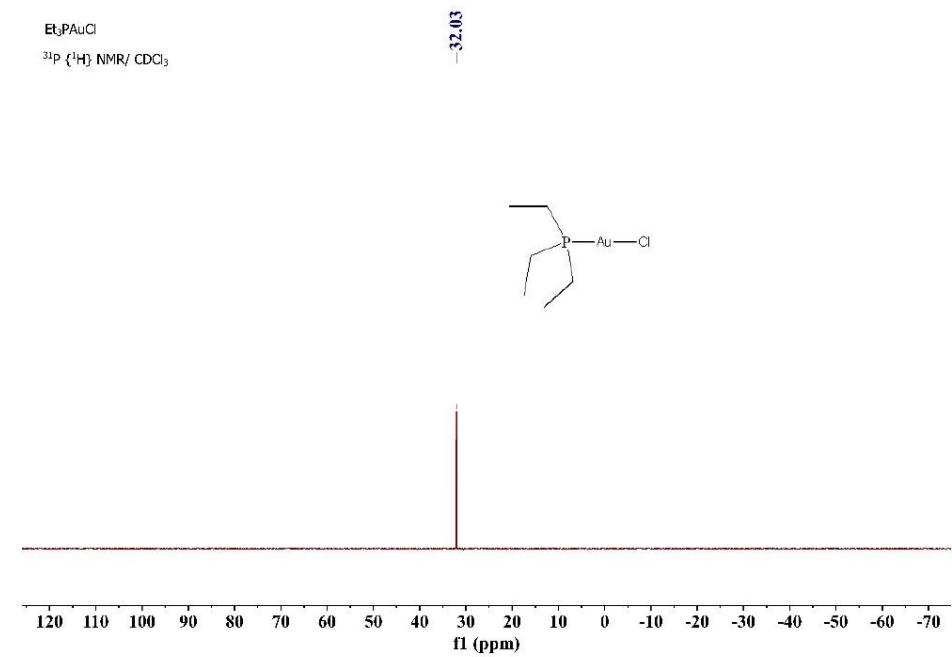
Fig. A. 10. $^{31}P\{^1H\}$ NMR of Et$_3$PAuCl top in CDCl$_3$ and bottom in CH$_2$Cl$_2$-d_2.
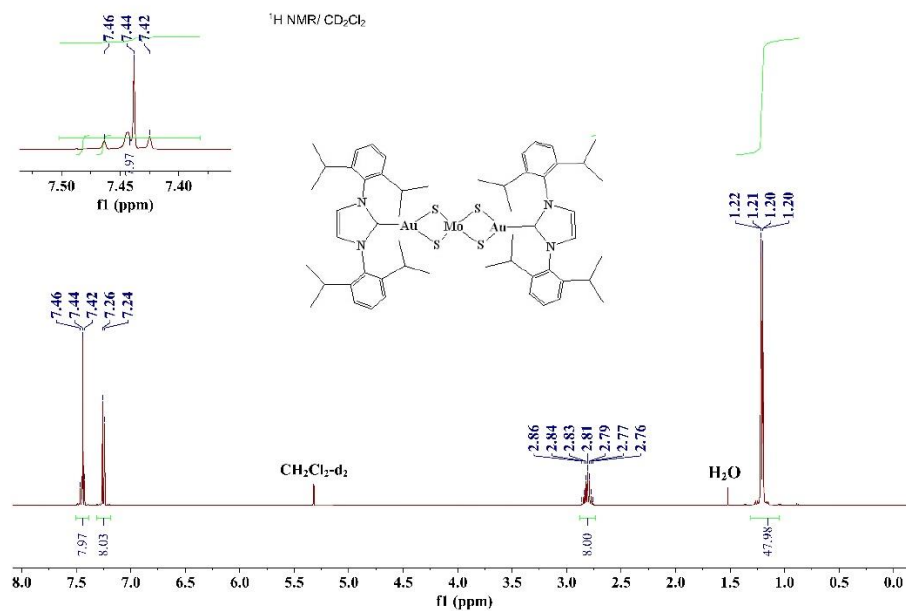
Fig. A. 11. ^{1}H NMR of **C-1** in CH_2Cl_2-d_2.
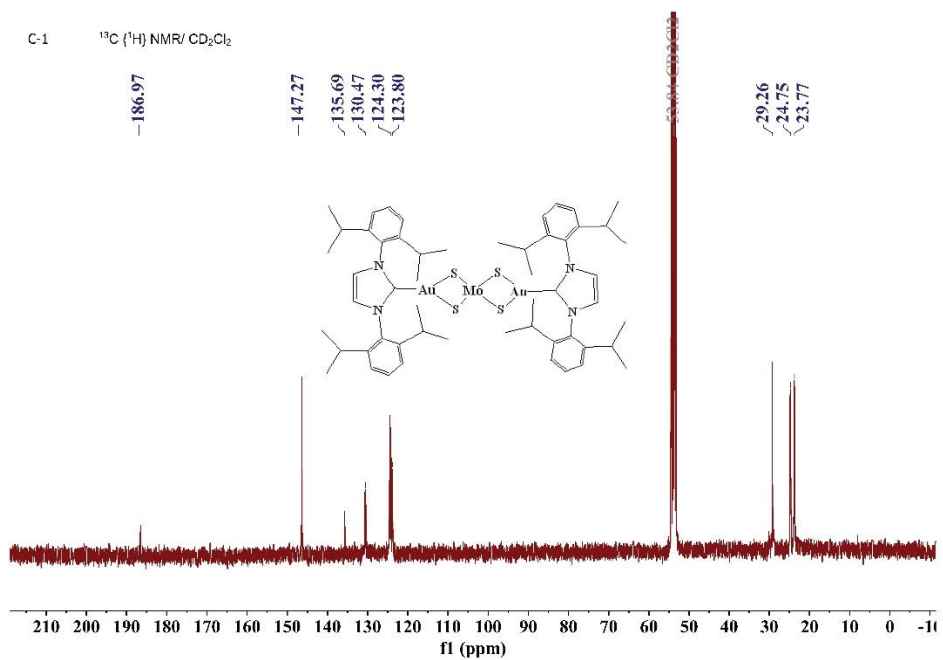
Fig. A. 12. $^{13}C\{^1H\}$ NMR of **C-1** in CH_2Cl_2-d_2.

Fig. A. 13. ^{1}H NMR of **C-2** in CH_2Cl_2-d_2.

Fig. A. 14. ^{13}C{^{1}H} NMR of **C-2** in CH_2Cl_2-d_2.
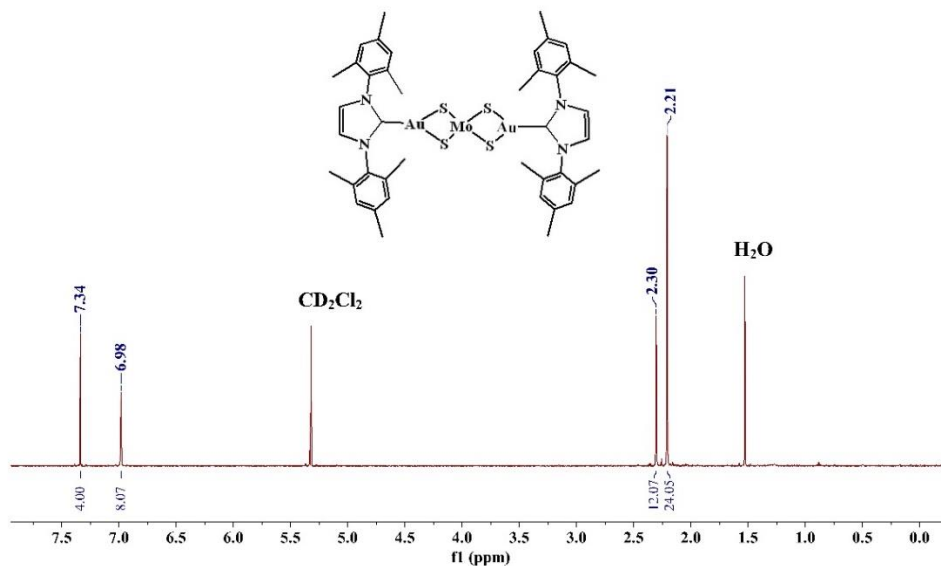
Fig. A. 15. ^{1}H NMR of **C-3** in CH$_2$Cl$_2$-d_2.
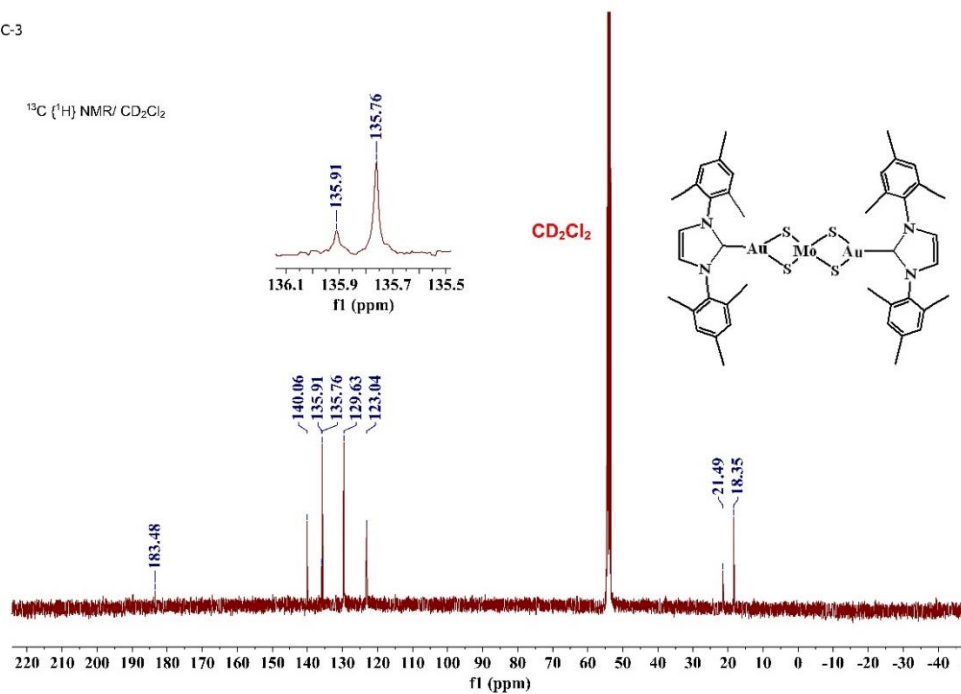
Fig. A. 16. ^{13}C{^{1}H} NMR of **C-3** in CH$_2$Cl$_2$-d_2.
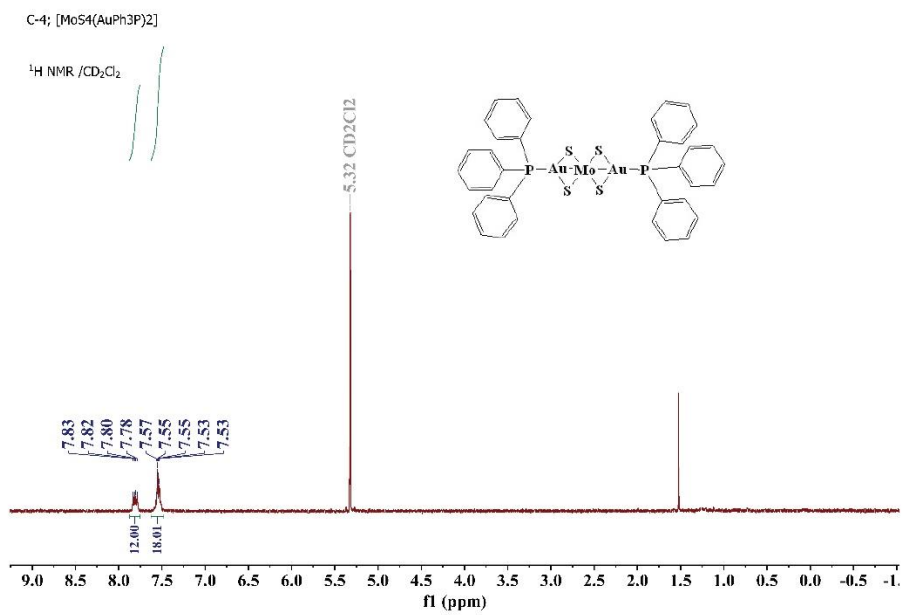
Fig. A. 17. ^{1}H NMR of **C-4**; [MoS$_4$(AuPh$_3$P)$_2$] in CH$_2$Cl$_2$-d_2.

C-4; [MoS4(AuPh3P)2]

¹H NMR /CDCl₃

42.99

| 60 | 55 | 50 | 45 | 40 | 35 | 30 | 25 | 20 | 15 | 10 | 5 | 0 | -5 | -10 | -15 | -20 | -25 | -30 | -35 | -40 | -45 | -50 | -55 |

f1 (ppm)
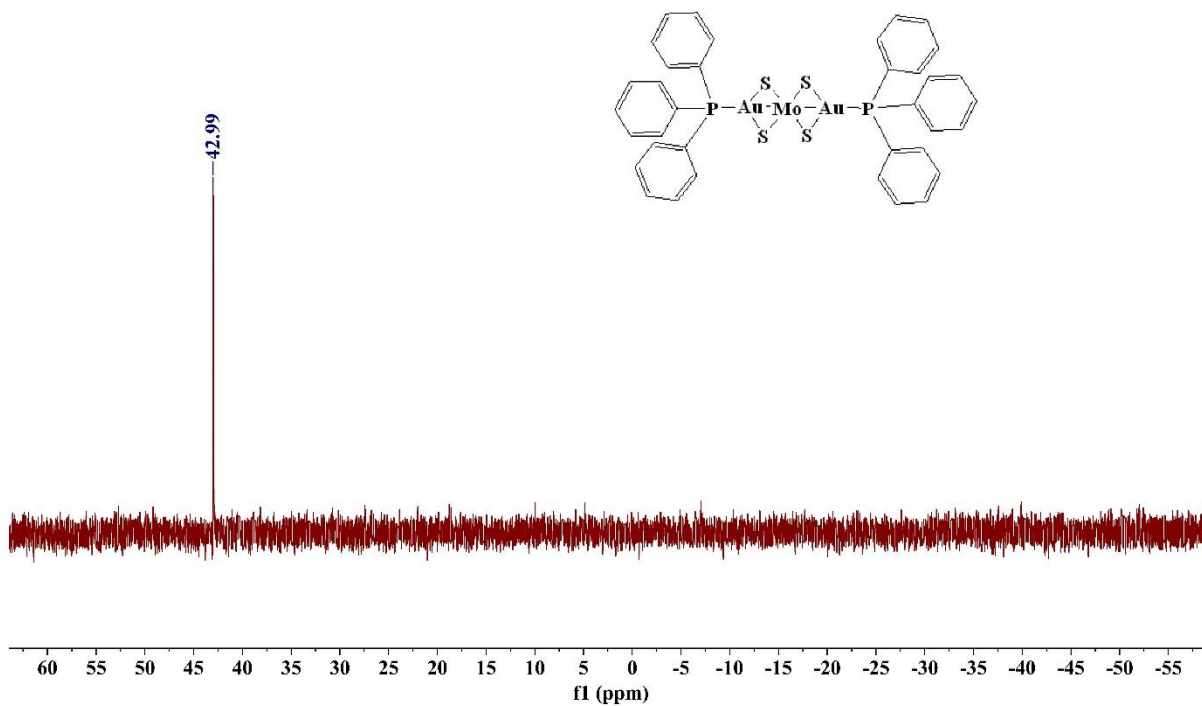
C-4; [MoS₄(AuPh₃P)₂]

³¹P {¹H} NMR/CD₂Cl₂

42.59

| 60 | 55 | 50 | 45 | 40 | 35 | 30 | 25 | 20 | 15 | 10 | 5 | 0 | -5 | -10 | -15 | -20 | -25 |

f1 (ppm)
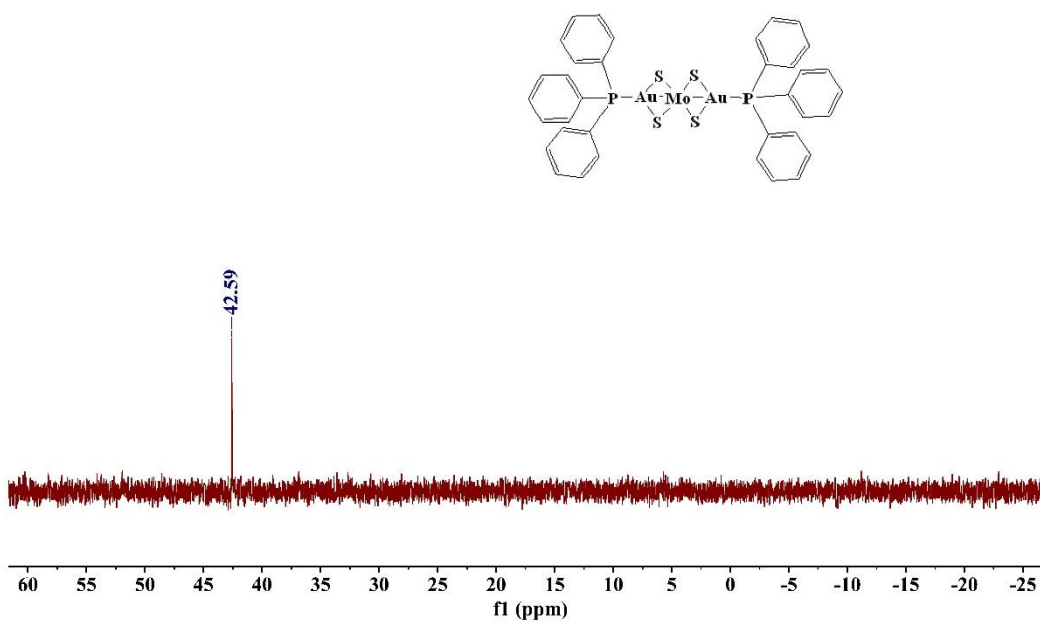
Fig. A. 18. ³¹P{¹H} NMR of **C-4**; [MoS₄(AuPh₃P)₂] the top in CDCl₃ and bottom in CH₂Cl₂-*d₂*.

159

C-5; [MoS₄(AuEt₃P)₂]

¹H NMR /CD₂Cl₂
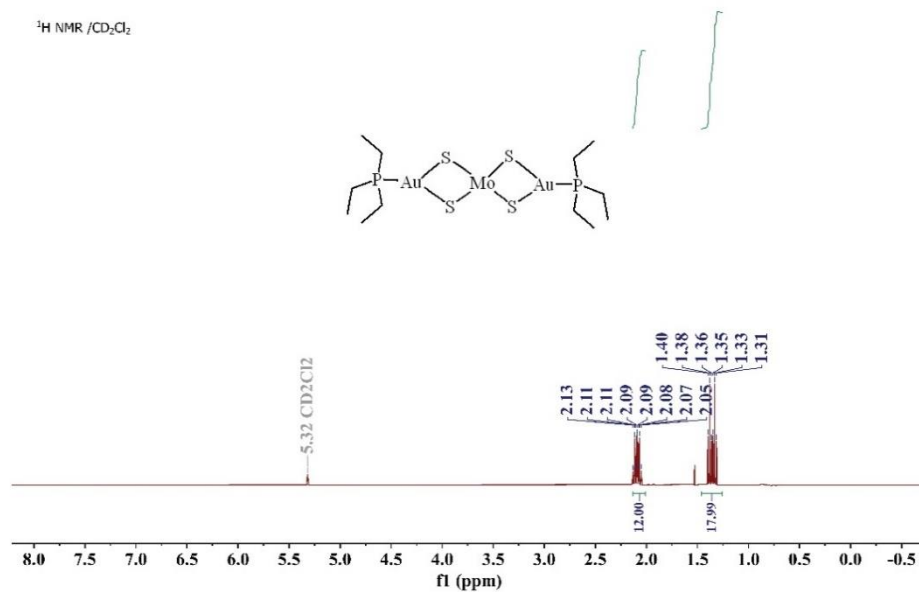
Fig. A. 19. ¹H NMR of **C-5**; [MoS$_4$(AuEt$_3$P)$_2$] in CH$_2$Cl$_2$-d_2.

C-5; [MoS₄(AuEt₃P)₂]

³¹P {¹H}NMR /CD₃CN
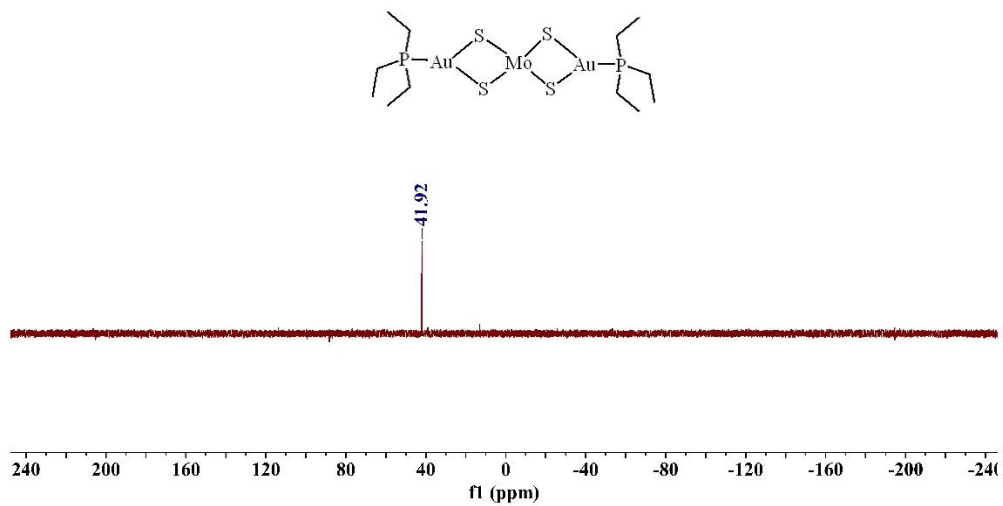
C-5; [MoS₄(AuEt₃P)₂]

³¹P {¹H} NMR/CD₂Cl₂
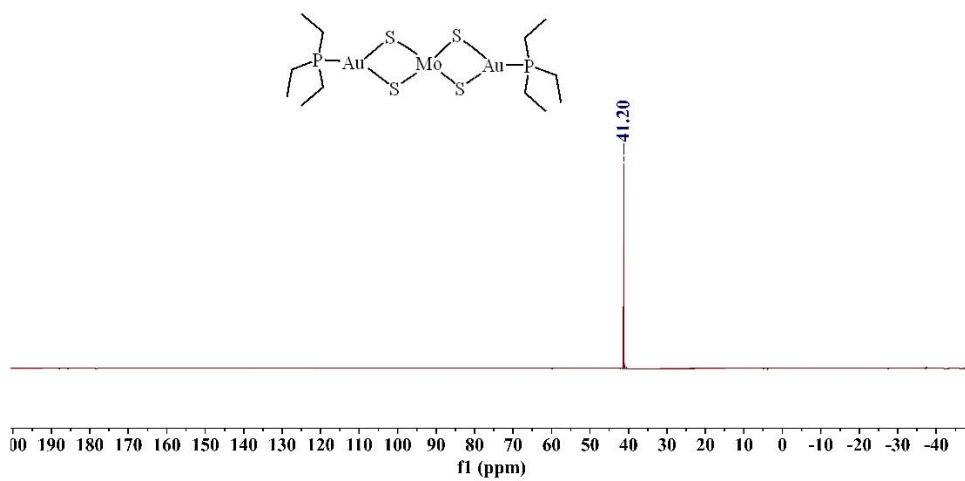
Fig. A. 20. ³¹P{¹H} NMR of **C-5**; [MoS₄(AuEt₃P)₂] the top in CD₃CN and the bottom in CH₂Cl₂-*d₂*.

```
Gamma         =    4.258e+03 Hz/G
Little Delta  =       2.000m
Big Delta     =      99.900m
RSS   =    2.288e-06
SD    =    3.025e-04
```

Point	Gradient	Expt	Calc	Difference
1	2.408e+00	4.927e-01	4.925e-01	-1.422e-04
2	4.213e+00	4.785e-01	4.783e-01	-1.130e-04
3	6.019e+00	4.564e-01	4.572e-01	7.864e-04
4	7.824e+00	4.301e-01	4.301e-01	2.503e-05
5	9.630e+00	3.983e-01	3.982e-01	-1.007e-04
6	1.144e+01	3.631e-01	3.628e-01	-2.711e-04
7	1.324e+01	3.254e-01	3.254e-01	-4.216e-05
8	1.505e+01	2.874e-01	2.871e-01	-2.419e-04
9	1.685e+01	2.495e-01	2.494e-01	-6.397e-05
10	1.866e+01	2.131e-01	2.132e-01	1.448e-04
11	2.046e+01	1.794e-01	1.794e-01	-5.598e-05
12	2.227e+01	1.490e-01	1.485e-01	-4.997e-04
13	2.408e+01	1.215e-01	1.210e-01	-5.034e-04
14	2.588e+01	9.678e-02	9.707e-02	2.900e-04
15	2.769e+01	7.612e-02	7.663e-02	5.152e-04
16	2.949e+01	5.961e-02	5.953e-02	-8.561e-05
17	3.130e+01	4.506e-02	4.551e-02	4.545e-04
18	3.310e+01	3.419e-02	3.425e-02	5.633e-05
19	3.491e+01	2.507e-02	2.536e-02	2.958e-04
20	3.671e+01	1.827e-02	1.849e-02	2.209e-04
21	3.852e+01	1.293e-02	1.326e-02	3.289e-04
22	4.033e+01	9.007e-03	9.360e-03	3.527e-04
23	4.213e+01	6.594e-03	6.504e-03	-8.974e-05
24	4.394e+01	4.484e-03	4.447e-03	-3.671e-05
25	4.574e+01	2.866e-03	2.993e-03	1.264e-04

```
=========================================================
25 points for Integral 4,  Integral Region from 4.111 to 4.055 ppm
Converged after 39 iterations!
Results      Comp. 1
I[0]          =    7.133e-01
Diff Con.     =    8.571e-10 m2/s
Gamma         =    4.258e+03 Hz/G
Little Delta  =       2.000m
Big Delta     =      99.900m
RSS   =    1.592e-06
SD    =    2.524e-04
```

(3/5)

25 points for Integral 2, Integral Region from 7.305 to 7.170 ppm
Converged after 43 iterations!
Results   Comp. 1
I[0]   =   4.852e-01
Diff Con.   =   8.484e-10 m2/s
Gamma   =   4.258e+03 Hz/G
Little Delta =   2.000m
Big Delta   =   99.900m
RSS   =   5.187e-06
SD   =   4.555e-04

Point	Gradient	Expt	Calc	Difference
1	2.408e+00	4.786e-01	4.785e-01	-1.581e-04
2	4.213e+00	4.649e-01	4.649e-01	-8.794e-06
3	6.019e+00	4.452e-01	4.446e-01	-5.933e-04
4	7.824e+00	4.180e-01	4.187e-01	6.880e-04
5	9.630e+00	3.878e-01	3.880e-01	2.093e-04
6	1.144e+01	3.540e-01	3.540e-01	9.074e-06
7	1.324e+01	3.174e-01	3.180e-01	6.216e-04
8	1.505e+01	2.811e-01	2.812e-01	8.039e-06
9	1.685e+01	2.453e-01	2.447e-01	-6.040e-04
10	1.866e+01	2.094e-01	2.097e-01	3.254e-04
11	2.046e+01	1.773e-01	1.769e-01	-4.750e-04
12	2.227e+01	1.477e-01	1.468e-01	-8.227e-04
13	2.408e+01	1.199e-01	1.200e-01	9.761e-05
14	2.588e+01	9.673e-02	9.657e-02	-1.646e-04
15	2.769e+01	7.653e-02	7.649e-02	-3.979e-05
16	2.949e+01	5.957e-02	5.964e-02	6.742e-05
17	3.130e+01	4.470e-02	4.578e-02	1.074e-03
18	3.310e+01	3.460e-02	3.459e-02	-5.861e-06
19	3.491e+01	2.560e-02	2.573e-02	1.280e-04
20	3.671e+01	1.905e-02	1.884e-02	-2.130e-04
21	3.852e+01	1.276e-02	1.358e-02	8.214e-04
22	4.033e+01	9.265e-03	9.634e-03	3.691e-04
23	4.213e+01	7.285e-03	6.730e-03	-5.549e-04
24	4.394e+01	4.664e-03	4.627e-03	-3.670e-05
25	4.574e+01	2.737e-03	3.132e-03	3.945e-04

==
25 points for Integral 3, Integral Region from 5.672 to 5.621 ppm
Converged after 40 iterations!
Results   Comp. 1
I[0]   =   4.996e-01
Diff Con.   =   8.610e-10 m2/s

```
SIMFIT RESULTS
==============
Dataset : D:/nmrdata/user/Dhirgam/dosy/C125M1/5/pdata/1/ct1t2.txt
AREA fit : Diffusion : Variable Gradient :
I=I[0]*exp(-D*SQR(2*PI*gamma*Gi*LD)*(BD-LD/3)*1e4)
25 points for Integral 1,  Integral Region from 7.507 to 7.336 ppm
Converged after 36 iterations!
Results      Comp. 1
I[0]          =   1.015e+00
Diff Con.     =   8.552e-10 m2/s
Gamma         =   4.258e+03 Hz/G
Little Delta  =      2.000m
Big Delta     =     99.900m
RSS   =    7.284e-06
SD    =    5.398e-04
Point     Gradient       Expt         Calc       Difference
    1     2.408e+00    1.000e+00    1.000e+00     4.191e-04
    2     4.213e+00    9.719e-01    9.718e-01    -1.572e-04
    3     6.019e+00    9.288e-01    9.291e-01     3.672e-04
    4     7.824e+00    8.740e-01    8.744e-01     3.791e-04
    5     9.630e+00    8.107e-01    8.100e-01    -7.405e-04
    6     1.144e+01    7.396e-01    7.385e-01    -1.139e-03
    7     1.324e+01    6.627e-01    6.627e-01     5.980e-05
    8     1.505e+01    5.848e-01    5.854e-01     6.070e-04
    9     1.685e+01    5.087e-01    5.089e-01     2.625e-04
   10     1.866e+01    4.352e-01    4.355e-01     3.809e-04
   11     2.046e+01    3.666e-01    3.668e-01     2.149e-04
   12     2.227e+01    3.052e-01    3.042e-01    -1.025e-03
   13     2.408e+01    2.487e-01    2.482e-01    -5.140e-04
   14     2.588e+01    1.992e-01    1.994e-01     1.685e-04
   15     2.769e+01    1.574e-01    1.576e-01     2.376e-04
   16     2.949e+01    1.228e-01    1.227e-01    -1.618e-04
   17     3.130e+01    9.358e-02    9.394e-02     3.550e-04
   18     3.310e+01    7.053e-02    7.083e-02     2.972e-04
   19     3.491e+01    5.193e-02    5.256e-02     6.214e-04
   20     3.671e+01    3.852e-02    3.839e-02    -1.241e-04
   21     3.852e+01    2.707e-02    2.760e-02     5.277e-04
   22     4.033e+01    1.933e-02    1.953e-02     1.986e-04
   23     4.213e+01    1.450e-02    1.360e-02    -8.935e-04
   24     4.394e+01    9.440e-03    9.325e-03    -1.147e-04
   25     4.574e+01    5.216e-03    6.292e-03     1.076e-03
==========================================================
```

(1/5)

Fig. A. 21. The diffusion coefficient measurements of **C-2** by DOSY ^{1}H NMR

164

B.1. Ultraviolet-Visible spectroscopy
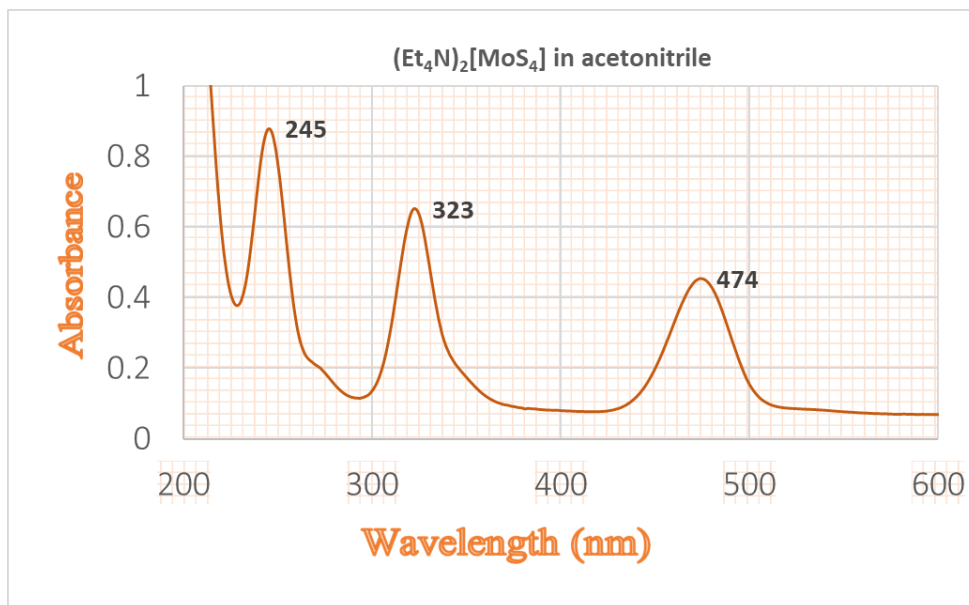
Fig. B. 1. UV-vis. Scan of $[Et_4N]_2[MoS_4]$ in acetonitrile
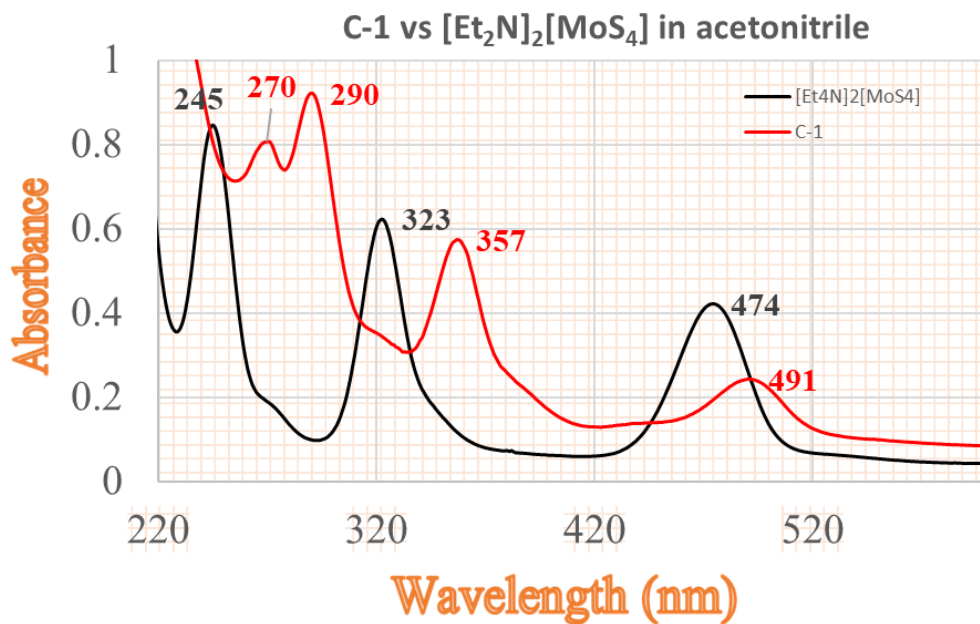
Fig. B. 2. UV-vis. Scan of **C-1** vs $[Et_4N]_2[MoS_4]$ in acetonitrile
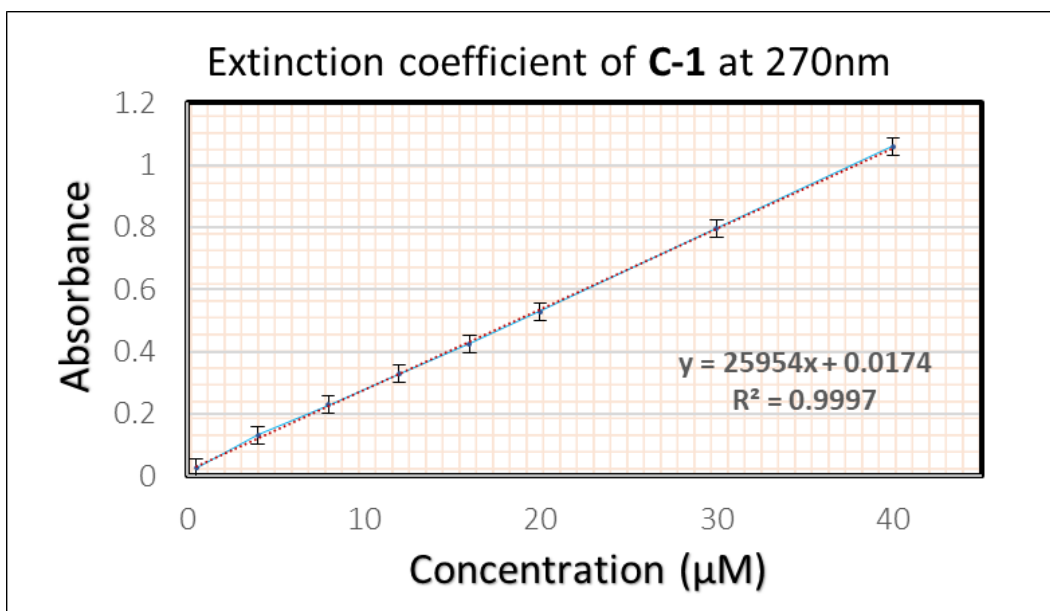
Fig. B. 3. UV-vis. **Ɛ** calculations curve of **C-1** (25k) in acetonitrile at 270nm
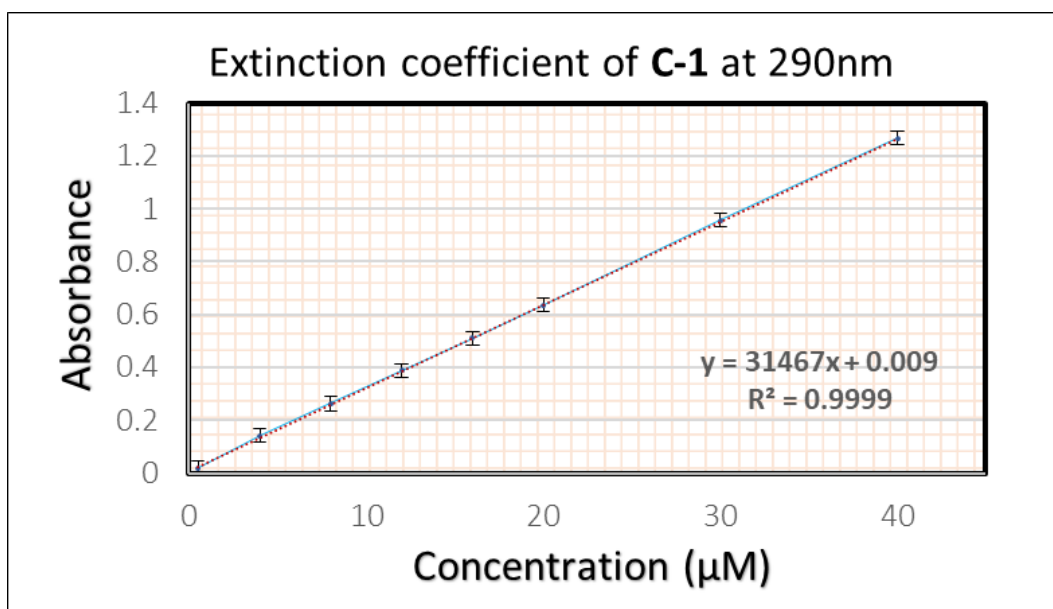
Fig. B. 4. UV-vis. **Ɛ** calculations curve of C-1 (31k) in acetonitrile at 290nm
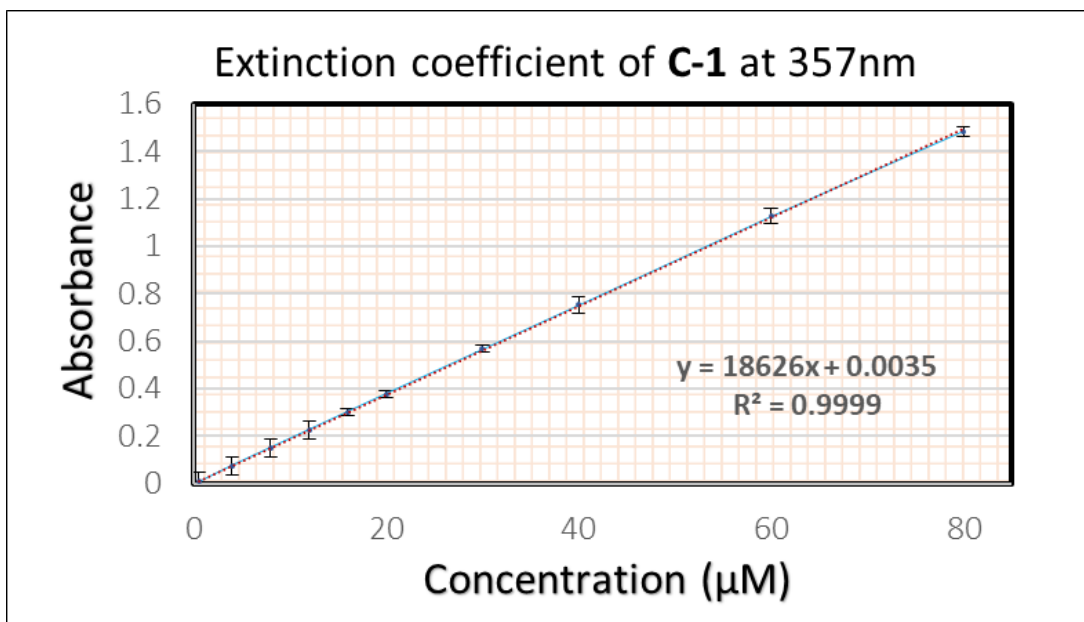
Fig. B. 5. UV-vis. **ε** calculations curve of **C-1** (18k) in acetonitrile at 357nm
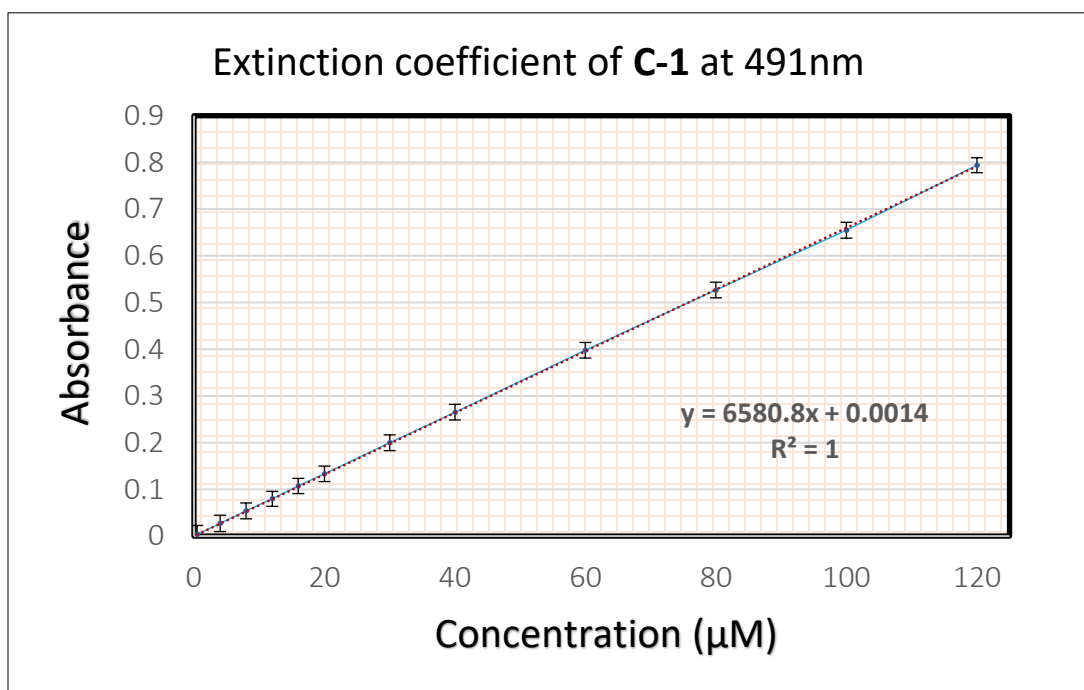
Fig. B. 6. UV-vis. **ε** calculations curve of **C-1** (7k) in acetonitrile at 491nm
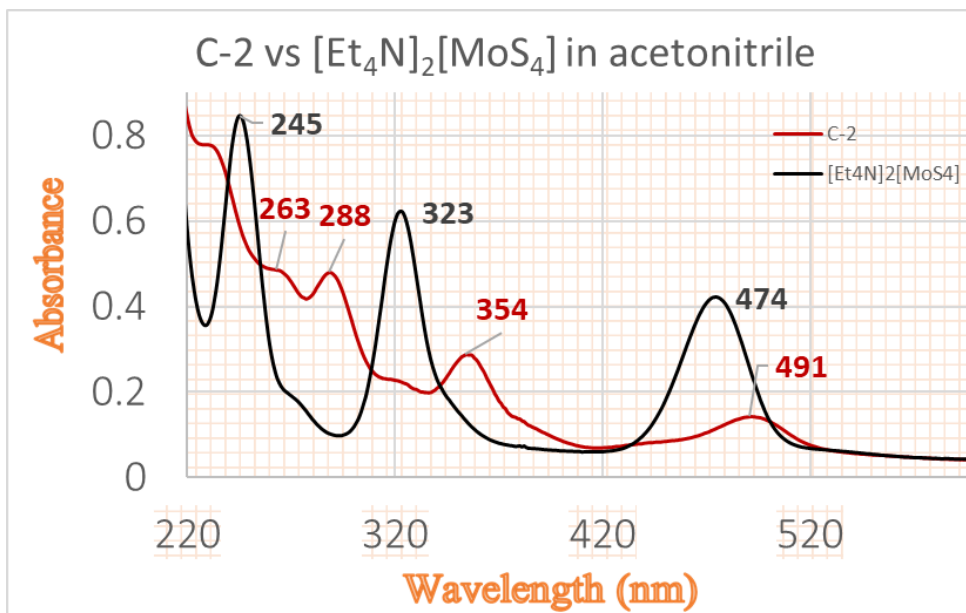
Fig. B. 7. UV-vis. Scan of **C-2** vs [Et₄N]₂[MoS₄] in acetonitrile
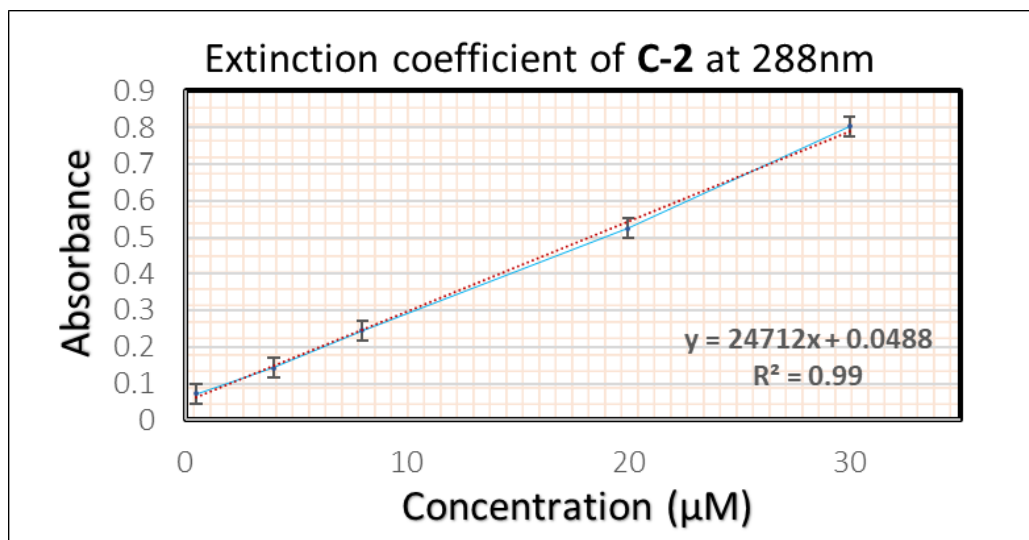
Fig. B. 8. UV-vis. **ε** calculations curve of **C-2** (25k) in acetonitrile at 288nm
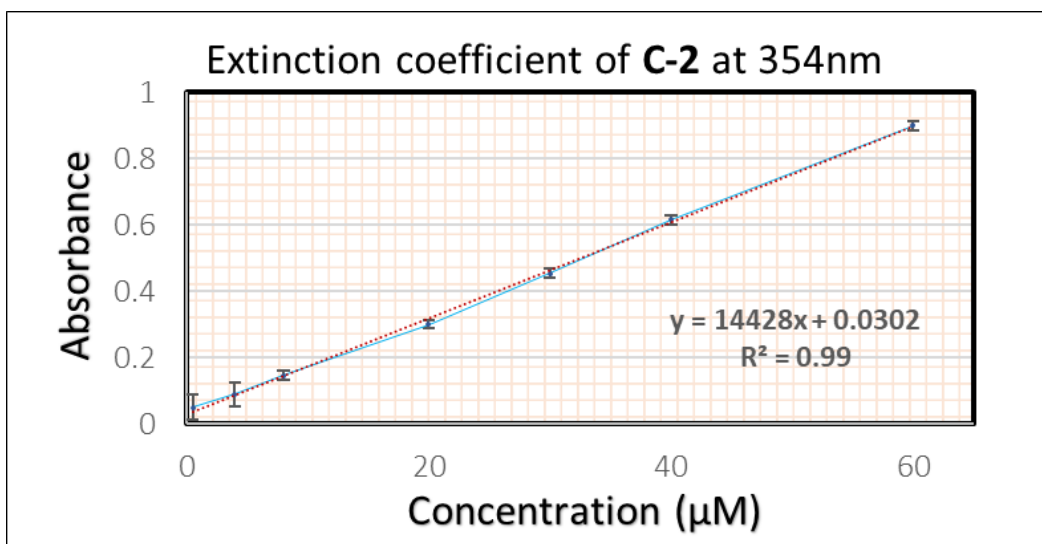
Fig. B. 9. UV-vis. **ε** calculations curve of **C-2** (14k) in acetonitrile at 354 nm
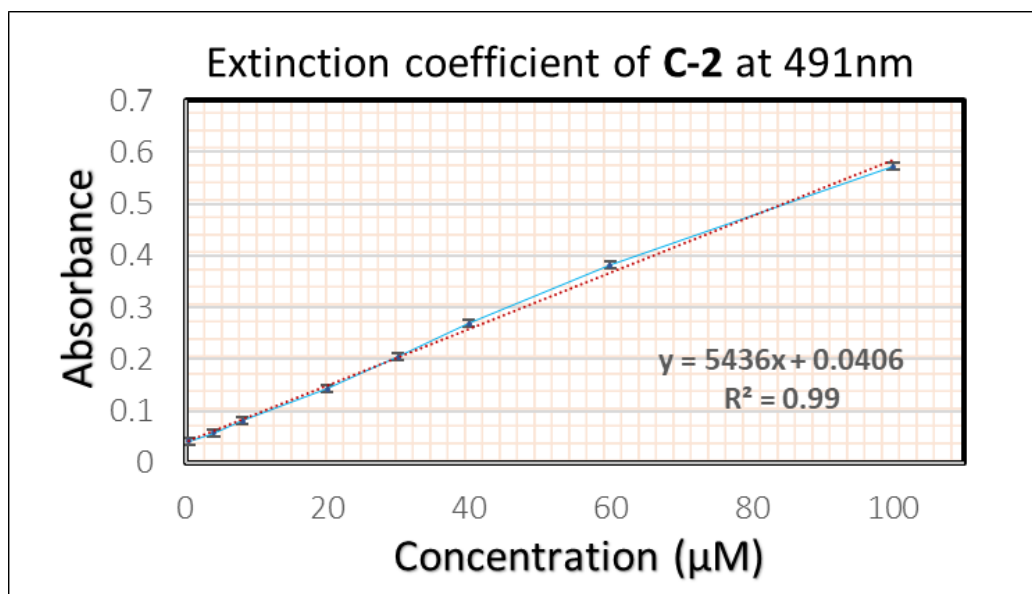
Fig. B. 10. UV-vis. **ε** calculations curve of **C-2** (5k) in acetonitrile at 491 nm
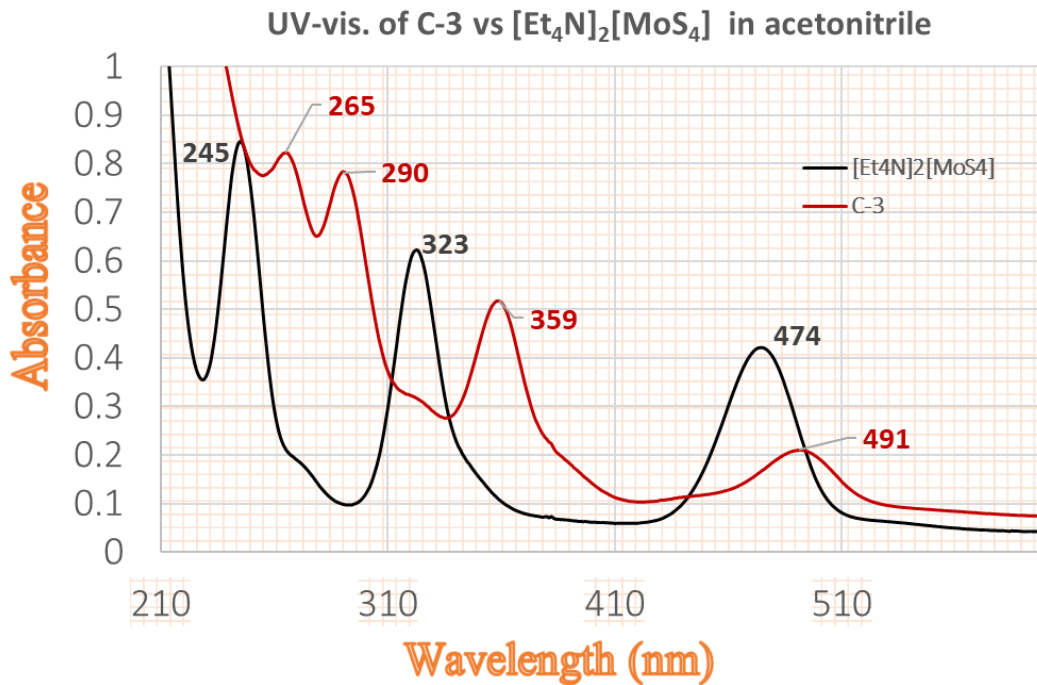
Fig. B. 11. UV-vis. Scan of **C-3** vs [Et$_4$N]$_2$[MoS$_4$] in acetonitrile
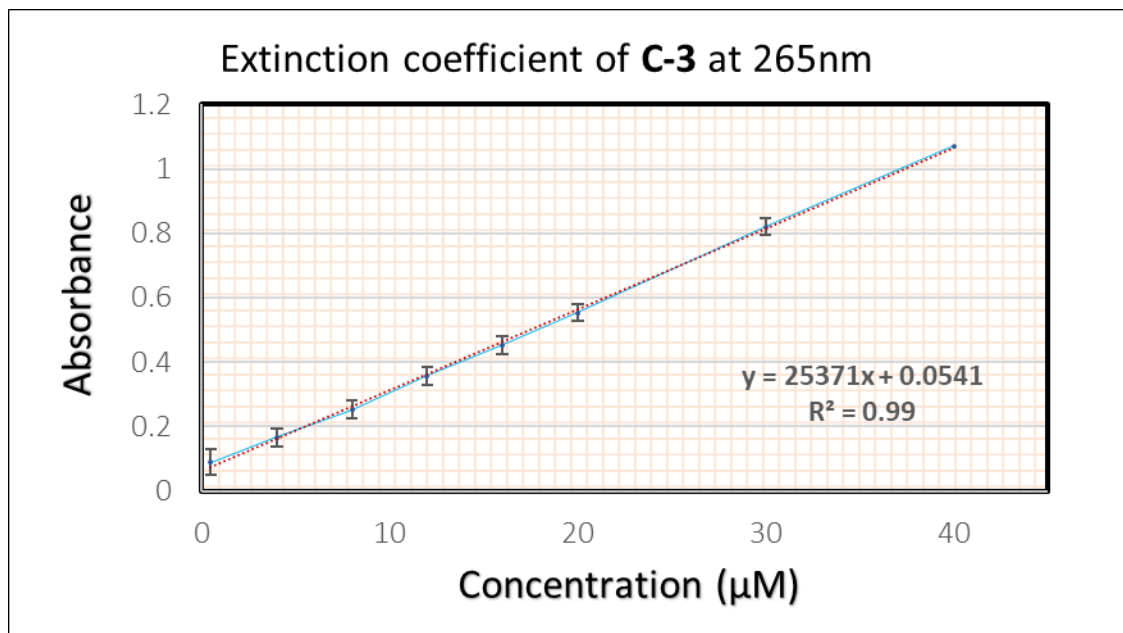
Fig. B. 12. UV-vis. **Ɛ** calculations curve of **C-3** (25k) in acetonitrile at 265 nm

170
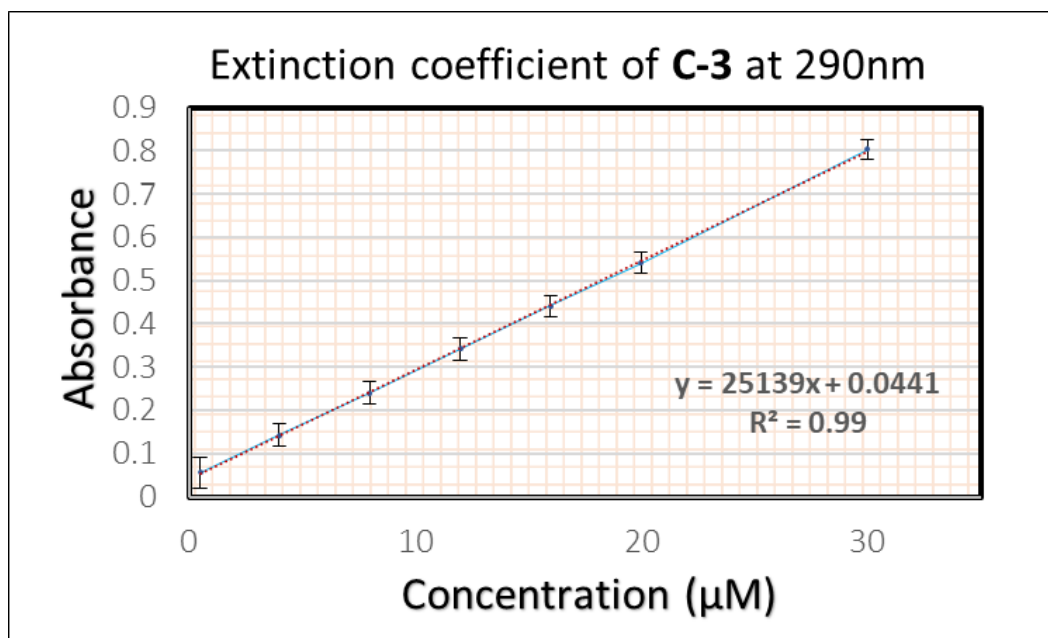
Fig. B. 13. UV-vis. Ɛ calculations curve of **C-3** (25k) in acetonitrile at 290 nm
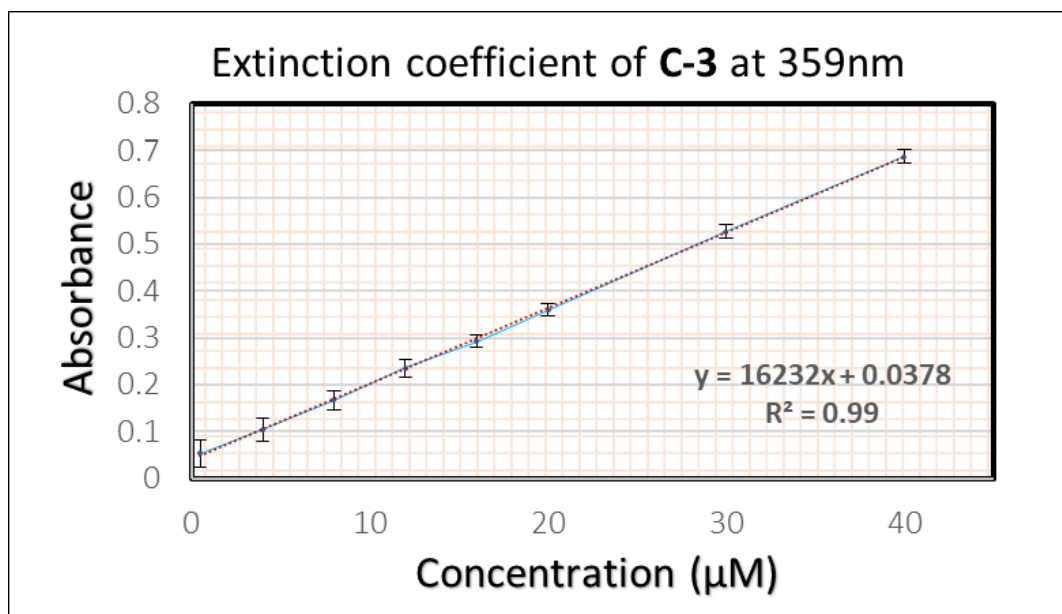
Fig. B. 14. UV-vis. Ɛ calculations curve of **C-3** (16k) in acetonitrile at 359 nm
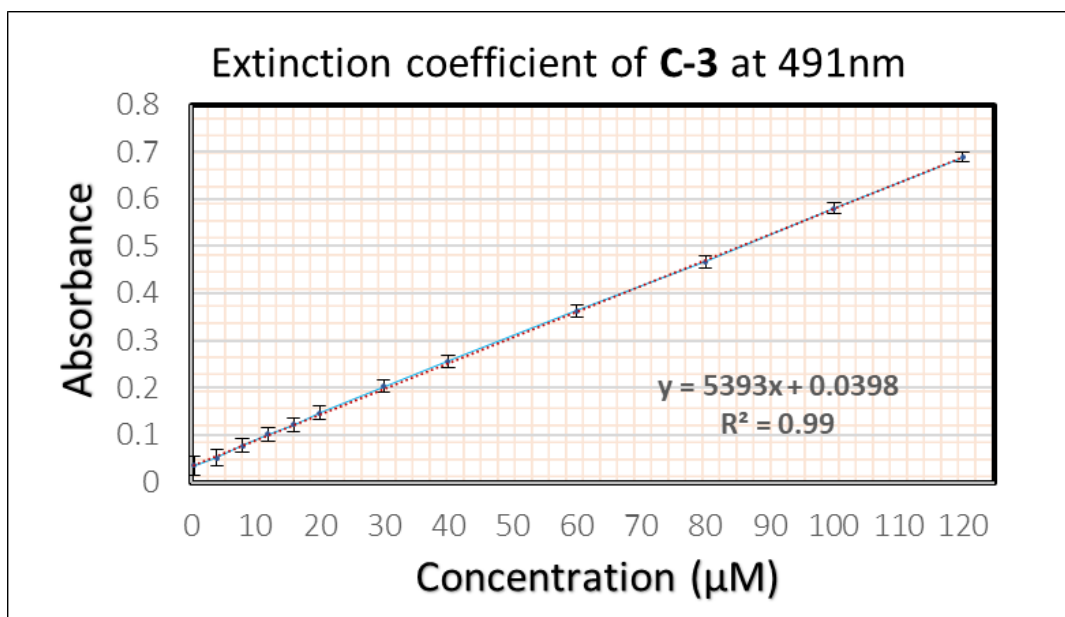
Fig. B. 15. UV-vis. **Ɛ** calculations curve of **C-3** (5k) in acetonitrile at 491 nm
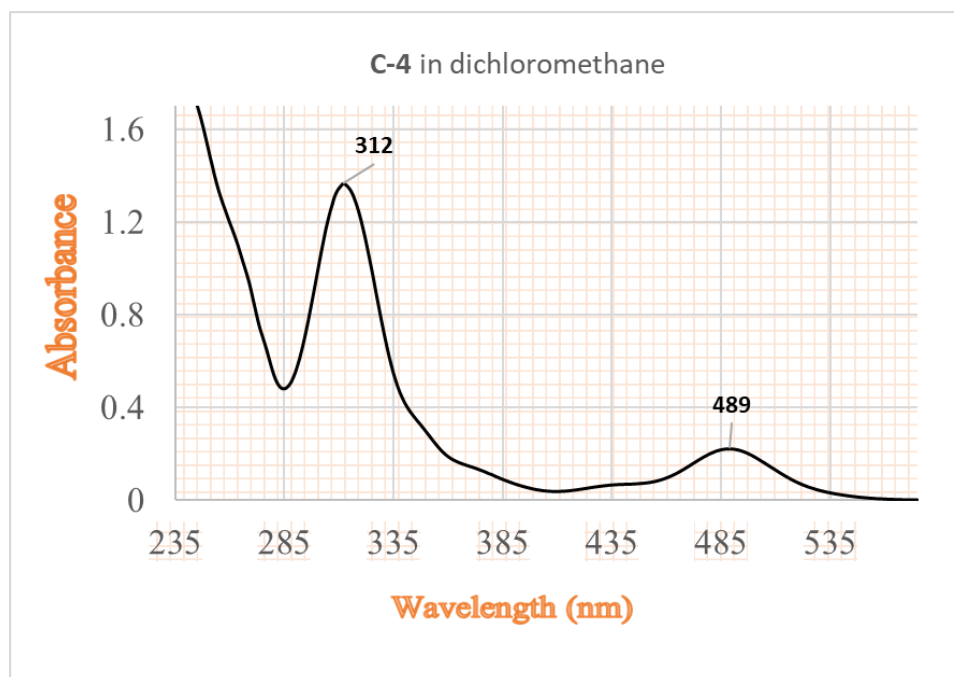
Fig. B. 16. UV-vis. Scan of **C-4** in dichloromethane
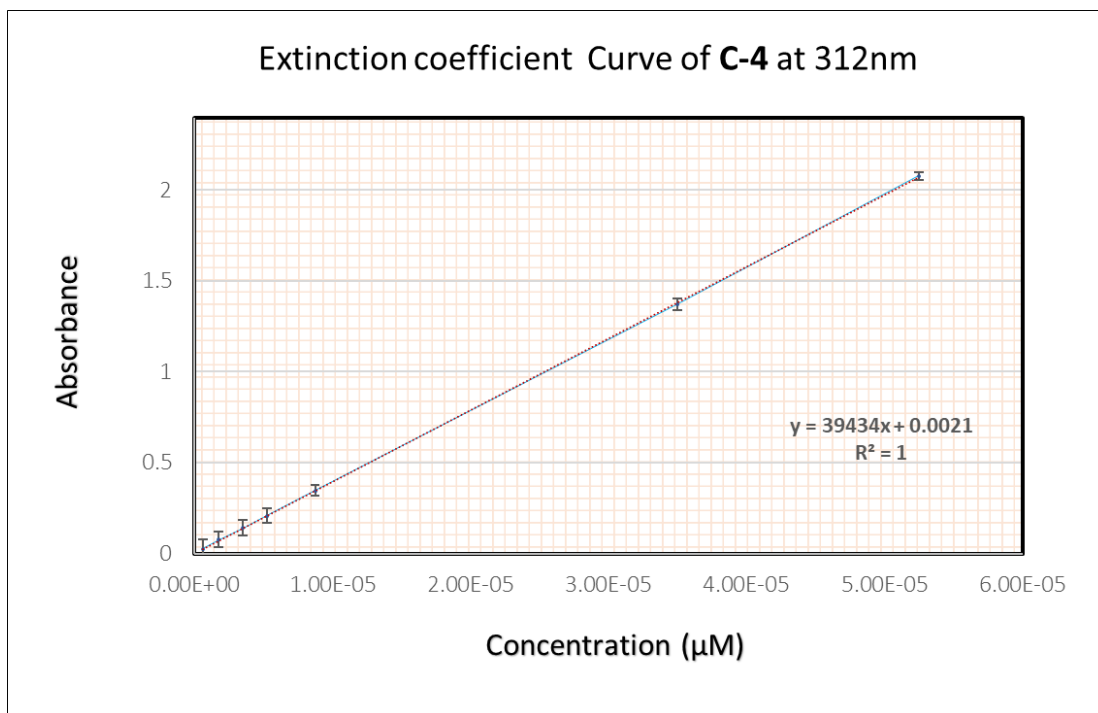
Fig. B. 17. UV-vis. **ε** calculations curve of **C-4** (40k) in dichloromethane at 312nm
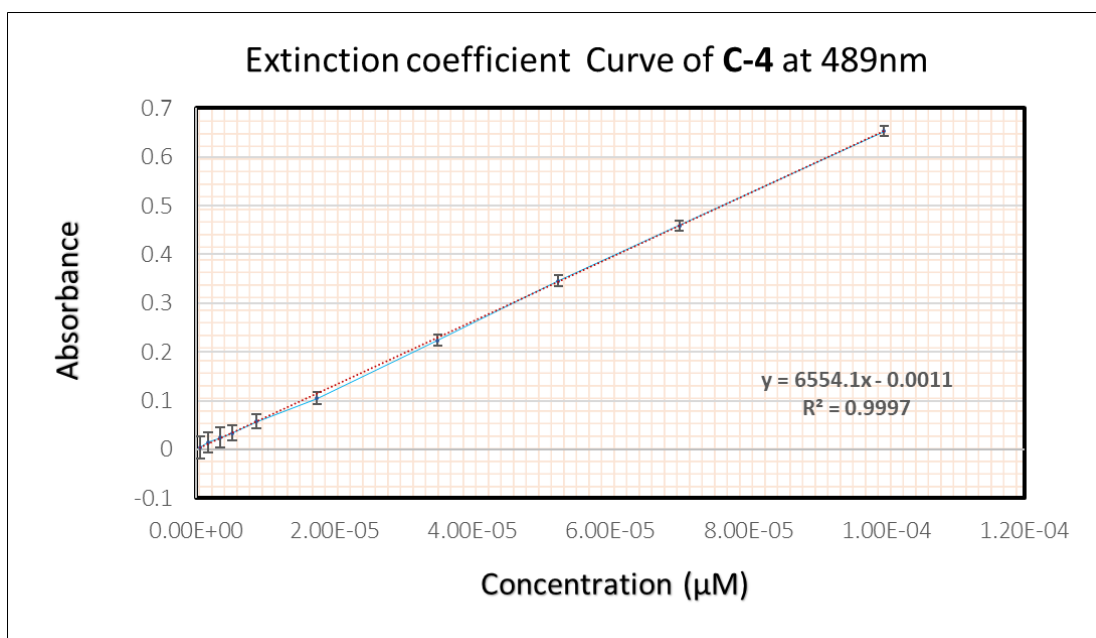
Fig. B. 18. UV-vis. **ε** calculations curve of **C-4** (7k) in dichloromethane at 489nm
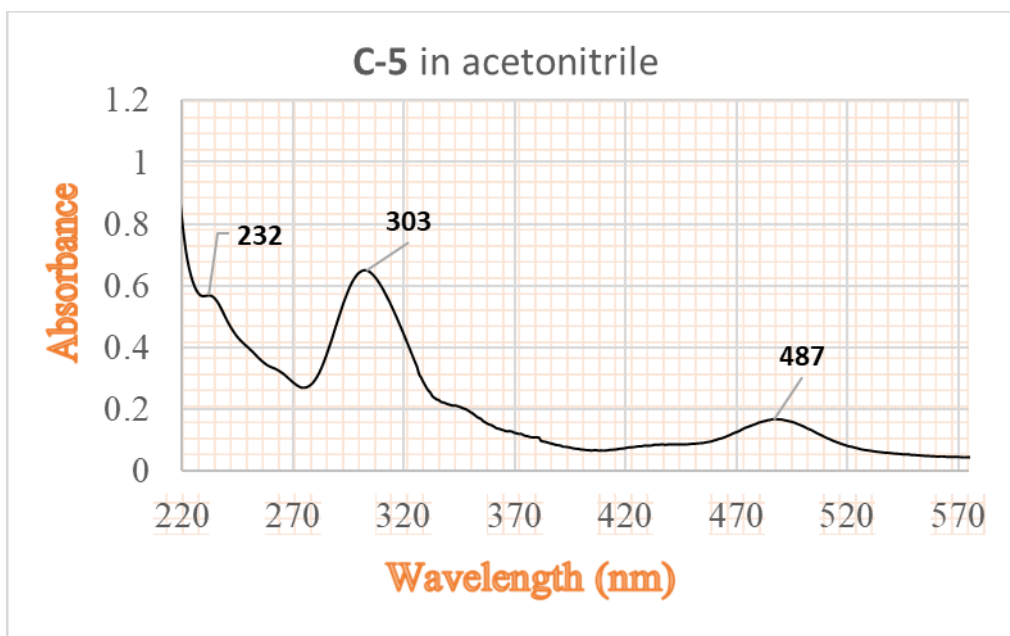
Fig. B. 19. UV-vis. Scan of **C-5** in acetonitrile
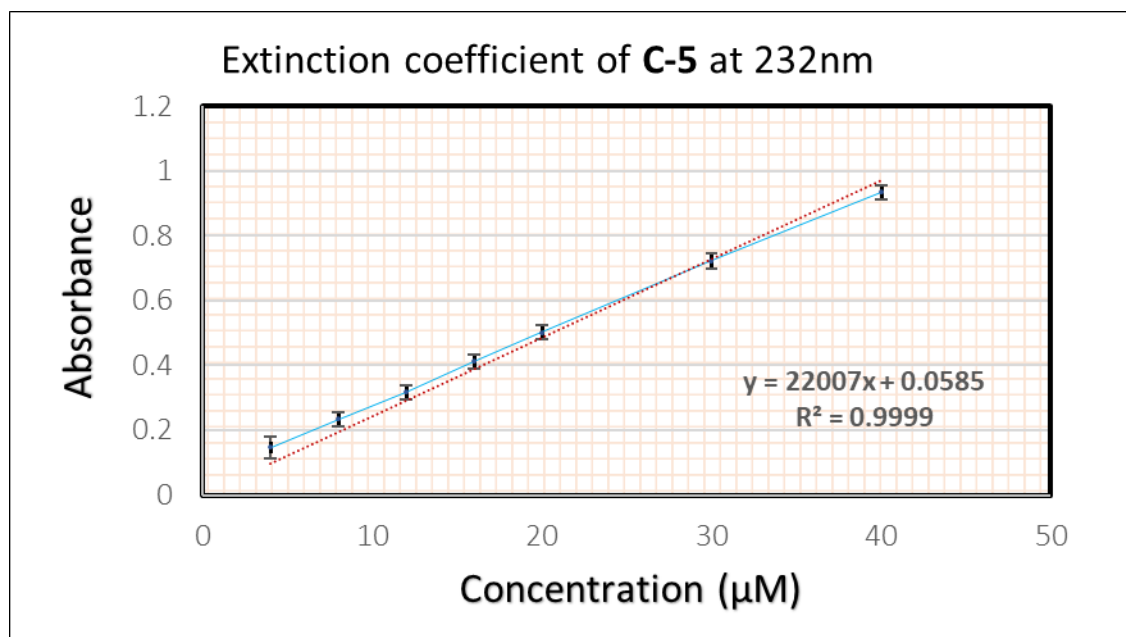
Fig. B. 20. UV-vis. **Ɛ** calculations curve of **C-5** (22k) in acetonitrile at 232nm
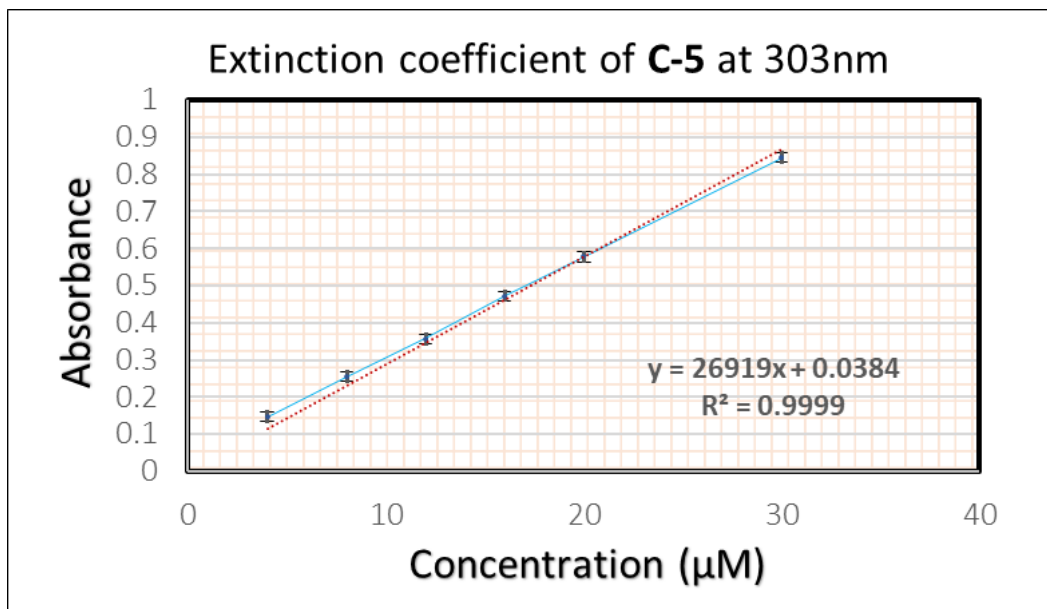
Fig. B. 21. UV-vis. Ɛ calculations curve of **C-4** (26k) in acetonitrile at 303nm
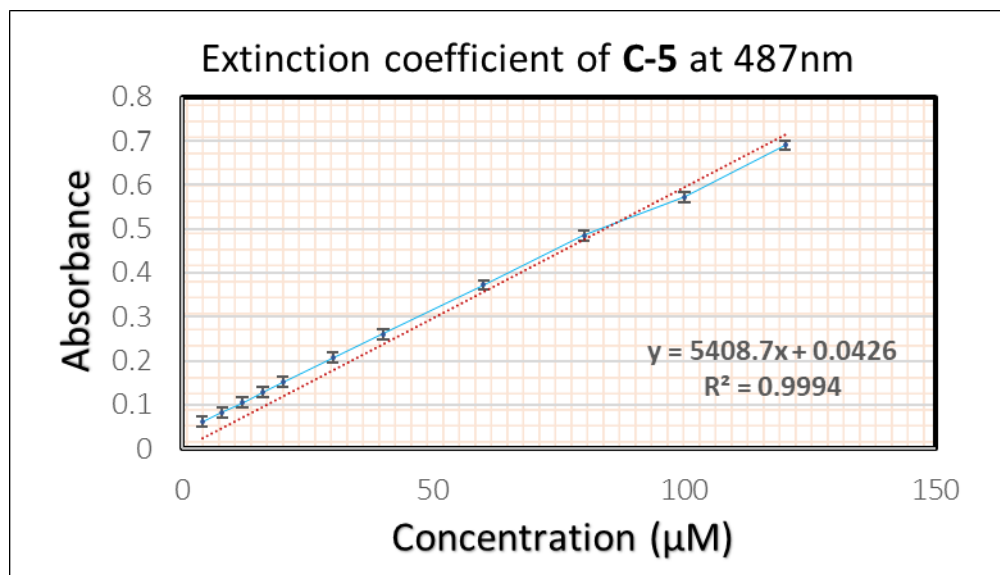
Fig. B. 22. UV-vis. Ɛ calculations curve of **C-4** (5k) in acetonitrile at 487nm

B.2. Cyclic Voltammetry (CV)

Cyclic voltammetry studies were utilized to analyze the electrochemical properties of **C-1 to C-5**. One compartment cell was used to perform the CV experiments. The working electrode used was platinum disk (1mm) . A platinum coil and saturated calomel (SCE, Hg_2Cl_2) were used as counter and reference electrodes, respectively. The scan rates and voltage rages were optimized and mentioned in each figure. The electrolyte solution was tetrabutylammonium hexafluorophosphate (TBAH; 0.1 M) in the dichloromethane or acetonitrile. The analyzed compounds (1.5mM) were prepared in electrolyte solution. Monocrystalline Diamond Suspension (1 μm), polish disk, Kimwipe were used to clean the tip of the working electrode between each scan. All experiments were repeated a minimum of three times.
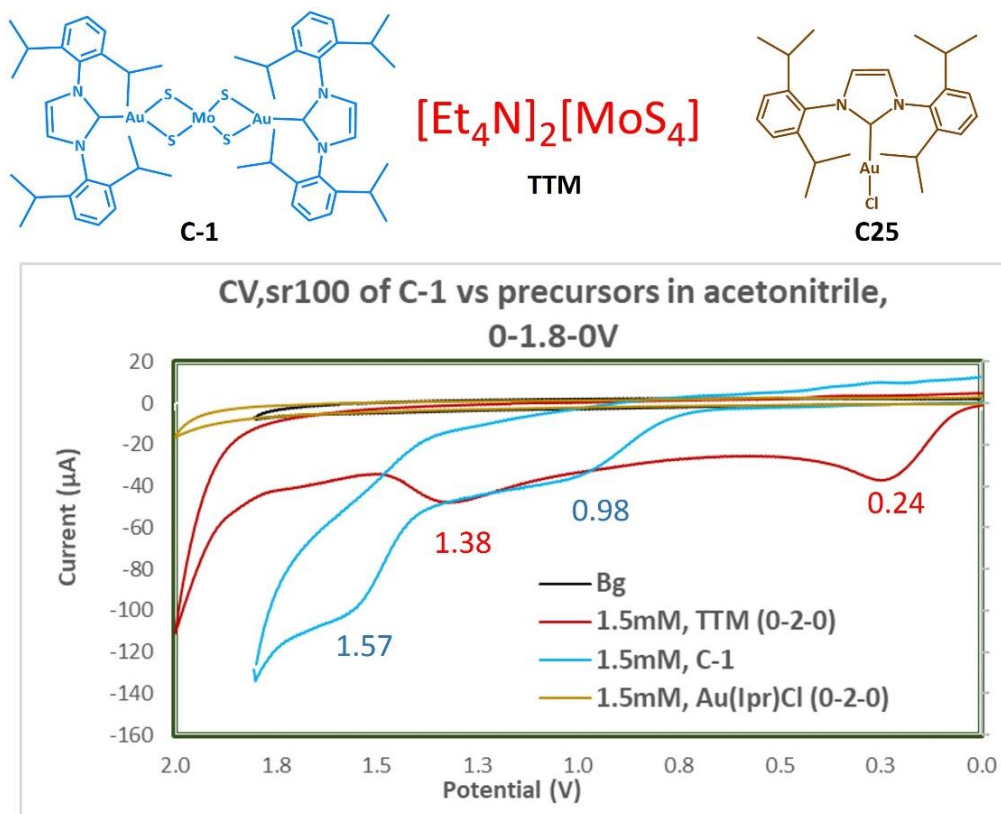
Fig. B. 23. CV of **C-1** vs its precursors in acetonitrile
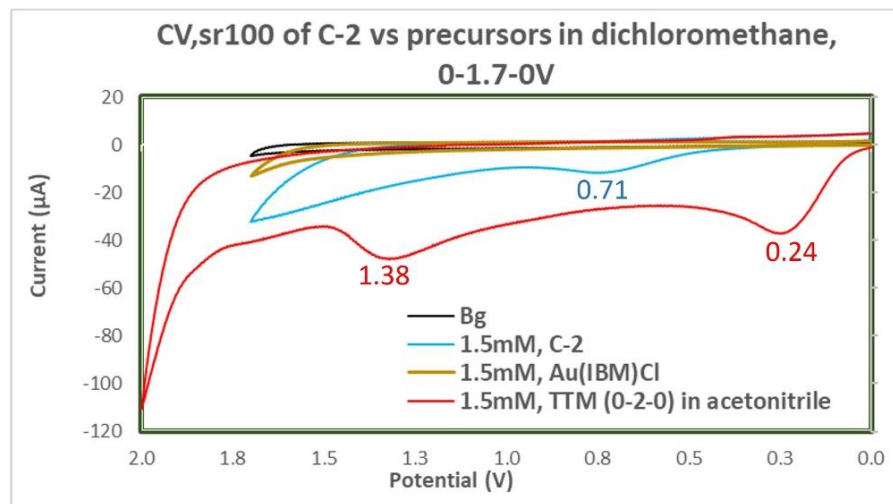
Fig. B. 24. CV of **C-2** vs its precursors in dichloromethane
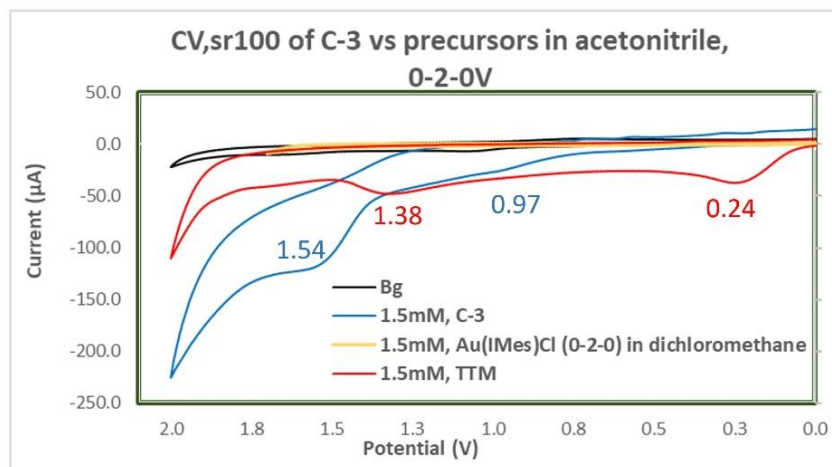
Fig. B. 25. CV of **C-3** vs its precursors in acetonitrile
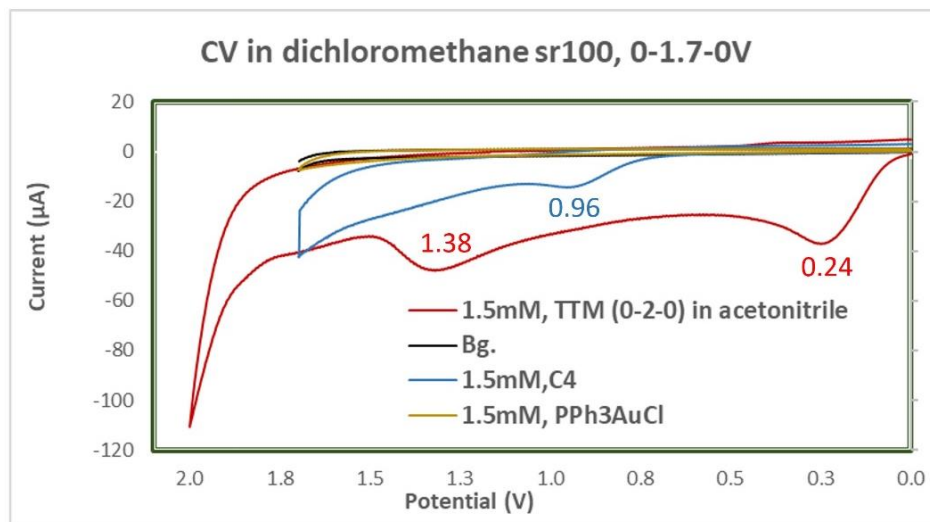
Fig. B. 26. CV of **C-4** vs its precursors in dichloromethane
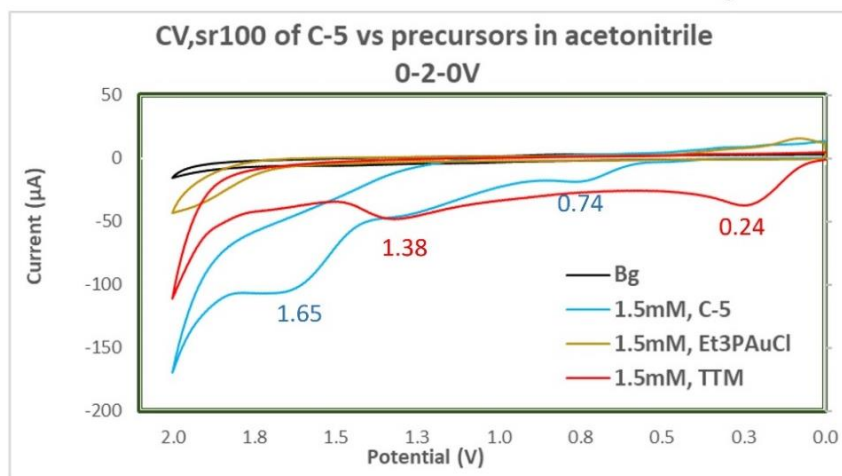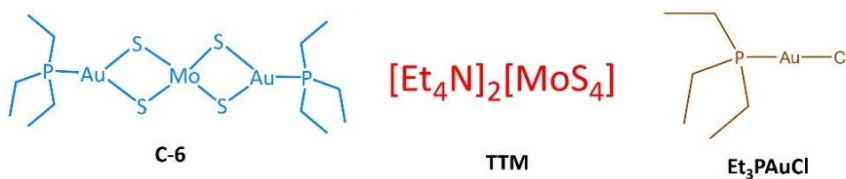
Fig. B. 27. CV of **C-5** vs its precursors in acetonitrile

APPENDIX C: SCXRD DATA

Table C. 1. SCXRD data of **C-1**

Crystal Data= **C-1**	
Chemical formula	$[MoS_4Au_2N_4C_{54}H_{72}]$
M_r	1395.28
Crystal system, space group	Tetragonal, $I\ 41/a$
Temperature (K)	296
a, b, c (Å)	18.5116(8), 18.5116(8), 17.4697(8)
α, β, γ (°)	90, 90, 90
V (Å^3)	5986.5(6)
Z	4
Radiation type	Mo $K\alpha$
μ (mm^{-1})	5.270
Crystal size (mm)	0.760 × 0.737 × 0.574
Data collection	
Diffractometer	Bruker D8 Quest ECO
Absorption correction	Multi-scan (SADABS: Krause et al., 2016)
T_{min}, T_{max}	0.090, 0.150
No. of measured, independent, and observed [$I > 2\sigma(I)$] reflections	8494, 3701, 2401
R_{int}	0.0904
(sin θ/λ)$_{max}$ (Å^{-1})	0.667
Refinement	
$R[F^2 > 2\sigma\ (F^2)]$, $wR(F^2)$, S	0.0399, 0.1118, 1.076
No. of reflections	31875
No. of parameters	163
No. of restraints	162
H-atom treatment	H-atom parameters constrained
Δρ_{max}, Δρ_{min} (e Å^{-3})	1.950 , -0.804

Table C. 2. SCXRD data of **C-2**

Crystal Data= **C-2**	
Chemical formula	$[MoS_4Au_2(C_{11}H_{12}N_2)_2]$
M_r	962.56
Crystal system, space group	Triclinic, *P -1*
Temperature (K)	293
a, b, c (Å)	10.5919(6), 11.0031(6), 13.8204(7)
α, β, γ (°)	93.932(3), 103.082(3), 117.507(2)
V (Å$^{3)}$	1363.30(13)
Z	2
Radiation type	Mo *K*α
μ (mm^{-1})	11.512
Crystal size (mm)	0.760 × 0.737 × 0.574
Data collection	
Diffractometer	Bruker D8 Quest ECO
Absorption correction	Multi-scan (SADABS: Krause et al., 2016)
$T_{min,}$ T_{max}	0.4467, 0.7452
No. of measured, independent, and observed [*I* > 2σ(*I*)] reflections	19028, 4810, 3814
R_{int}	0.0419
(sin θ/λ)$_{max}$ (Å $^{-1}$)	0.596
Refinement	
R[F^2 > 2σ (F^2)], wR(F^2), S	0.0320, 0.0700, 1.068
No. of reflections	4810
No. of parameters	300
No. of restraints	0
H-atom treatment	H-atom parameters constrained
Δρ_{max}, Δρ_{min} (e Å^{-3})	0.742, -1.163

Table C. 3. SCXRD data of **C-3**

Crystal Data= C-3	
Chemical formula	$[MoS_4Au_2(C_{21}H_{24}N_2)_2]$
M_r	1226.97
Crystal system, space group	Triclinic, *P -1*
Temperature (K)	296
a, b, c (Å)	9.5740(19),15.415(3),16.586(4)
α, β, γ (°)	93.971(10), 91.067(10, 99.438(10)
V (Å$^{3)}$)	2407.8(9)
Z	2
Radiation type	Mo *K*α
μ (mm^{-1})	6.539
Crystal size (mm)	1.385 × 0.918 × 0.310
Data collection	
Diffractometer	Bruker D8 Quest ECO
Absorption correction	Multi-scan (SADABS: Krause et al., 2016)
$T_{min,}$ T_{max}	0.001,0.132
No. of measured, independent, and observed [$I > 2σ(I)$] reflections	68282, 12438, 7477
R_{int}	0.1698
(sin θ/λ)$_{max}$ (Å $^{-1}$)	0.675
Refinement	
$R[F^2 > 2σ (F^2)], wR(F^2), S$	0.1106, 0.3497, 1.023
No. of reflections	12374
No. of parameters	470
No. of restraints	0
H-atom treatment	H-atom parameters constrained
$Δρ_{max}, Δρ_{min}$ (e Å^{-3})	4.854, -4.310

Table C. 4. Selected bonds data of **C-1**

Atoms	Distance (Å)
N-C$_{Au}$	1.35
Au-C$_{imd}$	1.99
Au-Mo	2.78
Au-S	2.39
Mo-S	2.23
	Angles
Au-Mo-Au	180˚
Au-S-Mo	73.9
N-C-N	107.2

Table C. 5. Selected bonds data of **C-2**

Atoms	Distance (Å)
N-C$_{Au}$	1.33 benzyl, 1.36 methyl
Au-C$_{imd}$	2.02
Au-Mo	2.80
Au-S	2.38
Mo-S	2.20
	Angles
Au-Mo-Au	176˚
Au-S-Mo	74.6 ±0.3
N-C-N	104.3

Table C. 6. Selected bonds data of **C-3**

Atoms	Distance (Å)
N-C$_{Au}$	1.35, 1.33
Au-C$_{imd}$	2.01
Au-Mo	2.84, 2.79
Au-S	2.4 ± 0.1
Mo-S	2.20
	Angles
Au-Mo-Au	170˚
Au-S-Mo	74.9 ±1.3
N-C-N	105.1 ±1.5

C-1/ checkCIF/PLATON report

Structure factors have been supplied for datablock(s) Dhirgam
THIS REPORT IS FOR GUIDANCE ONLY. IF USED AS PART OF A REVIEW PROCEDURE
FOR PUBLICATION, IT SHOULD NOT REPLACE THE EXPERTISE OF AN EXPERIENCED
CRYSTALLOGRAPHIC REFEREE.
No syntax errors found. CIF dictionary Interpreting this report
Datablock: C-1
Bond precision: C-C = 0.0469 A Wavelength=0.71073
Cell: a=18.5116(8) b=18.5116(8) c=17.4697(8)
alpha=90 beta=90 gamma=90
Temperature: 296 K
Calculated Reported
Volume 5986.5(6) 5986.5(5)
Space group I 41/a I 41/a
Hall group -I 4ad -I 4ad
Moiety formula C54 H72 Au2 Mo N4 S2 C54 H72 Au2 Mo N4 S2
Sum formula C54 H72 Au2 Mo N4 S2 C54 H72 Au2 Mo N4 S2
Mr 1331.16 1331.20
Dx,g cm-3 1.477 1.477
Z 4 4
Mu (mm-1) 5.199 5.199
F000 2624.0 2604.6
F000' 2603.24
h,k,lmax 24,24,23 24,24,23
Nref 3707 3701
Tmin,Tmax 0.072,0.052 0.100,0.150
Tmin' 0.037
Correction method= # Reported T Limits: Tmin=0.100 Tmax=0.150
AbsCorr = MULTI-SCAN
Data completeness= 0.998 Theta(max)= 28.310
R(reflections)= 0.1081(2401) wR2(reflections)= 0.3503(3701)
S = 1.337 Npar= 154
The following ALERTS were generated. Each ALERT has the format
test-name_ALERT_alert-type_alert-level.
Click on the hyperlinks for more details of the test.
Alert level A
SHFSU01_ALERT_2_A The absolute value of parameter shift to su ratio > 0.20
Absolute value of the parameter shift to su ratio given 1.369
Additional refinement cycles may be required.
PLAT080_ALERT_2_A Maximum Shift/Error .... 1.37 Why ?
PLAT245_ALERT_2_A U(iso) H14C Smaller than U(eq) C14 by 0.150 Ang**2
PLAT721_ALERT_1_A Bond Calc 1.0(2), Rep 0.96000 Dev... 0.04 Ang.
C11 -H11B 1.555 1.555 .... # 32 Check
PLAT721_ALERT_1_A Bond Calc 1.0(2), Rep 0.96000 Dev... 0.04 Ang.
C12 -H12A 1.555 1.555 .... # 34 Check
PLAT721_ALERT_1_A Bond Calc 1.0(2), Rep 0.96000 Dev... 0.04 Ang.

C12 -H12C 1.555 1.555 .... # 36 Check
PLAT721_ALERT_1_A Bond Calc 1.0(3), Rep 0.96000 Dev... 0.04 Ang.
C13 -H13A 1.555 1.555 .... # 37 Check
PLAT721_ALERT_1_A Bond Calc 1.0(2), Rep 0.96000 Dev... 0.04 Ang.
C13 -H13C 1.555 1.555 .... # 39 Check
PLAT971_ALERT_2_A Check Calcd Resid. Dens. 2.21A From Mo1 9.53 eA-3
PLAT973_ALERT_2_A Check Calcd Positive Resid. Density on Au1 3.93 eA-3
Alert level B
PLAT094_ALERT_2_B Ratio of Maximum / Minimum Residual Density .... 6.53 Report
PLAT097_ALERT_2_B Large Reported Max. (Positive) Residual Density 11.52 eA-3
PLAT342_ALERT_3_B Low Bond Precision on C-C Bonds .... 0.04692 Ang.
PLAT722_ALERT_1_B Angle Calc 107(13), Rep 109.50 Dev... 2.50 Degree
H13B -C13 -C9 1.555 1.555 1.555 # 61 Check
PLAT971_ALERT_2_B Check Calcd Resid. Dens. 0.39A From S2 3.37 eA-3
PLAT973_ALERT_2_B Check Calcd Positive Resid. Density on Mo1 1.82 eA-3
Alert level C
DIFMX02_ALERT_1_C The maximum difference density is > 0.1*ZMAX*0.75
The relevant atom site should be identified.
PLAT068_ALERT_1_C Reported F000 Differs from Calcd (or Missing)... Please Check
PLAT082_ALERT_2_C High R1 Value .... 0.11 Report
PLAT084_ALERT_3_C High wR2 Value (i.e. > 0.25) .... 0.35 Report
PLAT213_ALERT_2_C Atom C10 has ADP max/min Ratio ..... 3.8 prolat
PLAT220_ALERT_2_C Non-Solvent Resd 1 C Ueq(max)/Ueq(min) Range 3.2 Ratio
PLAT222_ALERT_3_C Non-Solv. Resd 1 H Uiso(max)/Uiso(min) Range 9.7 Ratio
PLAT234_ALERT_4_C Large Hirshfeld Difference Au1 --S2 . 0.22 Ang.
PLAT234_ALERT_4_C Large Hirshfeld Difference Au1 --C1 . 0.16 Ang.
PLAT234_ALERT_4_C Large Hirshfeld Difference Mo1 --S2 . 0.16 Ang.
PLAT234_ALERT_4_C Large Hirshfeld Difference C7 --C8 . 0.24 Ang.
PLAT241_ALERT_2_C High 'MainMol' Ueq as Compared to Neighbors of C5 Check
PLAT242_ALERT_2_C Low 'MainMol' Ueq as Compared to Neighbors of Au1 Check
PLAT242_ALERT_2_C Low 'MainMol' Ueq as Compared to Neighbors of Mo1 Check
PLAT242_ALERT_2_C Low 'MainMol' Ueq as Compared to Neighbors of C2 Check
PLAT242_ALERT_2_C Low 'MainMol' Ueq as Compared to Neighbors of C9 Check
PLAT260_ALERT_2_C Large Average Ueq of Residue Including Au1 0.127 Check
PLAT412_ALERT_2_C Short Intra XH3 .. XHn H11A ..H12B . 1.89 Ang.
x,y,z = 1_555 Check
PLAT413_ALERT_2_C Short Inter XH3 .. XHn H11A ..H13A . 2.10 Ang.
1/2+x,y,3/2-z = 16_556 Check
PLAT721_ALERT_1_C Bond Calc 0.94(14), Rep 0.96000 Dev... 0.02 Ang.
C11 -H11A 1.555 1.555 .... # 31 Check
PLAT721_ALERT_1_C Bond Calc 0.94(13), Rep 0.96000 Dev... 0.02 Ang.
C13 -H13B 1.555 1.555 .... # 38 Check
PLAT722_ALERT_1_C Angle Calc 108(5), Rep 109.50 Dev... 1.50 Degree
H14B -C14 -C9 1.555 1.555 1.555 # 67 Check
PLAT722_ALERT_1_C Angle Calc 111(10), Rep 109.50 Dev... 1.50 Degree
H14C -C14 -H14B 1.555 1.555 1.555 # 71 Check
PLAT910_ALERT_3_C Missing # of FCF Reflection(s) Below Theta(Min). 5 Note
PLAT918_ALERT_3_C Reflection(s) with I(obs) much Smaller I(calc) . 1 Check

PLAT925_ALERT_1_C The Reported and Calculated Rho(max) Differ by . 1.99 eA-3
PLAT926_ALERT_1_C Reported and Calculated R1 Differ by .... -0.0023 Check
PLAT927_ALERT_1_C Reported and Calculated wR2 Differ by .... -0.0012 Check
PLAT934_ALERT_3_C Number of (Iobs-Icalc)/SigmaW > 10 Outliers .... 1 Check
PLAT972_ALERT_2_C Check Calcd Resid. Dens. 1.29A From C10 -2.17 eA-3
PLAT972_ALERT_2_C Check Calcd Resid. Dens. 0.82A From Mo1 -1.75 eA-3
PLAT972_ALERT_2_C Check Calcd Resid. Dens. 0.82A From Mo1 -1.75 eA-3
PLAT972_ALERT_2_C Check Calcd Resid. Dens. 0.80A From Mo1 -1.71 eA-3
PLAT972_ALERT_2_C Check Calcd Resid. Dens. 1.37A From Mo1 -1.67 eA-3
PLAT972_ALERT_2_C Check Calcd Resid. Dens. 0.57A From S2 -1.58 eA-3
PLAT972_ALERT_2_C Check Calcd Resid. Dens. 0.90A From Au1 -1.56 eA-3
PLAT977_ALERT_2_C Check Negative Difference Density on H10 -0.95 eA-3
PLAT977_ALERT_2_C Check Negative Difference Density on H11A -0.40 eA-3
PLAT977_ALERT_2_C Check Negative Difference Density on H14C -0.51 eA-3
PLAT978_ALERT_2_C Number C-C Bonds with Positive Residual Density. 0 Info
Alert level G
PLAT002_ALERT_2_G Number of Distance or Angle Restraints on AtSite 6 Note
PLAT003_ALERT_2_G Number of Uiso or Uij Restrained non-H Atoms ... 18 Report
PLAT072_ALERT_2_G SHELXL First Parameter in WGHT Unusually Large 0.20 Report
PLAT176_ALERT_4_G The CIF-Embedded .res File Contains SADI Records 2 Report
PLAT177_ALERT_4_G The CIF-Embedded .res File Contains DELU Records 1 Report
PLAT178_ALERT_4_G The CIF-Embedded .res File Contains SIMU Records 1 Report
PLAT187_ALERT_4_G The CIF-Embedded .res File Contains RIGU Records 1 Report
PLAT300_ALERT_4_G Atom Site Occupancy of S2 Constrained at 0.5 Check
PLAT301_ALERT_3_G Main Residue Disorder ....(Resd 1) 3% Note
PLAT335_ALERT_2_G Check Large C6 Ring C-C Range C2 -C7 0.19 Ang.
PLAT722_ALERT_1_G Angle Calc 114.00, Rep 109.50 Dev... 4.50 Degree
H11B -C11 -H11A 1.555 1.555 1.555 # 50 Check
PLAT722_ALERT_1_G Angle Calc 108.00, Rep 109.50 Dev... 1.50 Degree
H11C -C11 -H11A 1.555 1.555 1.555 # 52 Check
PLAT722_ALERT_1_G Angle Calc 114.00, Rep 109.50 Dev... 4.50 Degree
H12B -C12 -H12A 1.555 1.555 1.555 # 56 Check
PLAT722_ALERT_1_G Angle Calc 106.00, Rep 109.50 Dev... 3.50 Degree
H12C -C12 -H12B 1.555 1.555 1.555 # 59 Check
PLAT722_ALERT_1_G Angle Calc 114.00, Rep 109.50 Dev... 4.50 Degree
H13B -C13 -H13A 1.555 1.555 1.555 # 62 Check
PLAT722_ALERT_1_G Angle Calc 113.00, Rep 109.50 Dev... 3.50 Degree
H13C -C13 -H13A 1.555 1.555 1.555 # 64 Check
PLAT722_ALERT_1_G Angle Calc 104.00, Rep 109.50 Dev... 5.50 Degree
H13C -C13 -H13B 1.555 1.555 1.555 # 65 Check
PLAT860_ALERT_3_G Number of Least-Squares Restraints .... 76 Note
PLAT883_ALERT_1_G No Info/Value for _atom_sites_solution_primary . Please Do !
PLAT912_ALERT_4_G Missing # of FCF Reflections Above STh/L= 0.600 3 Note
PLAT913_ALERT_3_G Missing # of Very Strong Reflections in FCF .... 1 Note
PLAT933_ALERT_2_G Number of OMIT Records in Embedded .res File ... 4 Note
PLAT960_ALERT_3_G Number of Intensities with I < - 2*sig(I) ... 8 Check
PLAT982_ALERT_1_G The Au-f'= -1.8451 Deviates from IT-value = -2.0133 Check
PLAT983_ALERT_1_G The Au-f"= 8.8704 Deviates from IT-Value = 8.8022 Check

PLAT983_ALERT_1_G The Mo-f"= 0.7034 Deviates from IT-Value = 0.6857 Check
PLAT983_ALERT_1_G The S-f"= 0.1244 Deviates from IT-Value = 0.1234 Check
10 **ALERT level A** = Most likely a serious problem - resolve or explain
6 **ALERT level B** = A potentially serious problem, consider carefully
40 **ALERT level C** = Check. Ensure it is not caused by an omission or oversight
27 **ALERT level G** = General information/check it is not something unexpected
27 ALERT type 1 CIF construction/syntax error, inconsistent or missing data
36 ALERT type 2 Indicator that the structure model may be wrong or deficient
10 ALERT type 3 Indicator that the structure quality may be low
10 ALERT type 4 Improvement, methodology, query or suggestion
0 ALERT type 5 Informative message, check

186
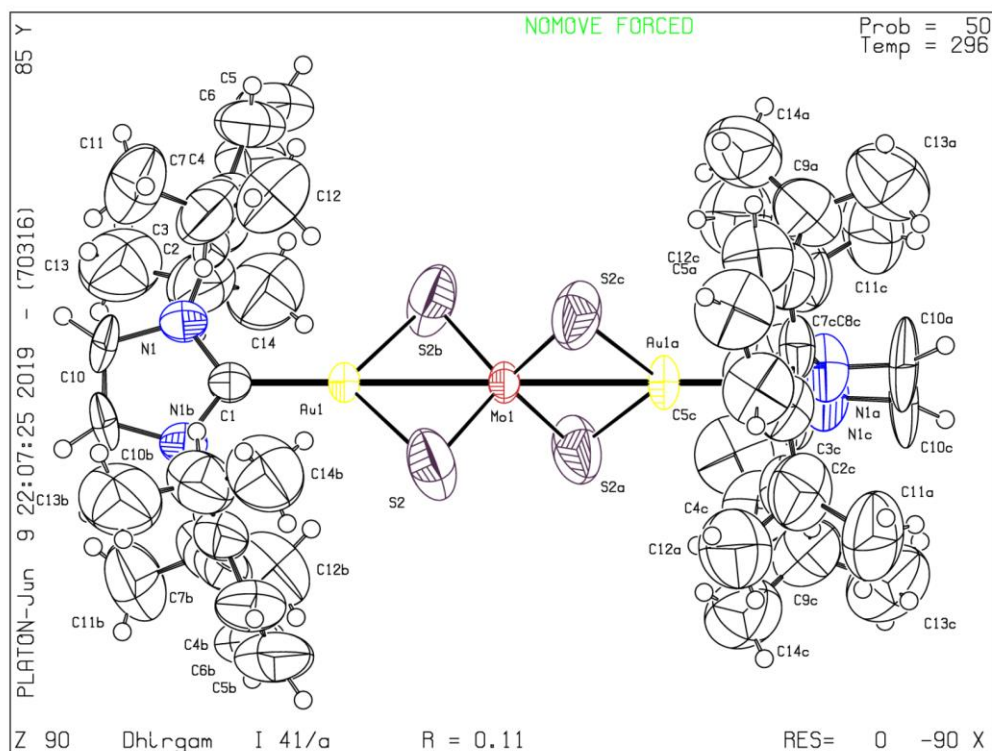
C-2/ checkCIF/PLATON report

You have not supplied any structure factors. As a result the full set of tests cannot be run.
THIS REPORT IS FOR GUIDANCE ONLY. IF USED AS PART OF A REVIEW PROCEDURE
FOR PUBLICATION, IT SHOULD NOT REPLACE THE EXPERTISE OF AN EXPERIENCED
CRYSTALLOGRAPHIC REFEREE.
No syntax errors found. CIF dictionary Interpreting this report
Datablock: DHC55
Bond precision: C-C = 0.0129 A Wavelength=0.71076
Cell: a=10.5919(6) b=11.0031(6) c=13.8204(7)
alpha=93.932(3) beta=103.082(3) gamma=117.507(2)
Temperature: 293 K
Calculated Reported
Volume 1363.30(13) 1363.30(13)
Space group P -1 P -1
Hall group -P 1 -P 1
Moiety formula C22 H24 Au2 Mo N4 S4 [MOS4(AU(MBI))2]
Sum formula C22 H24 Au2 Mo N4 S4 C22 H24 Au2 Mo N4 S4
Mr 962.57 962.56
Dx,g cm-3 2.345 2.345
Z 2 2
Mu (mm-1) 11.512 11.512
F000 896.0 896.0
F000' 886.23
h,k,lmax 12,13,16 12,13,16
Nref 4858 4810
Tmin,Tmax 0.009,0.042 0.450,0.750
Tmin' 0.005
Correction method= # Reported T Limits: Tmin=0.450 Tmax=0.750
AbsCorr = MULTI-SCAN
Data completeness= 0.990 Theta(max)= 25.090
R(reflections)= 0.0320(3814) wR2(reflections)= 0.0700(4810)
S = 1.061 Npar= 300
The following ALERTS were generated. Each ALERT has the format
test-name_ALERT_alert-type_alert-level.
Click on the hyperlinks for more details of the test.
Alert level B
PLAT232_ALERT_2_B Hirshfeld Test Diff (M-X) Au1 --S1 . 10.4 s.u.
Alert level C
RADNW01_ALERT_1_C The radiation wavelength lies outside the expected range
for the supplied radiation type. Expected range 0.71065-0.71075
Wavelength given = 0.71076
PLAT232_ALERT_2_C Hirshfeld Test Diff (M-X) Au1 --S4 . 6.5 s.u.
PLAT232_ALERT_2_C Hirshfeld Test Diff (M-X) Au2 --S2 . 9.7 s.u.
PLAT232_ALERT_2_C Hirshfeld Test Diff (M-X) Au2 --S3 . 6.3 s.u.
PLAT241_ALERT_2_C High 'MainMol' Ueq as Compared to Neighbors of S1 Check
PLAT241_ALERT_2_C High 'MainMol' Ueq as Compared to Neighbors of S3 Check

PLAT241_ALERT_2_C High 'MainMol' Ueq as Compared to Neighbors of S4 Check
PLAT241_ALERT_2_C High 'MainMol' Ueq as Compared to Neighbors of C4 Check
PLAT241_ALERT_2_C High 'MainMol' Ueq as Compared to Neighbors of C13 Check
PLAT242_ALERT_2_C Low 'MainMol' Ueq as Compared to Neighbors of Mo1 Check
PLAT242_ALERT_2_C Low 'MainMol' Ueq as Compared to Neighbors of C6 Check
PLAT242_ALERT_2_C Low 'MainMol' Ueq as Compared to Neighbors of C14 Check
PLAT342_ALERT_3_C Low Bond Precision on C-C Bonds .... 0.01288 Ang.
Alert level G
FORMU01_ALERT_1_G There is a discrepancy between the atom counts in the
_chemical_formula_sum and _chemical_formula_moiety. This is
usually due to the moiety formula being in the wrong format.
Atom count from _chemical_formula_sum: C22 H24 Au2 Mo1 N4 S4
Atom count from _chemical_formula_moiety:
PLAT042_ALERT_1_G Calc. and Reported MoietyFormula Strings Differ Please Check
PLAT199_ALERT_1_G Reported _cell_measurement_temperature ..... (K) 293 Check
PLAT200_ALERT_1_G Reported _diffrn_ambient_temperature ..... (K) 293 Check
PLAT883_ALERT_1_G No Info/Value for _atom_sites_solution_primary . Please Do !
0 **ALERT level A** = Most likely a serious problem - resolve or explain
1 **ALERT level B** = A potentially serious problem, consider carefully
13 **ALERT level C** = Check. Ensure it is not caused by an omission or oversight
5 **ALERT level G** = General information/check it is not something unexpected
6 ALERT type 1 CIF construction/syntax error, inconsistent or missing data
12 ALERT type 2 Indicator that the structure model may be wrong or deficient
1 ALERT type 3 Indicator that the structure quality may be low
0 ALERT type 4 Improvement, methodology, query or suggestion
0 ALERT type 5 Informative message, check
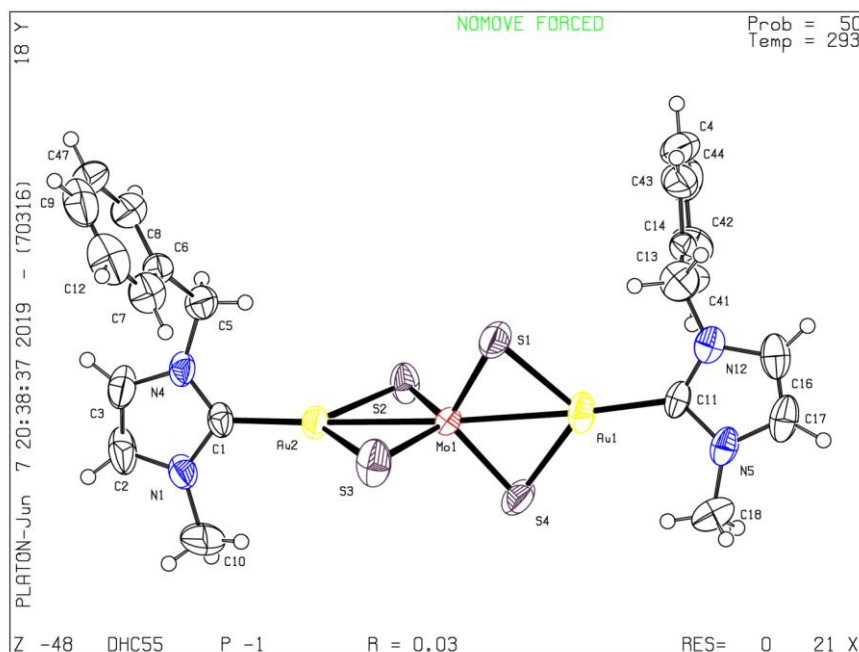
C-3/ checkCIF/PLATON report

You have not supplied any structure factors. As a result the full set of tests cannot be run.
THIS REPORT IS FOR GUIDANCE ONLY. IF USED AS PART OF A REVIEW PROCEDURE
FOR PUBLICATION, IT SHOULD NOT REPLACE THE EXPERTISE OF AN EXPERIENCED
CRYSTALLOGRAPHIC REFEREE.
No syntax errors found. CIF dictionary Interpreting this report
Datablock: C78D021019
Bond precision: C-C = 0.0358 A Wavelength=0.71073
Cell: a=9.5740(19) b=15.415(3) c=16.586(4)
alpha=93.971(10) beta=91.067(10) gamma=99.438(10)
Temperature: 296 K
Calculated Reported
Volume 2407.8(9) 2407.8(9)
Space group P -1 P -1
Hall group -P 1 -P 1
Moiety formula C42 H48 Au2 Mo N4 S4 ?
Sum formula C42 H48 Au2 Mo N4 S4 C42 H48 Au2 Mo N4 S4
Mr 1226.97 1226.95
Dx,g cm-3 1.692 1.692
Z 2 2
Mu (mm-1) 6.539 6.539
F000 1184.0 1184.0
F000' 1174.13
h,k,lmax 12,20,22 12,20,22
Nref 12438 12374
Tmin,Tmax 0.001,0.132 0.050,0.240
Tmin' 0.000
Correction method= # Reported T Limits: Tmin=0.050 Tmax=0.240
AbsCorr = MULTI-SCAN
Data completeness= 0.995 Theta(max)= 28.700
R(reflections)= 0.1106(7477) wR2(reflections)= 0.3497(12374)
S = 1.023 Npar= 470
The following ALERTS were generated. Each ALERT has the format
test-name_ALERT_alert-type_alert-level.
Click on the hyperlinks for more details of the test.
Alert level A
EXPT005_ALERT_1_A _exptl_crystal_description is missing
Crystal habit description.
The following tests will not be performed.
CRYSR_01
PLAT601_ALERT_2_A Structure Contains Solvent Accessible VOIDS of . 240 Ang**3
Alert level B
CRYSS02_ALERT_3_B The value of _exptl_crystal_size_mid is > 0.8
Mid crystal size given = 0.918
CRYSS02_ALERT_3_B The value of _exptl_crystal_size_max is > 1.0
Maximum crystal size given = 1.385
PLAT201_ALERT_2_B Isotropic non-H Atoms in Main Residue(s) .... 4 Report

C7 C11 C12 C23
PLAT213_ALERT_2_B Atom C22 has ADP max/min Ratio ..... 5.0 oblate
PLAT342_ALERT_3_B Low Bond Precision on C-C Bonds .... 0.03579 Ang.
Alert level C
RINTA01_ALERT_3_C The value of Rint is greater than 0.12
Rint given 0.170
PLAT020_ALERT_3_C The Value of Rint is Greater Than 0.12 .... 0.170 Report
PLAT082_ALERT_2_C High R1 Value .... 0.11 Report
PLAT084_ALERT_3_C High wR2 Value (i.e. > 0.25) .... 0.35 Report
PLAT213_ALERT_2_C Atom C9 has ADP max/min Ratio ..... 3.3 prolat
PLAT220_ALERT_2_C Non-Solvent Resd 1 C Ueq(max)/Ueq(min) Range 5.3 Ratio
PLAT222_ALERT_3_C Non-Solv. Resd 1 H Uiso(max)/Uiso(min) Range 4.9 Ratio
PLAT234_ALERT_4_C Large Hirshfeld Difference C14 --C19 . 0.22 Ang.
PLAT241_ALERT_2_C High 'MainMol' Ueq as Compared to Neighbors of S1 Check
PLAT241_ALERT_2_C High 'MainMol' Ueq as Compared to Neighbors of S3 Check
PLAT241_ALERT_2_C High 'MainMol' Ueq as Compared to Neighbors of S4 Check
PLAT241_ALERT_2_C High 'MainMol' Ueq as Compared to Neighbors of C2 Check
PLAT241_ALERT_2_C High 'MainMol' Ueq as Compared to Neighbors of C6 Check
PLAT241_ALERT_2_C High 'MainMol' Ueq as Compared to Neighbors of C8 Check
PLAT242_ALERT_2_C Low 'MainMol' Ueq as Compared to Neighbors of Mo1 Check
PLAT242_ALERT_2_C Low 'MainMol' Ueq as Compared to Neighbors of C5 Check
PLAT242_ALERT_2_C Low 'MainMol' Ueq as Compared to Neighbors of C7 Check
PLAT242_ALERT_2_C Low 'MainMol' Ueq as Compared to Neighbors of C9 Check
PLAT334_ALERT_2_C Small Aver. Benzene C-C Dist C4 -C9 1.37 Ang.
Alert level G
PLAT002_ALERT_2_G Number of Distance or Angle Restraints on AtSite 16 Note
PLAT003_ALERT_2_G Number of Uiso or Uij Restrained non-H Atoms ... 2 Report
PLAT063_ALERT_4_G Crystal Size Likely too Large for Beam Size .... 1.38 mm
PLAT072_ALERT_2_G SHELXL First Parameter in WGHT Unusually Large 0.15 Report
PLAT083_ALERT_2_G SHELXL Second Parameter in WGHT Unusually Large 151.07 Why ?
PLAT154_ALERT_1_G The s.u.'s on the Cell Angles are Equal ..(Note) 0.01 Degree
PLAT172_ALERT_4_G The CIF-Embedded .res File Contains DFIX Records 8 Report
PLAT174_ALERT_4_G The CIF-Embedded .res File Contains FLAT Records 4 Report
PLAT176_ALERT_4_G The CIF-Embedded .res File Contains SADI Records 1 Report
PLAT177_ALERT_4_G The CIF-Embedded .res File Contains DELU Records 1 Report
PLAT232_ALERT_2_G Hirshfeld Test Diff (M-X) Au1 --S1 . 5.3 s.u.
PLAT721_ALERT_1_G Bond Calc 0.97000, Rep 0.96000 Dev... 0.01 Ang.
C19 -H19C 1.555 1.555 .... # 61 Check
PLAT721_ALERT_1_G Bond Calc 0.97000, Rep 0.96000 Dev... 0.01 Ang.
C20 -H20A 1.555 1.555 .... # 62 Check
PLAT721_ALERT_1_G Bond Calc 0.97000, Rep 0.96000 Dev... 0.01 Ang.
C32 -H32C 1.555 1.555 .... # 87 Check
PLAT721_ALERT_1_G Bond Calc 0.97000, Rep 0.96000 Dev... 0.01 Ang.
C40 -H40B 1.555 1.555 .... # 103 Check
PLAT860_ALERT_3_G Number of Least-Squares Restraints .... 32 Note
PLAT883_ALERT_1_G No Info/Value for _atom_sites_solution_primary . Please Do !
2 **ALERT level A** = Most likely a serious problem - resolve or explain
5 **ALERT level B** = A potentially serious problem, consider carefully

19 **ALERT level C** = Check. Ensure it is not caused by an omission or oversight
17 **ALERT level G** = General information/check it is not something unexpected
7 ALERT type 1 CIF construction/syntax error, inconsistent or missing data
22 ALERT type 2 Indicator that the structure model may be wrong or deficient
8 ALERT type 3 Indicator that the structure quality may be low
6 ALERT type 4 Improvement, methodology, query or suggestion
0 ALERT type 5 Informative message, check

It is advisable to attempt to resolve as many as possible of the alerts in all categories. Often the minor alerts point to easily fixed oversights, errors and omissions in your CIF or refinement strategy, so attention to these fine details can be worthwhile. In order to resolve some of the more serious problems it may be necessary to carry out additional measurements or structure refinements. However, the purpose of your study may justify the reported deviations and the more serious of these should normally be commented upon in the discussion or experimental section of a paper or in the "special_details" fields of the CIF. checkCIF was carefully designed to identify outliers and unusual parameters, but every test has its limitations and alerts that are not important in a particular case may appear. Conversely, the absence of alerts does not guarantee there are no aspects of the results needing attention. It is up to the individual to critically assess their own results and, if necessary, seek expert advice.

Publication of your CIF in IUCr journals

A basic structural check has been run on your CIF. These basic checks will be run on all CIFs submitted for publication in IUCr journals (*Acta Crystallographica*, *Journal of Applied Crystallography*, *Journal of Synchrotron Radiation*); however, if you intend to submit to *Acta Crystallographica Section C* or *E* or *IUCrData*, you should make sure that full publication checks are run on the final version of your CIF prior to submission.
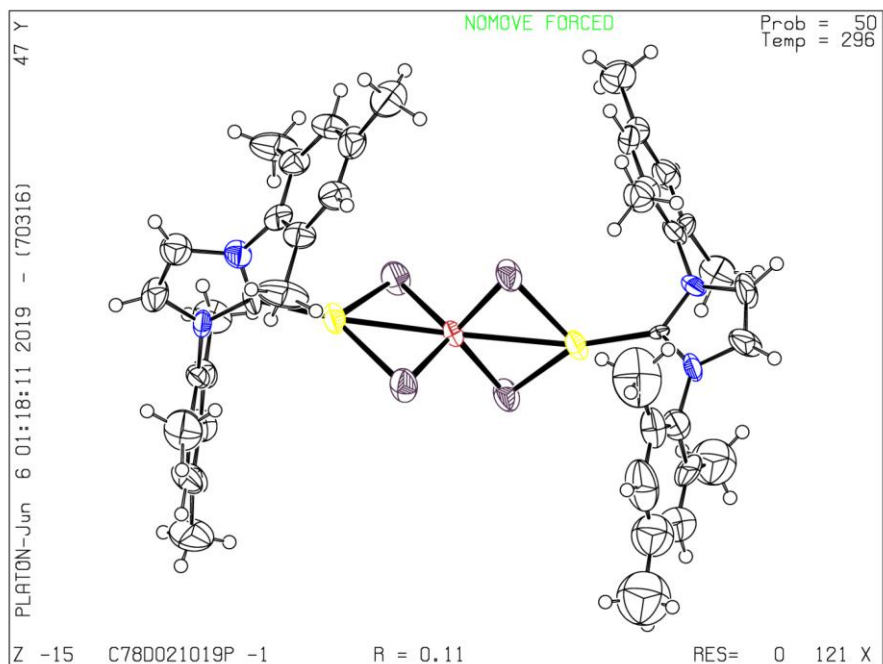
APPENDIX D: ELEMENTAL ANALYSES (CHN) and IM-MS

Laboratory Report

Report prepared for:
Dhirgam Humaidy
University of Maine
Chemistry Dept
5706 Aubert Hall
Orono, ME 04469
Phone: 207-581-1182
Email: Dhirgam.Humaidy@maine.edu

Sample: C4 (DH-4-1)
Lab ID: 2019-I-4483   **Received:** 2019-03-20

Analysis	Method	Result	Basis	Sample Amount Used	Date (Time)
C : Carbon					
	GLI Procedure ME-14	37.91 %	As Received	1.570 mg	2019-03-28
H : Hydrogen					
	GLI Procedure ME-14	2.86 %	As Received	1.570 mg	2019-03-28

Sample: C6 (DH-37-1)
Lab ID: 2019-I-4484   **Received:** 2019-03-20

Analysis	Method	Result	Basis	Sample Amount Used	Date (Time)
C : Carbon					
	GLI Procedure ME-14	44.69 %	As Received	1.527 mg	2019-03-28
H : Hydrogen					
	GLI Procedure ME-14	6.09 %	As Received	1.527 mg	2019-03-28
N : Nitrogen					
	GLI Procedure ME-14	4.54 %	As Received	1.527 mg	2019-03-28

Sample: C3 (DH-78-2)
Lab ID: 2019-I-4485   **Received:** 2019-03-20

Analysis	Method	Result	Basis	Sample Amount Used	Date (Time)
C : Carbon					
	GLI Procedure ME-14	41.34 %	As Received	1.450 mg	2019-03-28
H : Hydrogen					
	GLI Procedure ME-14	4.11 %	As Received	1.450 mg	2019-03-28
N : Nitrogen					
	GLI Procedure ME-14	4.91 %	As Received	1.450 mg	2019-03-28

Page 1 of 2

Fig. D. 1. Elemental analysis report for **C-4**, **C-6** and **C-3**

GALBRAITH
LABORATORIES, INC.

Laboratory Report

Report prepared for:
Dhirgam Humaidy
Univ of Maine
Chemistry Dept
5706 Aubert Hall
Orono, ME 04469
Phone: 207-581-1182
Fax: 207-581-1191
Email: Dhirgam.Humaidy@maine.edu

Report prepared by:
Christy Love

Purchase Order:
5100432223

For further assistance, contact:
Christy Love
Report Coordinator
PO Box 51610
Knoxville, TN 37950 -1610
(865) 546-1335
christylove@galbraith.com

Sample: C-1 (DH-29-1)
Lab ID: 2018-G-6190   **Received:** 2018-05-25

Analysis	Method	Result	Basis	Sample Amount Used	Date (Time)
C : Carbon					
	GLI Procedure ME-14	46.50 %	As Received	2.583 mg	2018-06-05
	GLI Procedure ME-14	46.42 %	As Received	2.223 mg	2018-06-05
H : Hydrogen					
	GLI Procedure ME-14	5.10 %	As Received	2.223 mg	2018-06-05
N : Nitrogen					
	GLI Procedure ME-14	4.19 %	As Received	2.583 mg	2018-06-05
	GLI Procedure ME-14	3.98 %	As Received	2.223 mg	2018-06-05

Sample: C-2 (DH-55-1)
Lab ID: 2018-G-6191   **Received:** 2018-05-25

Analysis	Method	Result	Basis	Sample Amount Used	Date (Time)
C : Carbon					
	GLI Procedure ME-14	27.38 %	As Received	4.636 mg	2018-06-05
	GLI Procedure ME-14	27.40 %	As Received	2.165 mg	2018-06-05
H : Hydrogen					
	GLI Procedure ME-14	2.53 %	As Received	2.165 mg	2018-06-05
N : Nitrogen					
	GLI Procedure ME-14	5.82 %	As Received	4.636 mg	2018-06-05
	GLI Procedure ME-14	5.73 %	As Received	2.165 mg	2018-06-05

Signatures:

Created By:	Christy.Love	2018-06-06T20:32:34.547-04:00
Published By:	Christy.Love	2018-06-06T20:32:54.843-04:00

Fig. D. 2. Elemental analysis report for **C-1** and **C-2**

GALBRAITH
LABORATORIES, INC.

Sample: C-5 (DH-84-2)
Lab ID: 2019-I-4486   **Received:** 2019-03-20

Analysis	Method	Result	Basis	Sample Amount Used	Date (Time)
C : Carbon					
	GLI Procedure ME-14	16.96 %	As Received	3.264 mg	2019-03-28
H : Hydrogen					
	GLI Procedure ME-14	3.57 %	As Received	3.264 mg	2019-03-28

Signatures:

Published By:	Christy.Love	2019-03-29T19:07:24.483-04:00
Created By:	Christy.Love	2019-03-29T19:06:55.67-04:00

- Physical signatures are on file.
- "Published By" signature indicates authorized release of data.

Fig. D. 3. Elemental analysis report for **C-5**
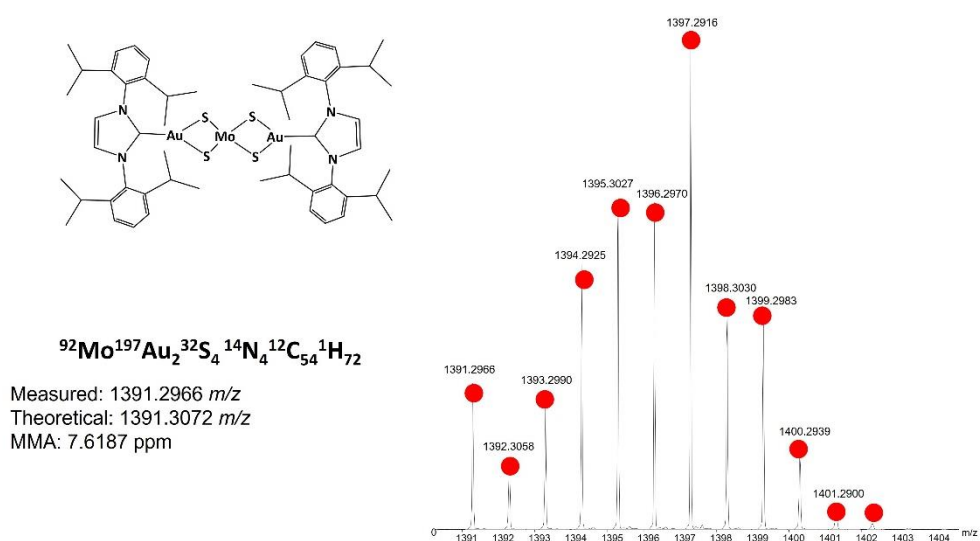
$^{92}Mo^{197}Au_2{}^{32}S_4{}^{14}N_4{}^{12}C_{54}{}^1H_{72}$

Measured: 1391.2966 *m/z*
Theoretical: 1391.3072 *m/z*
MMA: 7.6187 ppm

Fig. D. 4. ESI-MS in acetonitrile (positive ion mode) of **C-1**; corresponding theoretically calculated isotopic patterns are indicated with red dots. MMA: mass measurement accuracy values for [M+H]+

$^{92}Mo^{197}Au_2{}^{32}S_4{}^{14}N_4{}^{12}C_{22}{}^1H_{24}$

Measured: 958.9260 *m/z*
Theoretical: 958.9295 *m/z*
MMA: 3.6499 ppm
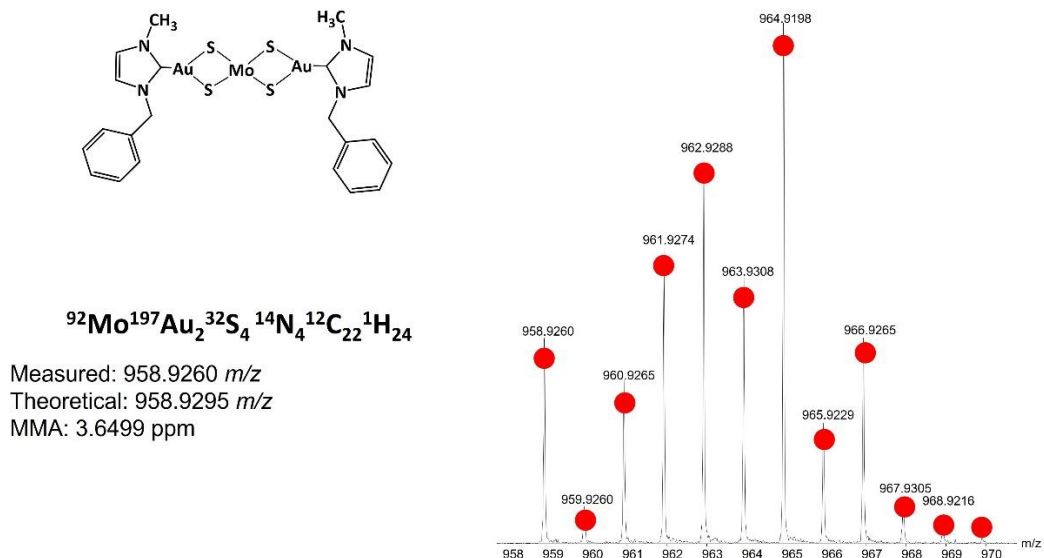
Fig. D. 5. ESI-MS in acetonitrile (positive ion mode) of **C-2**; corresponding theoretically calculated isotopic patterns are indicated with red dots. MMA: mass measurement accuracy values for [M+H]+

195

$^{92}Mo^{197}Au_2{}^{32}S_4{}^{14}N_4{}^{12}C_{42}{}^{1}H_{48}$

Measured: 1223.1176 *m/z*
Theoretical: 1223.1225 *m/z*
MMA: 3.6791 ppm
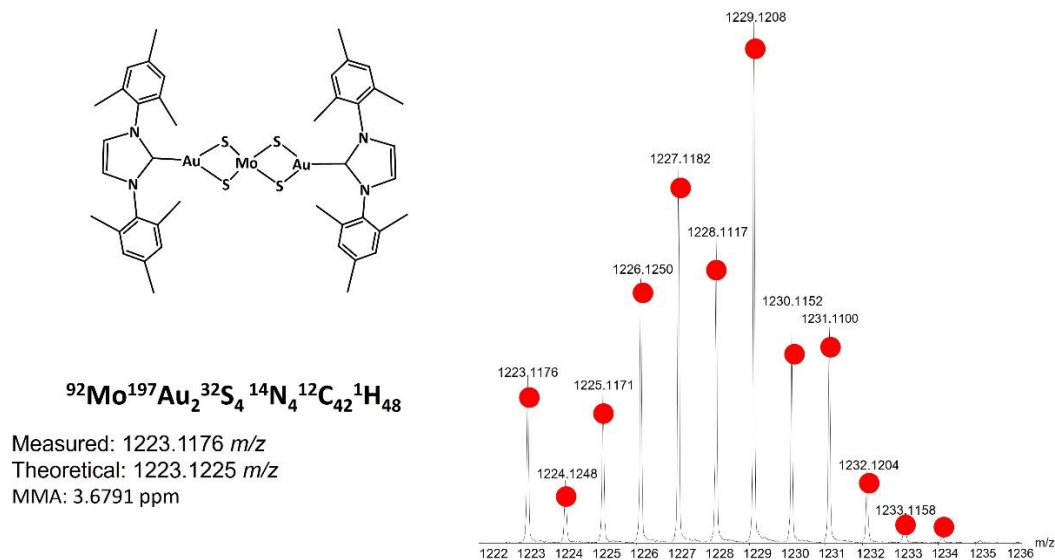
Fig. D. 6. ESI-MS in acetonitrile (positive ion mode) of **C-3**; corresponding theoretically calculated isotopic patterns are indicated with red dots. MMA: mass measurement accuracy values for [M+H]⁺

$^{92}Mo^{197}Au_2{}^{32}S_4{}^{31}P_2{}^{12}C_{36}{}^{1}H_{30}$

Measured: 1138.9188 *m/z*
Theoretical: 1138.9242 *m/z*
MMA: 4.7413 ppm
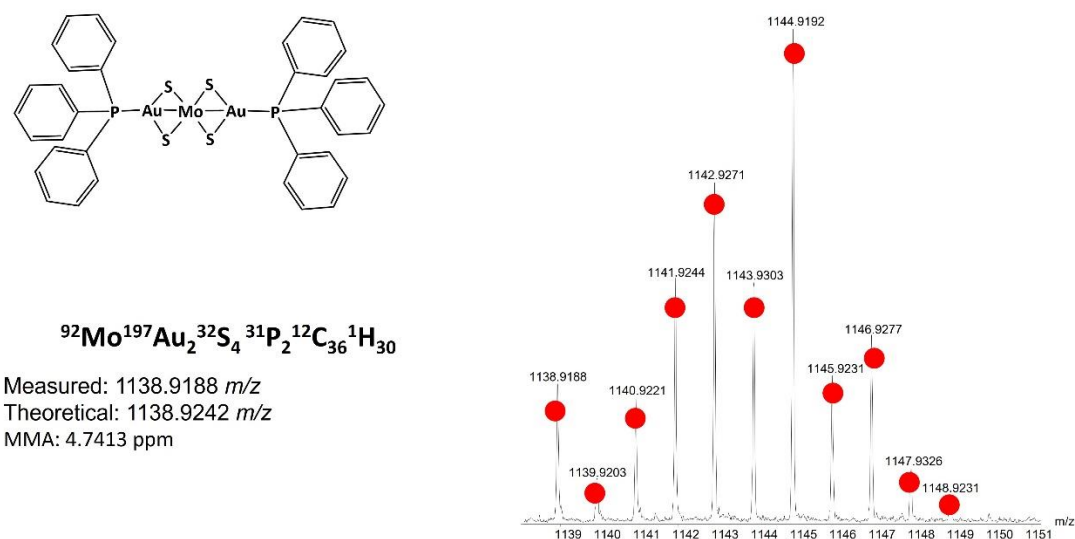
Fig. D. 7. ESI-MS in acetonitrile (positive ion mode) of **C-4**; corresponding theoretically calculated isotopic patterns are indicated with red dots. MMA: mass measurement accuracy values for [M+H]+

Article

Metal Complexes as Antifungals? From a Crowd-Sourced Compound Library to the First *In Vivo* Experiments

Angelo Frei,* Alysha G. Elliott, Alex Kan, Hue Dinh, Stefan Bräse, Alice E. Bruce, Mitchell R. Bruce, Feng Chen, Dhirgam Humaidy, Nicole Jung, A. Paden King, Peter G. Lye, Hanna K. Maliszewska, Ahmed M. Mansour, Dimitris Matiadis, María Paz Muñoz, Tsung-Yu Pai, Shyam Pokhrel, Peter J. Sadler, Marina Sagnou, Michelle Taylor, Justin J. Wilson, Dean Woods, Johannes Zuegg, Wieland Meyer, Amy K. Cain, Matthew A. Cooper, and Mark A. T. Blaskovich*

Cite This: https://doi.org/10.1021/jacsau.2c00308

Read Online

ACCESS | Metrics & More | Article Recommendations | Supporting Information

ABSTRACT: There are currently fewer than 10 antifungal drugs in clinical development, but new fungal strains that are resistant to most current antifungals are spreading rapidly across the world. To prevent a second resistance crisis, new classes of antifungal drugs are urgently needed. Metal complexes have proven to be promising candidates for novel antibiotics, but so far, few compounds have been explored for their potential application as antifungal agents. In this work, we report the evaluation of 1039 metal-containing compounds that were screened by the Community for Open Antimicrobial Drug Discovery (CO-ADD). We show that 20.9% of all metal compounds tested have antimicrobial activity against two representative *Candida* and *Cryptococcus* strains compared with only 1.1% of the >300,000 purely organic molecules tested through CO-ADD. We identified 90 metal compounds (8.7%) that show antifungal activity while not displaying any cytotoxicity against mammalian cell lines or hemolytic properties at similar concentrations. The structures of 21 metal complexes that display high antifungal activity (MIC ≤1.25 μM) are discussed and evaluated further against a broad panel of yeasts. Most of these have not been previously tested for antifungal activity. Eleven of these metal complexes were tested for toxicity in the *Galleria mellonella* moth larva model, revealing that only one compound showed signs of toxicity at the highest injected concentration. Lastly, we demonstrated that the organo-Pt(II) cyclooctadiene complex **Pt1** significantly reduces fungal load in an *in vivo G. mellonella* infection model. These findings showcase that the structural and chemical diversity of metal-based compounds can be an invaluable tool in the development of new drugs against infectious diseases.

KEYWORDS: *metal complexes, antifungal, antimicrobial resistance, inorganic, organometallic, antimycotic*

Crowdsourced Metal-based Antifungals
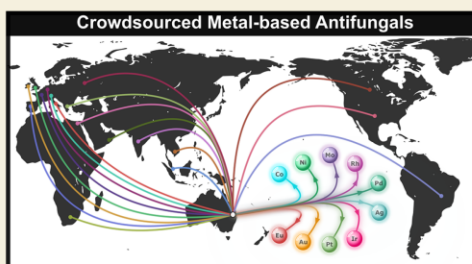
■ INTRODUCTION

Fungal infections are currently widely overlooked, failing to attract attention despite a recent focus on the antibacterial drug crisis. However, it is well-documented that fungal infections are proliferating around the world with an estimated 1.5 million deaths per year.[1−3] While healthy humans are generally not affected by fungal infections, they are a major concern to immunocompromised individuals.[4] Modern medical treatments such as chemotherapy, transplantations, and broad-spectrum antibiotic courses lead to an increased population of people susceptible to fungal infections.[5] Of particular concern are *Candida, Aspergillus*, and *Cryptococcus* species, which are responsible for >90% of fungal infection deaths. *Candida* species, and *Candida albicans* in particular, are the most prevalent cause of healthcare-associated bloodstream infections in the US. Despite the availability of antifungal

drugs, these infections have a mortality rate of around 40%.[3] Over the last few years, *Candida glabrata* has caused a continuously increasing number of identified cases,[6] while *Candida auris*, first reported in 2009, has already been identified in over 30 countries across 6 continents. *C. auris* generally displays resistance against at least one class of antifungal drugs and, in some cases, resistance against all three major antifungal drug classes (polyenes, azoles, and echinocandins),[7] leading to the 2019 Centers for Disease Control and

A
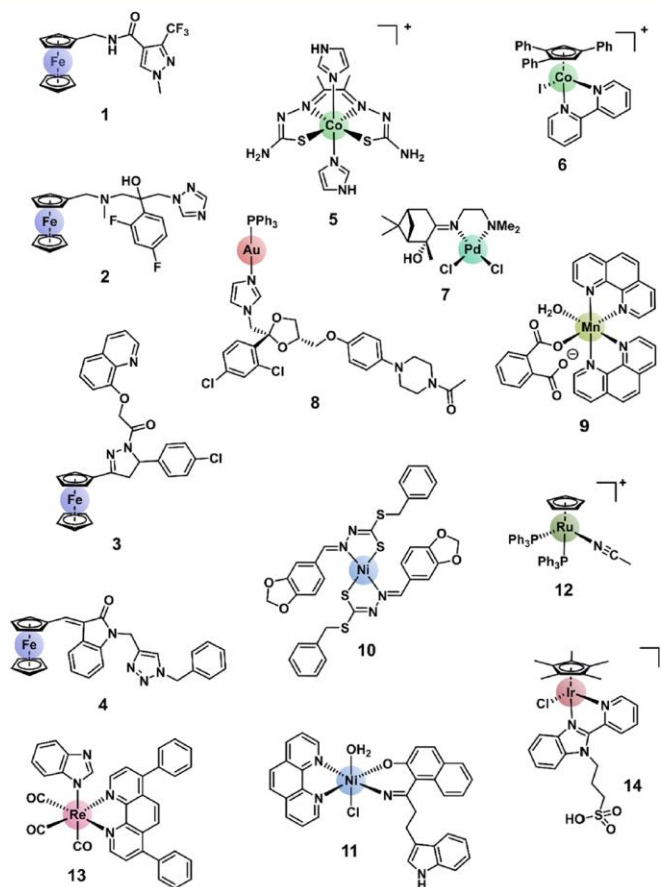
Figure 1. Selected structures of metal complexes with reported antifungal activity containing iron (1,[34,35]2,[35]3,[36]4[37]), cobalt (5,[28]6[38]), palladium (7[39]), gold (8[40]), manganese (9[41]), nickel (10,[42]11[43]), ruthenium (12[44]), rhenium (13[30]), and iridium (14[45]).

Prevention (CDC) report on "Antibiotic Resistance Threats in the United States" listing *C. auris* as an "Urgent Threat". Reported cases increased 318% in 2018 when compared to the average number of cases reported in 2015 to 2017.[8]

Despite the growing threat of fungal infections to global health, the current development pipeline for antifungal agents is even sparser than the already meager antibacterial drug landscape, with fewer than 10 drugs in various phases of clinical development.[5,9] Promisingly, some of these compounds represent new classes with novel modes of action. However, with the high attrition rates of compounds during clinical trials, few can be expected to be approved for clinical use in the coming years. To prevent drug resistance from overwhelming the capabilities of the global healthcare system, a richer and more diverse antifungal drug pipeline is urgently needed.

While all current antifungal drugs and antifungal drug candidates are exclusively organic molecules, metal-containing compounds have been a cornerstone of medicine since the beginning of the 20th century. Today, metal complexes are present mainly in the field of anticancer therapies where

platinum-based drugs (e.g., cisplatin) are still the most frequently used chemotherapeutics despite having been introduced over 40 years ago.[10] Since then, metal compounds that contain titanium, iron, copper, gallium, molybdenum, ruthenium, palladium, silver, gold, and bismuth have entered clinical trials.[11] Indeed, in 2020, 12 metal complexes were in clinical trials for anticancer indications alone.[12] In the field of infectious diseases, the iron-based antimalaria drug-candidate ferroquine advanced to phase II clinical trials, though it was not successful.[13] Recently, a spin-off company was established to advance a series of dinuclear ruthenium complexes with promising antimicrobial properties.[14−18]

While metal-based drugs are still a niche field, interest in their clinical use is increasing. Metal complexes offer two potentially advantageous properties that set them apart from their purely organic counterparts. First, the various oxidation states and multivalency of transition metals allow them to combine with a myriad of different organic and inorganic ligands, with coordination numbers from 2 to as high as 15,[19] forming highly diverse three-dimensional structures. This opens an entire realm of chemical space that is not accessible

B
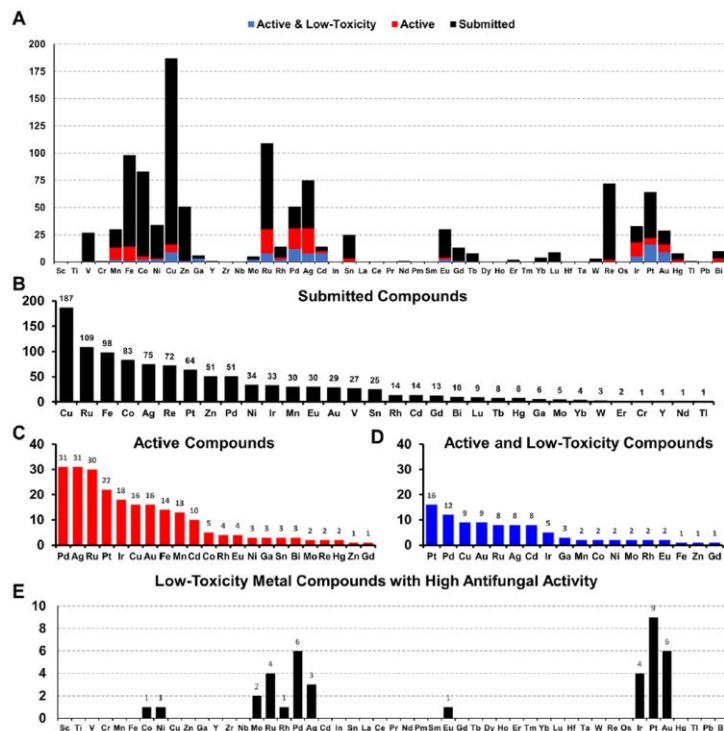
Figure 2. (A) Elemental distribution for all 1039 metal-containing compounds submitted to CO-ADD (black); 218/1039 submitted metal-containing compounds with at least one MIC lower or equal to 16 μg mL^{-1} or 10 μM (red) against the tested fungal organisms; 90/218 metal-containing compounds with antifungal activity and no cytotoxicity or hemolytic activity at the highest concentration tested (blue). (B) Metal frequency among the 1039 metal-containing compounds submitted to CO-ADD. (C) Metal frequency among the 218 metal complexes that possess some activity against the tested fungal organisms. (D) Metal frequency among the 90 compounds that are active against fungi as well as "low-toxicity" (see text for definition). (E) Elemental distribution of the 36 metal compounds (including two di-nuclear compounds) with high activity against the tested fungal strains, i.e., at least one MIC lower or equal to 2 μg mL^{-1} or 1.25 μM.

to carbon-based scaffolds and provides the "escape from flatland" advocated by some medicinal chemists: a higher three-dimensional character correlates with higher clinical success rates.[20,21] The superior geometrical diversity of metal complexes was recently demonstrated with a small library of 71 metallofragments (metal complexes with fragment-like ligands) that were shown to cover more three-dimensional chemical space than a representative organic fragment-library containing 18,000 molecules.[22]

The second unique characteristic of metal complexes is their ability to access multiple different and unique modes of actions. These range from redox reactions, generation of reactive oxygen species or catalytic generation of other active species, ligand exchange, or triggered ligand release. Different metals, and different types of metal complexes, are likely to act via widely varying, and potentially multiple, mechanisms. Overall, there are many ways for metal-based drugs to make a significant difference in the field of medicine and complement the organic drug arsenal currently available to us.[23]

While some metals, such as silver, have long been known to possess antimicrobial properties, there have been few systematic studies of anti-infective metal complexes until recently.[24−27] In the last few years, several reports have described

promising antibacterial properties of metal complexes,[28−31] including our systematic study on the antimicrobial properties of ~1000 metal-containing compounds contained within a screening collection of >300,000 molecules.[32] These data were collected *via* the crowd-sourced Community for Open Antimicrobial Drug Discovery initiative (CO-ADD, co-add.org) funded by The Wellcome Trust and the University of Queensland. CO-ADD provides free antimicrobial screening to chemists around the world.[33] Our analysis found that metal-containing complexes displayed significantly superior hit rates (9.9%) compared to purely organic molecules (0.87%), with cytotoxicity and hemolysis counter-screening assays showing similar toxicity rates for both classes, undermining the commonly held belief that metal-containing compounds are inherently (more) toxic.[32]

The antifungal activity of metal compounds has been investigated even less than their antibacterial properties.[28,30,34−51] Figure 1 presents an overview of selected metal compounds with measured antifungal activity. Gasser and coworkers recently published an expansive review of the metal-based antifungals research field.[52] One issue that the authors noted, in addition to the small number of systematic studies into antifungal metal complexes, is the lack of mode of action

C

studies and the often less than ideal antifungal data collection and reporting with regard to methodology and controls. Furthermore, there are only a few studies reporting *in vivo* evaluation of antifungal metal-based compounds.[28,30,35,51,53,54] A series of phenanthroline complexes containing copper, manganese, or silver showed no toxicity in a *G. mellonella* (moth larvae) *in vivo* model at 10 μg/larva, and most complexes reduced the fungal burden of larvae infected with *Candida haemulonii*.[41,53] Silver complexes of 1,10-phenanthroline-5,6-dione protected *G. mellonella* larvae from infection with *Phialophora verrucose*.[51] A series of cobalt complexes (e.g., **5**, Figure 1) showed excellent *in vitro* activity against several fungal strains and displayed no toxicity in a *G. mellonella in vivo* model at doses up to 266 mg/kg.[28] In 2021, a ferrocene-bearing fluconazole derivative with excellent *in vitro* antifungal activity (**2**, Figure 1) was evaluated in an *in vivo* mouse *Candida* infection model, where it both reduced the fungal burden and improved the inflammatory pathology of the mouse's kidney and colon.[35] The same year, rhenium complexes active against Gram-positive bacteria and fungi were tested for toxicity *via* a series of *in vitro* and *in vivo* assays, with the most promising complexes (e.g., **13**, Figure 1) showing no signs of cardio-, hepato-, or hematotoxicity or teratogenicity and inhibiting fungal filamentation in a *C. albicans* infection study in zebrafish.[30]

While these reports are encouraging, more systematic studies into metal-based antifungals are needed. The CO-ADD screening panel, while focused on five bacteria, also includes the pathogenic yeasts *Candida albicans* and *Cryptococcus neoformans*. Hence, we have access to an unprecedented array of systematically collected data on the antifungal properties of >300,000 compounds, including >1000 metal compounds. We now report on a large number of active and low-toxicity metal complexes identified during the screening of our library, with the most active ones subsequently tested against an extended panel of relevant fungal strains. A selection of compounds with the best activity profile was then evaluated for toxicity in the *in vivo* insect model *G. mellonella*, with most compounds exhibiting no toxicity at the tested concentrations. Finally, two nontoxic antifungal metal compounds were assessed in an *in vivo G. mellonella* efficacy (infection model) assay.

■ RESULTS AND DISCUSSION

As in our previous work, our use of the term "metal complex" refers to compounds containing d-block elements and lanthanides, as well as the post-transition metals gallium, indium, tin, thallium, lead, and bismuth. Actinides, the d-elements beyond atomic number 100, and the radioactive elements technetium and promethium are excluded. As of June 2020, a total of 1039 metal-containing compounds had been received and tested by CO-ADD. These compounds were submitted by 50 different research groups from 17 countries (and cover 32 of the 49 possible metal elements). The overall elemental distribution of the compounds has not changed significantly since our 2020 report. The most represented element is copper, with 187 compounds submitted to date.

Compounds were submitted to CO-ADD as dry powders, confirmed to be at >95% purity by the collaborators, and then tested as received. Characterization of the complexes were carried out by the submitting research group. No quality control check of purity was performed by CO-ADD due to the volume of compounds received. False positives are therefore

possible, and promising compounds should be checked thoroughly before further development. The procedure reported in our previous study for antimicrobial testing by CO-ADD has been followed.[32]

Of the 1039 tested metal compounds (Figure 2A,B), 320 (30.8%) showed activity against a bacterial and/or fungal strain (MIC $\leq$32 μg/mL). Two hundred eighteen (21.0%, Figure 2C) compounds had at least one MIC value that was less than or equal to 16 μg/mL or 10 μM against a fungal strain. Of these 218 antifungal metal compounds, 90 (10.4%, Figure 2D) complexes showed no cytotoxicity against HEK293 (human embryonic kidney) mammalian cells or hemolysis against human red blood cells up to 32 μg/mL or 20 μM. "Low-toxicity" compounds were defined as compounds with HEK293 CC_{50} >32 μg/mL or >20 μM and hemolytic HC_{10} >32 μg/mL or >20 μM (HC_{10} is the concentration causing 10% hemolysis).

The number of metal complexes with antifungal activity and low toxicity was further reduced by including only compounds with "high" antifungal activity, which was defined as having at least one MIC lower or equal to 2 μg/mL or 1.25 μM. This reduced the data set to 36 metal complexes (Figure 2E). It is worth noting that obtaining 36/1039 (3.5%) compounds with high antifungal activity and low toxicity from a crowd-sourced screen is a remarkable outcome. For comparison purposes, of the 287,534 small organic molecules for which an MIC was determined through CO-ADD against at least one fungal strain, only 3076 (1.1%) were found to be active. About half of these were further classified as toxic, leaving 1586 (0.6%) small organic molecules with activity against fungi and no toxicity at the measured concentrations. Applying the same "high-activity" filter to these compounds leaves 409 highly active "low-toxicity" organic molecules or 0.14% of all compounds tested, a 25-fold lower "hit rate".

Two observations stand out when comparing the data for organic molecules with those for metal complexes. First, the overall antifungal hit rate for metal complexes is 23 times higher than that for small organic molecules, reconfirming our previous finding that metal compounds have superior hit rates against microbial organisms (Figure 3). The caveat is that the (metal) compounds tested by CO-ADD are not randomly selected. While some collaborators may have submitted compounds that are expected to have biological activities (e.g., against cancer), many compounds submitted to CO-
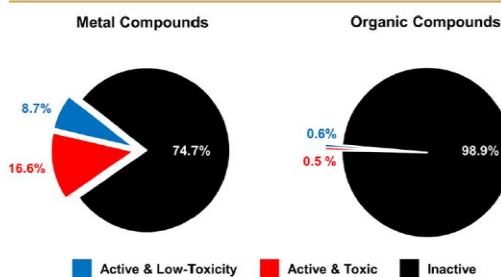
Figure 3. Percentage of submitted metal-containing compounds with antifungal activity with or without associated cytotoxicity and/or hemolysis compared to the overall hit rate for organic small molecules within the CO-ADD collection.

D

Table 1. Initial CO-ADD Dose−Response Screening Data for 21 Metal Complexes with Potent Antifungal Activity and No Cell Toxicity up to 32 μg/mL or 20 μM, for which Fresh Stocks Could be Obtained (Values Given in μg/mL or μM Depending on How Compounds Were Originally Submitted to CO-ADD)[a]

ID	Ab	Ec	Kp	Pa	MRSA	Ca	Cn	HEK CC50	RBC HC10	Unit
Co1	>32	>32	32	>32	>32	0.5	0.5	>32	>32	μg/mL
Ni1	>32	>32	>32	>32	≤0.25	32	≤0.25	>32	>32	μg/mL
Rh1	>32	>32	>32	>32	>32	4	2	>32	>32	μg/mL
Pd1	>20	>20	>20	>20	>20	1.25	0.63	>20	>20	μM
Pd2	>20	>20	>20	>20	>20	1.25	0.31	>20	>20	μM
Pd3	>32	>32	>32	>32	>32	0.5	1	>32	>32	μg/mL
Ag1	>32	>32	>32	>32	>32	≤0.25	≤0.25	>32	>32	μg/mL
Ag2	>32	>32	>32	>32	>32	≤0.25	≤0.25	>32	>32	μg/mL
Eu1	>20	>20	>20	>20	>20	≤0.16	≤0.16	>20	>20	μM
Ir1	>32	>32	>32	>32	1	2	2	>32	>32	μg/mL
Ir2	>32	>32	>32	>32	1	2	2	>32	>32	μg/mL
Ir3	>32	>32	>32	>32	0.5	2	1	>32	>32	μg/mL
Pt1	>20	>20	>20	>20	1.25	10	2.5	>20	>20	μM
Pt2	>20	>20	>20	>20	0.625	10	1.25	>20	>20	μM
Pt3	>20	>20	>20	>20	>20	>20	1.25	>20	>20	μM
Pt4	>20	>20	>20	>20	>20	10	1.25	>20	>20	μM
Pt5	>32	>32	>32	>32	>32	1	2	>32	>32	μg/mL
Au1	n.d.	n.d.	n.d.	>32	≤0.25	≤0.25	≤0.25	>32	n.d.	μg/mL
Au2	>32	>32	>32	>32	≤0.25	≤0.25	≤0.25	>32	>32	μg/mL
Au3	>32	>32	>32	>32	≤0.25	>32	≤0.25	>32	>32	μg/mL
Au4*	32	32	32	>32	0.5	2	≤0.25	>32	>32	μg/mL

[a]Ab, *Acinetobacter baumannii* ATCC 19606 type strain; Ec, *Escherichia coli* ATCC 25922 FDA control strain; Kp, *Klebsiella pneumoniae* ATCC 700603 ESBL; Pa, *Pseudomonas aeruginosa* ATCC 27853 QC control strain; MRSA, methicillin-resistant *Staphylococcus aureus* ATCC 43300; Ca, *Candida albicans* ATCC 90028 NCCLS11; Cn, *Cryptococcus neoformans* H99 ATCC 208821 type strain; HEK, HEK-293 human embryonic kidney cells ATCC CRL-1573; RBC, human red blood cells. N.d., not determined. Reference antifungal and antibiotics data provided in the Supporting Information. [b]**Au4** was originally submitted to CO-ADD as a 1:2 mixture of **Au4a** and **Au4b**.

ADD were originally made with very different applications in mind (*vide infra*).

When all the compounds displaying cytotoxicity are removed, the metal complexes still show a vastly superior rate of active and low-toxicity compounds (8.7 vs 0.6%, Figure 3). It is notable that the toxicity rate in the class of metal compounds was somewhat higher than that within the organic molecule group; *i.e.*, 66% of active metal complexes also showed toxicity against mammalian cell lines and/or hemolysis, whereas this was the case for only 48% of organic molecules. This contrasts our analysis focused on antibacterial activity where both organic and metal compounds had similar toxicity rates.[32]

Comparison of the distribution of all submitted compounds (Figure 2A,B) with the distribution of the active and low-toxicity compounds (Figure 2C,D) reinforces a trend that was observed previously, namely, that the first-row transition metals seem to be vastly under-represented in the active and low-toxicity group. Indeed, first-row transition metals make up 47% of submitted compounds but only 21% of all active and low-toxicity ones. With the still limited number of complexes, it is too early to dismiss these metals for antifungal applications altogether, but the current trends certainly seem to favor second- and third-row d-elements.

There may be good chemical reasons for this. Complexes of first-row transition metals tend to be less kinetically stable than those of the second row and especially the third row of transition metals. Also, essential transition (d-block) metals (Mn, Fe, Co, Cu, Zn, and Mo) have metabolic pathways specifically designed to control their homeostasis (uptake,

transport, storage, and usage), so they may become diverted into targets other than the desired ones in the infective organisms.

To further explore the properties of these compounds, we reached out to the contributors of the 36 high-activity hit compounds to obtain fresh samples for further testing. Through this effort, we were able to obtain new stocks for 21/36 (58%) of the compounds shipped to our laboratories (Table 1). This number is impressive since these compounds were originally submitted for testing over a range of 5 years and the requests for more samples were sent out at the height of the COVID-19 pandemic when many laboratories were shut down for extended amounts of time.

The structures of the 21 obtained highly active metal complexes are shown in Figure 4. They comprise the nine elements cobalt(III), nickel(II), rhodium(III), palladium(II), silver(I), europium(III), iridium(III), platinum(II), molybdenum(VI), gold(I), and gold(III), with ruthenium the only element for which we were not able to obtain a second sample. The majority of these compounds (15/21) have not previously been studied for their antifungal activity. Synthesis protocols and characterization data have been reported elsewhere or are provided in the Supporting Information (Table S13). Notably, only five of these compounds are present in both this analysis and contained within the 30 metal complexes highlighted for their antibacterial activity in our earlier work.[32] This indicates that somewhat different features are required to obtain activity against bacteria vs fungi. At the same time, the elements cobalt, ruthenium, silver, europium, iridium, and platinum are well represented in both data sets.
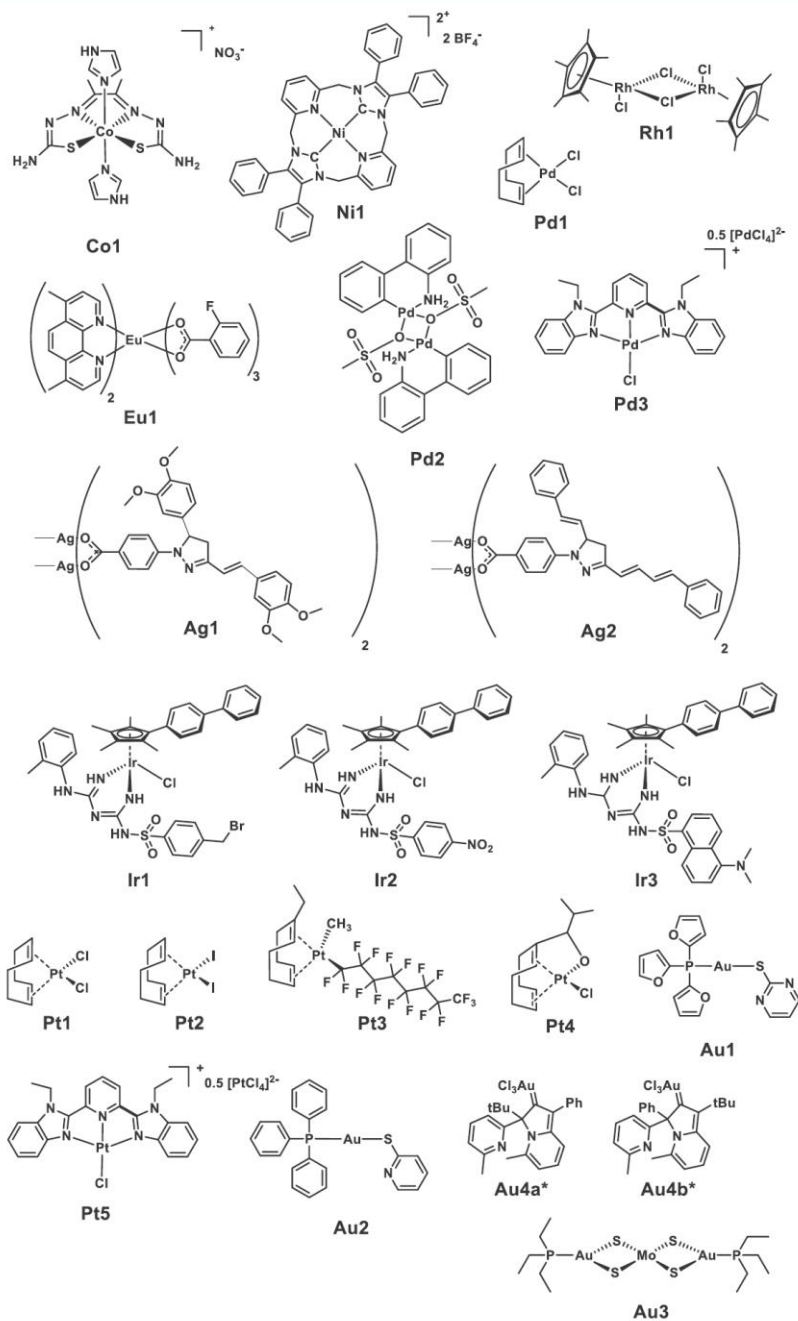
Figure 4. Chemical structures of the 21 metal complexes in the CO-ADD screening with high antifungal activity and no associated cytotoxicity and hemolysis. *Au4 is a mixture of two isomers (**Au4a** and **Au4b**); several samples were submitted with differing ratios.

While this can partly be explained by the high submission rates for compounds containing some of these elements, it perhaps suggests a trend in the activity patterns of metal-containing compounds. Increasing the number and diversity of tested

F

203

Table 2. Extended MIC Testing against a Panel of Fungal Strains with Compounds for Which a Second Batch Could Be Obtained (MIC Is Displayed as ≥80 or ≥50% Inhibition in μM)[a]

ID	Candida albicans ATCC 90028 NCCLS 11	Candida auris CBS10913 JCM 15448	Candida auris CBS12373 KCTC 17810	Candida glabrata ATCC 90030 NCCLS 84	Candida tropicalis ATCC 750 QC strain for susceptibility testing	Cryptococcus deuterogattii CBS7750 VGII; Serotype B	Cryptococcus deuterogattii ATCC 32609 VGII	Cryptococcus neoformans ATCC 208821 H99; VN1
				MIC [μM]				
Co1	0.78 - 1.56	0.39 - 0.78	0.39 - 0.78	100	0.39	1.56	0.78 - 1.56	0.39 - 0.78
Ni1	>160	>160	2.5 - 20	>160	160	5 - 10	5 - 10	2.5 - 5
Rh1	0.39 - 1.56	0.781-1.56	0.78	6.25	0.391 - 0.781	0.391	0.781 - 1.56	0.195 - 0.391
Pd1	3.12	≤0.78	≤0.78	3.12	6.25	≤0.78	1.56 - 3.12	≤0.78
Pd2	0.05 - 0.2	0.024-0.098	0.024 - 0.049	0.049 - 0.195	0.195 - 0.391	0.098	0.024 - 0.049	0.024
Pd3	0.012 - 0.024	0.098 - 0.2	0.098 - 0.2	0.012 - 0.024	0.006 - 0.024	0.2 - 0.78	0.2	0.012 - 0.024
Ag1	≤0.006	0.006	≤0.006	≤0.006	≤0.006 - 0.012	0.006	0.006 - 0.024	≤0.006
Ag2	≤0.006 - 0.098	0.006 - 0.098	0.006 - 0.098	0.006 - 0.195	≤0.006 - 0.049	0.006 - 0.098	0.006 - 0.098	≤0.006 - 0.098
Eu1	≤0.006 - 0.012	0.006	0.006	0.024 - 0.098	≤0.006 - 0.049	0.024 - 0.098	0.024	≤0.006
Ir1	0.098	0.098	0.049	0.195	0.098 - 0.195	0.024	0.098 - 0.195	0.024 - 0.049
Ir2	0.049 - 0.098	0.049 - 0.098	0.024	0.098	0.098 - 0.195	0.024	0.098 - 0.195	0.024 - 0.049
Ir3	0.024 - 0.098	0.024 - 0.098	0.012 - 0.49	0.098	0.098	0.024 - 0.049	0.049 - 0.2	0.024
Pt1	12.5 - 25	6.25 - 12.5	3.13	25	25	1.56 - 3.13	3.125 - 6.25	1.56 - 3.13
Pt2	12.5 - 25	12.5	3.13 - 6.25	50	50	≤0.78 - 3.13	6.25 - 12.5	1.56 - 3.13
Pt3	25	25	12.5 - 25	50	100	12.5-25	12.5	12.5 - 25
Pt4	6.25 - 12.5	6.25 - 12.5	1.56 - 3.12	12.5 - 25	12.5 - 25	≤0.78 - 1.56	3.12 - 6.25	≤0.78 - 1.56
Pt5	0.006 - 0.2	0.024 - 0.098	0.024 - 0.098	0.006 - 0.098	0.006 - 0.098	0.006 - 0.098	0.006 - 0.049	0.006 - 0.098
Au1	0.049 - 0.391	0.098	0.098 - 0.391	0.098 - 0.781	0.049 - 0.391	0.024 - 0.391	0.098 - 0.391	0.098 - 0.195
Au2	NA	0.195	0.195	>200	>200	0.098	0.049 - 0.391	0.024 - 0.195
Au3	50 - 200	3.13 - 6.25	NA	100 - 200	NA	NA	3.125 - 6.25	3.12 - 6.25
Au4*	0.391	0.195 - 0.391	≤0.006 - 0.049	0.781 - 6.25	1.56 - 6.25	0.098 - 0.195	0.024 - 0.049	0.098 - 0.195

[a]Underscored = MIC values that were inactive or gave a wide replicate variation when analyzed for ≥80% inhibition (optically clear to slightly hazy). These were re-analyzed at 50% inhibition (e.g., an MIC score of 2 = prominent decrease in visible growth as per CLSI M27 guidelines for evaluating MICs of yeasts) which gave more consistent and active values; see Table S9. NA: MIC value not available due to wide replicate variation. [b]Two new samples of **Au4** (1:2 and 1:0.7, **Au4a/Au4b**) were received for further testing. Both mixtures gave the same MIC values across all assays.

metal complexes will be the only way to further support or contradict this finding.

These 21 complexes were tested against an extended panel of eight *Candida* and *Cryptococcus* strains. We used the same panel for the extended testing of a series of cobalt complexes (including **Co1**) in an earlier study.[28] The panel comprises strains with different resistance profiles, including clinical isolates that are resistant to multiple classes of antifungal drugs. We also repeated the cytotoxicity and hemolysis assays with the new batch of compounds to verify earlier results and measure any possible adverse effects at higher concentrations (up to at least 100 μM).

From the initial set of antimicrobial testing and filtering for good activity, we expected a high degree of activity from the obtained 21 metal compounds. Indeed, we were pleased to find that most of the complexes showed good to excellent activity against most of the tested strains in the extended panel (Table 2).

As mentioned above, **Co1** is part of a series of Schiff-base complexes that were previously explored for both their anticancer[55,56] and antifungal[28] properties. The compound showed high levels of antifungal activity across the range of strains, with the notable exception of *Candida glabrata*. Importantly, we found no cytotoxicity or hemolysis up to the highest measured concentrations.

The nickel carbene complex **Ni1** was originally prepared to investigate the effect of structural changes upon the properties of N-heterocyclic carbene (NHC) complexes as catalysts for the electrochemical reduction of carbon dioxide, illustrating how compounds submitted were originally synthesized for a range of reasons. The first compound of this class was reported in 2004,[57] with some more described in the recent work by Su et al.[58] In the initial CO-ADD screening, this complex showed high activity against *Cryptococcus* spp. and the Gram-positive bacteria methicillin-resistant *Staphylococcus aureus* (MRSA) but none against the *Candida* spp. or any of the Gram-negative strains tested (Table 1). In the extended fungal panel, **Ni1**

G

showed good activity against all the *Cryptococcus* spp. but no measurable effect against the *Candida* strains except *C. auris*. The complex also showed no toxicity or hemolysis up to the highest concentration measured, 160 μM. This heterogeneity in the fungal activity profile of this compound is notable as it is the only complex in this data set that shows this behavior. Culture media contributions can be ruled out as a factor as all tested yeasts were grown under the same conditions. Further studies on analogues of **Ni1** to investigate the origin of this *Cryptococcus* selectivity could lead to interesting, targeted antifungal candidates.

Rhodium complex **Rh1** is a useful synthon for the synthesis of rhodium piano-stool complexes.[59] This compound showed high levels of activity against the entire panel of fungi, with MIC values in the nanomolar range and no cytotoxicity up to 200 μM. However, we found significant hemolysis in our second round of assays (Table S7 in SI), which was not observed in the initial CO-ADD screening. Previous studies of **Rh1** showed cytotoxicity against the human ovarian carcinoma cell line A2780 after prolonged (96 h) exposure (IC_{50} = 7.3 ± 1.5 μM).[60] The strong hemolytic effect of **Rh1** precludes it from further testing.

Compounds **Pd1**, **Pd2**, and **Pd3** provide examples of the different structures that can be obtained within the chemical space of the same metal, oxidation state, and coordination geometry. All three square-planar palladium(II) complexes showed exclusively antifungal activity in the initial CO-ADD screening. The cyclooctadiene compound **Pd1** was part of a series of similar platinum complexes that we studied for their antibacterial potency, with some also showing antifungal activity (*vide infra*).[61] Although **Pd1** showed good antifungal activity across all tested strains and no cytotoxicity up to 100 μM, it caused hemolysis at low concentrations, with a therapeutic index of 13. **Pd2** is a synthon for palladium catalysts.[62] High levels of activity across the fungal panel were observed, with MIC values in the low nanomolar range, but were accompanied by some cytotoxicity and significant hemolysis (Table S7 in SI). Palladium complexes with ligands similar to **Pd3** have found some applications as catalysts for Suzuki-type reactions,[63] while the ligand has been explored in other coordination complexes formed with lanthanides,[64–66] cobalt,[67] ruthenium,[68,69] platinum,[70] and chromium.[71]

Of note, compound **Pt5** is identical to **Pd3** in all aspects except the platinum metal center. Indeed, there are a total of nine complexes in the CO-ADD database with very similar structures, as well as the free ligand. The latter showed no activity at all in the CO-ADD primary screening and was not evaluated further. The biological evaluation of these analogue compounds has been reported separately.[72,73] The fact that both **Pd3** and **Pt5** have similar activity profiles against the fungal panel but the free ligand alone shows no activity suggests that a metal is essential to obtain the observed antifungal activity. The cytotoxic and hemolytic properties of the two compounds are slightly different, with **Pd3** displaying low cytotoxicity and significant hemolysis. On the other hand, no hemolysis up to 200 μM could be detected for **Pt5**, and the cytotoxicity was similar to **Pd3**, resulting in a promising therapeutic index of >2500 (Table S7 in SI).

Silver compounds, silver ions, and silver nanoparticles have all been shown to be good antibacterial agents,[74–78] but there have been comparatively very few studies into their antifungal properties,[79–81] mostly focusing on silver nanoparticles.[82,83] Compounds **Ag1** and **Ag2** are interesting as they show

exclusive antifungal activity, with no inhibition of bacterial growth, suggesting that the activity is not due to free (weakly bound) silver ions; e.g., $AgNO_3$ effectively inhibits both bacteria and fungi but also causes some degree of hemolysis in our assays (Table S2 in SI). The ligands for these complexes (**Ligand-Ag1** and **Ligand-Ag2** in the SI) were originally studied for their solvatochromism and were later coordinated with silver to investigate their potential antimicrobial activity.[84] The carboxylate ion is able to coordinate to silver with monodentate, chelating, and/or bridging modes. Since the difference in frequencies ($\Delta \nu$) between symmetric and asymmetric vibrations of the −COO group in FT-IR peaks is well under 200 cm^{-1}, the bridging mode is suggested.[85,86] The stability of complexes **Ag1** and **Ag2** was assessed. Solid samples kept at room temperature and protected from light exhibited identical NMR spectra over a period of 2 years. Complexes in DMSO solution also showed no changes in NMR (Figures S3 and S4 in SI) or UV−vis (Figure S5 in SI) spectra after 24 h.

Both silver compounds showed good antifungal activity with MICs ranging from 6 to 98 nM, but cytotoxicity CC_{50} values were in the low micromolar range (Table S7 in SI), though this still resulted in a good therapeutic index of 33,333 for **Ag2**. The free ligands of **Ag1** and **Ag2** were inactive (Table S2 in SI). **Ag1** and **Ag2** showed similar biological properties despite differing ligands, but a third silver complex with a very similar ligand showed significantly lower antifungal activity (**Ag-S4** in the SI). The antibacterial mode of action of silver ions has been studied in detail by the group of Sun *et al.*,[87,88] but the antifungal mode of action remains unknown. Some reports have indicated that silver nanoparticles exert their antifungal activity through disruption of the cellular envelope, causing plasma membrane damage with subsequent cell leakage.[83,89] It is noteworthy that *C. albicans*, but not *C. parapsilosis*, *C. tropicalis*, or *C. glabrata*, was shown to be able to convert Ag(I) ions into less toxic silver nanoparticles, thereby evading the antifungal effect of silver.[79]

Europium complexes have been studied for their versatile photophysical properties.[90−93] There have been a few sparse reports on the potential antimicrobial properties of lanthanide complexes, including europium,[94] and one europium complex with antibacterial activity was found in our previous analysis of CO-ADD data. A series of similar europium complexes (**Eu-S1-S8**, Figure S7 in the SI) are also in the CO-ADD collection. Several of these complexes show mild activity against Gram-positive MRSA and against the two tested fungal strains (Table S3 in SI). However, all but two complexes (**Eu-S1** and **Eu1**) also displayed cytotoxicity and/or hemolytic properties as well. The varied activity profile indicates a direct relationship between their structure and antimicrobial activity, toxicity, and hemolysis, suggesting that further optimization could lead to better compounds. In the extended panel, **Eu1** showed very high levels of activity against all the tested fungal strains (MIC values between 6 and 98 nM) and no cytotoxicity or hemolysis up to 200 μM, resulting in a therapeutic index of 33,333 (Table S7 in SI). Future studies could leverage the strong luminescence of this compound class for mode of action investigations.

The iridium complexes **Ir1−3**, with *N*,*N*-chelated ligands from the metformin (a biguanide anti-diabetic drug) family, were already highlighted in our previous antibacterial analysis for their ability to inhibit MRSA at low concentrations. Indeed, these complexes were already reported by the group of Sadler in an in-depth study on their antimicrobial properties.[95] These

H

three complexes maintained similar high levels of activity across the extended screening panel and exhibited moderate levels of cytotoxicity (CC_{50} values in the 50−100 μM range) with significant hemolysis (Table S7 in SI). Overall, the favorable therapeutic indices of 2600−3383 for **Ir1−3** are promising.

Compounds **Pt1−Pt4** are part of a series of cyclooctadiene compounds that were discovered through CO-ADD to have quite potent antibacterial activity,[61] with some modest antifungal activity now reported. Compounds **Pt1**, **Pt2**, and **Pt4** were more active against the three *Cryptococcus* strains compared to the *Candida* strains. Promisingly, none of the four compounds showed any cytotoxicity or hemolysis up to 100 μM.

The antimicrobial properties of gold were first described by Robert Koch back in 1890, when he reported on the activity of potassium dicyanidoaurate(I) against *Mycobacterium tuberculosis*.[96] More recent reports on the antimicrobial properties of gold complexes have been summarized in several review articles.[97−99] The FDA-approved oral antirheumatic gold(I) drug auranofin exhibits excellent antibacterial properties *in vitro* and *in vivo*.[100,101] Compounds **Au1** and **Au2** were originally part of a series of gold(I) phosphine thiolate complexes synthesized to investigate their biological properties.[102] In the initial CO-ADD screening, where six other analogues were also tested (**Au-S1-S6**, Figure S8 in the SI), the two compounds stand out for their high activity against the two fungal strains as well as MRSA. The drastic change in activity profile with only a few atoms of difference between the compounds (Table S4 in SI) implies that both metal and ligands are responsible for the observed activity. For example, combining 2-sulfanylpyrimidine with a trifuran-2-yl-phosphane ligand gave complex **Au1** that had high activity against both MRSA and the fungal strains. In contrast, the gold complex with the same 2-sulfanylpyrimidine ligand but with triphenylphosphine (**Au-S4**, Figure S8 in SI) showed no activity against any of the tested strains. Conversely, the triphenylphosphine gold complex with a 2-sulfanylpyridine ligand (**Au2**) had high activity against MRSA and the fungal strains, but the same thiolate ligand with the trifuran-2-yl-phosphane gold complex (**Au-S1**) possessed only moderate activity. Interestingly, the introduction of a trifluoromethyl group on the thiolate ligand seemed to increase specificity toward bacteria, as no antifungal activity was observed for these compounds (**Au-S3** and **Au-S6**). In the extended panel, some slight differences in the activity patterns of **Au1** and **Au2** appeared. While **Au1** showed high antifungal activity against all fungal strains, **Au2** was not active against the *C. glabrata* and *C. tropicalis* strains. While the compounds showed only low to no hemolysis, they both displayed significant cytotoxicity in the repeated assays.

Complex **Au3** is perhaps the structurally most intriguing compound that we report in this study. Its synthesis was first described by Kinsch and Stephan in 1985,[103] and it is the only heteronuclear bimetallic compound in this set of highly antifungal metal complexes. It is also the only one of five CO-ADD compounds that contains the element molybdenum, as Mo(VI). Notably, the related compound tetrathiomolybdate is currently in phase III clinical trials as a decoppering agent.[104,105] All five molybdenum-containing compounds are of similar structures (**Au-S7-S10**, Figure S5 in SI), two containing phosphine ligands (**Au3** and **Au-S7**) and three with NHC ligands (**Au-S8-S10**). Again, we observed that depending on the exact structure of the compound, the observed

activity was markedly different. Switching from a triethylphosphine ligand to triphenylphosphine resulted in complete loss of activity. A similar effect was observed with the NHC ligand. Unfortunately, we were not able to obtain more of **Au-S10** for further studies at this stage. It is notable that **Au3** seemed to possess high activity against MRSA and the *C. neoformans* strain while being not very active against *C. albicans*. Conversely, **Au-S10** only showed activity against *C. albicans*. Unfortunately, with **Au3**, we obtained wide ranges of activity for several of the fungal strains. Consistently good activity was observed against *C. auris* as well as with two *Cryptococcus* strains. Promisingly, **Au3** showed no hemolysis up to 200 μM and CC_{50} values in the range of 139−170 μM (Table S7 in SI), resulting in a therapeutic index of 44. The low toxicity values combined with signs of structure-dictated activity profiles suggest that synthetic explorations could yield even better compounds of this class.

Lastly, **Au4** (Figure 4) was part of a series of complexes containing an intact bis(pyridyl)allene framework (formed with palladium(II), platinum(IV), and gold(III)), a vinyl-platinum(II) metallacycle, and a series of gold(I) and gold(III) carbenes formed by the nucleophilic attack of an allenic pyridine into the allene moiety (Figure S10 in SI). Allene-containing complexes have recently been reported as potential anticancer agents, among other activities.[106] The free ligands (**Au-Ligand1** and **Au-Ligand2**), as well as the corresponding platinum(IV) complexes, did not show any antimicrobial activity (Table S6 in SI). The palladium(II) analogues showed good activity against MRSA and the two yeasts tested but were cytotoxic. The two gold(III) analogues with allene ligands coordinated through the pyridyl nitrogens (**Au-S11** and **Au-S12**) showed moderate to good activity against the two fungal strains tested but varied dramatically in hemolytic activity despite only varying by a phenyl to a *tert*-butyl group on the ligand framework. The vinyl-Pt(II) metallacycle derivative showed good activity against MRSA and the two yeasts tested but also exhibited high levels of cytotoxicity. This platinum complex and the novel gold carbenes series were originally studied for their application as potential catalysts for the cyclization of 1,6-enynes, and no biological activity for them has been reported to date.[107]

From this series, only the gold(III) carbene **Au-S13** showed some moderate activity against any of the tested Gram-negative strains as well as high activity against MRSA and yeasts. However, both **Au-S13** and its gold(I) analogue (**Au-S14**) showed high toxicity levels, leaving only the gold(I) complex **Au-S15** as an active and low-toxicity candidate. Unfortunately, we were unable to obtain more of it for further testing. Gold(III) complex **Au4** showed good levels of activity across the antifungal panel and no cytotoxicity or hemolysis up to 200 μM, resulting in a therapeutic index of 33,333 (Table S7 in SI). The original sample of **Au4** submitted to CO-ADD was received as a 1:2 mixture of nonseparable but well-characterized isomers (**Au4a/Au4b**). For the expanded panel, two new samples were obtained with ratios of 1:2 and 1:0.7 (**Au4a/Au4b**), respectively. Both samples showed virtually identical MIC values, indicating that both isomers are responsible for the observed activity.

General Observations

Some overall observations can be made upon analysis of the results from the extended antifungal and toxicity assays. The level of activity for the most active compounds is comparable

206

to the activity of the control antifungal drugs against the respective pathogen (Tables S10 and S11 in SI). And, generally, good activity in the initial CO-ADD screening translates to good activity across the whole panel of *Candida* and *Cryptococcus* strains used in this work.

The same cannot be said for the cytotoxicity and hemolysis counter-screening data, with significant variations often seen between different assay runs. Part of this can be attributed to the fact that the highest concentration measured in the initial CO-ADD screening is 32 μg/mL (standard units for antimicrobial screening), which, depending on the molecular weight of the compound, can vary dramatically when translated to molar units. Because the molecular weight of metal complexes generally covers an expanded range compared to organic compounds, all subsequent assays were conducted with molar units to generate comparable data. In essence, this work highlights that the cytotoxicity of these compounds needs to be evaluated rigorously. It should be noted that the therapeutic indices for most (14/21) compounds tested in the extended panel were still over 50 and many (9/21) were >1000, indicating the significant potential for further development (Table S7 in SI). As can be seen in this study, conducting all assays in the same laboratory and under the same conditions can still produce variable results. This underscores the need to standardize the testing conditions for metal-based antimicrobials to obtain reliable data and advance the field.

Based on criteria of overall antifungal activity, cytotoxicity, and hemolysis as well as compound availability, we selected compounds **Co1**, **Ag2**, **Eu1**, **Ir1**, **Pt1**, **Pt2**, **Pt4**, **Pt5**, **Au1**, **Au2**, and **Au4** to conduct a preliminary *in vivo* toxicity assay. For these initial *in vivo* assessments, we used the greater wax moth *G. mellonella* instead of a rodent model,[28,61] as it is significantly less resource- and cost-intensive, allowing us to screen far more compounds than would otherwise be possible. Results obtained in *G. mellonella* have been shown to be robust, reproducible, and correlate well with toxicity study results obtained in rodent models.[108−110] The compounds were dissolved in DMSO and diluted to the highest possible final concentration (Table 3). Larvae were injected with 10 μL of the compound (at the maximum concentration indicated in Table 3) or DMSO control. The larvae were then monitored for 6 days for survival and health using the *G. mellonella* Health Index Scoring System.[111] Of the 11 tested compounds, only

Table 3. Results of the *In Vivo* Toxicity Assay in *G. mellonella* (10 μL of the Highest Concentration Was Injected into the Larvae)

compound	max conc.	max dose	toxicity
Co1	10 mM	244 mg/kg	nontoxic
Ag2	1 mM	53 mg/kg	nontoxic
Eu1	1 mM	49 mg/kg	nontoxic
Ir1	1 mM	47 mg/kg	nontoxic
Pt1	0.4 mM	7 mg/kg	nontoxic
Pt2	0.4 mM	11 mg/kg	nontoxic
Pt4	0.4 mM	8 mg/kg	nontoxic
Pt5	1 mM	38 mg/kg	nontoxic
Au1	1 mM	27 mg/kg	nontoxic
Au2	1 mM	28 mg/kg	toxic at 1 mM
Au4[a]	1 mM	33 mg/kg	nontoxic

[a]For the *in vivo* testing, the **Au4** sample with a ratio of 1:0.7 (**Au4a**/**Au4b**) was used.

Au2 showed signs of toxicity at the highest tested concentration (1 mM). For the other compounds, no detrimental effects could be observed in the larvae over the monitoring period. These data contribute to our understanding that metal complexes need not be considered as generally toxic. Nevertheless, factors such as the metabolism, excretion, and/or accumulation of the various metal complexes and their metabolites will still need to be studied more rigorously in rodent models if they are to be advanced into the preclinical pipeline. Of note, the maximum concentration reached in the larvae in these assays is anticipated to be significantly lower than the concentrations measured in the *in vitro* toxicity/hemolysis assays.

With these results in hand, we proceeded to conduct an exploratory *in vivo* efficacy study with compounds **Co1**, **Eu1**, **Ir1**, **Pt1**, **Pt2**, **Pt4**, **Au1**, and **Au4** (**Ag2** and **Pt5** had to be excluded due to solubility issues in these assays). In an initial survival assay, *G. mellonella* larvae were inoculated with *C. albicans* (ATCC 90028). The larvae were then injected with 10 μL of the compound solution, and their survival was monitored for the next 5 days. Fluconazole and 10% DMSO injections were used as controls. Compounds **Pt1** and **Pt2** and the fluconazole control resulted in significant larva survival (at least three larvae alive after 5 days at the tested concentrations) compared to the untreated control.

To quantify the possible protective effect of **Pt1** and **Pt2** in *G. mellonella* challenged with *C. albicans*, we conducted a CFU reduction assay with these compounds. Briefly, *G. mellonella* larvae were inoculated with *C. albicans* (ATCC 90028) and incubated for 2 h at 37 °C. The larvae were then injected with 10 μL of the corresponding compound solution (1 mM) or control (same concentration and injection volume) and incubated for 24 h at 37 °C. The larvae were then anesthetized, macerated, and serially diluted onto SDA (Sabouraud dextrose agar) plates. After 48 h of incubation, the CFUs were counted.

Pt2-treated larvae showed CFUs comparable to the DMSO control, indicating that no significant biological effect was achieved by this compound at the tested concentration (Figure 5). On the other hand, a significant reduction in CFUs was detected for the control compound fluconazole (1.1 log10) and for compound **Pt1** (0.7 log10). These data indicate that **Pt1** is able to reduce the fungal burden in a living organism. Together with the data on its promising antibacterial properties, **Pt1** and its related compounds seem to be a promising starting point for a novel class of antimicrobial agents.

◼ CONCLUSIONS

This work represents the first large-scale investigation of metal complexes as antifungal agents. Through CO-ADD, over 1000 metal-containing compounds submitted by a range of research groups were tested for their antifungal activity against *C. albicans* and *C. neoformans*. Similar to our analysis of data for antibacterial properties,[32] we found that metal complexes had a significantly higher (23×) hit rate against these fungal strains when compared with the over 300,000 tested organic molecules. These data should still be regarded as preliminary since the number of metal complexes tested is still relatively low, particularly if the immense chemical space accessible through all possible metal−ligand combinations is considered. Nevertheless, this study makes a strong case that a more systematic and thorough study of metal-based compounds for antimicrobial applications is warranted.

Figure 5. Average weight-standardized log10 CFU counts for *G. mellonella* larvae challenged with *C. albicans* and corresponding compounds **Pt1** (19 mg/kg), **Pt2** (28 mg/kg), and the controls, fluconazole (12 mg/kg) and 10% DMSO, after 24 h incubation at 37 °C. Statistical significance calculated by one-way ANOVA analysis with Tukey's pairwise test: ns = not significant.

In our previous antibacterial study, both metal compounds and organic molecules displayed roughly equal rates of cytotoxicity and hemolysis (around two-thirds of all tested compounds displayed toxicity at the tested concentrations). In the current antifungal analysis, we found that the incidence of toxicity for metal complexes (66%) was moderately elevated compared to the organic molecules tested (48%). It should be noted that the toxicity rate for metal compounds was very similar to that reported in our earlier study, whereas the rate for organic molecules was reduced. However, even with their relatively higher toxicity rate, the overall percentage of metal complexes that were active against the tested fungi yet exhibited low toxicity was still significantly higher than their organic counterparts (8.7 vs 0.6%).

To further evaluate the potential of these metal complexes, we obtained fresh samples for 21 of the most promising compounds and assessed their antifungal potential against a panel of eight relevant fungi. We found that the high activity observed in the initial assay against *C. albicans* and *C. neoformans* generally translated to high activity against the broader panel. We also studied the potential cytotoxicity and hemolysis of these compounds at higher concentrations and found that, in several cases, some toxicity or hemolysis was now observed. Wishing to understand the potential toxicity of metal compounds in living systems, where they have been assessed far less often than organic drug candidates, we tested 11 of these active metal complexes in a *G. mellonella* larva toxicity model. Ten exhibited no toxicity at the highest injected concentration. These data, together with results from other recent studies, indicate that metal complexes in general are well tolerated by the *G. mellonella* model.[14,28,61,112]

Compounds submitted to CO-ADD are generally not optimized for biological applications; hence, any hits obtained through this screening will most likely have to undergo medicinal chemistry optimization before a potential drug candidate is obtained. Regardless, we were interested to see if the excellent *in vitro* antifungal activity observed for metal complexes would translate to *in vivo* efficacy prior to any

structural optimization for solubility, stability, and other properties. To this end, we evaluated the ability of eight metal complexes to prolong survival in *G. mellonella* larvae infected with *C. albicans*. Compounds **Pt1** and **Pt2** showed some efficacy, and treatment with **Pt1**, but not **Pt2**, resulted in a significant 0.7 log10 reduction in the treated larvae compared to the DMSO control. As mentioned earlier, we have previously reported on **Pt1** and related compounds for their activity against Gram-positive bacteria. Interestingly, in an analogous *in vivo* assay with *G. mellonella* infected with MRSA, compound **Pt1** did not elicit a significant reduction in bacterial load.[61] It is notable that this compound class seems to perform well in assays against microbes while showing no toxicity against human cell lines or in *G. mellonella*.

These results warrant further studies into the structure–activity relationship of this compound class. Initial insights showed that substitution of the chloride ligands on **Pt1** generally results in a reduction of antibacterial activity, suggesting that chemical alterations of the COD-fragment may be more favorable.[61] One concern with **Pt1** is its potential stability under biological conditions. In a preliminary stability study, incubation of **Pt1** in DMSO for 7 days at room temperature resulted in no changes of the ^{1}H NMR spectrum, suggesting that the compound is stable under these conditions (Figure S6 in SI). Future work will be aimed toward more comprehensive examinations of the chemical and biological stability of these and related compounds, as well as investigations into their mode of action.

In summary, this study continues our efforts to showcase the vast potential of metal-containing compounds as antimicrobial agents. We have shown that metal complexes have promise as antifungal agents, displaying hit rates that vastly surpass those of a similarly sourced set of organic molecules. While metal compounds did show slightly higher rates of toxicity, they are overall still 14× times more likely to be active against *C. albicans* or *C. neoformans* in our data set. We further showed that this activity is generally retained against other fungal species and strains, including drug-resistant isolates. Lastly, we

K

demonstrate that most of these metal complexes are well tolerated by *G. mellonella*, displaying no signs of toxicity, and we identify one compound, **Pt1**, with the ability to significantly reduce the load of *C. albicans* in a moth larva infection model.

The results also validate the hypothesis behind the founding of CO-ADD, i.e., that searching for new antimicrobials without excluding potential new chemotypes due to the many dogmas of drug discovery may help to refill the antibiotic pipeline. We do note that the selection of metal complexes tested is biased by the collaborator's motive in making and submitting compounds, but the same caveat applies to submitted organic compounds. CO-ADD's phenotypic screening approach, traditionally used for antimicrobial discovery, is currently undergoing a renaissance for other therapeutic areas.[113]

Together with our recent studies, this work strongly supports further investigations into metal complexes as potential antimicrobial agents. We encourage other researchers to conduct more extensive studies into these compound classes. In particular, future work should focus on more systematic structure–activity relationship studies as well as elucidating the mode of action of active metal compounds. The few in-depth studies on the mechanism of action of metallobiotics in recent years have indicated that metal compounds are likely to affect multiple targets inside of microbes.[17,26,114,115] This makes them well suited to avoid rapid resistance development but also increases the difficulty in narrowing down their exact mode of action.[116] On behalf of CO-ADD, we invite researchers around the world to submit their (well-characterized) metal complexes for antimicrobial testing to advance our collective knowledge on this promising and underexplored compound class.

■ METHODS

Purity of Compounds

All compounds were obtained as dried powders from collaborators and confirmed by the collaborators to be at >95% purity. No further purification was performed by CO-ADD. The dry compounds were dissolved to a final concentration of 10 mg/mL or 10 mM in DMSO and used for the screenings as such.

Antibacterial Assays

For the all the bacterial assays, each bacterial strain was cultured in cation-adjusted Mueller Hinton broth (CAMHB; Bacto Laboratories 212322) at 37 °C overnight. A sample of each culture was then diluted 40-fold in fresh CAMHB and incubated at 37 °C for 1.5–3 h. The resultant mid-log phase cultures were diluted with CAMHB (CFU/mL measured by OD_{600}) and then added to each well of the compound-containing plates (384-well non-binding surface (NBS) plates; Corning CLS3640), giving a cell density of 5×10^5 CFU/mL and a total volume of 50 μL. Plates were covered and incubated at 37 °C for 18 h without shaking. Inhibition of bacterial growth was determined by measuring the absorbance at 600 nm (OD_{600}) using media only as negative control and bacteria without inhibitors as positive control. MIC values were determined as the lowest concentration at which the growth was inhibited by ≥80% (equivalent to no visible growth by the eye). Colistin sulfate (Sigma C4461) and vancomycin HCl (Sigma 861987) were used as internal controls on each plate for Gram-negative and Gram-positive bacteria, respectively. All compounds were tested as two technical replicates in two independent biological assays, $n = 4$ final data.

Antifungal Assays

For the fungal assays, both fungi (yeast) strains were cultured for 3 days on Yeast Extract-Peptone Dextrose (YPD; Becton Dickinson 242720) agar at 30 °C. A yeast suspension of 1×10^6 to 5×10^6 CFU/mL (as determined by OD_{530}) was prepared from five colonies

from the agar plates, subsequently diluted with Yeast Nitrogen Base media (YNB; Becton Dickinson 233520), and added to each well of the compound containing plates (384-well plates, NBS; Corning CLS3640), giving a final cell density of 2.5×10^3 CFU/mL and a total volume of 50 μL. Plates were covered and incubated at 35 °C for 36 h without shaking. The growth inhibition of *C. albicans* was determined by measuring the absorbance at 630 nm (OD_{630}), while the growth inhibition of *C. neoformans* was determined by measuring the difference in the absorbance between 600 and 570 nm ($OD_{600-570}$), after the addition of resazurin (0.001% final concentration; Sigma R7017) and incubation at 35 °C for 2 h, using media only as negative control and fungi without inhibitors as positive control. MIC values were recorded as the lowest concentration at which the growth was inhibited by ≥80%, equivalent to "optically clear-to-slightly hazy" or MIC score of 0–1 as per CLSI guidelines M27 Reference Method for Broth Dilution Antifungal Susceptibility Testing of Yeasts. Using this same scoring method, MICs were calculated at score 2 or 50% inhibition, with results displayed in the Supporting Information. Fluconazole (Sigma F8929) was used as internal control on each plate for all strains. All compounds were tested as two technical replicates in two to four independent biological assays, $n = 4–8$ final data. Those compounds that showed greater variability in data were tested at the higher replicate number.

Cytotoxicity Assays

HEK-293 ATCC CRL-1573 human embryonic kidney cells were counted manually in a Neubauer hemocytometer and added to compound-containing plates (384-well plates, tissue culture treated (TC); Corning CLS3712), giving a final density of 5000 cells/well and a total volume of 50 μL, using Dulbecco's modified Eagle medium (DMEM; Life Technologies 11995-073) with 10% fetal bovine serum (FBS; GE SH30084.03). The cells were incubated together with the compounds for 20 h at 37 °C in 5% CO_2. Cytotoxicity (or cell viability) was measured by fluorescence, ex: 560/10 nm, em: 590/10 nm (F560/590), after addition of 5 μL of 25 μg/mL resazurin (2.3 μg/mL final concentration; Sigma R7017) and after further incubation for 3 h at 37 °C in 5% CO_2, using media only as negative control and cells without inhibitors as positive control. CC_{50} (concentration at 50% cytotoxicity) values were calculated by curve fitting the inhibition values vs log(concentration) using a sigmoidal dose–response function, with variable fitting values for the bottom, top, and slope. Tamoxifen (Sigma T5648) was used as internal control on each plate.

Hemolysis Assays

Human whole blood (Australian Red Cross) was washed three times with 3 vol of 0.9% NaCl and resuspended in a concentration of 0.5×10^8 cells/mL, determined by a manual cell count in a Neubauer hemocytometer. Washed cells were added to compound-containing plates (384-well polypropylene plates (PP); Corning 3657) for a final volume of 50 μL, shaken, and incubated for 1 h at 37 °C. After incubation, the plates were centrifuged at 1000g for 10 min to pellet cells and debris; 25 μL of the supernatant was then transferred to reading plates (384-well, polystyrene plated (PS), Corning CLS3680), with hemolysis determined by measuring the supernatant absorbance at 405 mm (OD405) using cells without inhibitors as negative control and cells with 1% Triton X-100 (Sigma T8787) as positive control. HC10 and HC50 (concentration at 10 and 50% hemolysis, respectively) were calculated by curve fitting the inhibition values vs log(concentration) using a sigmoidal dose–response function with variable fitting values for the top, bottom, and slope. Melittin (Sigma M2272) was used as internal control on each plate. The use of human blood (sourced from the Australian Red Cross Blood Service) for hemolysis assays was approved by the University of Queensland Institutional Human Research Ethics Committee, Approval Number 2014000031.

Galleria mellonella In Vivo Toxicity Assay

The toxicity of compounds was tested *in vivo* using the *G. mellonella* model using our previously described methods,[61] Briefly, *G. mellonella* larvae were reared in a controlled environmental room at Macquarie

University, Sydney, Australia, at 30 °C and 65% humidity with a 12-h light/dark cycle. Larvae (200−250 mg) were individually injected with 10 μL of chemical into the last right pro-leg using a 100 μL syringe (Hamilton Ltd.). Each compound was dissolved in DMSO at the maximum concentration given in Table 3 and also diluted in water to final concentrations of 100, 10, and 1 μM. We injected five larvae in triplicate for each of the four dilutions for each compound. Larvae injected with different dilutions of DMSO (10^{-1}, 10^{-2}, and 10^{-3}) were included as negative controls. Following injection, the larvae were incubated at 30 °C and monitored every 24 h for 6 days. Larval performance was assessed according to the *G. mellonella* Health Index Scoring System.[111] The experiments were repeated over three separate days for biological triplicates.

Galleria mellonella Infection (Survival) Assay

The globally available strains for *C. albicans* and *C. neoformans*, namely, ATCC 90028 and H99, respectively, were used to assess the antifungal potential of the panel of cobalt complex compounds in the *G. mellonella* insect model. Each strain was cultured on Sabouraud dextrose agar (SDA) for 24−48 h at 27 °C prior to inoculation. Yeast colonies were then suspended in a phosphate-buffered saline solution (PBS), and cells' concentrations were adjusted using a Neubauer counting chamber to 5×10^7 cells for ATCC 90028 and 1×10^8 cells for H99. Compounds were prepared by dissolving in 100% dimethylsulfoxide (DMSO) to 4 or 10 mM depending on compound solubility before being further diluted with water to 0.4 or 1 mM for injection into larvae.

For each compound, five sixth instar *G. mellonella* larvae of similar size (ranging from 200 to 250 mg) were selected for each fungal species and injected with 10 μL of the fungal inoculum in the last left pro-leg using a Hamilton (USA) 1710 TLL syringe with a 27-gauge needle. Each group of larvae was subsequently incubated at 37 °C for 2 h in 90 mm Petri dishes. After incubation, larvae were injected with 10 μL of the compound into the last right pro-leg and returned to Petri dishes to incubate at 37 °C for 5 days. In addition to the panel of metal compounds, fluconazole (FLC) was included as a positive control (1 and 0.4 mM) and reference antifungal. Larvae inoculated with just the fungal strains and the fungal strains with 10% DMSO were also included as comparison groups. Larvae injected concurrently with PBS instead of fungal inoculum and compounds were used as negative controls. All larvae were checked daily for survival.

Galleria mellonella Infection (Log CFU Reduction) Assay

A log CFU reduction assay was conducted for two compounds and two control groups. The compounds examined were **Pt1** (1 mM) and **Pt2** (1 mM), both of which showed observed *in vivo* antifungal potential with the *G. mellonella* survival assay against the *C. albicans* strain ATCC 90028. Fluconazole (1 mM) and 10% DMSO were used once again as the control groups. Fifteen *G. mellonella* larvae (200−250 mg) per test group were selected and inoculated with 10 μL of *C. albicans* at a concentration of 5×10^7 cells/mL and incubated on 90 mm Petri dishes in groups of five larvae for 2 h at 37 °C. Larvae were then subsequently injected with 10 μL of the corresponding test compound or control and returned to Petri dishes to incubate for 24 h at 37 °C.

Larvae were then anesthetized on ice for 5 to 10 min before being placed in individual prefilled 2 mL tubes with 3.0 mm diameter zirconium beads with 1000 μL of PBS. They were then macerated briefly using the BeadBug 6 Homogenizer (Benchmark Scientific, USA) in two 45 s intervals at 4350 rpm. After homogenization, serial dilutions of 1:100, 1:1000, and 1:10,000 were then made for each larva/tube, and 100 μL of the dilution was spread plated onto SDA plates with 50 μg/mL chloramphenicol. Plates were then incubated at 27 °C for 48 h before CFUs were counted.

A one-way ANOVA was conducted to compare the CFU counts for **Pt1**, **Pt2**, and both controls. After a significant difference was observed between the groups, a subsequent Tukey's pairwise test was used to compare the individual test groups with each other.

■ ASSOCIATED CONTENT

Ⓢ Supporting Information

The Supporting Information is available free of charge at https://pubs.acs.org/doi/10.1021/jacsau.2c00308.

Experimental details, characterization data, and additional data (PDF)

■ AUTHOR INFORMATION

Corresponding Authors

Angelo Frei − *Centre for Superbug Solutions, Institute for Molecular Bioscience, The University of Queensland, St. Lucia, Queensland 4072, Australia; Department of Chemistry, Biochemistry & Pharmaceutical Sciences, University of Bern, 3012 Bern, Switzerland;* Email: angelo.frei@unibe.ch

Mark A. T. Blaskovich − *Centre for Superbug Solutions, Institute for Molecular Bioscience, The University of Queensland, St. Lucia, Queensland 4072, Australia;* ● orcid.org/0000-0001-9447-2292; Email: m.blaskovich@uq.edu.au

Authors

Alysha G. Elliott − *Centre for Superbug Solutions, Institute for Molecular Bioscience, The University of Queensland, St. Lucia, Queensland 4072, Australia;* ● orcid.org/0000-0002-2983-0484

Alex Kan − *Molecular Mycology Research Laboratory, Centre for Infectious Diseases and Microbiology, Faculty of Medicine and Health, Sydney Medical School, Westmead Clinical School, Sydney Institute for Infectious Diseases, Westmead Hospital-Research and Education Network, Westmead Institute for Medical Research, University of Sydney, Sydney, NSW 2145, Australia*

Hue Dinh − *School of Natural Sciences, ARC Centre of Excellence in Synthetic Biology, Macquarie University, Sydney, NSW 2109, Australia*

Stefan Bräse − *Institute of Organic Chemistry, Karlsruhe Institute of Technology, 76131 Karlsruhe, Germany; Institute of Biological and Chemical Systems - Functional Molecular Systems, Karlsruhe Institute of Technology, 76344 Eggenstein-Leopoldshafen, Germany*

Alice E. Bruce − *Department of Chemistry, University of Maine, Orono, Maine 04469, United States;* ● orcid.org/0000-0002-4556-8180

Mitchell R. Bruce − *Department of Chemistry, University of Maine, Orono, Maine 04469, United States;* ● orcid.org/0000-0002-6428-3842

Feng Chen − *Department of Chemistry, University of Warwick, Coventry CV4 7AL, U.K.*

Dhirgam Humaidy − *Department of Chemistry, University of Maine, Orono, Maine 04469, United States*

Nicole Jung − *Karlsruhe Nano Micro Facility (KNMF), Karlsruhe Institute of Technology, 76344 Eggenstein-Leopoldshafen, Germany; Institute of Biological and Chemical Systems - Functional Molecular Systems, Karlsruhe Institute of Technology, 76344 Eggenstein-Leopoldshafen, Germany;* ● orcid.org/0000-0001-9513-2468

A. Paden King − *Department of Chemistry and Chemical Biology, Cornell University, Ithaca, New York 14853, United States*

210

Peter G. Lye − School of Science and Technology, University of New England, Armidale, NSW 2351, Australia

Hanna K. Maliszewska − School of Chemistry, University of East Anglia, Norwich NR4 7TJ, U.K.

Ahmed M. Mansour − Chemistry Department, Faculty of Science, Cairo University, Giza 12613, Egypt; orcid.org/0000-0002-0877-3636

Dimitris Matiadis − Institute of Biosciences & Applications, National Centre for Scientific Research "Demokritos", 15310 Athens, Greece; orcid.org/0000-0003-0059-952X

María Paz Muñoz − School of Chemistry, University of East Anglia, Norwich NR4 7TJ, U.K.

Tsung-Yu Pai − Molecular Mycology Research Laboratory, Centre for Infectious Diseases and Microbiology, Faculty of Medicine and Health, Sydney Medical School, Westmead Clinical School, Sydney Institute for Infectious Diseases, Westmead Hospital-Research and Education Network, Westmead Institute for Medical Research, University of Sydney, Sydney, NSW 2145, Australia

Shyam Pokhrel − Department of Chemistry, University of Maine, Orono, Maine 04469, United States

Peter J. Sadler − Department of Chemistry, University of Warwick, Coventry CV4 7AL, U.K.; orcid.org/0000-0001-9160-1941

Marina Sagnou − Institute of Biosciences & Applications, National Centre for Scientific Research "Demokritos", 15310 Athens, Greece; orcid.org/0000-0002-4231-6658

Michelle Taylor − School of Science and Technology, University of New England, Armidale, NSW 2351, Australia

Justin J. Wilson − Department of Chemistry and Chemical Biology, Cornell University, Ithaca, New York 14853, United States; orcid.org/0000-0002-4086-7982

Dean Woods − School of Science and Technology, University of New England, Armidale, NSW 2351, Australia

Johannes Zuegg − Centre for Superbug Solutions, Institute for Molecular Bioscience, The University of Queensland, St. Lucia, Queensland 4072, Australia; orcid.org/0000-0001-6240-6020

Wieland Meyer − Molecular Mycology Research Laboratory, Centre for Infectious Diseases and Microbiology, Faculty of Medicine and Health, Sydney Medical School, Westmead Clinical School, Sydney Institute for Infectious Diseases, Westmead Hospital-Research and Education Network, Westmead Institute for Medical Research, University of Sydney, Sydney, NSW 2145, Australia

Amy K. Cain − School of Natural Sciences, ARC Centre of Excellence in Synthetic Biology, Macquarie University, Sydney, NSW 2109, Australia

Matthew A. Cooper − Centre for Superbug Solutions, Institute for Molecular Bioscience, The University of Queensland, St. Lucia, Queensland 4072, Australia; orcid.org/0000-0003-3147-3460

Complete contact information is available at:
https://pubs.acs.org/10.1021/jacsau.2c00308

Author Contributions

A.F. conceived the project concept to analyze CO-ADD data for metal complexes. A.F. analyzed the data and generated the graphics. M.A.T.B, M.A.C., J.Z., and A.G.E. founded the screening initiative CO-ADD and collected the microbiological data. A.F, A.G.E., and M.A.T.B. composed the manuscript. A.K., H.D., W.M., T.P., and A.C. conducted the in vivo

experiments in G. mellonella. A.E.B., M.R.B, F.C., D.H., N.J., A.P.K., P.G.L., H.K.M., A.M.M., D.M., M.P.M., S.P., P.J.S., M.S., M.T., J.J.W., and W.D. prepared, characterized, and submitted the compounds highlighted in this work. All authors discussed, commented, and approved the final manuscript.

Notes

The authors declare no competing financial interest.

REFERENCES

(1) Brown, G. D.; Denning, D. W.; Gow, N. A. R.; Levitz, S. M.; Netea, M. G.; White, T. C. Hidden Killers: Human Fungal Infections. Sci. Transl. Med. 2012, 4, 165rv13−165rv13.

(2) Fisher, M. C.; Hawkins, N. J.; Sanglard, D.; Gurr, S. J. Worldwide Emergence of Resistance to Antifungal Drugs Challenges Human Health and Food Security. Science 2018, 360, 739−742.

(3) Lee, Y.; Puumala, E.; Robbins, N.; Cowen, L. E. Antifungal Drug Resistance: Molecular Mechanisms in Candida Albicans and Beyond. Chem. Rev. 2021, 121, 3390−3411.

(4) Park, B. J.; Wannemuehler, K. A.; Marston, B. J.; Govender, N.; Pappas, P. G.; Chiller, T. M. Estimation of the Current Global Burden of Cryptococcal Meningitis among Persons Living with Hiv/Aids. *AIDS* **2009**, *23*, 525−530.

(5) Perfect, J. R. The Antifungal Pipeline: A Reality Check. *Nat. Rev. Drug Discovery* **2017**, *16*, 603−616.

(6) Pfaller, M. A.; Diekema, D. J.; Turnidge, J. D.; Castanheira, M.; Jones, R. N. Twenty Years of the Sentry Antifungal Surveillance Program: Results for Candida Species from 1997−2016. *Open Forum Infect. Dis.* **2019**, *6*, S79−S94.

(7) Chakrabarti, A.; Singh, S. Multidrug-Resistant Candida Auris: An Epidemiological Review. *Expert Rev. Anti-infect. Ther.* **2020**, *18*, 551−562.

(8) CDC Antibiotic Resistance Threats in the United States. https://www.cdc.gov/DrugResistance/Biggest-Threats.html (accessed 15.05.2022).

(9) Gintjee, T. J.; Donnelley, M. A.; Thompson, G. R. Aspiring Antifungals: Review of Current Antifungal Pipeline Developments. *J. of Fungi* **2020**, *6*, 28.

(10) Rosenberg, B.; Vancamp, L.; Trosko, J. E.; Mansour, V. H. Platinum Compounds: A New Class of Potent Antitumour Agents. *Nature* **1969**, *222*, 385−386.

(11) Medina-Franco, J. L.; López-López, E.; Andrade, E.; Ruiz-Azuara, L.; Frei, A.; Guan, D.; Zuegg, J.; Blaskovich, M. A. T. Bridging Informatics and Medicinal Inorganic Chemistry: Toward a Database of Metallodrugs and Metallodrug Candidates. *Drug Discovery Today* **2022**, 1420−1430.

(12) Anthony, E. J.; Bolitho, E. M.; Bridgewater, H. E.; Carter, O. W. L.; Donnelly, J. M.; Imberti, C.; Lant, E. C.; Lermyte, F.; Needham, R. J.; Palau, M.; Sadler, P. J.; Shi, H.; Wang, F.-X.; Zhang, W.-Y.; Zhang, Z. Metallodrugs Are Unique: Opportunities and Challenges of Discovery and Development. *Chem. Sci.* **2020**, *11*, 12888−12917.

(13) Adoke, Y.; Zoleko-Manego, R.; Ouoba, S.; Tiono, A. B.; Kaguthi, G.; Bonzela, J. E.; Duong, T. T.; Nahum, A.; Bouyou-Akotet, M.; Ogutu, B.; Ouedraogo, A.; Macintyre, F.; Jessel, A.; Laurijssens, B.; Cherkaoui-Rbati, M. H.; Cantalloube, C.; Marrast, A. C.; Bejuit, R.; White, D.; Wells, T. N. C.; Wartha, F.; Leroy, D.; Kibuuka, A.; Mombo-Ngoma, G.; Ouattara, D.; Mugenya, I.; Phuc, B. Q.; Bohissou, F.; Mawili-Mboumba, D. P.; Olewe, F.; Soulama, I.; Tinto, H.; Ramharter, M.; Nahum, D.; Zohou, H.; Nzwili, I.; Ongecha, J. M.; Thompson, R.; Kiwalabye, J.; Diarra, A.; Coulibaly, A. S.; Bougouma, E. C.; Kargougou, D. G.; Tegneri, M.; Castin Vuillerme, C.; Djeriou, E.; Ansary, A. F.; the ALCI Study Group. A Randomized, Double-Blind, Phase 2b Study to Investigate the Efficacy, Safety, Tolerability and Pharmacokinetics of a Single-Dose Regimen of Ferroquine with Artefenomel in Adults and Children with Uncomplicated Plasmodium Falciparum Malaria. *Malar. J.* **2021**, *20*, 222−222.

(14) Smitten, K. L.; Southam, H. M.; de la Serna, J. B.; Gill, M. R.; Jarman, P. J.; Smythe, C. G. W.; Poole, R. K.; Thomas, J. A. Using Nanoscopy to Probe the Biological Activity of Antimicrobial Leads That Display Potent Activity against Pathogenic, Multidrug Resistant, Gram-Negative Bacteria. *ACS Nano* **2019**, *13*, 5133−5146.

(15) Smitten, K. L.; Fairbanks, S. D.; Robertson, C. C.; Bernardino de la Serna, J.; Foster, S. J.; Thomas, J. A. Ruthenium Based Antimicrobial Theranostics − Using Nanoscopy to Identify Therapeutic Targets and Resistance Mechanisms in Staphylococcus Aureus. *Chem. Sci.* **2020**, *11*, 70−79.

(16) Smitten, K. L.; Thick, E. J.; Southam, H. M.; Bernardino de la Serna, J.; Foster, S. J.; Thomas, J. A. Mononuclear Ruthenium(Ii) Theranostic Complexes That Function as Broad-Spectrum Antimicrobials in Therapeutically Resistant Pathogens through Interaction with DNA. *Chem. Sci.* **2020**, *11*, 8828−8838.

(17) Varney, A. M.; Smitten, K. L.; Thomas, J. A.; McLean, S. Transcriptomic Analysis of the Activity and Mechanism of Action of a Ruthenium(Ii)-Based Antimicrobial That Induces Minimal Evolution of Pathogen Resistance. *ACS Pharmacol. Transl. Sci.* **2021**, *4*, 168−178.

(18) https://www.metallobio.com/ (accessed 03/08/2021).

(19) Lawrance, G. A. *Introduction to Coordination Chemistry*; John Wiley & Sons Ltd.: Chichester, United Kingdom, 2010.

(20) Lovering, F.; Bikker, J.; Humblet, C. Escape from Flatland: Increasing Saturation as an Approach to Improving Clinical Success. *J. Med. Chem.* **2009**, *52*, 6752−6756.

(21) Lovering, F. Escape from Flatland 2: Complexity and Promiscuity. *MedChemComm* **2013**, *4*, 515−519.

(22) Morrison, C. N.; Prosser, K. E.; Stokes, R. W.; Cordes, A.; Metzler-Nolte, N.; Cohen, S. M. Expanding Medicinal Chemistry into 3d Space: Metallofragments as 3d Scaffolds for Fragment-Based Drug Discovery. *Chem. Sci.* **2020**, *11*, 1216−1225.

(23) Boros, E.; Dyson, P. J.; Gasser, G. Classification of Metal-Based Drugs According to Their Mechanisms of Action. *Chem* **2020**, *6*, 41−60.

(24) Pandey, A.; Boros, E. Coordination Complexes to Combat Bacterial Infections: Recent Developments, Current Directions and Future Opportunities. *Chem. − Eur. J.* **2021**, *27*, 7340−7350.

(25) Frei, A. Metal Complexes, an Untapped Source of Antibiotic Potential? *Antibiotics* **2020**, *9*, 90.

(26) Li, F.; Collins, J. G.; Keene, F. R. Ruthenium Complexes as Antimicrobial Agents. *Chem. Soc. Rev.* **2015**, *44*, 2529−2542.

(27) Frei, A.; Verderosa, A. D.; Elliott, A. G.; Zuegg, J.; Blaskovich, M. A. T., Leveraging Metals to Combat Antimicrobial Resistance. *Nature Chem. Rev.* **2022**, (submitted).

(28) Frei, A.; King, A. P.; Lowe, G. J.; Cain, A. K.; Short, F. L.; Dinh, H.; Elliott, A. G.; Zuegg, J.; Wilson, J. J.; Blaskovich, M. A. T. Nontoxic Cobalt(Iii) Schiff Base Complexes with Broad-Spectrum Antifungal Activity. *Chem. − Eur. J.* **2021**, *27*, 2021−2029.

(29) Frei, A.; Amado, M.; Cooper, M. A.; Blaskovich, M. A. T. Light-Activated Rhenium Complexes with Dual Mode of Action against Bacteria. *Chem. − Eur. J.* **2020**, *26*, 2852−2858.

(30) Sovari, S. N.; Radakovic, N.; Roch, P.; Crochet, A.; Pavic, A.; Zobi, F. Combatting Amr: A Molecular Approach to the Discovery of Potent and Non-Toxic Rhenium Complexes Active against C. albicans-Mrsa Co-Infection. *Eur. J. Med. Chem.* **2021**, *226*, No. 113858.

(31) Sovari, S. N.; Vojnovic, S.; Bogojevic, S. S.; Crochet, A.; Pavic, A.; Nikodinovic-Runic, J.; Zobi, F. Design, Synthesis and In vivo Evaluation of 3-Arylcoumarin Derivatives of Rhenium(I) Tricarbonyl Complexes as Potent Antibacterial Agents against Methicillin-Resistant Staphylococcus Aureus (Mrsa). *Eur. J. Med. Chem.* **2020**, *205*, No. 112533.

(32) Frei, A.; Zuegg, J.; Elliott, A. G.; Baker, M.; Braese, S.; Brown, C.; Chen, F.; Dowson, C. G.; Dujardin, G.; Jung, N.; King, A. P.; Mansour, A. M.; Massi, M.; Moat, J.; Mohamed, H. A.; Renfrew, A. K.; Rutledge, P. J.; Sadler, P. J.; Todd, M. H.; Willans, C. E.; Wilson, J. J.; Cooper, M. A.; Blaskovich, M. A. T. Metal Complexes as a Promising Source for New Antibiotics. *Chem. Sci.* **2020**, *11*, 2627−2639.

(33) Blaskovich, M. A. T.; Zuegg, J.; Elliott, A. G.; Cooper, M. A. Helping Chemists Discover New Antibiotics. *ACS Infect. Dis.* **2015**, *1*, 285−287.

(34) Rubbiani, R.; Blacque, O.; Gasser, G. Sedaxicenes: Potential New Antifungal Ferrocene-Based Agents? *Dalton Trans.* **2016**, *45*, 6619−6626.

(35) Rubbiani, R.; Weil, T.; Tocci, N.; Mastrobuoni, L.; Jeger, S.; Moretto, M.; Ng, J.; Lin, Y.; Hess, J.; Ferrari, S.; Kaech, A.; Young, L.; Spencer, J.; Moore, A. L.; Cariou, K.; Renga, G.; Pariano, M.; Romani, L.; Gasser, G. In Vivo Active Organometallic-Containing Antimycotic Agents. *RSC Chemical Biology* **2021**, *2*, 1263−1273.

(36) Parveen, H.; Alatawi, R. A. S.; Alsharif, M. A.; Alahmdi, M. I.; Mukhtar, S.; Khan, S. A.; Hasan, S.; Khan, A. U. Novel Pyrazoline-Based Organometallic Compounds Containing Ferrocenyl and Quinoline Units: Synthesis, Characterization and Microbial Susceptibilities. *Appl. Organomet. Chem.* **2018**, *32*, No. e4257.

(37) Yagnam, S.; Rami Reddy, E.; Trivedi, R.; Krishna, N. V.; Giribabu, L.; Rathod, B.; Prakasham, R. S.; Sridhar, B. 1,2,3-Triazole Derivatives of 3-Ferrocenylidene-2-Oxindole: Synthesis, Character-

o

212

ization, Electrochemical and Antimicrobial Evaluation. *Appl. Organomet. Chem.* **2019**, *33*, No. e4817.

(38) Efimov, N. N.; Loginov, D. A.; Sharipov, M. Y.; Nazarov, A. A.; Nelyubina, Y. V.; Perekalin, D. S. Unexpected Antifungal Activity of Half-Sandwich Complexes with Metal−Iodine Bonds. *J. Organomet. Chem.* **2020**, *916*, No. 121272.

(39) Zalevskaya, O.; Gur'eva, Y.; Kutchin, A.; Hansford, K. A. Antimicrobial and Antifungal Activities of Terpene-Derived Palladium Complexes. *Antibiotics* **2020**, *9*, 277.

(40) Gagini, T.; Colina-Vegas, L.; Villarreal, W.; Borba-Santos, L. P.; de Souza Pereira, C.; Batista, A. A.; Kneip Fleury, M.; de Souza, W.; Rozental, S.; Costa, L. A. S.; Navarro, M. Metal−Azole Fungistatic Drug Complexes as Anti-Sporothrix Spp. Agents. *New J. Chem.* **2018**, *42*, 13641−13650.

(41) Gandra, R. M.; Mc Carron, P.; Fernandes, M. F.; Ramos, L. S.; Mello, T. P.; Aor, A. C.; Branquinha, M. H.; McCann, M.; Devereux, M.; Santos, A. L. S. Antifungal Potential of Copper(Ii), Manganese-(Ii) and Silver(I) 1,10-Phenanthroline Chelates against Multidrug-Resistant Fungal Species Forming the Candida Haemulonii Complex: Impact on the Planktonic and Biofilm Lifestyles. *Front. Microbiol.* **2017**, *8*, 1−11.

(42) Malik, M. A.; Lone, S. A.; Wani, M. Y.; Talukdar, M. I. A.; Dar, O. A.; Ahmad, A.; Hashmi, A. A. S-Benzyldithiocarbazate Imine Coordinated Metal Complexes Kill Candida Albicans by Causing Cellular Apoptosis and Necrosis. *Bioorg. Chem.* **2020**, *98*, No. 103771.

(43) Dar, O. A.; Lone, S. A.; Malik, M. A.; Wani, M. Y.; Ahmad, A.; Hashmi, A. A. New Transition Metal Complexes with a Pendent Indole Ring: Insights into the Antifungal Activity and Mode of Action. *RSC Adv.* **2019**, *9*, 15151−15157.

(44) Golbaghi, G.; Groleau, M.-C.; López de los Santos, Y.; Doucet, N.; Déziel, E.; Castonguay, A. Cationic Ruii Cyclopentadienyl Complexes with Antifungal Activity against Several Candida Species. *ChemBioChem* **2020**, *21*, 3112−3119.

(45) Mansour, A. M.; Radacki, K. Antimicrobial Properties of Half-Sandwich Ir(Iii) Cyclopentadienyl Complexes with Pyridylbenzimidazole Ligands. *Dalton Trans.* **2020**, *49*, 4491−4501.

(46) Mansour, A. M. Ruii−Carbonyl Photocorms with N,N-Benzimidazole Bidentate Ligands: Spectroscopic, Lysozyme Binding Affinity, and Biological Activity Evaluation. *Eur. J. Inorg. Chem.* **2018**, *2018*, 852−860.

(47) Dar, O. A.; Lone, S. A.; Malik, M. A.; Aqlan, F. M.; Wani, M. Y.; Hashmi, A. A.; Ahmad, A. Synthesis and Synergistic Studies of Isatin Based Mixed Ligand Complexes as Potential Antifungal Therapeutic Agents. *Heliyon* **2019**, *5*, No. e02055.

(48) Bomfim Filho, L. F. O.; Oliveira, M. R. L.; Miranda, L. D. L.; Vidigal, A. E. C.; Guilardi, S.; Souza, R. A. C.; Ellena, J.; Ardisson, J. D.; Zambolim, L.; Rubinger, M. M. M. Syntheses, Characterization and Antifungal Activity of Novel Dimethylbis(N-R-Sulfonyldithiocarbimato)Stannate(Iv) Complexes. *J. Mol. Struct.* **2017**, *1129*, 60−67.

(49) de Azevedo-França, J. A.; Borba-Santos, L. P.; de Almeida Pimentel, G.; Franco, C. H. J.; Souza, C.; de Almeida Celestino, J.; de Menezes, E. F.; dos Santos, N. P.; Vieira, E. G.; Ferreira, A. M. D. C.; de Souza, W.; Rozental, S.; Navarro, M. Antifungal Promising Agents of Zinc(Ii) and Copper(Ii) Derivatives Based on Azole Drug. *J. Inorg. Biochem.* **2021**, *219*, No. 111401.

(50) Lobana, T. S.; Indoria, S.; Sood, H.; Arora, D. S.; Kaur, M.; Jasinski, J. P. Synthesis of (3-Nitro-2-Oxo-Benzaldehyde Thiosemicarbazonato)−Zinc(Ii) Complexes: The Position of Nitro Group in Phenyl Ring Alters Antimicrobial Activity against K. Pneumoniae 1, S. Typhimurium 2, Mrsa and C. Albicans. *Dalton Trans.* **2021**, *50*, 6823−6833.

(51) Granato, M. Q.; Mello, T. P.; Nascimento, R. S.; Pereira, M. D.; Rosa, T. L. S. A.; Pessolani, M. C. V.; McCann, M.; Devereux, M.; Branquinha, M. H.; Santos, A. L. S.; Kneipp, L. F. Silver(I) and Copper(Ii) Complexes of 1,10-Phenanthroline-5,6-Dione against Phialophora Verrucosa: A Focus on the Interaction with Human Macrophages and Galleria Mellonella Larvae. *Front. Microbiol.* **2021**, *12*, 1−12.

(52) Lin, Y.; Betts, H.; Keller, S.; Cariou, K.; Gasser, G. Recent Developments of Metal-Based Compounds against Fungal Pathogens. *Chem. Soc. Rev.* **2021**, 10346−10402.

(53) Gandra, R. M.; McCarron, P.; Viganor, L.; Fernandes, M. F.; Kavanagh, K.; McCann, M.; Branquinha, M. H.; Santos, A. L. S.; Howe, O.; Devereux, M. In Vivo Activity of Copper(Ii), Manganese-(Ii), and Silver(I) 1,10-Phenanthroline Chelates against Candida Haemulonii Using the Galleria Mellonella Model. *Front. Microbiol.* **2020**, *11*, 1−15.

(54) Ge, M.; Feng, J.; Huang, H.; Gou, X.; Hua, C.; Chen, B.; Zhao, J. No2-Fe (Ii)Pc-Catalyzed Synthesis of 2-Ferrocenyl-5-Aryl-1,3,4-Oxadiazoles and Study of Antifungal Activity. *J. Heterocycl. Chem.* **2019**, *56*, 3297−3302.

(55) King, A. P.; Gellineau, H. A.; Ahn, J.-E.; MacMillan, S. N.; Wilson, J. J. Bis(Thiosemicarbazone) Complexes of Cobalt(Iii). Synthesis, Characterization, and Anticancer Potential. *Inorg. Chem.* **2017**, *56*, 6609−6623.

(56) King, A. P.; Gellineau, H. A.; MacMillan, S. N.; Wilson, J. J. Physical Properties, Ligand Substitution Reactions, and Biological Activity of Co(Iii)-Schiff Base Complexes. *Dalton Trans.* **2019**, *48*, 5987−6002.

(57) Baker, M. V.; Skelton, B. W.; White, A. H.; Williams, C. C. Synthesis and Characterization of a Saddle-Shaped Nickel−Carbene Complex Derived from an Imidazolium-Linked Meta-Cyclophane. *Organometallics* **2002**, *21*, 2674−2678.

(58) Su, X.; McCardle, K. M.; Panetier, J. A.; Jurss, J. W. Electrocatalytic Co2 Reduction with Nickel Complexes Supported by Tunable Bipyridyl-N-Heterocyclic Carbene Donors: Understanding Redox-Active Macrocycles. *Chem. Commun.* **2018**, *54*, 3351−3354.

(59) Guimond, N.; Gorelsky, S. I.; Fagnou, K. Rhodium(Iii)-Catalyzed Heterocycle Synthesis Using an Internal Oxidant: Improved Reactivity and Mechanistic Studies. *J. Am. Chem. Soc.* **2011**, *133*, 6449−6457.

(60) Geisler, H.; Harringer, S.; Wenisch, D.; Urban, R.; Jakupec, M. A.; Kandioller, W.; Keppler, B. K. Systematic Study on the Cytotoxic Potency of Commonly Used Dimeric Metal Precursors in Human Cancer Cell Lines. *ChemistryOpen* **2022**, No. e202200019.

(61) Frei, A.; Ramu, S.; Lowe, G. J.; Dinh, H.; Semenec, L.; Elliott, A. G.; Zuegg, J.; Deckers, A.; Jung, N.; Bräse, S.; Cain, A. K.; Blaskovich, M. A. T. Platinum Cyclooctadiene Complexes with Activity against Gram-Positive Bacteria. *ChemMedChem* **2021**, *16*, 3165−3171.

(62) Bruno, N. C.; Buchwald, S. L. Synthesis and Application of Palladium Precatalysts That Accommodate Extremely Bulky Di-Tert-Butylphosphino Biaryl Ligands. *Org. Lett.* **2013**, *15*, 2876−2879.

(63) Şengül, A.; Hanhan, M. E. Water Soluble Benzimidazole Containing Ionic Palladium(Ii) Complex for Rapid Microwave-Assisted Suzuki Reaction of Aryl Chlorides. *Appl. Organomet. Chem.* **2018**, *32*, No. e4288.

(64) Piguet, C.; Bünzli, J.-C. G.; Bernardinelli, G.; Bochet, C. G.; Froidevaux, P. Design of Luminescent Building Blocks for Supramolecular Triple-Helical Lanthanide Complexes. *J. Chem. Soc., Dalton Trans.* **1995**, 83−97.

(65) Escande, A.; Guénée, L.; Buchwalder, K.-L.; Piguet, C. Complexation of Trivalent Lanthanides with Planar Tridentate Aromatic Ligands Tuned by Counteranions and Steric Constraints. *Inorg. Chem.* **2009**, *48*, 1132−1147.

(66) Lemonnier, J.-F.; Guénée, L.; Bernardinelli, G.; Vigier, J.-F.; Bocquet, B.; Piguet, C. Planned Failures from the Principle of Maximum Site Occupancy in Lanthanide Helicates. *Inorg. Chem.* **2010**, *49*, 1252−1265.

(67) Gong, D.; Jia, X.; Wang, B.; Zhang, X.; Jiang, L. Synthesis, Characterization, and Butadiene Polymerization of Iron(Iii), Iron(Ii) and Cobalt(Ii) Chlorides Bearing 2,6-Bis(2-Benzimidazolyl)Pyridyl or 2,6-Bis(Pyrazol)Pyridine Ligand. *J. Organomet. Chem.* **2012**, *702*, 10−18.

(68) Yu, Q.-Y.; Lei, B.-X.; Liu, J.-M.; Shen, Y.; Xiao, L.-M.; Qiu, R.-L.; Kuang, D.-B.; Su, C.-Y. Ruthenium Dyes with Heteroleptic

P

213

Tridentate 2,6-Bis(Benzimidazol-2-Yl)-Pyridine for Dye-Sensitized Solar Cells: Enhancement in Performance through Structural Modifications. *Inorg. Chim. Acta* **2012**, *392*, 388−395.

(69) Mansour, A. M.; Shehab, O. R. Photoactivatable Co-Releasing Properties of {Ru(CO)2}-Core Pyridylbenzimidazole Complexes and Reactivity Towards Lysozyme. *Eur. J. Inorg. Chem.* **2017**, *2017*, 4299−4310.

(70) Chan, K.; Chung, C. Y.-S.; Yam, V. W.-W. Conjugated Polyelectrolyte-Induced Self-Assembly of Alkynylplatinum(II) 2,6-Bis(Benzimidazol-2′-Yl)Pyridine Complexes. *Chem. − Eur. J.* **2015**, *21*, 16434−16447.

(71) Zare, D.; Doistau, B.; Nozary, H.; Besnard, C.; Guénée, L.; Suffren, Y.; Pelé, A.-L.; Hauser, A.; Piguet, C. CrIII as an Alternative to Ruii in Metallo-Supramolecular Chemistry. *Dalton Trans.* **2017**, *46*, 8992−9009.

(72) Mansour, A. M. Pd(Ii) and Pt(Ii) Complexes of Tridentate Ligands with Selective Toxicity against Cryptococcus Neoformans and Candida Albicans. *RSC Adv.* **2021**, *11*, 39748−39757.

(73) Mansour, A. M.; Radacki, K.; Shehab, O. R. Role of the Ancillary Ligand in Determining the Antimicrobial Activity of Pd(Ii) Complexes with N^N^N-Tridentate Coligand. *Polyhedron* **2022**, *221*, No. 115857.

(74) Hill, W. R.; Pillsbury, D. M., *Argyria: The Pharmacology of Silver*. Williams & Wilkins: Baltimore, 1939.

(75) Kascatan-Nebioglu, A.; Panzner, M. J.; Tessier, C. A.; Cannon, C. L.; Youngs, W. J. N-Heterocyclic Carbene−Silver Complexes: A New Class of Antibiotics. *Coord. Chem. Rev.* **2007**, *251*, 884−895.

(76) Medici, S.; Peana, M.; Crisponi, G.; Nurchi, V. M.; Lachowicz, J. I.; Remelli, M.; Zoroddu, M. A. Silver Coordination Compounds: A New Horizon in Medicine. *Coord. Chem. Rev.* **2016**, *327-328*, 349−359.

(77) Eckhardt, S.; Brunetto, P. S.; Gagnon, J.; Priebe, M.; Giese, B.; Fromm, K. M. Nanobio Silver: Its Interactions with Peptides and Bacteria, and Its Uses in Medicine. *Chem. Rev.* **2013**, *113*, 4708−4754.

(78) Matiadis, D.; Karagiaouri, M.; Mavroidi, B.; Nowak, K. E.; Katsipis, G.; Pelecanou, M.; Pantazaki, A.; Sagnou, M. Synthesis and Antimicrobial Evaluation of a Pyrazoline-Pyridine Silver(I) Complex: DNA-Interaction and Anti-Biofilm Activity. *BioMetals* **2021**, *34*, 67−85.

(79) Cardoso, J. M. S.; Guerreiro, S. I.; Lourenço, A.; Alves, M. M.; Montemor, M. F.; Mira, N. P.; Leitão, J. H.; Carvalho, M. F. N. N. Ag(I) Camphorimine Complexes with Antimicrobial Activity Towards Clinically Important Bacteria and Species of the Candida Genus. *PLoS One* **2017**, *12*, No. e0177355.

(80) Andrejević, T. P.; Nikolić, A. M.; Glišić, B. Đ.; Wadepohl, H.; Vojnovic, S.; Zlatović, M.; Petković, M.; Nikodinovic-Runic, J.; Opsenica, I. M.; Djuran, M. I. Synthesis, Structural Characterization and Antimicrobial Activity of Silver(I) Complexes with 1-Benzyl-1h-Tetrazoles. *Polyhedron* **2018**, *154*, 325−333.

(81) Savić, N. D.; Petković, B. B.; Vojnovic, S.; Mojicevic, M.; Wadepohl, H.; Olaifa, K.; Marsili, E.; Nikodinovic-Runic, J.; Djuran, M. I.; Glišić, B. Đ. Dinuclear Silver(I) Complexes with a Pyridine-Based Macrocyclic Type of Ligand as Antimicrobial Agents against Clinically Relevant Species: The Influence of the Counteranion on the Structure Diversification of the Complexes. *Dalton Trans.* **2020**, *49*, 10880−10894.

(82) Panáček, A.; Kolář, M.; Večeřová, R.; Prucek, R.; Soukupová, J.; Kryštof, V.; Hamal, P.; Zbořil, R.; Kvítek, L. Antifungal Activity of Silver Nanoparticles against Candida Spp. *Biomaterials* **2009**, *30*, 6333−6340.

(83) Kim, K.-J.; Sung, W. S.; Suh, B. K.; Moon, S.-K.; Choi, J.-S.; Kim, J. G.; Lee, D. G. Antifungal Activity and Mode of Action of Silver Nano-Particles on Candida Albicans. *BioMetals* **2009**, *22*, 235−242.

(84) Matiadis, D.; Nowak, K. E.; Alexandratou, E.; Hatzidimitriou, A.; Sagnou, M.; Papadakis, R. Synthesis and (Fluoro)-Solvatochromism of Two 3-Styryl-2-Pyrazoline Derivatives Bearing Benzoic Acid Moiety: A Spectral, Crystallographic and Computational Study. *J. Mol. Liq.* **2021**, *331*, No. 115737.

(85) Azócar, M. I.; Gómez, G.; Levín, P.; Paez, M.; Muñoz, H.; Dinamarca, N. Review: Antibacterial Behavior of Carboxylate Silver(I) Complexes. *J. Coord. Chem.* **2014**, *67*, 3840−3853.

(86) Deacon, G. B.; Phillips, R. J. Relationships between the Carbon-Oxygen Stretching Frequencies of Carboxylato Complexes and the Type of Carboxylate Coordination. *Coord. Chem. Rev.* **1980**, *33*, 227−250.

(87) Wang, H.; Yan, A.; Liu, Z.; Yang, X.; Xu, Z.; Wang, Y.; Wang, R.; Koohi-Moghadam, M.; Hu, L.; Xia, W.; Tang, H.; Wang, Y.; Li, H.; Sun, H. Deciphering Molecular Mechanism of Silver by Integrated Omic Approaches Enables Enhancing Its Antimicrobial Efficacy in *E. coli*. *PLoS Biol.* **2019**, *17*, No. e3000292.

(88) Wang, H.; Wang, M.; Yang, X.; Xu, X.; Hao, Q.; Yan, A.; Hu, M.; Lobinski, R.; Li, H.; Sun, H. Antimicrobial Silver Targets Glyceraldehyde-3-Phosphate Dehydrogenase in Glycolysis of *E. coli*. *Chem. Sci.* **2019**, *10*, 7193−7199.

(89) Mikhailova, E. O. Silver Nanoparticles: Mechanism of Action and Probable Bio-Application. *J. Funct. Biomater.* **2020**, *11*, 84.

(90) Kalyakina, A. S.; Utochnikova, V. V.; Bushmarinov, I. S.; Ananyev, I. V.; Eremenko, I. L.; Volz, D.; Rönicke, F.; Schepers, U.; Van Deun, R.; Trigub, A. L.; Zubavichus, Y. V.; Kuzmina, N. P.; Bräse, S. Highly Luminescent, Water-Soluble Lanthanide Fluorobenzoates: Syntheses, Structures and Photophysics, Part I: Lanthanide Pentafluorobenzoates. *Chem. − Eur. J.* **2015**, *21*, 17921−17932.

(91) Kalyakina, A. S.; Utochnikova, V. V.; Zimmer, M.; Dietrich, F.; Kaczmarek, A. M.; Van Deun, R.; Vashchenko, A. A.; Goloveshkin, A. S.; Nieger, M.; Gerhards, M.; Schepers, U.; Bräse, S. Remarkable High Efficiency of Red Emitters Using Eu(Iii) Ternary Complexes. *Chem. Commun.* **2018**, *54*, 5221−5224.

(92) Kalyakina, A. S.; Utochnikova, V. V.; Bushmarinov, I. S.; Le-Deygen, I. M.; Volz, D.; Weis, P.; Schepers, U.; Kuzmina, N. P.; Bräse, S. Lanthanide Fluorobenzoates as Bio-Probes: A Quest for the Optimal Ligand Fluorination Degree. *Chem. − Eur. J.* **2017**, *23*, 14944−14953.

(93) Utochnikova, V. V.; Latipov, E. V.; Dalinger, A. I.; Nelyubina, Y. V.; Vashchenko, A. A.; Hoffmann, M.; Kalyakina, A. S.; Vatsadze, S. Z.; Schepers, U.; Bräse, S.; Kuzmina, N. P. Lanthanide Pyrazolecarboxylates for Oleds and Bioimaging. *J. Lumin.* **2018**, *202*, 38−46.

(94) Cota, I.; Marturano, V.; Tylkowski, B. Ln Complexes as Double Faced Agents: Study of Antibacterial and Antifungal Activity. *Coord. Chem. Rev.* **2019**, *396*, 49−71.

(95) Chen, F.; Moat, J.; McFeely, D.; Clarkson, G.; Hands-Portman, I. J.; Furner-Pardoe, J. P.; Harrison, F.; Dowson, C. G.; Sadler, P. J. Biguanide Iridium(Iii) Complexes with Potent Antimicrobial Activity. *J. Med. Chem.* **2018**, *61*, 7330−7344.

(96) Koch, R. *Dtsche med. Wochenschr.* **1890**, *16*, 756−757.

(97) Glišić, B. Đ.; Djuran, M. I. Gold Complexes as Antimicrobial Agents: An Overview of Different Biological Activities in Relation to the Oxidation State of the Gold Ion and the Ligand Structure. *Dalton Trans.* **2014**, *43*, 5950−5969.

(98) Dominelli, B.; Correia, J. D. G.; Kühn, F. E. Medicinal Applications of Gold(I/Iii)-Based Complexes Bearing N-Heterocyclic Carbene and Phosphine Ligands. *J. Organomet. Chem.* **2018**, *866*, 153−164.

(99) Mora, M.; Gimeno, M. C.; Visbal, R. Recent Advances in Gold−Nhc Complexes with Biological Properties. *Chem. Soc. Rev.* **2019**, *48*, 447−462.

(100) Harbut, M. B.; Vilchèze, C.; Luo, X.; Hensler, M. E.; Guo, H.; Yang, B.; Chatterjee, A. K.; Nizet, V.; Jacobs, W. R.; Schultz, P. G.; Wang, F. Auranofin Exerts Broad-Spectrum Bactericidal Activities by Targeting Thiol-Redox Homeostasis. *Proc. Natl. Acad. Sci.* **2015**, *112*, 4453−4458.

(101) Wu, B.; Yang, X.; Yan, M. Synthesis and Structure−Activity Relationship Study of Antimicrobial Auranofin against Eskape Pathogens. *J. Med. Chem.* **2019**, *62*, 7751−7768.

(102) Usón, R.; Laguna, A.; Laguna, M.; Jiménez, J.; Gómez, M. P.; Sainz, A.; Jones, P. G. Gold Complexes with Heterocyclic Thiones as Ligands. X-Ray Structure Determination of [Au(C5h5ns)2]Clo4. *J. Chem. Soc., Dalton Trans.* **1990**, 3457−3463.

Q

214

(103) Kinsch, E. M.; Stephan, D. W. Synthesis and Crystal and Molecular Structure of Mos4(Aupet3)2: A Linear Trinuclear Heterobimetallic Species. *Inorg. Chim. Acta* **1985**, *96*, L87–L90.

(104) Kim, P.; Zhang, C. C.; Thoröe-Boveleth, S.; Buhl, E. M.; Weiskirchen, S.; Stremmel, W.; Merle, U.; Weiskirchen, R. Analyzing the Therapeutic Efficacy of Bis-Choline-Tetrathiomolybdate in the Atp7b$^{-/-}$ Copper Overload Mouse Model. *Biomedicines* **2021**, *9*, 1861.

(105) Nct05047523. https://clinicaltrials.gov/ct2/show/NCT05047523?term=ALXN1840&draw=2&rank=9 (accessed 02.05.2022).

(106) Maliszewska, H. K.; Arnau del Valle, C.; Xia, Y.; Marín, M. J.; Waller, Z. A. E.; Muñoz, M. P. Precious Metal Complexes of Bis(Pyridyl)Allenes: Synthesis and Catalytic and Medicinal Applications. *Dalton Trans.* **2021**, *50*, 16739–16750.

(107) Maliszewska, H. K.; Hughes, D. L.; Muñoz, M. P. Allene-Derived Gold and Platinum Complexes: Synthesis and First Applications in Catalysis. *Dalton Trans.* **2020**, *49*, 4034–4038.

(108) Cook, S. M.; McArthur, J. D. Developing Galleria Mellonella as a Model Host for Human Pathogens. *Virulence* **2013**, *4*, 350–353.

(109) Ignasiak, K.; Maxwell, A. Galleria Mellonella (Greater Wax Moth) Larvae as a Model for Antibiotic Susceptibility Testing and Acute Toxicity Trials. *BMC Res. Notes* **2017**, *10*, 428.

(110) Martin, J. K.; Sheehan, J. P.; Bratton, B. P.; Moore, G. M.; Mateus, A.; Li, S. H.-J.; Kim, H.; Rabinowitz, J. D.; Typas, A.; Savitski, M. M.; Wilson, M. Z.; Gitai, Z. A Dual-Mechanism Antibiotic Kills Gram-Negative Bacteria and Avoids Drug Resistance. *Cell* **2020**, 1518–1532.

(111) Tsai, C. J.-Y.; Loh, J. M. S.; Proft, T. Galleria Mellonella Infection Models for the Study of Bacterial Diseases and for Antimicrobial Drug Testing. *Virulence* **2016**, *7*, 214–229.

(112) Güntzel, P.; Nagel, C.; Weigelt, J.; Betts, J. W.; Pattrick, C. A.; Southam, H. M.; La Ragione, R. M.; Poole, R. K.; Schatzschneider, U. Biological Activity of Manganese(I) Tricarbonyl Complexes on Multidrug-Resistant Gram-Negative Bacteria: From Functional Studies to in Vivo Activity in Galleria Mellonella†. *Metallomics* **2019**, *11*, 2033–2042.

(113) Vincent, F.; Nueda, A.; Lee, J.; Schenone, M.; Prunotto, M.; Mercola, M. Phenotypic Drug Discovery: Recent Successes, Lessons Learned and New Directions. *Nat. Rev. Drug Discovery* **2022**, 1.

(114) Mendes, S. S.; Marques, J.; Mesterházy, E.; Straetener, J.; Arts, M.; Pissarro, T.; Reginold, J.; Berscheid, A.; Bornikoel, J.; Kluj, R. M.; Mayer, C.; Oesterhelt, F.; Friães, S.; Royo, B.; Schneider, T.; Brötz-Oesterhelt, H.; Romão, C. C.; Saraiva, L. M.Synergetic Antimicrobial Activity and Mechanism of Clotrimazole-Linked Co-Releasing Molecules. *ACS Bio & Med Chem Au* 2022, DOI: 10.1021/acsbiomedchemau.2c00007.

(115) Wenzel, M.; Patra, M.; Senges, C. H. R.; Ott, I.; Stepanek, J. J.; Pinto, A.; Prochnow, P.; Vuong, C.; Langklotz, S.; Metzler-Nolte, N.; Bandow, J. E. Analysis of the Mechanism of Action of Potent Antibacterial Hetero-Tri-Organometallic Compounds: A Structurally New Class of Antibiotics. *ACS Chem. Biol.* **2013**, *8*, 1442–1450.

(116) Romero-Canelón, I.; Sadler, P. J. Systems Approach to Metal-Based Pharmacology. *PNAS* **2015**, *112*, 4187–4188.

(117) Fisher, M. C.; Alastruey-Izquierdo, A.; Berman, J.; Bicanic, T.; Bignell, E. M.; Bowyer, P.; Bromley, M.; Brüggemann, R.; Garber, G.; Cornely, O. A.; Gurr, S. J.; Harrison, T. S.; Kuijper, E.; Rhodes, J.; Sheppard, D. C.; Warris, A.; White, P. L.; Xu, J.; Zwaan, B.; Verweij, P. E. Tackling the emerging threat of antifungal resistance to human health. *Nat Rev Microbiol.* **2022**, *9*, 557–571.

■ NOTE ADDED IN PROOF

An excellent review on the emerging threat of antifungal resistance was published during proof corrections.[117]

Angelo Frei*[a,b], Alysha G. Elliott[a], Alex Kan[c], Hue Dinh[d], Stefan Bräse[e], Alice E. Bruce[f], Mitchell R. Bruce[f], Feng Chen[g], Dhirgam Humaidy[f], Nicole Jung[e], A. Paden King[h], Peter G. Lye[i], Hanna K. Maliszewska[j], Ahmed M. Mansour[k], Dimitris Matiadis[l], María Paz Muñoz[j], Tsung-Yu Pai[k], Shyam Pokhrel[f], Peter J. Sadler[g], Marina Sagnou[l], Michelle Taylor[i], Justin J. Wilson[h], Dean Woods[i], Johannes Zuegg[a], Wieland Meyer[c], Amy K. Cain[d], Matthew A. Cooper[a], Mark A. T. Blaskovich*[a]

[a] Centre for Superbug Solutions, Institute for Molecular Bioscience, The University of Queensland, St. Lucia, Queensland 4072 (Australia).

[b] Dept. of Chemistry, Biochemistry & Pharmaceutical Sciences, University of Bern, Freiestrasse 3, 3012 Bern, Switzerland

[c] Molecular Mycology Research Laboratory, Centre for Infectious Diseases and Microbiology, Faculty of Medicine and Health, Sydney Medical School, Westmead Clinical School, Sydney Institute for Infectious Diseases, Westmead Hospital-Research and Education Network, Westmead Institute for Medical Research, University of Sydney, Sydney, NSW, Australia

[d] School of Natural Sciences, ARC Centre of Excellence in Synthetic Biology, Macquarie University, Sydney, NSW 2109 (Australia)

[e] Institute of Organic Chemistry, Karlsruhe Institute of Technology, Fritz-Haber-Weg 6, 76131 Karlsruhe (Germany). Institute of Toxicology and Genetics, Karlsruhe Institute of Technology, Hermann-von-Helmholtz-Platz 1, 76344 Eggenstein-Leopoldshafen (Germany).

[f] University of Maine, Department of Chemistry, Orono, ME, USA

[g] Department of Chemistry, University of Warwick, Gibbet Hill Road, Coventry CV4 7AL (UK).

[h] Department of Chemistry and Chemical Biology, Cornell University, Ithaca, NY 14853 (USA).

[i] School of Science and Technology, University of New England, Armidale, NSW 2351, Australia

[j] School of Chemistry, University of East Anglia, Norwich Research Park, Norwich, NR4 7TJ

[k] Chemistry Department, Faculty of Science, Cairo University (Egypt).

[l] Institute of Biosciences & Applications, National Centre for Scientific Research "Demokritos", 15310 Athens, Greece

*angelo.frei@unibe.ch, m.blaskovich@uq.edu.au

1

216

Microbial Strain and Other Abbreviations

Table S1. Glossary of abbreviations used in this document

G-ve	Gram negative
G+ve	Gram positive
Ab	*Acinetobacter baumannii* ATCC 19606 type strain
Ec	*Escherichia coli* ATCC 25922 FDA control strain
Kp	*Klebsiella pneumoniae* ATCC 700603 ESBL
Pa	*Pseudomonas aeruginosa* ATCC 27853 QC control strain
MRSA	Methicillin resistant *Staphylococcus aureus* ATCC 43300
Ca	*Candida albicans* ATCC 90028 NCCLS11
Cn H99	*Cryptococcus neoformans* H99 ATCC 208821 type strain
HEK	HEK-293 human embryonic kidney cells ATCC CRL-1573
RBC	Human red blood cells
CC50	cytotoxicity concentration 50%
HC10	hemolysis concentration 10% against RBC

Experimental Details

Synthesis of complexes Ag1 and Ag2.

A solution of the corresponding pyrazolines[1] (0.16 mmol) in MeOH (1 mL) was added slowly to an aqueous KOH solution (1%, 0.9 mL) at room temperature under stirring. A solution of $AgNO_3$ (27 mg, 0.16 mmol) in H_2O (0.3 mL) was subsequently added in the absence of light. A yellow solid precipitated immediately occurred. The mixture was stirred for 30 more minutes and then, the dark brown solid was filtered using Büchner funnel, washed with ethanol (x2) and water (x2) and dried under vacuum and P_2O_5. The products were protected from light at any time.

*(E)-1-(4-Carboxyphenyl)-5-(3,4-dimethoxyphenyl)-3-(3,4-dimethoxystyryl)-2-pyrazoline silver(I) complex Ag1*

Dark green solid (45 mg, 48% calculated for 0.08 mmol maximum yield); FT-IR (KBr, cm^{-1}): 1595, 1510, 1375, 1260, 1135, 1025, 770, 515; ^{1}H NMR (DMSO-d_6) δ: 2.98 (1H, dd, J_{MX} = 4.9 Hz, J_{AM} = 16.9 Hz, CH$_A$H$_M$), 3.69 (3H, s, MeO),

2

3.71 (3H, s, MeO), 3.76 (1H, overlapped, CH_AH$_M$), 3.76 (3H, s, MeO), 3.81 (3H, s, MeO), 5.43 (1H, dd, J_{MX} = 5.1 Hz, J_{AX} = 11.9 Hz, CH_X), 6.68 (1H, d, J = 8.3 Hz, H28), 6.73 (1H, d, J = 16.2 Hz, H16), 6.87-6.91 (4H, m, H21, H29, H32), 6.93 (1H, d, J = 8.4 Hz, H21), 7.06 (1H, d, J = 8.4 Hz, H22), 7.19 (1H, d, J = 16.2 Hz, H15), 7.24 (1H, s, H18), 7.71 (2H, d, J = 8.6 Hz, H8, H10); ^{13}C NMR (DMSO-d_6) δ: 41.9 (C4), 55.4 (CH$_3$O-), 55.5 (CH$_3$O-), 62.2 (C5), 109.2 (C18), 109.6 (C32), 111.6 (C7, C11), 111.7 (C29), 112.2 (C21), 117.4 (C28), 119.1 (C15), 121.7 (C9), 120.5 (C22), 129.4 (C17), 130.8 (C8, C10), 134.0 (C27), 134.5 (C16), 145.4 (C6), 148.0 (C30), 149.0 (C31), 149.1 (C20), 149.2 (C19), 150.3 (C3), 170.0 (-COOH).

1-(4-Carboxyphenyl)-3-{(1E,3E)-4-phenylbuta-1,3-dien-1-yl}-5-{(E)-styryl}-2-pyrazoline silver(I) complex Ag2

Dark brown solid (43 mg, 51% calculated for 0.08 mmol maximum yield); FT-IR (KBr, cm^{-1}): 1595, 1535, 1510, 1370, 1320, 1125, 980, 745, 690, 500; ^{1}H NMR (DMSO-d_6) δ: 3.01 (1H, dd, J_{MX} = 5.2 Hz, J_{AM} = 16.8 Hz, CH_AH$_M$), 3.51 (1H, dd, J_{AX} = 11.5 Hz, J_{AM} = 16.8 Hz, CH_AH$_M$), 5.19 (1H, ddd, J_{MX} = 5.2 Hz, J_{AX} = 11.5 Hz, J_{XH15b}= 7.6 Hz, CH_X), 6.28 (1H, dd, $J_{H15bH16b}$ = 16.0 Hz, $J_{H15'X}$ = 7.6 Hz, H-15b), 6.67 (1H, d, J = 16.0 Hz, H-16b), 6.69 (1H, d, J = 15.8 Hz, H-16), 6.77 (2H, d overlapped, H-15a, H-16a), 7.06 (d, 2H, J = 8.7 Hz, H-7, H-11), 7.13-7.27 (3H, m, H-15, H-20, H-30), 7.30 (2H, t, J = 7.6 Hz, H-29, H-31), 7.36 (2H, t, J = 7.6 Hz, H-19, H-21), 7.43 (2H, d, J = 7.6 Hz, H-28, H-32), 7.52 (2H, d, J = 7.6 Hz, H-18, H-22), 7.79 (d, 2H, J = 8.7 Hz, H-8, H-10); ^{13}C NMR (DMSO-d_6) δ: 38.7 (C-4), 61.2 (C-5), 112.0 (C-7, C-11), 122.7 (C-9), 125.1 (C-15), 126.49 (Ph), 126.52 (C-18, C-22), 127.9 (C-15b), 128.4, 128.6, 128.8, 128.83, 128.93 (Ph), 130.8 (C-8, C-10), 131.2 (C-16b), 134.0, 134.6, 136.0 (C-16, C-15a, C-16a), 136.8 (C-17), 142.3 (C-27), 145.6 (C-6), 150.7 (C-3), 168.4 (-COOH).
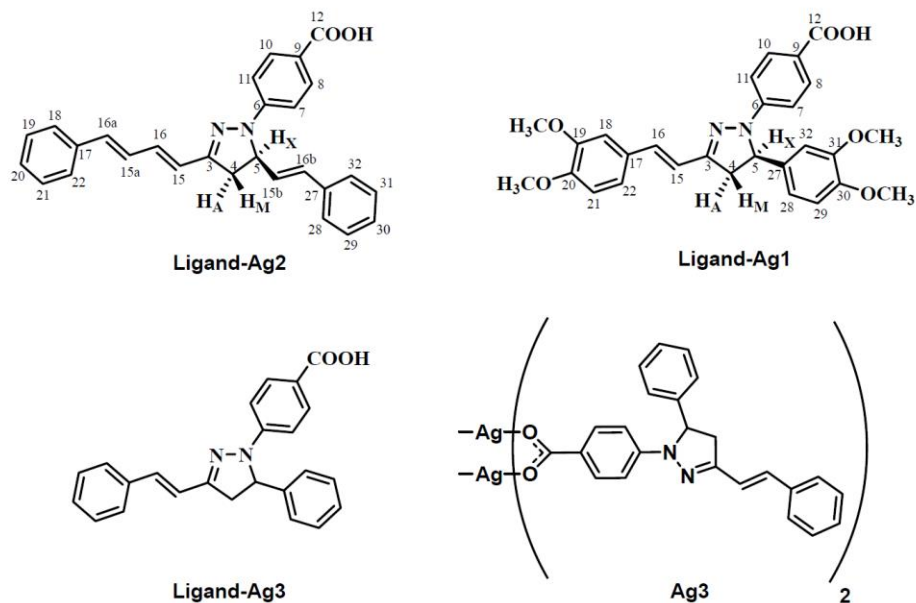
Figure S1. Structures of complex **Ag3** and ligands used to prepare the complexes **Ag1**, **Ag2** and **Ag3**. Numbering of compounds **Ligand-S1** and **Ligand-S2** is according to the numbering of published X-ray structure [1] to describe the AMX system and the NMR assignments of the products **Ag1** and **Ag2**. The products are racemic but single molecules are shown for clarity and simplicity purposes.

Table S2. MIC, CC50 and HC10 values for selected **silver** analogues (values given in μg/mL).

	G-ve				G+ve	Fungi		HEK CC$_{50}$	RBC HC$_{10}$	
	Ab	Ec	Kp	Pa	MRSA	Ca	Cn			Unit
Ligand-Ag2#	>32	>32	>32	>32	>32	>32	>32	n.d.	n.d.	μg/mL
Ligand-Ag1#	>32	>32	>32	>32	>32	>32	>32	n.d.	n.d.	μg/mL

3

Ligand-Ag3#	>32	>32	>32	>32	>32	>32	>32	n.d.	n.d.	µg/mL
Ag3	>32	>32	>32	>32	>32	16	16	>32	>32	µg/mL
AgNO₃	≤0.25	≤0.25	≤0.25	≤0.25	2	≤0.25	≤0.25	>32	8.9	µg/mL

#This compound showed no inhibition in the single concentration (32 µg/mL) CO-ADD Primary Screening and was hence not evaluated in a dose-response assay. n.d.: not determined
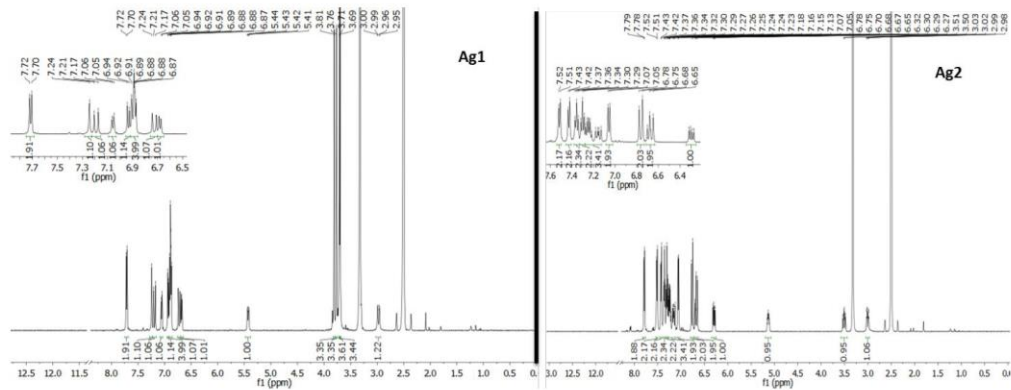

Figure S2. ^{1}H NMR spectra of complexes **Ag1** and **Ag2** in DMSO-d_6.
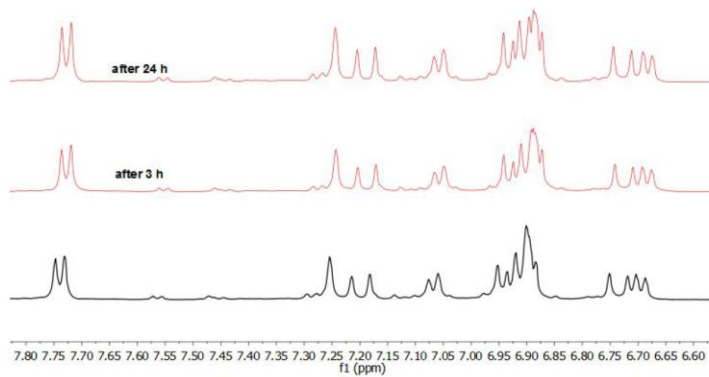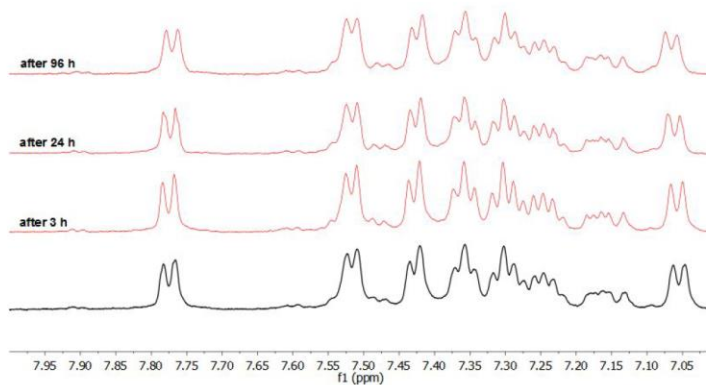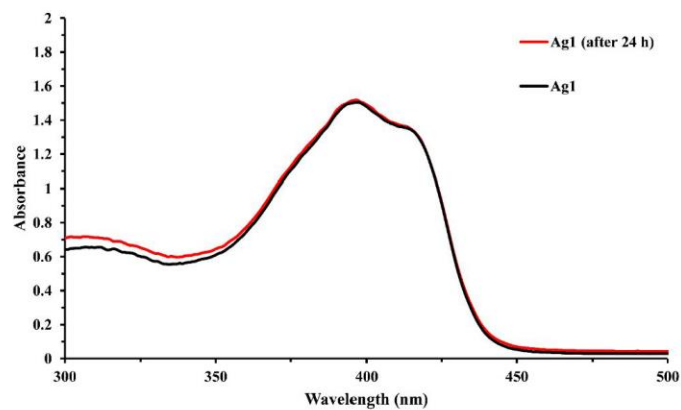

Figure S3. Superimposed ^{1}H NMR spectra of silver(I) complex **Ag1** for stability test – t = 0, 3, 24 h.

Figure S4. Superimposed ^{1}H NMR spectra of silver(I) complex **Ag2** (red) with ligand (black). For stability – t = 0, 3, 24, 96 h.

Figure S5. UV-Vis Stability test for compound **Ag1** in 10% DMSO (20 µM) over 24 h.

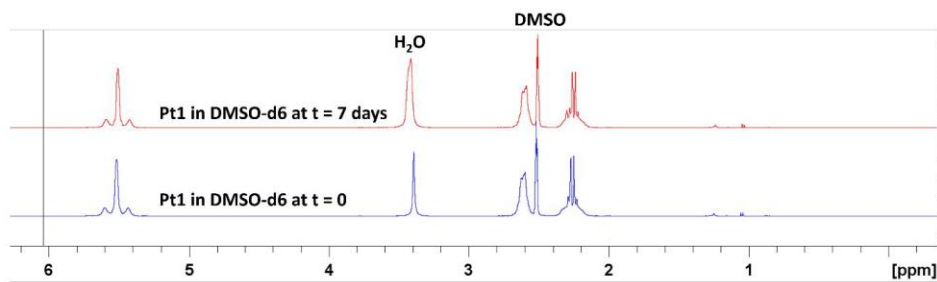**Figure S6.** 1H NMR spectrum of **Pt1** in DMSO-d6 after 0 days and after 7 days at room temperature.

Eu-S1

Eu-S2

Eu-S3

Eu1

Eu-S4

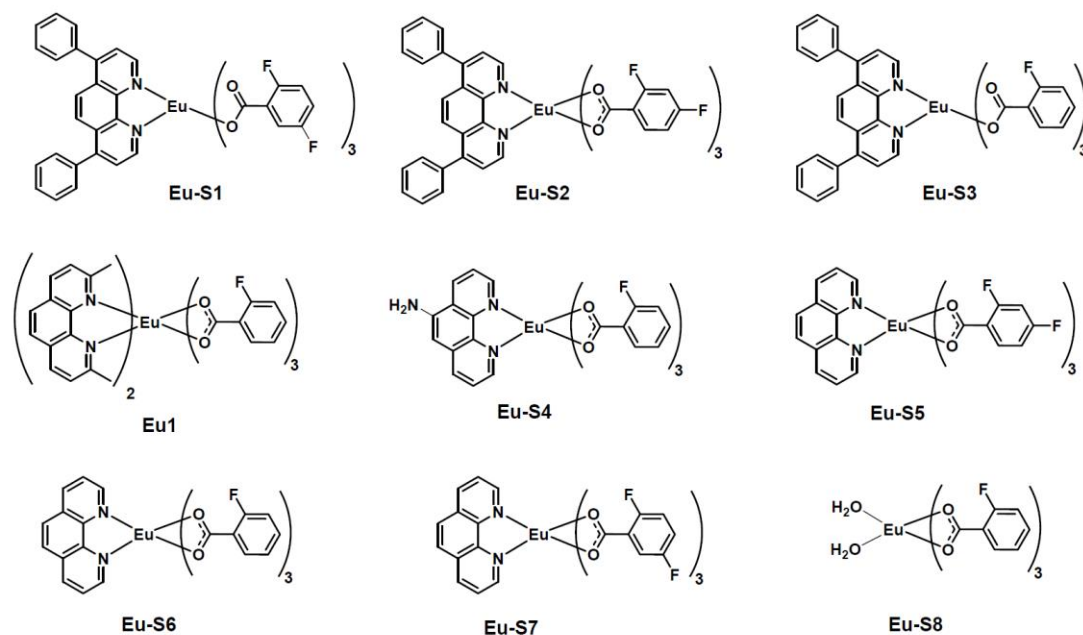Eu-S5

Eu-S6

Eu-S7

Eu-S8

Figure S7. Structures of selected **europium** analogues.

Table S3. MIC, CC50 and HC10 values for selected **europium** analogues (values given in µg/mL).

	G-ve				G+ve	Fungi		HEK CC$_{50}$	RBC HC$_{10}$	Unit
	Ab	Ec	Kp	Pa	Sa	Ca	Cn			
Eu-S1	>20	>20	>20	>20	10	>20	5	>20	>20	µM
Eu-S2	>20	>20	>20	>20	1.25	10	0.625	15.9	0.7	µM
Eu-S3	>20	>20	>20	>20	10	20	5	14.7	>20	µM
Eu1	>20	>20	>20	>20	>20	≤0.16	≤0.16	>20	>20	µM
Eu-S4	>20	>20	>20	>20	>20	>20	20	3.3	1.2	µM
Eu-S5	>20	>20	>20	>20	>20	>20	20	13.6	0.5	µM
Eu-S6	>20	>20	>20	>20	>20	20	20	9.9	>20	µM
Eu-S7[#]	n.a.	n.a.	n.a.	n.a.	n.a.	n.a.	n.a.	n.a.	n.a.	µM
Eu-S8[#]	n.a.	n.a.	n.a.	n.a.	n.a.	n.a.	n.a.	n.a.	n.a.	µM

6

#This compound showed no inhibition in the single concentration (20 μM) CO-ADD Primary Screening and was hence not evaluated in a dose-response assay.
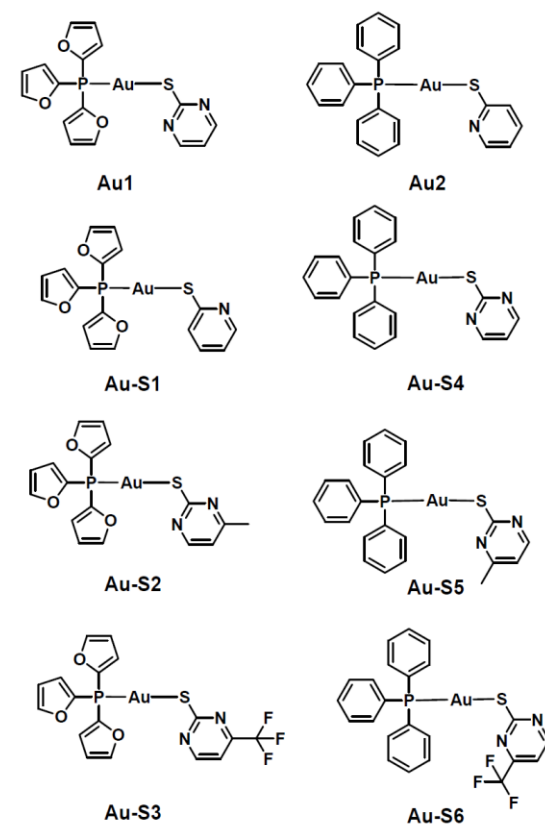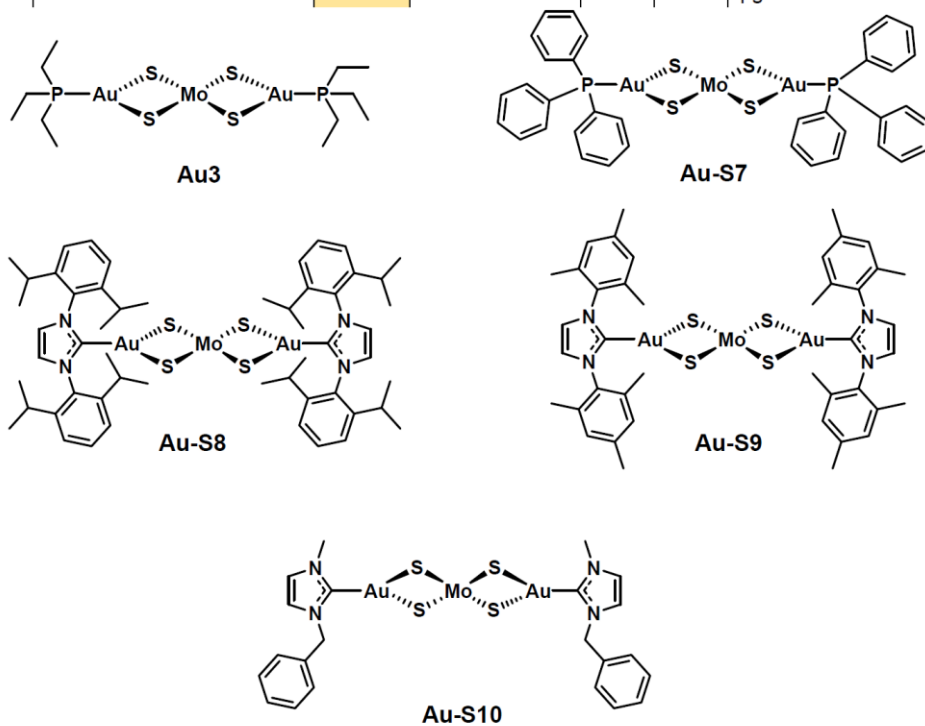

Figure S8. Structures of selected **gold** analogues.

Table S4. MIC, CC50 and HC10 values for selected **gold** analogues (values given in μg/mL).

	G-ve		G+ve	Fungi			

	Ab	Ec	Kp	Pa	Sa	Ca	Cn	HEK CC_{50}	RBC HC_{10}	
Au1	n.d.	n.d.	n.d.	>32	≤0.25	≤0.25	≤0.25	>32	>32	µg/mL
Au-S1	>32	>32	>32	>32	16	16	16	>32	>32	µg/mL
Au-S2	>32	>32	>32	>32	>32	>32	>32	1.38	>32	µg/mL
Au-S3	>32	>32	>32	>32	≤0.25	>32	>32	>32	>32	µg/mL
Au2	>32	>32	>32	>32	≤0.25	≤0.25	≤0.25	>32	>32	µg/mL
Au-S4	>32	>32	>32	>32	>32	>32	>32	>32	>32	µg/mL
Au-S5	>32	>32	>32	>32	>32	>32	>32	>32	>32	µg/mL
Au-S6	>32	>32	>32	>32	≤0.25	>32	>32	>32	>32	µg/mL

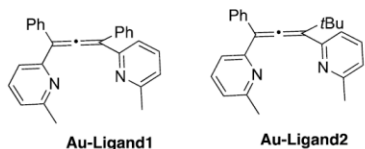

Au3

Au-S7

Au-S8

Au-S9

Au-S10

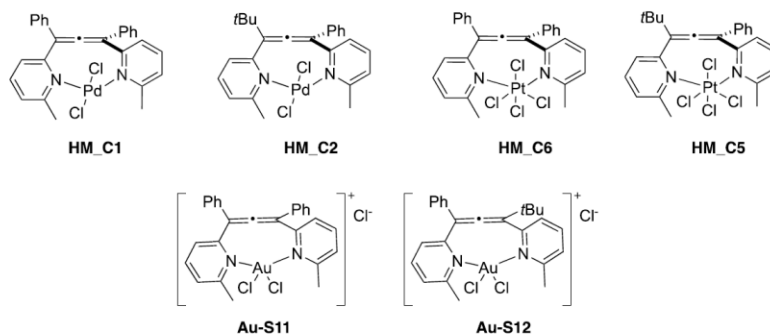**Figure S9.** Structures of selected **gold-molybdenum** analogues.

Table S5. MIC, CC50 and HC10 values for selected **gold-molybdenum** analogues (values given in µg/mL).

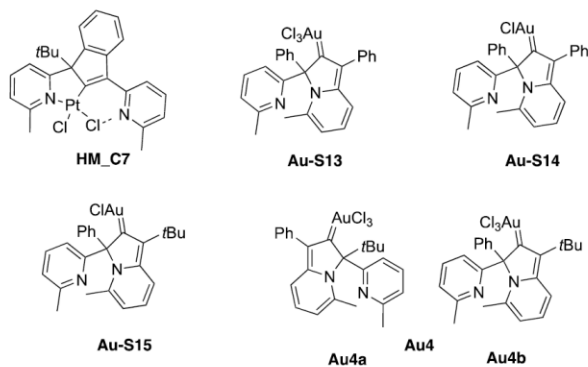|	G-ve				G+ve	Fungi		HEK	RBC	
	Ab	Ec	Kp	Pa	Sa	Ca	Cn	CC_{50}	HC_{10}	
Au3	>32	>32	>32	>32	≤0.25	16	≤0.25	>32	>32	µg/mL
Au-S7#	>32	>32	>32	>32	>32	>32	>32	n.d.	n.d.	µg/mL
Au-S8#	>32	>32	>32	>32	>32	>32	>32	n.d.	n.d.	µg/mL
Au-S9#	>32	>32	>32	>32	>32	>32	>32	n.d.	n.d.	µg/mL
Au-S10	>32	>32	>32	>32	>32	≤0.25	>32	>32	>32	µg/mL

#This compound showed no inhibition in the single concentration (32 µg/mL) CO-ADD Primary Screening and was hence not evaluated in a dose-response assay for MIC evaluation. Values shown for these compounds as >32 µg/mL was a single point concentration assay, n=2.

8

Figure S10. Structures of selected **gold/platinum/palladium** analogues.

Table S6. MIC, CC50 and HC10 values for selected **gold/platinum/palladium** analogues (values given in µg/mL).[2]

| | G-ve | | | | G+ve | Fungi | | HEK | RBC | |
	Ab	Ec	Kp	Pa	Sa	Ca	Cn	CC$_{50}$	HC$_{10}$	
Au-Ligand1	n.a.	n.a.	n.a.	n.a.	n.a.	n.a.	n.a.	n.a.	n.a.	µg/mL
Au-Ligand1	n.a.	n.a.	n.a.	n.a.	n.a.	n.a.	n.a.	n.a.	n.a.	µg/mL
Au-S11	>32	32	>32	>32	16	4	16	>32	>32	µg/mL
Au-S12	>32	>32	>32	>32	16	4	<=0.25	>32	<=0.25	µg/mL
Au-S13	32	16	16	>32	<=0.25	2	<=0.25	>32	19.3	µg/mL
Au-S14	32	>32	32	>32	<=0.25	<=0.25	<=0.25	0.7	23.7	µg/mL
Au-S15	32	>32	32	32	2	<=0.25	<=0.25	>32	>32	µg/mL
Au4	32	32	32	>32	0.5	1	<=0.25	>32	>32	µg/mL
HM_C1	>32	>32	>32	>32	2	16	1	1.0	>32	µg/mL
HM_C2	32	>32	>32	>32	<=0.25	<=0.25	<=0.25	1.1	>32	µg/mL
HM_C5	>32	>32	>32	>32	>32	32	>32	>32	>32	µg/mL

9

HM_C6	n.a.	n.a.	n.a.	n.a.	n.a.	n.a.	n.a.	n.a.	n.a.	µg/mL
HM_C7	>32	>32	>32	>32	2	4	2	14.5	>32	µg/mL

Table S7. Cytotoxicity (CC_{50}) and haemolysis (HC_{10}) ranges obtained for highly active compounds upon retesting. Therapeutic Index (**TI**) with respect to cytotoxicity (**TI_CC50**) and haemoysis (**TI_HC10**) is given against the best MIC measured. The **Minimum TI** is the lowest TI obtained in either TI_CC50 or TI_HC10. Highlighted compounds were advanced to *in vivo* toxicity screening in *G. mellonella* based on TI and compound availability.

	HEK293 CC50	RBC HC10	TI_CC50	TI_HC10	Minimum TI
Co1	>100	>100	256	256	256
Ni1	>200	>200	80	80	80
Rh1	>200	0.4-3	513	1-9	1
Pd1	>100	10	128	13	13
Pd2	38-53	0.2-3	1563 - 2192	10-130	10
Pd3	89-123	17-56	14,733 - 20,433	2900-9350	2900
Ag1	3-4	13-154	417 - 683	2117-25,600	2117
Ag2	6-7	>200	933 -1117	33,333	933
Eu1	>200	>200	33,333	33,333	33,333
Ir1	73-96	23-200	3029 - 3992	8333	3029
Ir2	62-65	2-76	2600 - 2717	3154	2600
Ir3	54-76	3-41	4450 - 6300	3383	3383
Pt1	>100	>100	64	64	64
Pt2	>100	>100	128	128	128
Pt3	>100	>100	8	8	8
Pt4	>100	>100	128	128	128
Pt5	16-130	>200	2667 - 21,667	33,333	2667
Au1	0.1-0.6	90-200	5 - 25	3746-8333	5
Au2	0.8-200	>200	35 - 8333	8333	35
Au3	139-170	200	44 - 54	64	44
Au4	200	200	33,333	33,333	33,333

10

Table S8. Molecular Formula and Molecular Weight for highly active compounds highlighted in the paper.

ID	Molecular Formula	MW
Co1	C12H18CoN11O3S2	487.4037
Ni1	C44H34B2F8N6Ni	705.4914
Rh1	C20H30Cl4Rh2	618.0710
Pd1	C8H12Cl2Pd	285.5040
Pd2	C26H24N2O6Pd2S2	737.4460
Pd3	C23H21Cl3N5Pd1.5	633.4365
Ag1	C64H62Ag2N4O12	1190.80
Ag2	C56H46Ag2N4O4	1054.74
Eu1	C49H36EuF3N4O6	985.8082
Ir1	C38H42BrClIrN5O2S	940.4180
Ir2	C36H36ClIrN6O4S	876.4490
Ir3	C42H44ClIrN6O2S	924.5810
Pt1	C8H12Cl2Pt	374.1680
Pt2	C8H12I2Pt	557.0769
Pt3	C36H36ClIrN6O4S	876.4490
Pt4	C12H19ClOPt	409.8170
Pt5	C23H21Cl3N5Pt1.5-	766.4325
Au1	C16H12AuN2O3PS	540.2833
Au2	C23H19AuNPS	569.4123
Au3	C12H30Au2MoP2S4	854.4437
Au4	C25H26AuCl3N2	657.8136

11

Table S9. Extended panel MICs (*50% inhibition, MIC score 2, μM)

MIC*	Candida albicans	Candida auris	Candida auris	Candida glabrata	Candida tropicalis	Cryptococcus deuterogattii	Cryptococcus deuterogattii	Cryptococcus neoformans
	ATCC 90028	CBS10913	CBS12373	ATCC 90030	ATCC 750	CBS7750	ATCC 32609	ATCC 208821
	NCCLS 11	JCM 15448;DSM 21092; CBS 10913	KCTC 17810	NCCLS 84	QC strain for susceptibility testing	VGII; Serotype B	VGII	H99; VN1
ID	MIC50 [μM] *							
Co1								
Ni1	>160	≥160	2.5 - 20	≥160	160	5 - 10	5 - 10	2.5 - 5
Rh1	0.391 - 1.56	0.781- 1.56	0.391 - 0.781	0.391 - 6.25	0.391 - 0.781	0.391	0.78 - 1.56	0.195 - 0.391
Pd1								
Pd2	0.049 - 0.195	0.024 - 0.098	0.024 - 0.049	0.012 - 0.195	0.195 - 0.391	≤0.006	0.024 - 0.098	≤0.006 - 0.024
Pd3	0.012 - 0.024	≤0.006	≤0.006	0.012 - 0.024	≤0.006 - 0.024	0.012 - 0.024	0.012 - 0.024	0.012 - 0.049
Ag1	≤0.006	≤0.006	≤0.006	≤0.006	≤0.006	≤0.006	≤0.006 - 0.024	≤0.006
Ag2	≤0.006 - 0.098	≤0.006 - 0.049	≤0.006 - 0.098	0.006 - 0.195	≤0.006 - 0.049	≤0.006 - 0.049	≤0.006 - 0.098	≤0.006 - 0.098
Eu1	≤0.006 - 0.012	≤0.006	≤0.006	0.012 - 0.049	≤0.006 - 0.049	0.024 - 0.098	0.024	≤0.006
Ir1	0.049 - 0.098	0.098	0.049	0.098 - 0.195	0.098 - 0.195	0.024	0.098 - 0.195	0.024 - 0.049
Ir2	0.049 - 0.098	0.049 - 0.098	0.024	0.098 - 0.195	0.098 - 0.195	0.012 - 0.024	0.098 - 0.195	0.024 - 0.098
Ir3	0.049	0.098	0.024 - 0.049	0.098	0.098	0.024	0.049 - 0.098	0.024
Pt1								
Pt2								
Pt3								
Pt4								
Pt5	≤0.006 - 0.049	≤0.006 - 0.024	≤0.006 - 0.024	≤0.006 - 0.024	≤0.006 - 0.024	≤0.006 - 0.098	≤0.006 - 0.049	≤0.006 - 0.049
Au1	0.049 - 0.391	0.098 - 0.195	0.098 - 0.391	0.098 - 0.391	0.049 - 0.391	0.024 - 0.098	0.024 - 0.049	0.098 - 0.195
Au2	0.098 - >200	0.098 - 1.56	0.098 - 0.195	>200	≥200	0.049 - 1.56	0.049 - 0.195	0.024 - 0.195
Au3	3.13 - 200	3.13 - 6.25	3.13 - 200		6.25 - 100	3.12 - 100	3.12 - 6.25	3.12 - 6.25
Au4*	0.195 - 0.391	0.195 - 0.391	≤0.006 - 0.049	0.781 - 6.25	1.56 - 6.25	0.098 - 0.195	0.024 - 0.049	0.098 - 0.195

*Two new samples of Au4 (1:2 and 1:0.7 (Au4a:Au4b)) were received for further testing. Both mixtures gave the same MIC values across all assays. NA: MIC value not available due to wide replicate variation.

12

Table S10. Comparator MICs of antifungals, µg/mL

	Candida albicans	Candida auris	Candida auris	Candida glabrata	Candida tropicalis
	ATCC 90028	CBS10913	CBS12373	ATCC 90030	ATCC 750
(*) MIC = ≥80% inhibition	NCCLS 11	JCM 15448	KCTC 17810	NCCLS 84	QC strain for susceptibility testing
ID	**MIC* [µg/mL]**				
Itraconazole	0.062 - 0.25	0.063	2	32	2
Amphotericin B	0.125 - 1	16	>128	≥64	2 - 4
Micafungin	≤0.0005	≤0.001	2	4 - 32	0.008 - 0.063
5-Fluorocytosine	≤0.001	≤0.002	≤0.002	>32	0.001 - 0.002
Posaconazole	0.001 - 0.031	0.031 - 0.063	2	2	0.125
Ketoconazole	0.002 - 0.004	0.004 - 0.016	≤0.004	NT	NT
Fluconazole	0.004	≤0.004	≤0.004	NT	NT
Voriconazole	0.008	0.004 - 0.008	0.156	NT	NT
Caspofungin	0.391 - 1.56	6.25	12.5	6.25 - 12.5	1.56
Anidulafungin	0.031 - 0.125	0.031 - 0.125	0.25	0.008	0.004 - 0.008

	Cryptococcus deuterogattii	Cryptococcus deuterogattii	Cryptococcus neoformans
	CBS7750	ATCC 32609	ATCC 208821
(*) MIC = ≥80% inhibition	VGII; Serotype B	VGII	H99; VN1

13

ID	MIC* [µg/mL]		
Itraconazole	2 - 4	2 - 8	1 - 2
Amphotericin B	1 - 8	4 - 16	2 - 8
Micafungin	0.06 - 0.125	0.016 - 0.125	0.015 - 0.063
5-Fluorocytosine	0.06 - 0.25	0.002 - 0.25	0.001 - 0.016
Posaconazole	0.06 - 0.125	0.015 - 0.25	0.016 - 0.125
Ketoconazole	NT	NT	>64
Fluconazole	NT	NT	2 - 4
Voriconazole	NT	NT	≥64
Caspofungin	0.06 - 0.1	0.1 - 0.63	0.098 - 1.56
Anidulafungin	0.06 - 0.25	0.003 - 0.25	0.016 - 0.125

Table S11. Comparator MICs of antifungals, μM

	Candida albicans	Candida auris	Candida auris	Candida glabrata	Candida tropicalis
	ATCC 90028	CBS10913	CBS12373	ATCC 90030	ATCC 750
(*) MIC = ≥80% inhibition	NCCLS 11	JCM 15448	KCTC 17810	NCCLS 84	QC strain for susceptibility testing
ID	MIC* [µM]				
Itraconazole	0.089 - 0.354	0.089	2.83	45	2.83
Amphotericin B	0.192 - 1.53	24.5	≥196	≥98.2	3.01 - 6.13
Micafungin	≤0.0007	≤0.0014	2.23	4.45 - 35.7	0.009 - 0.070
5-Fluorocytosine	≤0.012	≤0.021	≤0.021	>351	0.012 - 0.021
Posaconazole	0.002 - 0.063	0.063- 0.126	4.04	4.04	0.253
Ketoconazole	0.005 - 0.010	0.010 - 0.042	≤0.01	NT	NT
Fluconazole	0.018	≤0.018	≤0.018	NT	NT
Voriconazole	0.032	0.016 - 0.032	0.447	NT	NT
Caspofungin	0.357 - 1.43	5.72	11.4	5.72 - 11.4	1.43
Anidulafungin	0.027 - 0.110	0.027 - 0.110	0.219	0.007	0.003 - 0.007

	Cryptococcus deuterogattii	Cryptococcus deuterogattii	Cryptococcus neoformans
	CBS7750	ATCC 32609	ATCC 208821
(*) MIC = ≥80% inhibition	VGII; Serotype B	VGII	H99; VN1
ID	MIC* [µM]		
Itraconazole	2.83 - 5.67	2.83 - 11.3	1.42 - 2.83
Amphotericin B	1.53 - 12.3	6.13 - 24.5	3.01 - 12.3

14

Micafungin	0.070 - 0.139	0.017 - 0.139	0.017 - 0.070
5-Fluorocytosine	0.686 - 2.75	0.021 - 2.75	0.0107 - 0.172
Posaconazole	0.126 - 0.253	0.032 - 0.506	0.032 - 0.253
Ketoconazole	NT	NT	>170
Fluconazole	NT	NT	9.25 - 18.5
Voriconazole	NT	NT	≥260
Caspofungin	0.029 - 0.089	0.089 - 0.057	0.089 - 1.43
Anidulafungin	0.055 - 0.219	0.003 - 0.219	0.014 - 0.110

Table S12. Antifungal MW (g/mol) used for concentration conversion.

ID	Abbreviation	Class	MW
Itraconazole	ITC/ITR	azole	705.64
Amphotericin B	AMB	polyene	924.079
Micafungin	MFG/MICA	echinocandins	1270.28
5-Fluorocytosine	5FC	pyrimidine	129.093
Posaconazole	POS	azole	700.8
Ketoconazole	KCZ/KTC	azole	531.43
Fluconazole	FCZ/FLC	azole	306.271
Voriconazole	VRC/VOR	azole	349.311
Caspofungin	CAS	echinocandins	1093.3
Anidulafungin	AFG/ANI	echinocandins	1140.2

Table S13. Characterization Data reference for the highly active compounds highlighted in the manuscript.

Compound	Data	Reference
Co1	Published, Complex **1**	https://doi.org/10.1002/chem.202003545
Ni1	Added below	unpublished
Rh1	Published (common synthon)	e.g. https://doi.org/10.1002/ejic.201700199
Pd1	Published, **Pd1**	https://doi.org/10.1002/cmdc.202100157
Pd2	Added below	https://doi.org/10.14272/reaction/SA-FUHFF-UHFFFADPSC-HWRAKXKBWA-UHFFFADPSC-NUHFF-LUHFF-NUHFF-ZZZ
Pd3	published Complex **1**	https://doi.org/10.1039/D1RA06559A
Ag1	Added above	unpublished
Ag2	Added above	unpublished
Eu1	Added below	https://doi.org/10.14272/reaction/SA-FUHFF-UHFFFADPSC-XSDMQMVIDC-UHFFFADPSC-NUHFF-KUHFF-NUHFF-ZZZ
Ir1	Published, **11**	https://pubs.acs.org/doi/10.1021/acs.jmedchem.8b00906
Ir2	Published, **13**	https://pubs.acs.org/doi/10.1021/acs.jmedchem.8b00906
Ir3	Published, **14**	https://pubs.acs.org/doi/10.1021/acs.jmedchem.8b00906
Pt1	Published, **Pt1**	https://doi.org/10.1002/cmdc.202100157

15

Pt2	Published, **Pt2**	https://doi.org/10.1002/cmdc.202100157
Pt3	Published **Pt9**	https://doi.org/10.1002/cmdc.202100157
Pt4	Published **Pt 8**	https://doi.org/10.1002/cmdc.202100157
Pt5	Published, 2	https://doi.org/10.1039/D1RA06559A
Au1	Added below	unpublished
Au2	Added below	unpublished
Au3	Added below	unpublished
Au4*	Published, **3b**	https://pubs.rsc.org/en/content/articlelanding/2020/dt/d0dt00665c

Characterization Data for unpublished compounds

Ni1. ^{1}H NMR (500 MHz, DMSO-d_6): δ 5.46 (d, J = 15.75 Hz, 4H, CH$_2$), 5.46 (d, J = 15.75 Hz, 4H, CH2), 6.01 (d, J = 15.65 Hz, 4H, CH$_2$), 7.35-7.37 (m, 8H, Ar-H), 7.50-7.52 (m, 8H, Ar-H), 7.98 (d, J = 7.75 Hz, 4H, Pyr-m-H), 8.19 (d, J = 7.75 Hz, 4H, Pyr-m-H) ppm.
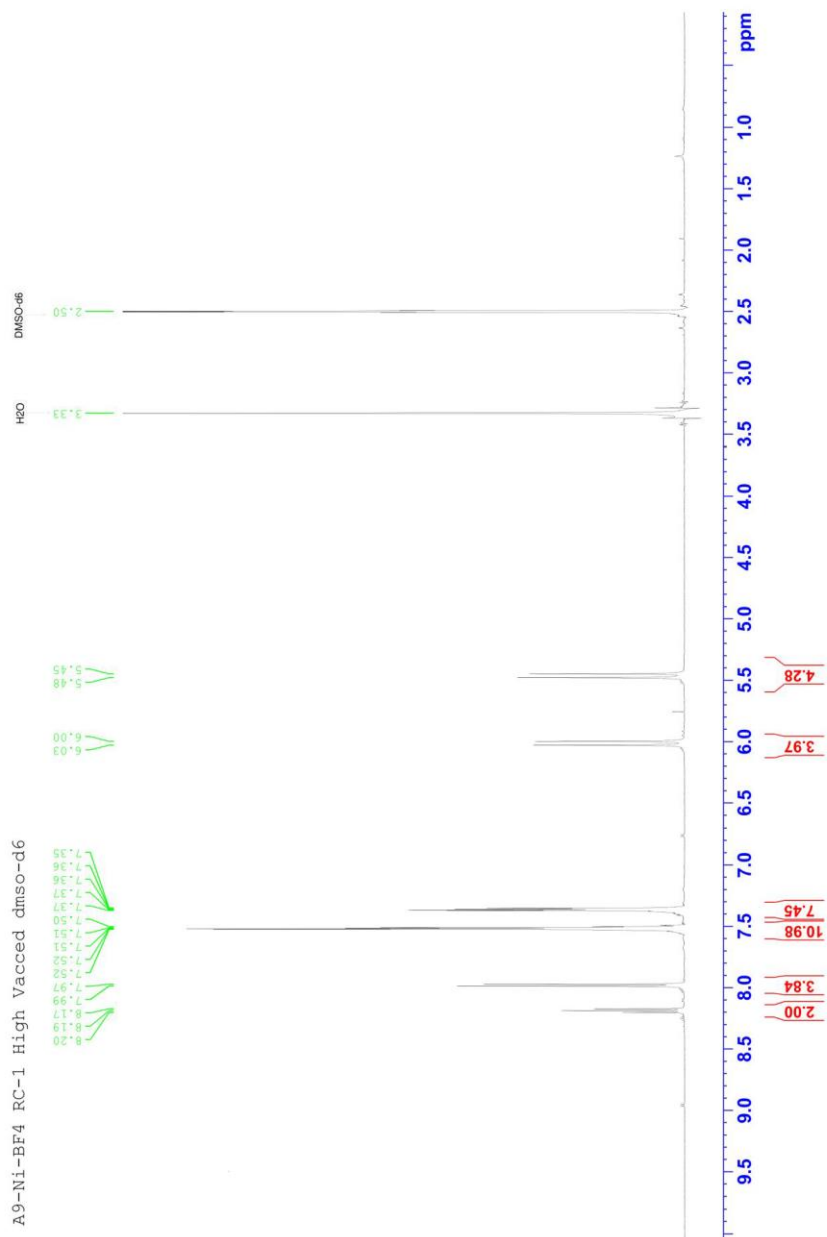
Figure S11. 1H NMR spectrum of **Ni1** in DMSO-d6.

Pd2.

17
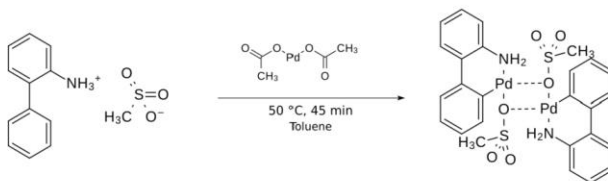
Formula: $C_{26}H_{26}N_2O_6Pd_2S_2$;

Smiles: Nc1ccccc1c1ccccc1[Pd]OS(=O)(=O)C.Nc1ccccc1c1ccccc1[Pd]OS(=O)(=O)C

InChIKey: HWRAKXKBWAQMFD-UHFFFAOYSA-L

A 20 mL Schlenk flask was charged with methanesulfonic acid;2-phenylaniline (500 mg, 1.88 mmol, 1.00 equiv) and palladium(II) acetate (423 mg, 1.88 mmol, 1.00 equiv). Dry toluene (8.00 mL) was added and the mixture was stirred at 50 °C for 45 min until it became milky and brown in appearance. After cooling to 21 °C the suspension was filtered, washed with toluene (1.5 mL) and diethyl ether (3 x 1.5 mL) and dried under vacuum for 24 h. The isolated product Pd2 ($C_{26}H_{26}N_2O_6Pd_2S_2$)) was obtained as a grey solid in 44% yield (609 mg, 824 μmol).

^{1}H NMR (400 MHz, Methanol-d4 [3.31 ppm], ppm) δ = 7.62 (dd, J = 1.3 Hz, J = 7.3 Hz, 2H), 7.46 (d, J = 7.2 Hz, 2H), 7.31–7.21 (m, 6H), 7.16–7.11 (m, 2H), 7.07–7.04 (m, 4H), 2.72 (s, 6H). Missing two H from 2 x NH$_2$ (4H); ^{13}C NMR (100 MHz, Methanol-d4 [49.1 ppm], ppm) δ = 140.1 (2C), 139.7 (2C), 138.4 (4C), 137.6 (2C), 134.8 (2C), 129.0 (2C), 128.8 (2C), 127.9 (2C), 127.2 (2C), 125.7 (2C), 120.9 (2C), 39.7 (2C). Impurities at 130.0, 129.4, 126.4 ppm; IR (ATR, ṽ) = 3259 (w), 3210 (w), 3054 (w), 3020 (w), 1612 (vw), 1571 (w), 1497 (w), 1465 (vw), 1439 (w), 1425 (w), 1332 (vw), 1320 (vw), 1234 (vs), 1181 (w), 1167 (w), 1160 (w), 1126 (vs), 1106 (vs), 1061 (w), 1048 (w), 1024 (vs), 1001 (w), 983 (w), 965 (w), 941 (vw), 932 (vw), 868 (vw), 827 (vw), 775 (m), 759 (s), 739 (vs), 728 (m), 713 (w), 663 (vw), 615 (vw), 591 (m), 567 (w), 551 (vs), 511 (vs), 470 (s), 452 (w), 405 (w), 387 (w) cm^{-1}.

Additional information on the chemical synthesis is available via Chemotion repository:

https://doi.org/10.14272/reaction/SA-FUHFF-UHFFFADPSC-HWRAKXKBWA-UHFFFADPSC-NUHFF-LUHFF-NUHFF-ZZZ

Additional information on the analysis of the target compound is available via Chemotion repository:

https://doi.org/10.14272/HWRAKXKBWAQMFD-UHFFFAOYSA-L.1

Eu1.

18

EU1 (75 %)
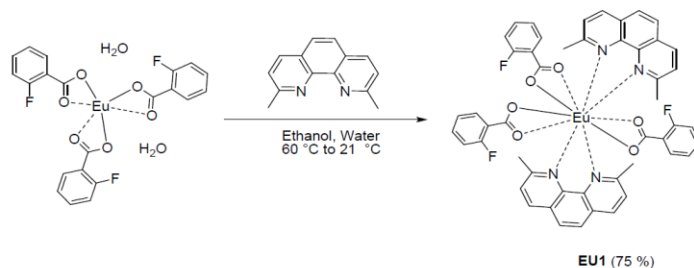
Formula: $C_{49}H_{36}EuF_3N_4O_6$; Smiles:
O=C(c1ccccc1F)O[Eu](OC(=O)c1ccccc1F)OC(=O)c1ccccc1F.Cc1ccc2c(n1)c1nc(C)ccc1cc2.Cc1ccc2c(n1)c1nc(C)ccc1cc2

InChIKey: XSDMQMVIDCRHRR-UHFFFAOYSA-K

A solution of 2,9-dimethyl-1,10-phenanthroline (86.7 mg, 416 μmol, 2.00 equiv) in ethanol (12.0 mL) was slowly added to a solution of tris-europium-2-fluorobenzoate dihydrate (126 mg, 208 μmol, 1.00 equiv) in ethanol (12.0 mL) and water (4.0 mL) and the reaction mixture was heated to 60 °C for 1 hour and then allowed to cool to 21 °C. The precipitate was gained by filtration, washed with cold ethanol and dried in vacuo. The isolated product EU1 (C49H36EuF3N4O6) was obtained as a light brown solid in 75% yield (154 mg, 156 μmol).

^{1}H NMR (400 MHz, DMSO-d6 [2.50 ppm], ppm) δ = 8.33 (d, J = 8.2 Hz, 4H), 7.86 (s, 4H), 7.61 (d, J = 8.2 Hz, 4H), 7.18 (bs, 4H), 6.74 (bs, 8H), 2.78 (s, 12H); ^{13}C NMR (100 MHz, DMSO-d6 [39.5 ppm], ppm) δ = 160.6 (d, J = 254 Hz, 3C), 158.3 (4C), 144.7 (4C), 136.4 (4C), 132.4 (d, J = 6.9 Hz), 131.6 (4C), 126.6 (4C), 125.5 (4C), 123.4 (4C), 123.1 (d, J = 2.3 Hz, 3C), 114.6 (d, J = 20.8 Hz, 3C), 25.0 (4C). Missing signals due to line broadening (7 C); ^{19}F NMR (376 MHz, ppm) δ = −112.08; IR (ATR, ṽ) = 2918 (w), 1706 (w), 1609 (vs), 1594 (vs), 1545 (vs), 1496 (s), 1486 (s), 1449 (s), 1400 (vs), 1298 (m), 1261 (m), 1220 (vs), 1159 (m), 1145 (m), 1094 (s), 1028 (s), 958 (m), 863 (vs), 809 (s), 759 (vs), 734 (s), 696 (s), 681 (m), 657 (vs), 642 (s), 571 (m), 547 (s), 523 (m), 499 (m), 450 (m), 418 (m), 411 (m), 391 (m), 380 (m) cm^{-1}.

Additional information on the chemical synthesis is available via Chemotion repository:

https://doi.org/10.14272/reaction/SA-FUHFF-UHFFFADPSC-XSDMQMVIDC-UHFFFADPSC-NUHFF-KUHFF-NUHFF-ZZZ

Additional information on the analysis of the target compound is available via Chemotion repository:

https://doi.org/10.14272/XSDMQMVIDCRHRR-UHFFFAOYSA-K.1
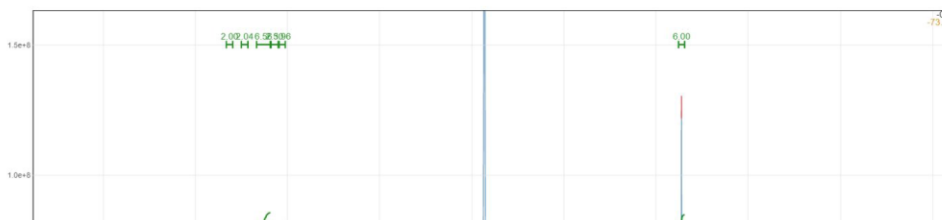
19

Figure S12. 1H NMR spectrum of **Pd2** in CD$_3$OD.
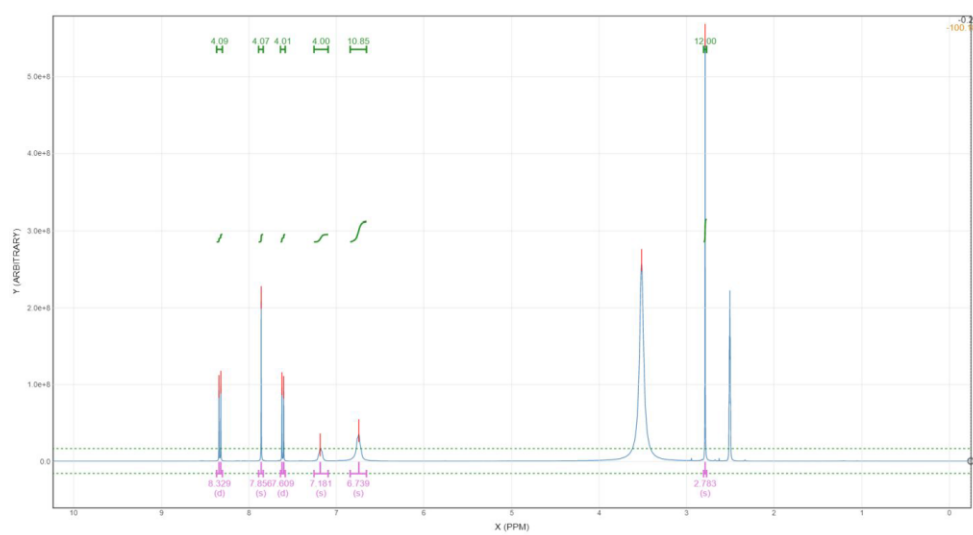
Figure S13. 1H NMR spectrum of **Eu1** in DMSO-d6.

Au1.

MS: Mass-to-charge ratio (*m/z*) values for observed ions with relative abundance (RA) > 10% in ESI mass spectrum: 541.0045 [M+H]+ (RA 100%)
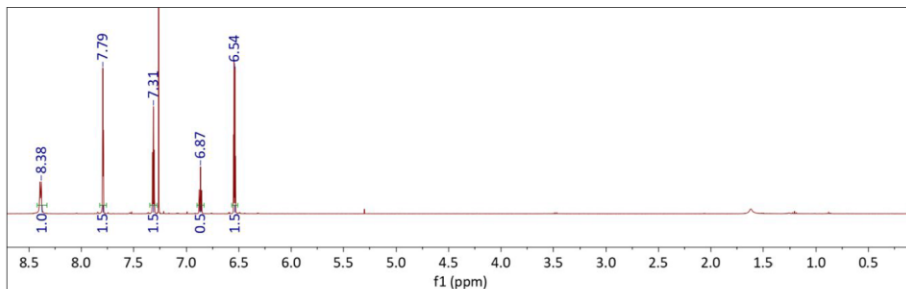
Figure S14. 1H NMR spectrum of **Au1** in CDCl₃.
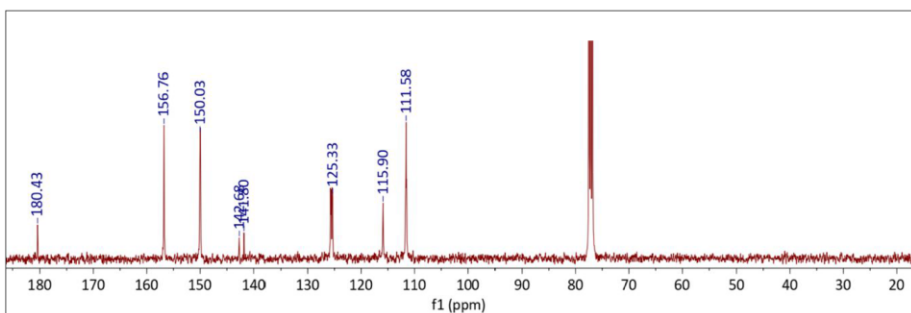

Figure S15. 13C NMR spectrum of **Au1** in CDCl₃.
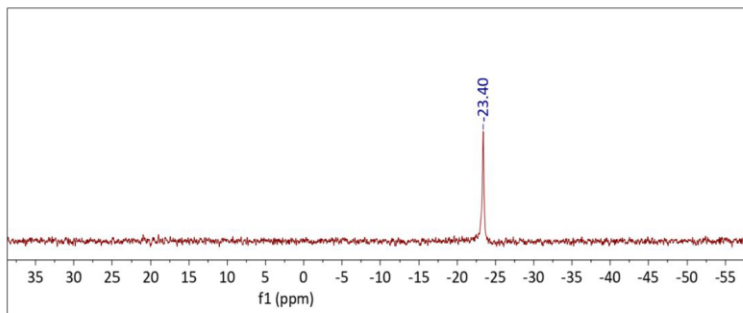
Figure S16. 31P NMR spectrum of **Au1** in CDCl₃

21

Au2.

MS for $C_{23}H_{19}NPSAu$: Mass-to-charge ratio (*m/z*) values for observed ions with relative abundance (RA) > 10% in ESI mass spectrum: 570.0714 [M+H]⁺ (RA 100%)
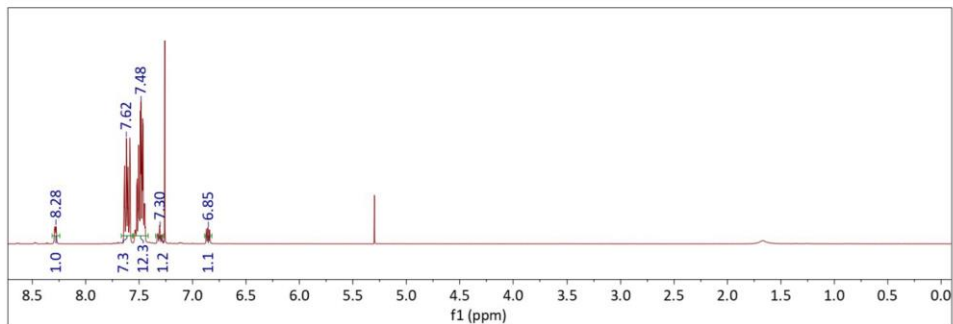
Figure S17. 1H NMR spectrum of **Au2** in CDCl₃.
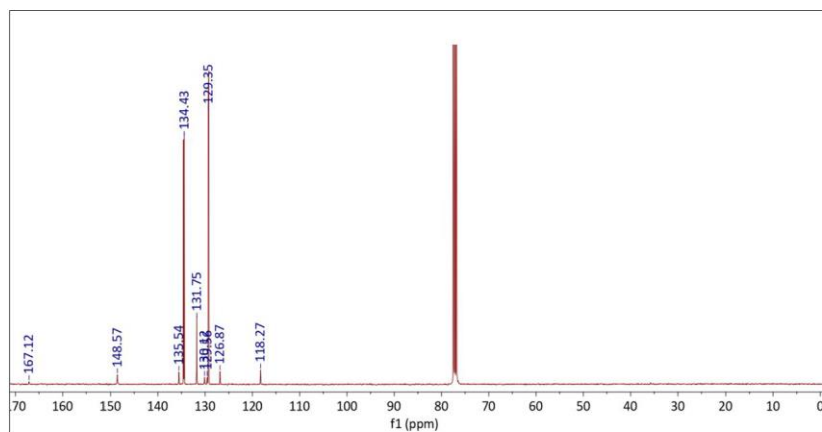
Figure S18. 13C NMR spectrum of **Au2** in CDCl₃.
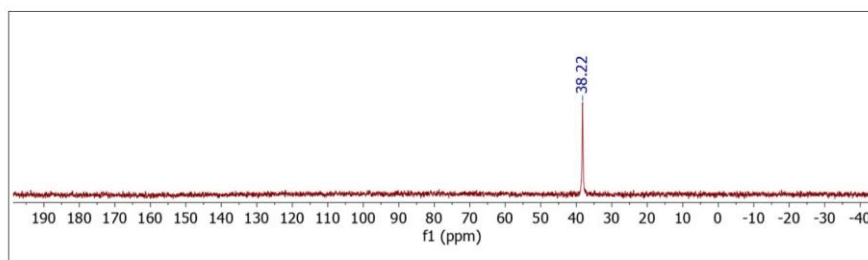
Figure S19. 31P NMR spectrum of **Au2** in CDCl₃.

Au3.

EA for $C_{12}H_{30}S_4P_2Au_2Mo$

Experimental % (calculated %)

C: 16.96 (16.87); H: 3.57 (3.54)
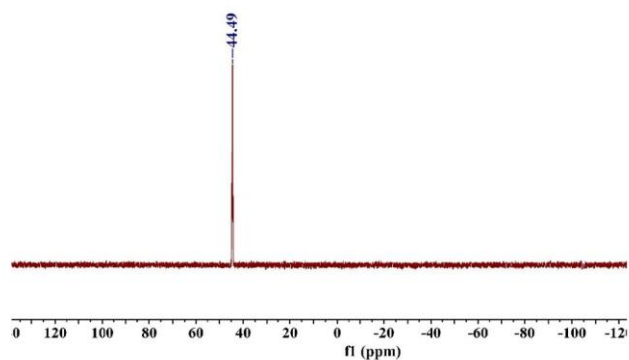
Figure S20. 31P NMR spectrum of **Au3** in DMSO-d6.

References

1.　　Matiadis, D.; Nowak, K. E.; Alexandratou, E.; Hatzidimitriou, A.; Sagnou, M.; Papadakis, R., Synthesis and (Fluoro)Solvatochromism of Two 3-Styryl-2-Pyrazoline Derivatives Bearing Benzoic Acid Moiety: A Spectral, Crystallographic and Computational Study. *J. Mol. Liq.* **2021,** *331*, 115737.
2.　　Maliszewska, H. K.; Arnau del Valle, C.; Xia, Y.; Marín, M. J.; Waller, Z. A. E.; Muñoz, M. P., Precious Metal Complexes of Bis(Pyridyl)Allenes: Synthesis and Catalytic and Medicinal Applications. *Dalton Trans.* **2021,** *50* (45), 16739-16750.

23

APPENDIX F: FIGURES, SCHEMES, AND TABLES RIGHTS & PERMISSIONS

Figure 1.4. Au(I)NHC and Au(III)NHC halide complexes derived from 4,5-diarylimidazoles

ORGANOMETALLICS

Titanocene–Gold Complexes Containing N-Heterocyclic Carbene Ligands Inhibit Growth of Prostate, Renal, and Colon Cancers in Vitro

Yiu Fung Mui,[†,‡,#] Jacob Fernández-Gallardo,[†,#] Benelita T. Elie,[†,§] Ahmed Gubran,[†] Irene Maluenda,[∥] Mercedes Sanaú,[⊥] Oscar Navarro,[∥] and María Contel*[,†,‡,§]

[†]Department of Chemistry, Brooklyn College, The City University of New York, Brooklyn, New York 11210, United States
[‡]Chemistry and [§]Biology Ph.D. Programs, The Graduate Center, The City University of New York, 365 Fifth Avenue, New York, New York 10016, United States
[∥]Department of Chemistry, University of Sussex, Falmer, Brighton BN1 9QJ, U.K.
[⊥]Departamento de Química Inorgánica, Universidad de Valencia, Burjassot, Valencia 46100, Spain

ⓢ *Supporting Information*

ABSTRACT: We report on the synthesis, characterization, and stability studies of new titanocene complexes containing a methyl group and a carboxylate ligand (mba = $-OC(O)$-p-C_6H_4-$S-$) bound to gold(I)−N-heterocyclic carbene fragments through the thiolate group: $[(\eta^5$-$C_5H_5)_2TiMe(\mu$-mba)Au(NHC)]$. The cytotoxicities of the heterometallic compounds along with those of novel monometallic gold−N-heterocyclic carbene precursors $[(NHC)Au(mbaH)]$ have been evaluated against renal, prostate, colon, and breast cancer cell lines. The highest activity and selectivity and a synergistic effect of the resulting heterometallic species was found for the prostate and colon cancer cell lines. The colocalization of both titanium and gold metals (1:1 ratio) in PC3 prostate cancer cells was demonstrated for the selected compound **5a**, indicating the robustness of the heterometallic compound in vitro. We describe here preliminary mechanistic data involving studies on the interaction of selected mono- and bimetallic compounds with plasmid (pBR322) used as a model nucleic acid and the inhibition of thioredoxin reductase in PC3 prostate cancer cells. The heterometallic compounds, which are highly apoptotic, exhibit strong antimigratory effects on the prostate cancer cell line PC3.

Inhibition of Thioredoxin Reductase in PC3 cancer cell lines up to 76% in 24h

Cytotoxic towards prostate cancer cell lines (PC3 and DU145)
No interaction with DNA
Anti-migratory properties on PC3
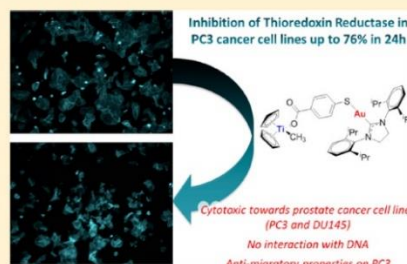
■ INTRODUCTION

The potential of heterometallic complexes as cancer chemo-therapeutics has been recently highlighted.[1] The improved activity of heteronuclear complexes as antitumor agents by incorporation of two different cytotoxic metals within the same molecule has been demonstrated. The beneficial influence may be due to a synergistic or cooperative effect. Bimetallic and trimetallic compounds with anticancer properties have been described. There have been reports on titanocenes incorporating Ru(II), Pt(II), and Pd(II) centers[2,3] and a number of complexes containing ferrocene moieties and other metals.[4] Bimetallic systems based on Ru(II)−Pt(II)[5] or Ru(II)−Ir(III)[6] have also been described. Ferrocenyl phosphanes were incorporated in the iminophosphorane skeleton of gold(III) and palladium(II) coordination complexes.[4] Heterometallic compounds based on gold(I) fragments have been reported for titanocene,[1,3,7,8] ruthenium(II),[9−12] platinum(II),[13] rhenium-(I),[14] and copper(II)[10] derivatives.

We have reported on a number of titanocene–gold derivatives with potential as anticancer agents (zero-, first-, and second-generation derivatives **1−3** in Chart 1).[1,3,8] We described cytotoxic species in which gold fragments coordinate

Chart 1. Potential Anticancer Titanocene−Gold Complexes Containing Different Linkers Described by Our Group[1,3,8]

Zero generation
First generation
Second generation
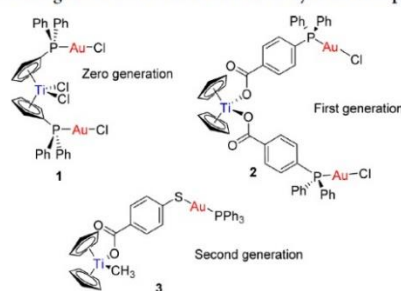
to cyclopentadienyl−phosphane ligands that displayed a synergistic effect (such as **1** in Chart 1).[3] In order to improve

Figure 1.5. [Au(NHC)(Hmba)] (Au) and [(η^5-C_5H_5)$_2$Ti(CH$_3$){OC(O)-p-C_6H_4SAu(NHC)}] (AuTi) complexes, NHC= IPr, SIPr and IMes

CCC Marketplace

Order Confirmation

> Thank you, your order has been placed. An email confirmation has been sent to you. Your order license details and printable licenses will be available within 24 hours. Please access Manage Account for final order details.

This is not an invoice. Please go to manage account to access your order history and invoices.

CUSTOMER INFORMATION

> Payment by invoice: You can cancel your order until the invoice is generated by contacting customer service.

Billing Address

Dhirgam Humaidy
168 College Ave
Orono, ME 04469
United States

+1 (207) 889-7232
dhirgam.humaidy@maine.edu

Customer Location

Dhirgam Humaidy
168 College Ave
Orono, ME 04469
United States

PO Number (optional)

N/A

Payment options

Invoice

PENDING ORDER CONFIRMATION

Confirmation Number: Pending

Order Date: 10-Dec-2022

1. CURRENT MEDICINAL CHEMISTRY   0.00 USD

Order License ID	Pending	Publisher	BENTHAM SCIENCE PUBLISHERS LTD.
ISSN	0929-8673		
Type of Use	Republish in a thesis/dissertation	Portion	Image/photo/illustration

LICENSED CONTENT

Publication Title	CURRENT MEDICINAL CHEMISTRY	**Country**	Netherlands
		Rightsholder	EUREKA SCIENCE (FZC)
Date	01/01/1994	**Publication Type**	Journal
Language	English		

REQUEST DETAILS

Portion Type	Image/photo/illustration	**Distribution**	Worldwide
Number of Images / Photos / Illustrations	1	**Translation**	Original language of publication
Format (select all that apply)	Print, Electronic	**Copies for the Disabled?**	No
Who Will Republish the Content?	Academic institution	**Minor Editing Privileges?**	No
		Incidental Promotional Use?	No
Duration of Use	Life of current edition		
Lifetime Unit Quantity	Up to 499	**Currency**	USD
Rights Requested	Main product and any product related to main product		

NEW WORK DETAILS

Title	GOLD (I) TETRATHIOMOLYBDATE CLUSTERS: SYNTHESIS, CHARACTERIZATION, COMPUTATIONAL STUDIES, AND REACTIVITY WITH THIOPHENOL AND SELENOPHENOL	**Institution Name**	University of Maine
		Expected Presentation Date	2022-12-31
Instructor Name	Dhirgam Humaidy		

ADDITIONAL DETAILS

Order Reference Number	N/A	**The Requesting Person/Organization to Appear on the License**	Dhirgam Humaidy

REUSE CONTENT DETAILS

Title, Description or Numeric Reference of the Portion(s)	GOLD (I) TETRATHIOMOLYBDATE CLUSTERS: SYNTHESIS, CHARACTERIZATION, COMPUTATIONAL STUDIES, AND REACTIVITY WITH THIOPHENOL AND SELENOPHENOL	**Title of the Article/Chapter the Portion Is From**	Molybdenum Metallopharmaceuticals Candidate Compounds - The "Renaissance" of Molybdenum Metallodrugs?
		Author of Portion(s)	N/A
		Issue, if Republishing an Article From a Serial	N/A
Editor of Portion(s)	N/A		

Figure 1.7. Ball-and-stick model of the $S_6Cu_4MoS_4$ cluster structure (yellow balls, sulfur atoms; blue balls, copper atoms; lime ball, molybdenum atoms)

Anti-Arthritic Activity in Rats of Some Phosphinegold(I) Thionucleobases and Related Thiolates

Michael W. Whitehouse,[1,2] Peter D. Cookson,[3] George Siasios,[3] and Edward R. T. Tiekink[3]

Show more

Abstract

A number of phosphinegold(I) thiolates where, generally, the thiolate is derived from a thionucleobase, have been screened for anti-arthritic activity in Dark Agouti rats, a gold sensitive model for arthritis. Potency and toxicity data showed that, generally, the Ph3P derivatives and species based on thiopurines were the most effective and that with other complexes enhanced activity was accompanied by greater toxicity.

Copyright

More related articles

No related content is available yet for this article.

Hindawi

Table 1.1. Anticancer activity of complexes R_3PAuCl vs colon cancer (HT-29) and breast cancer (MCF-7) cells (IC_{50} is the half maximal inhibitory concentration).

CCC   Marketplace

Order Confirmation

Thank you, your order has been placed. An email confirmation has been sent to you. Your order license details and printable licenses will be available within 24 hours. Please access Manage Account for final order details.

This is not an invoice. Please go to manage account to access your order history and invoices.

CUSTOMER INFORMATION

Payment by invoice: You can cancel your order until the invoice is generated by contacting customer service.

PENDING ORDER CONFIRMATION

Confirmation Number: Pending

Order Date: 10-Dec-2022

1. New journal of chemistry   0.00 USD

Article: Cytotoxic effects of gold(I) complexes against colon, cervical and osteo carcinoma cell lines: A mechanistic approach

Order License ID	Pending	**Publisher**	ROYAL SOCIETY
ISSN	1144-0546		OF CHEMISTRY
Type of Use	Republish in a thesis/dissertation	**Portion**	Image/photo/illustration

LICENSED CONTENT

Publication Title	New journal of chemistry	Rightsholder	Royal Society of Chemistry
Article Title	Cytotoxic effects of gold(I) complexes against colon, cervical and osteo carcinoma cell lines: A mechanistic approach	Publication Type	Journal
		Start Page	14565
		End Page	14574
		Issue	36
Author/Editor	CENTRE NATIONAL DE LA RECHERCHE SCIENTIFIQUE (FRAN, SOCIETE FRANCAISE DE CHIMIE.	Volume	43
Date	01/01/1987		
Language	English, French		
Country	United Kingdom of Great Britain and Northern Ireland		

REQUEST DETAILS

Portion Type	Image/photo/illustration	Distribution	Worldwide
Number of Images / Photos / Illustrations	1	Translation	Original language of publication
Format (select all that apply)	Print, Electronic	Copies for the Disabled?	No
Who Will Republish the Content?	Academic institution	Minor Editing Privileges?	No
Duration of Use	Life of current edition	Incidental Promotional Use?	Yes
Lifetime Unit Quantity	Up to 499	Currency	USD
Rights Requested	Main product and any product related to main product		

NEW WORK DETAILS

Title	GOLD (I) TETRATHIOMOLYBDATE CLUSTERS: SYNTHESIS, CHARACTERIZATION, COMPUTATIONAL STUDIES, AND REACTIVITY WITH THIOPHENOL AND SELENOPHENOL	Institution Name	University of Maine
		Expected Presentation Date	2022-12-31
Instructor Name	Dhirgam Humaidy		

ADDITIONAL DETAILS

Order Reference Number	N/A	The Requesting Person/Organization to Appear on the License	University of Maine

REUSE CONTENT DETAILS

Title, Description or Numeric Reference of the Portion(s)	GOLD (I) TETRATHIOMOLYBDATE CLUSTERS: SYNTHESIS, CHARACTERIZATION, COMPUTATIONAL STUDIES, AND REACTIVITY WITH THIOPHENOL AND SELENOPHENOL	Title of the Article/Chapter the Portion Is From	Cytotoxic effects of gold(I) complexes against colon, cervical and osteo carcinoma cell lines: A mechanistic approach
		Author of Portion(s)	Seleman, Adam; Kalia, Namarta; Bhatia, Gaurav; Kaur , Manpreet; Fettouhi, Mohammed; Altaf , Mohammad; Baig, Nadeem; Kawde, Abdel-Nasser; Isab, Anvarhusein
Editor of Portion(s)	Seleman, Adam; Kalia, Namarta; Bhatia, Gaurav; Kaur , Manpreet; Fettouhi, Mohammed; Altaf , Mohammad; Baig, Nadeem; Kawde, Abdel-Nasser; Isab, Anvarhusein		
		Issue, if Republishing an Article From a Serial	36
Volume of Serial or Monograph	43	Publication Date of Portion	2019-01-01
Page or Page Range of Portion	14565-14574		

Total Items: 1   **Total Due: 0.00 USD**

Accepted: Marketplace Order General Terms and Conditions and any applicable Publisher Terms and Conditions

Table 1.2. Anticancer activity of complexes (NHC)AuX and cisplatin vs HCT15, MG-63 and HeLa cancer cells.

×

Targeting antioxidant pathways with ferrocenylated N-heterocyclic carbene supported gold(I) complexes in A549 lung cancer cells

×

Table 1.3. Anticancer activity of complexes [Au(NHC)$_2$]$_+$ and auranofin vs A549 cancer cells.

Table 1.4. Anticancer activity of complexes (NHC)AuX, cisplatin and auranofin vs A2780S and A2780R cancer cells.

CCC Marketplace

Order Confirmation

Thank you, your order has been placed. An email confirmation has been sent to you. Your order license details and printable licenses will be available within 24 hours. Please access Manage Account for final order details.

This is not an invoice. Please go to manage account to access your order history and invoices.

CUSTOMER INFORMATION

Payment by invoice: You can cancel your order until the invoice is generated by contacting customer service.

目 Billing Address

Dhirgam Humaidy
168 College Ave
Orono, ME 04469
United States

+1 (207) 889-7232
dhirgam.humaidy@maine.edu

⚑ Customer Location

Dhirgam Humaidy
168 College Ave
Orono, ME 04469
United States

PO Number (optional)

N/A

Payment options

Invoice

PENDING ORDER CONFIRMATION

Confirmation Number: Pending

Order Date: 10-Dec-2022

1. MedChemComm   0.00 USD

Article: Biscarbene gold(i) complexes: structure-activity-relationships regarding antibacterial effects, cytotoxicity, TrxR inhibition and cellular bioavailability.

Order License ID	Pending	Publisher	Royal Society of Chemistry
ISSN	2040-2503		
Type of Use	Republish in a thesis/dissertation	Portion	Chart/graph/table/figure

LICENSED CONTENT

Publication Title	MedChemComm	**Rightsholder**	Royal Society of Chemistry
Article Title	Biscarbene gold(i) complexes: structure-activity-relationships regarding antibacterial effects, cytotoxicity, TrxR inhibition and cellular bioavailability.	**Publication Type**	Journal
		Start Page	1681
		End Page	1689
		Issue	8
		Volume	8
Author/Editor	Royal Society of Chemistry (Great Britain), European Federation for Medicinal Chemistry.		
Date	01/01/2010		
Language	English		
Country	United Kingdom of Great Britain and Northern Ireland		

REQUEST DETAILS

Portion Type	Chart/graph/table/figure	**Distribution**	Worldwide
Number of Charts / Graphs / Tables / Figures Requested	1	**Translation**	Original language of publication
		Copies for the Disabled?	No
Format (select all that apply)	Print, Electronic	**Minor Editing Privileges?**	No
Who Will Republish the Content?	Academic institution	**Incidental Promotional Use?**	No
Duration of Use	Life of current edition	**Currency**	USD
Lifetime Unit Quantity	Up to 499		
Rights Requested	Main product and any product related to main product		

NEW WORK DETAILS

Title	GOLD (I) TETRATHIOMOLYBDATE CLUSTERS: SYNTHESIS, CHARACTERIZATION, COMPUTATIONAL STUDIES, AND REACTIVITY WITH THIOPHENOL AND SELENOPHENOL	**Institution Name**	University of Maine
		Expected Presentation Date	2022-12-31
Instructor Name	Dhirgam Humaidy		

ADDITIONAL DETAILS

Order Reference Number	N/A

The Requesting
Person/Organization to   Dhirgam Humaidy
Appear on the License

REUSE CONTENT DETAILS

Title, Description or Numeric Reference of the Portion(s)	GOLD (I) TETRATHIOMOLYBDATE CLUSTERS: SYNTHESIS, CHARACTERIZATION, COMP	Title of the Article/Chapter the Portion Is From	Biscarbene gold(i) complexes: structure-activity-relationships regarding antibacterial effects, cytotoxicity, TrxR inhibition and cellular bioavailability.
Editor of Portion(s)	Schmidt, Claudia; Karge, Bianka; Misgeld, Rainer; Prokop, Aram; Brönstrup, Mark; Ott, Ingo	Author of Portion(s)	Schmidt, Claudia; Karge, Bianka; Misgeld, Rainer; Prokop, Aram; Brönstrup, Mark; Ott, Ingo
Volume of Serial or Monograph	8		
Page or Page Range of Portion	1681-1689	Issue, if Republishing an Article From a Serial	8
		Publication Date of Portion	2017-08-01

Total Items: 1   Total Due: 0.00 USD

Table 1.5. Anticancer and antibacterial activities, and TrxR inhibition of complexes $[Au(NHC)_2]^+$ and auranofin vs selected cancer cells, one strain of Gram-positive (MRSA DMS) and one strain of Gram-negative bacteria, and TrxR of rat and bacteria (*E. coli*).

🏠 Home   ❓ Help ∨   ✉ Email Support

N-Heterocyclic Carbenes: A New Concept in Organometallic Catalysis

Author: Wolfgang A. Herrmann

Publication: Angewandte Chemie International Edition

Publisher: John Wiley and Sons

Date: Apr 16, 2002

Order Completed

Your confirmation email will contain your order number for future reference.

License Number	5445341418094
License date	Dec 10, 2022

🖨 Printable Details

✅ Licensed Content

Licensed Content Publisher	John Wiley and Sons
Licensed Content Publication	Angewandte Chemie International Edition
Licensed Content Title	N-Heterocyclic Carbenes: A New Concept in Organometallic Catalysis
Licensed Content Author	Wolfgang A. Herrmann
Licensed Content Date	Apr 16, 2002
Licensed Content Volume	41
Licensed Content Issue	8
Licensed Content Pages	20

📋 Order Details

Type of use	Dissertation/Thesis
Requestor type	University/Academic
Format	Print and electronic
Portion	Figure/table
Number of figures/tables	1
Will you be translating?	No

📄 About Your Work

Title	GOLD (I) TETRATHIOMOLYBDATE CLUSTERS: SYNTHESIS, CHARACTERIZATION, COMPUTATIONAL STUDIES, AND REACTIVITY WITH THIOPHENOL AND SELENOPHENOL
Institution name	University of Maine
Expected presentation date	Dec 2022

📁 Additional Data

Portions	Convenient synthetic routes to imidazolium salts, a) the same R substituents, b) different R substituents where R = any aromatic or aliphatic group

Scheme 1.4. Convenient synthetic routes to imidazolium salts, a) the same R substituents, b) different R substituents where R = any aromatic or aliphatic group.
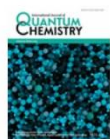
Electronic structure calculations on multiply charged anions containing M S bonds (M = Cr, Mo, W) and their heterobimetallic cluster complexes

Author: Athanassios C. Tsipis, Pedro Gili

Publication: International Journal of Quantum Chemistry

Publisher: John Wiley and Sons

Date: Sep 5, 2006

Copyright © 2006 Wiley Periodicals, Inc.

Order Completed

Your confirmation email will contain your order number for future reference.

License Number	5445361448430	🖶 Printable Details
License date	Dec 10, 2022	

Licensed Content

Licensed Content Publisher	John Wiley and Sons
Licensed Content Publication	International Journal of Quantum Chemistry
Licensed Content Title	Electronic structure calculations on multiply charged anions containing M S bonds (M = Cr, Mo, W) and their heterobimetallic cluster complexes
Licensed Content Author	Athanassios C. Tsipis, Pedro Gili
Licensed Content Date	Sep 5, 2006
Licensed Content Volume	107
Licensed Content Issue	2
Licensed Content Pages	22

Order Details

Type of use	Dissertation/Thesis
Requestor type	University/Academic
Format	Print and electronic
Portion	Figure/table
Number of figures/tables	1
Will you be translating?	No

About Your Work

Title	GOLD (I) TETRATHIOMOLYBDATE CLUSTERS: SYNTHESIS, CHARACTERIZATION, COMPUTATIONAL STUDIES, AND REACTIVITY WITH THIOPHENOL AND SELENOPHENOL
Institution name	University of Maine
Expected presentation date	Dec 2022

Additional Data

Portions	Reaction profile of the interconversion of the [MoOxS4-x] (x= 0-4) dianions

Requestor Location

Requestor Location	168 College Ave Department of Chemistry ORONO, ME 04469 United States Attn: Dhirgam Humaidy

Tax Details

Publisher Tax ID	EU826007151

Price

Total	0.00 USD

Total: 0.00 USD

CLOSE WINDOW   ORDER MORE

Scheme 1.5. Reaction profile of the interconversion of the [MoO$_x$S$_{4-x}$] (x= 0-4) dianions.

Figure 3.1. a) Tolman cone angle; b) sphere dimensions for steric parameter determination %VBur of NHC ligands

BIOGRAPHY OF THE AUTHOR

Dhirgam Humaidy was born in Najaf, Iraq on July 03, 1981. After graduating from Al-Najaf High School in Iraq, Dhirgam entered University of Kufa in Kufa to pursue a Bachelor's degree in Chemistry and graduated in 2005. Then, Dhirgam worked for seven years for Al-Najaf Refinery, and then Oil Products Distribution Company and Oil Pipelines Company / Alnajaf oil depot, Najaf, Iraq. During that time, he entered the graduate program at Nahrain University, Baghdad, Iraq and obtained his Master's degree in Biochemistry Chemistry in 2011. Dhirgam entered the graduate program of the Department of Chemistry at the University of Maine in the Spring of 2016. His study is funded by the Higher Committee for Education Development in Iraq (HCED). Dhirgam has been a Teaching Assistant for the General Chemistry program of the Department of Chemistry from 2020 to 2022. Dhirgam is a candidate for the Doctor of Philosophy degree in Chemistry from the University of Maine in December 2022.